Project no.:	**637268**
Project full title:	**Robust Internal Thermal Insulation of Historic Buildings**
Project Acronym:	**RIBuild**
Deliverable no.:	**D2.3**
Title of the deliverable:	**Impact of water repellent agents on hygric properties of porous building materials**

Contractual Date of Delivery to the CEC:	**M63**
Actual Date of Delivery to the CEC:	**M63**
Organisation name of lead contractor for this deliverable:	**KU Leuven**
Author(s):	**Hans Janssen, Daan Deckers, Evy Vereecken, Chi Feng, Vasilis Soulios, Angela Vanek, Tessa Kvist Hansen**
Participants(s):	**KUL, DTU, AAU, IFLEX**
Work package contributing to the deliverable:	**WP2**
Internal reviewers:	**Ernst Jan de Place Hansen, Tessa Kvist Hansen, Lukas Lång**
Nature:	**R**
Version:	**1**
Total number of pages:	**159**
Start date of project:	**01.01.2015**
Duration of project:	**5½ years**

Abstract:

The insight that hydrophobization should be regarded as a possible element in the spectrum of internal insulation solutions triggered the midway introduction of RIBuild's Task 2.4 'Impact of water repellent agents on hygric material properties' and this deliverable reports the findings of that task. While giving much new knowledge and insights in regard to water repellent agents and hydrophobization, it also reveals that the results and outcomes show significant limitations and incongruences still, and that much more work thus is needed before hydrophobization can be reliably considered as part of the solution spectrum for moisture damages possibly resulting from application of internal insulation. Therefore, the findings of Task 2.4 have not resulted in adopting hydrophobization in the simulation campaign for the webtool of RIBuild's WP6.

Keyword list: hydrophobization, ceramic brick, lime mortar, water repellent agents, hygric property measurements, case studies, impregnation depth

Table of Contents

EXECUTIVE SUMMARY **5**
1 GENERAL INTRODUCTION **7**
2 OVERVIEW OF LITERATURE **8**
2.1 INTRODUCTION 8
2.2 PHYSICS AND PRINCIPLES 8
2.3 HISTORY AND EVOLUTION 9
2.4 EFFICACY AND DURABILITY 10
2.5 WETTING AND DRYING 11
2.6 CONCLUSIONS 12
3 WATER REPELLENT AGENTS **14**
3.1 INTRODUCTION 14
3.2 THE NATURE OF WATER REPELLENCY 14
3.3 TYPES OF WATER REPELLENT AGENTS 15
3.4 PRODUCT IDENTIFICATION 17
3.5 CLASSIFICATION OF COMMERCIAL WATER REPELLENT AGENTS 20
3.6 GENERAL OVERVIEW OF THE MARKET ..... **FEJL! BOGMÆRKE ER IKKE DEFINERET.**
4 SIMULATION CAMPAIGN **33**
4.1 INTRODUCTION 33
4.2 VIRTUAL HYDROPHOBIZATION 33
4.3 HYGROTHERMAL PERFORMANCE OF HYDROPHOBIZED WALLS 36
4.4 CONCLUSIONS 53
5 HYGRIC PROPERTY MEASUREMENTS @ DTU **56**
5.1 GENERAL INTRODUCTION 56
5.2 HYDROPHOBIZED BRICK AND AIR LIME MORTAR 57
5.3 HYDROPHOBIZED MASONRY SECTIONS – WATER MIGRATION 69
5.4 REFERENCES 75

6 LABORATORY MEASUREMENTS @ KUL 77

6.1 HYGRIC PROPERTIES OF HYDROPHOBIZED BRICK AND MORTAR SAMPLES 77

6.2 HYGRIC BEHAVIOUR OF HYDROPHOBIZED BRICK AND MORTAR SAMPLES 84

6.3 DEVELOPMENT OF NEW METHODS FOR MEASURING HYGRIC PROPERTIES 87

6.4 MEASURING THE HYGRIC PROPERTIES OF POROUS BUILDING MATERIALS BEFORE AND AFTER HYDROPHOBIZATION 103

7 LABORATORY EXPERIMENTS ON IMPACT OF CRACKS 121

7.1 INTRODUCTION 121

7.2 DETERMINATION OF THE BREAKTHROUGH PRESSURE 121

7.3 OCCURING EXTERNAL PRESSURE ON A HYDROPHOBIZED FACADE 124

7.4 CONCLUSIONS 126

8 IN-SITU ASSESSMENT @ KLITGAARDEN, DENMARK 128

8.1 GENERAL INFORMATION 128

8.2 INTRODUCTION 128

8.3 HYDROPHOBIZATION 129

8.4 MEASUREMENTS 130

8.5 RESULTS 131

8.6 CONCLUSIONS 134

9 IN-SITU ASSESSMENT @ COPENHAGEN, DENMARK 135

9.1 INTRODUCTION ..... **FEJL! BOGMÆRKE ER IKKE DEFINERET.**

9.2 SET UP ..... **FEJL! BOGMÆRKE ER IKKE DEFINERET.**

9.3 RESULTS AND DISCUSSION ..... **FEJL! BOGMÆRKE ER IKKE DEFINERET.**

9.4 CONCLUSIONS ..... **FEJL! BOGMÆRKE ER IKKE DEFINERET.**

10 IN-SITU ASSESSMENT @ HEVERLEE, BELGIUM 147

10.1 INTRODUCTION 147

10.2 FIELD TEST SETUP 147

10.3 RESULTS 151

10.4 ANALYSIS OF THE IMPREGNATION DEPTH 157

10.5 CONCLUSIONS 157

Abbreviations

A	surface area (m^2)
A_{cap}	capillary absorption coefficient ($kg/m^2s^{0.5}$)
ACC	aerated cellular concrete
c	coefficient (kg/m^3)
CaSi	calcium silicate
G	volumetric flow rate (m^3/s)
$\dot{G}$	mass flow rate (kg/s)
g	gravitational acceleration (m/s^2)
$\dot{g}$	water flux (kg/m^2s)
H	water head (m)
H/NH	hydrophobized/non-hydrophobized
ICC	indoor climate class
K_l	liquid permeability (kg/msPa)
m_{K2SO4}	mass of K_2SO_4 (kg)
$m_{solution}$	mass of solution (kg)
m_{water}	water mass (kg)
p_c	capillary pressure (Pa)
p_l	liquid pressure (Pa)
PUR	polyurethane
$R_{membrane}$	membrane resistance (m^2sPa/kg)
R_{sample}	sample resistance (m^2sPa/kg)
R_{total}	total resistance (m^2sPa/kg)
R	electrical resistance (Ω)
RH	relative humidity (-)
r	pore radius (m)
S	intersection area (m^2)
s	solubility (kg/kg)
T	thickness (m)
t	time (s)
V	volume (m^3)
V_{K2SO4}	volume of K_2SO_4 (m^3)
V_{net}	net volume (m^3)
$V_{solution}$	volume of solution (m^3)
w	moisture content (kg/m^3)
w_{cap}	capillary moisture content (kg/m^3)
w_{sat}	saturated moisture content (kg/m^3)
WDR	wind-driven rain
XPS	extruded polystyrene
ϕ	open porosity (m^3/m^3)
ρ_{bulk}	bulk density (kg/m^3)
ρ_{K2SO4}	density of K_2SO_4 (kg/m^3)
$\rho_{solution}$	solution density (kg/m^3)
ρ_{water}	water density (kg/m^3)
μ	vapor diffusion resistance factor (-)

Executive Summary

(Hans Janssen, KUL)

The insight that hydrophobization should be regarded as a possible element in the spectrum of internal insulation solutions triggered the midway introduction of RIBuild's Task 2.4 'Impact of water repellent agents on hygric material properties', with KUL as leading partner and AAU and DTU as contributing partners. This deliverable D2.3 'Impact of water repellent agents on hygric properties of porous building materials' reports on the conclusions of that task.

In this research campaign, four elements have been central:

- A literature study collecting the current state-of-the-art with respect to water repellent agents and hydrophobization, firstly targeting the presently available knowledge in relation to hydrophobization and secondly surveying the presently available water repellent agents on the market. With respect to hydrophobization in general, the conclusion is that it can be a success, but only when the correct product is correctly used, and when proper maintenance is additionally applied. The literature also reveals that the impacts of hydrophobization on the hygric equilibrium of (internally insulated) wall assemblies has not been studied yet, not for walls in perfect condition, neither for walls with cracks or fissures. In relation to water repellent agents, the majority of these are silicon-based, and almost half of the the silicon-based products are mixtures of silanes and siloxanes. The majority of water repellent agents are also provided in liquid form, some of them as cream. Most products use water as a diluent, especially the creams. Although some products are recommended only for application in concrete and cementitious materials, most products are recommended for mineral substrates in general;
- A simulation study on the potential influence of water repellent agents on the moisture behaviour of massive facades with and without internal insulation, focusing primarily on the impacts of the hydrophobization strength, on the moisture contents and moisture damages. The simulations reveal that strong impregnations mostly result in lower levels of moisture content inside the masonry, while weak impregnations can have a negative impact on the moisture content levels, particularly in walls with a vapour tight interior insulation. In relation to wood decay and mold growth, strong impregnations generally lead to lower risks, while weak impregnations often increase the risk of moisture related damages. Regarding heat loss, hydrophobization is more effective when strong impregnations are combined with capillary active insulation systems. In general, it is shown that when hydrophobization succeeds in its main goal, preventing of liquid water from entering the masonry wall, there are many benefits for the hygrothermal performance of the wall. However, when there is rain penetration (through defects), the hygrothermal performance of the wall can deteriorate, resulting in increased risks for moisture-related damages;
- Laboratory analyses on the impact of water repellent agents on the hygric properties of porous building materials – ceramic brick and lime mortar –, with focus on the influence of the agents' formulation and concentration and on the effect of the agents' application and penetration. The study concludes that a hydrophobization treatment has the desired effect of reduced rainwater penetration on historic masonry, although this effect is more pronounced in brick relative to lime mortar. Drying of treated specimens is not significantly influenced for brick, the drying of lime mortar on the other hand is slightly impeded. Furthermore, the investigation shows that the vapor diffusion through both brick and mortar is not influenced by the hydrophobization treatments. It is also observed that

the water repellent agents can penetrate deeply into the materials, successfully blocking capillary effects. Moreover, the water repellent agent appears to spread in the material for a long time after the hydrophobic treatment. It is moreover shown that the impacts of hydrophobization depend on the material pore sizes and the imposed agent amounts. There is a material-dependent critical concentration of the water repellent agent, beyond which the impact of hydrophobization becomes clear. When a material is treated above the critical agent concentration, its capillarity is significantly influenced, while its hygroscopicity is moderately reduced. Finally, in the framework of this study on hygric properties, multiple new measurement approaches have been developed. Specifically, the psychrometer method, semi-permeable membrane method (for storage), adsorption pressure plate method and hanging water column method are innovated for measuring moisture storage. The water head method, semi-permeable membrane method (for transport) and tension infiltrometer test are designed for moisture transport.

- In-situ studies on the influence of hydrophobization on the moisture behaviour of solid facades with(out) internal insulation, in actual dwellings and test buildings, wherein the hygrothermal behaviour of solid facades with and without hydrophobization is monitored. In all three cases, the findings are mixed, not yielding definite answers yet. This is in all cases attributable to the limited time interval since the start of the measurement campaign, which causes built-in moisture (from earlier wind-driven rain, from the fresh glue mortar, from the water repellent agents, …) to have a strong influence still on the observations. All studies hence indicate that future results will probably more revealing. The preliminary findings are hence mixed, and no solid conclusions are currently within reach. The case study in Heverlee (Belgium) is however most evolved, and allows some first outcomes to be defined. It is found that the moisture levels in the hydrophobized masonry wall internally insulated with a capillary-active calcium silicate are lower than measured in the walls with a vapor tight extruded polystyrene. The moisture levels in the non-hydrophobized wall with calcium silicate, however, is often found to be higher than measured in the hydrophobized wall insutaled with XPS. Finally, with respect to the moisture levels in the glue mortar between the masonry and the internal insulation, the largest drying rate is measured for the walls with calcium silicate insulation. In the second winter period, however, the relative humidity in the calcium silicate glue mortar is seen to increase and to become higher than measured in the glue mortar layer between the hydrophobized wall and the vapor tight XPS-system.

Additionaly, exploratory research on the impact of cracks on the moisture response of facades has been executed. This shows that the wind pressure is the only driving force for water penetration in cracks. The wind pressure, often limited to a few tens of Pascals, has to be larger than the breakthrough pressure of a crack for water penetration to occur. Cracks with a width smaller than 0.5 mm need an external pressure of at least 100 Pa to 150 Pa for water entry. The common wind pressures are hence insufficient to force water into cracks. When the crack width exceeds 0.5 mm, regular water penetration, driven by the wind pressure, is more likely, which confirms the maximum allowable crack width of 0.3 to 0.4 mm often put forward in literature.

This deliverable confirms that much new knowledge and insights in relation to water repellent agents and hydrophobization has been gained. It however also establishes that the results and outcomes show significant limitations and incongruences still, and that much more work thus is needed before hydrophobization can be reliably considered as part of the solution spectrum for the moisture damages possibly resulting from application of internal insulation. Therefore, the findings of Task 2.4 have not resulted in an adoption of hydrophobization in the simulation campaign for the webtool of RIBuild's WP6.

1 General introduction

(Hans Janssen, KUL)

RIBuild Deliverable D1.1 'Report on historical building types and combinations of structural solutions' confirmed that many of the structural damages experienced with respect to internal insulation are linked to moisture. Exemplary cases are frost spalling of the exterior brick, fungal decay of structural wooden elements, or mold growth at surfaces or interfaces. Moisture inside the internal insulation material may moreover reduce its thermal resistance, thus (partially) compromising the thermal retrofit that is intended. The harmful impacts of moisture on internally insulated walls are closely linked to the absorption of rainwater at the exterior surface. When changes of the exterior appearance of the building facades are considered undesirable, then only water repellent agents can be applied to limit this rainwater absorption. Hydrophobization should hence be regarded as a possible element in the spectrum of internal insulation solutions.

That insight triggered the midway introduction of Task 2.4 'Impact of water repellent agents on hygric material properties' in RIBuild, with KUL as leading partner and AAU and DTU as contributing partners. This deliverable D2.3 'Impact of water repellent agents on hygric properties of porous building materials' reports on the findings and outcomes of that task. In this research campaign, four elements have been central:

- A literature study collecting the current state-of-the-art with respect to water repellent agents and hydrophobization, firstly targeting the presently available knowledge and insights in relation to hydrophobization and secondly surveying the presently available water repellent agents on the market. The outcomes of this literature study are brought together in Section 2 and 3;
- A simulation study on the potential influence of water repellent agents on the moisture behaviour of massive facades with and without internal insulation, focusing primarily on the impacts of the hydrophobization strength, on the moisture contents and moisture damages. The findings of this simulation study are collected in Section 4;
- Laboratory analyses on the impact of water repellent agents on the hygric properties of porous building materials – ceramic brick and lime mortar –, with focus on the influence of the agents' formulation and concentration and on the effect of the agents' application and penetration. The results of these laboratory studies are gathered in Section 5 and 6;
- In-situ studies on the effect of hydrophobization on the moisture behaviour of solid facades with(out) internal insulation, in actual dwellings as well as test buildings, wherein the hygrothermal behaviour of facades with and without hydrophobization is monitored. The conclusions of the in-situ studies are compiled in Section 8, 9 and 10;

Additionaly, exploratory research on the impact of cracks on the moisture response of facades has been executed, the results of which can be found in Section 7.

This deliverable confirms that much new knowledge and insights in relation to water repellent agents and hydrophobization has been gained. It however also establishes that the results and outcomes show significant limitations and incongruences still, and that much more work thus is needed before hydrophobization can be reliably considered as part of the solution spectrum for the moisture damages possibly resulting from application of internal insulation. Therefore, the findings of Task 2.4 have not resulted in an adoption of hydrophobization in the simulation campaign for the webtool of RIBuild's WP6.

2 Overview of literature

(Hans Janssen, KUL)

2.1 Introduction

Moisture transfer in building materials plays a decisive role in the health and comfort of building occupants and in the durability and sustainability of built structures. Two exemplary illustrations are mold formation on interior finishes due to excessive interior humidity levels and concrete rebar corrosion owing to chloride ingress via the pore water. Moisture is an equally important factor in internal insulation solutions: potential moisture damages linked to internal insulation are frost spalling of the exterior brick, fungal decay of structural wooden beams, or mold growth at the interior wall surface or at the interface between insulation and wall (Vereecken et al., 2015; Finken et al., 2016; among others). Moisture inside the insulation material may moreover reduce its thermal resistance, thus partially compromising the thermal retrofit that is intended (Vereecken et al., 2015; Finken et al., 2016).

These adverse impacts of moisture on the hygrothermal performances of internally insulated walls are closely connected to the absorption of rainwater at the wall's exterior surface (Vereecken et al., 2015; Finken et al., 2016). Such rainwater absorption can be restricted via various means: a sufficient overhang, an exterior render, a paint finish. However, such measures typically change the exterior appearance of the building, which often is neither permitted, nor desired. In that case hydrophobization can be considered (Engel et al., 2014): impregnation of the wall's exterior surface with a water repellent agent results in a low-permeability layer, hindering the rainwater absorption. One should be aware though that hydrophobization also impedes the drying of the wall (Carmeliet et al., 2002; Hilbert et al., 2012), possibly enclosing rainwater penetrating through cracks or fissures in the wall.

Given the potential advantages and disadvantages of hydrophobization in relation to internal insulation, its application should be carefully considered. To support that, further research of the effect of water repellent agents on the hygrothermal behaviour of wall assemblies is needed. To initiate that, a brief literature review is undertaken to recap the current knowledge, for which some 45 papers on the topic were collected and analysed. Most of the articles and books stem from the field of conservation of cultural built heritage, a small share relates to the hygrothermal performance of building components. The findings are collected below in sections: 2.2 Physics and principles, 2.3 History and evolution, 2.4 Efficacy and durability, 2.5 Wetting and drying.

2.2 Physics and principles

Moisture protection treatments should be differentiated by whether they are totally impermeable to moisture or just impermeable to liquid water. The former is called waterproofing, the latter hydrophobization. Waterproofing typically creates a fully closed barrier film at the exterior surface, which impedes both liquid and vapor transport. In hydrophobization, the pores of the material are surface-coated with a water repellent agent, largely reducing liquid transport without overly decreasing vapor transport. As waterproofing totally obstructs all drying of the wall, hydrophobization is generally the preferred measure (Charola, 1995).

The polarity of both water and inorganic porous building materials explains the innate attraction between water and material, thus leading to the spontaneous adsorption and/or absorption of moisture in the pores of building materials. A water repellent counteracts that natural attraction by rendering the pore walls non-polar. Water repellents commonly are molecules with a polar head and a non-polar tail. The former attach to the pore walls, while the latter effectively render the pore walls non-polar, thus non-attractive to moisture. Because such pore wall coatings do not (completely) block the pore, the diffusion of water vapor remains possible, thus not fully barring drying of the material (Charola, 1995; Carmeliet et al., 2002).

The primary function of hydrophobization is hence to reduce the absorption of liquid water in porous building materials without strongly weakening the diffusion permeance of the porous building material. To achieve a long-term performance, the water repellent agent should penetrate beyond the surface layer, into the interior substrate of the porous material. Good resistance against weathering and UV-radiation are also crucial requirements.The optical appearance of the substrate, such as colour, gloss or hue, should furthermore not be modified (Roos et al., 2008).

2.3 History and evolution

Hydrophobization has a long history in the field of cultural heritage. The earliest accounts on moisture protection treatments stem from Greek and Roman antiquity, where oils and waxes were applied (Charola, 1995). These water repellent agents were also used in post-classical and modern times (Charola, 1995). Currently mostly silicon-based agents are popular for the hydrophobization of brick, stone and masonry (Roos et al., 2008; Syed and Donadio, 2013). Silicones consist of an inorganic silicon-oxygen backbone chain (⋯-Si-O-Si-O-Si-O-⋯) with organic side groups attached to the silicon atoms, and have been used in industrial and consumer applications since the 1950's (Roos et al., 2008). For hydrophobization applications, the silicon-based water repellent agents can be based on siliconates, silanes, siloxanes and silicone resins, the order of which represents their increasing complexity and molecular weight (Charola, 1995; BBRI, 2002; Roos et al., 2008; Syed and Donadio, 2013).

In recent decades, these silicone-based water repellent agents have gone through a continuous process of change, driven by legislative or commercial aspects (Roos et al., 2008). The first representatives appeared in the 1960's when high molecular weight silicone resins dissolved in organic solvents, mainly alcohols containing about 60 -70 % of active material, were developed for this application. As these had specific drawbacks, low-molecular-weight oligomeric siloxanes were developed in the 1970's. Later on, mixed products with both silanes and siloxanes were marketed as more widely applicable products. To get ready-to-use products, the agents had to be diluted with white spirits or alcohols. Depending on the agent and the substrate, the active matter of the products ranged from 5 to 100 %. For environmental reasons the market asked for "greener products", with a lower content of volatile organic compounds (VOC), ideally without any solvents. In response, water-based emulsion products were developed. In the early 2000's, paste-like hydrophobization products have been introduced, to facilitate the correct application. Finally, in recent years, researchers have been looking at the addition of nanoparticles, for improved effectiveness (Lubelli and van Hees, 2011; MacMullen et al., 2012): the outcomes are ambiguous though and they are not commercially available (yet).

2.4 Efficacy and durability

In spite of the progressive development of water repellent agents, unsuccessful hydrophobizations abound in examples (van Hees et al., 1996; Charola, 2001; Hilbert et al., 2012), hence bringing severe doubts to their efficacy and durability. However, most of the research on the subject (Charola, 1995; van Hees et al., 1996; De Witte et al., 1996; Bruchertseifer et al., 1997; van Hees, 1998; Charola, 2001; De Clercq and De Witte, 2001, 2002) confirms both the efficacy and the durability of hydrophobization, if the correct product is correctly applied. The following factors are pointed out to have an effect:

- polymer chain length with respect to the material's pore radii (Carmeliet et al., 2002): the polymer chain length governs which pores will be coated, blocked or neither, and that determines the efficacy of the water repellent agent;
- alkyl group in the silicon relative to alkalinity of the material (Charola, 1995, 2001): it has been repeatedly suggested that both increased length and branching of that alkyl group improves the alkali-resistance of the water repellent;
- condition of wall and presence of humidity and/or salts (Charola, 1995; De Clercq, 2006): cracks or fissures in the exterior surface appear detrimental for the hydrophobization, no consensus exists on their minimal aperture though. The presence of moisture or salts prior to the hydrophobation is similarly seen to have a negative impact.
- formulation and application of the agent (Charola, 2001; De Clercq and De Witte, 2001): the formulation (nature of solvent and agent concentration) and application (delivery as spray, paint, cream, … as well as temperature of substrate) of the water repellent agent determine its impregnation depth, which in turn governs its efficacy and durability.

Many authors hence stress the importance of choosing the correct water repellent agent and application procedure relative to the substrate (Charola, 1995; De Witte et al., 1996; van Hees, 1998; Charola, 2001; De Clercq and De Witte, 2001; De Clercq 2002). Van Hees (1998) explicitly states that the key "reason for an insufficient performance of treatments lies in most cases in the lack of preliminary investigations" "to furnish the basis for 1) deciding on the necessity of a treatment, 2) selecting the most suitable treatment product." If these conditions are met though, the literature indicates a good durability of hydrophobization, which may remain efficient to up to 30 years (van Hees, 1998). The average life span of hydrophobization is commonly estimated at some 10 years however (BBRI, 2002), based on a study of in situ applications. This durability is though, as is the efficacy, strongly dependent on the nature of the water repellent agent, the substrate to be treated, the application procedure, … Most authors moreover recommend regular maintenance to maintain the desired performance of the water repellent agent.

Because of the intricacy of an efficient and durable hydrophobization and because of the variety of commercially available water repellent agents, the Belgian Building Research Institute published a technical reference on these products (BBRI, 2002). That documents surveys the state-of-the-art in relation to water repellent agents and hydrophobization and concludes with a proposal for national and European standardization. This standardization targets synchronization of the measurement protocol for the evaluation of such efficacy and durability of hydrophobization treatments.

In short, it contains the following components:

- agent identification: determination of the nature and amount of the active component and the applied solvent in the water repellent agent, with X-ray fluorescence, Fourier transformation infrared, gas chromatography-mass spectrometry, and titration;
- efficacy and durability: determination of the water absorption, before treatment, after treatment and after artificial weathering, via Karsten tube and free water uptake test. The application of the water repellent agent is similarly tightly specified, and typically four different substrates are used in this evaluation;
- influences on diffusion and drying: the water vapor diffusion resistance of a brick is tested before and after treatment, and the drying speed of a calcium silicate stone is measured before and after treatment, with the common vapor cups and drying test.
- impact on optical properties: colour and gloss are tested, before and after treatment, with a pulsed xenon arc lamp and a gloss meter respectively;

While this methodology does not cover all aspects of water repellent agents and hydrophobization treatments – given that the diffusion and drying is only evaluated on one material –, the test protocol does give a crucial first indication of the performances of the product, and has also been adopted by the CSTB (France) and the Instituto Eduardo Torroja (Spain).

However, in light of that intricacy of efficient and durable hydrophobization, there are multiple circumstances wherein hydrophobization may not be appropriate. To provide guidance for that decision of suitability, the WTA – Wissenschaftlich-Technische Arbeitsgemeinschaft für Bauwerkserhaltung und Denkmalpflege, Germany – recently published the WTA Code of Practice: 'Hydrophobization of Mineral Building Materials' (Hilbert et al., 2012). The questions therein mainly focuses on the a priori evaluation of potential benefits and damages.

2.5 Wetting and drying

Typically the efficacy of a hydrophobization treatment is assessed with a capillary absorption measurement: in the lab usually free water uptake tests are performed, in situ a Karsten tube test is commonly executed (van Hees et al., 1996; Carmeliet et al., 2002). A drop of the capillary absorption coefficient with one or two orders of magnitude is often observed. Generally producers also are very open about the efficacy of their water repellent agent, given that that is of course their primary selling point.

The impacts on the vapor diffusion and drying speed are commonly measured with vapor cups and drying tests, exclusively in laboratory environments. The outcomes of these measurements are much more scarce though, and these have usually been obtained on a single substrate only. The results do besides vary highly: Charola (1995) and Engel et al. (2014) indicate a vapor permeability reduction of some 5 to 10%, Carmeliet et al. (2002) on the other hand observe reductions up to a factor 6. Similar differences are found for the drying speed, where the reductions are sometimes as low as a few tens of percent (BBRI, 2002), or as high as a factor 10 (Carmeliet et al., 2002). The drying speed of course highly depends on the impregnation depth, contrary to the absorption coefficient or vapor permeability. The water in the material must escape via vapor diffusion through the impregnated layer, the resistance of which is determined by both its permeability and its depth.

In general, the combined impacts of hydrophobization on the wetting and drying of (internally insulated) walls have not been thoroughly analysed yet, not for walls in perfect condition, neither for walls with cracks or fissures. The recent article of Finken et al. (2016) provides a first onset though. There is currently thus no full basis for assessing the influence of water repellent agents on the hygrothermal performance of (internally insulated) walls. Such analysis is required though, to evaluate the potentials of hydrophobization to avoid moisture damages in relation to internal insulation.

2.6 Conclusions

Hilbert et al. (2012) explicitly refers to the "very emotional discussions" on whether to apply a hydrophobization. This is a consequence of the many ill-considered applications of water repellent agents in the past. The literature review does however yield a different final perspective: hydrophobization can be a success, but only when the correct product is correctly used, and when proper maintenance is additionally applied (Charola, 1995). However, the impacts of hydrophobization on the hygric equilibrium of (internally insulated) wall assemblies has not been examined yet, not for walls in perfect condition, neither for walls with cracks or fissures. Such analysis is the key to appraising the applicability of water repellent agents in relation to the hygrothermal performance of internal insulation solutions. This requires the characterization of the impact of water repellent agents on the moisture properties of building materials and the assessment of the effect of hydrophobization on the hygrothermal performance of internal insulation solutions.

References

Remark: while only a limited number of papers have been referenced in the text above, many more have been read and digested in relation to this literature review.

BBRI, 2002. Technical reference 224: Water repellent surface treatments. Belgian Building Research Institute, Brussels (in Dutch).

Bruchertseifer C., Brüggerhoff S., Stoppek-Langner K., Grobe J., Jursch M., Götze H.J. 1997. Organosilicon compounds for stone impregnation: long-term effectivity and weathering stability. In Organisilicon Chemistry III, Wiley-VCH, Weinheim, Germany, 531-537.

Carmeliet J., Houvenaghel G., Van Schijndel J., Roels S., 2002. Moisture phenomena in hydrophobic porous building material, Part 1: Measurements and physical interpretations. Restoration of Buildings and Monuments 8:165-183.

Charola A.E. 1995. Water-repellent treatments for building stones: A practical overview. APT Bulletin 26:10-17.

Charola A.E. 2001. Water repellents and other "protective" treatments: A critical review. In proceedings of 3rd International Conference on Surface Technology with Water Repellent Agents, 3-20.

De Clercq H., De Witte E. 2001.Effectiveness of silicon-based water repellent agents at different application conditions - Part II: commercial water repellents. Restoration of Buildings and Monuments 7:641-654.

De Clercq H., De Witte E. 2002. Effectiveness of commercial silicon-based water repellents applied under different conditions. Restoration of Buildings and Monuments 8:149-164.

De Clercq H. 2006, Performance of selected materials containing different mixtures of salts after water repellent treatment. Restoration of Buildings and Monuments 12:25-34.

De Witte E., De Clercq H., De Bruyn R., Pien A. 1996. Systematic testing of water repellent agents. Restoration of Buildings and Monuments 2:133-144.

Engel J., Heinze P., Plagge R. 2014. Adapting hydrophobizing impregnation agents to the object. Restoration of Buildings and Monuments 20:1-8.

Finken G.R., Bjarløv S.P., Peuhkuri R.H. 2016. Effect of façade impregnation on feasibility of capillary active thermal internal insulation for a historic dormitory – A hygrothermal simulation study. Construction and Building Materials 113:202-214.

Hilbert G., Neumann H.-H., Wendler E. 2012. Hydrophobization – One target, several possibilities. Restoration of Buildings and Monuments 18:3-12.

Lubelli B., van Hees R.P.J. 2011. Evaluation of the effect of nano-coatings with water repellent properties on the absorption and drying behaviour of brick. In proceedings of 6th International Conference on Surface Technology with Water Repellent Agents, 125-136.

MacMullen J., Zhang Z., Rirsch E., Dhakal H.N., Bennett N. 2011. Brick and mortar treatment by cream emulsion for an improved water repellence and thermal insulation. Energy and Buildings 43: 1560-1565.

Roos M., König F., Stadtmüller S., Weyershausen B. 2008. Evolution of silicone-based water repellents for modern building protection. In proceedings of 5th International Conference on Surface Technology with Water Repellent Agents, 3-16.

Syed A., Donadio M. 2013. Silane sealers/hydrophobic impregnation – The European perspective. Concrete Repair Bulletin, September/October 2013, 12-17.

van Hees R.P.J., van der Klugt L.J.A.R., De Witte E., De Clerq H., Binda L., Baronio G. 1996. Test methods for the evaluation of the in situ performance of water-repellent treatments. Restoration of Buildings and Monuments 2:117-132.

van Hees R.P.J. 1998. The performance of surface treatments for the conservation of historic brick masonry. In proceedings of the CIB World Building Congress 1998.

Vereecken E., Van Gelder L., Janssen H., Roels S. 2015. Internal insulation for wall retrofitting – A probabilistic analysis of energy savings and hygrothermal risks. Energy and Buildings 89:231-244.

3 Water repellent agents

(Vasilis Soulios, KUL[1])

3.1 Introduction

In this section, literature study including the nature of the water repellency, types of water repellent agents and identification of the products is provided. The section concludes with an overview of comercially available water repellent agents. The results are an extensive section of a part of a scientific paper (Soulios et al., 2020).

Hydrophobization is an old method for the protection of buildings from wind-driven rain induced moisture (Møller 2003). However, it remains an ambiguous practice. To understand the nature of water repellency it is important to examine how hydrophobization works, what the differences are between the existing products and how the properties of the substrate change after the treatment. Nowadays, different water repellent agents exist on the market. These water repellent agents can be categorized based on the type of substrate, their formulation, the concentration and the chemical composition of the active ingredient.

3.2 The nature of water repellency

The main function of water repellent agents is to prevent liquid water from entering the treated surface (Roos et al., 2008; Carmeliet et al., 2002; Møller, 2003). In contrast to waterproofing treatment, which renders the treated material completely impermeable to water, water repellency treatment does not prevent the treated building material from being permeable to water vapor (Charola, 1995). Since moisture that penetrates into porous building materials is a major reason for their deterioration and consequently the deterioration of the whole structure, water repellency treatment can prevent serious damages from occurring both at the material and the component level (Roos et al., 2008).

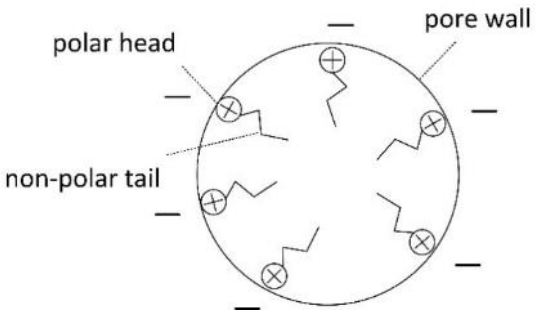

Figure 3-1. Water repellent molecules have a polar head and a non-polar tail. The polar end attaches itself to the polar pore wall of the substrate, effectively creating a non-polar film, which repels liquid water and allows water vapor diffusion, thus not fully impeding the drying of the material.

[1] Activities performed while at KUL, currently at AAU

Water is a polar material since it has positive charge at the hydrogen ends and negative charge at the oxygen end. Inorganic building materials, such as brick and stone, usually have negative surface charges and therefore attract the positive end of the water molecules (i.e. they are hydrophilic). A water-repellent molecule has a polar “head” and a non-polar “tail”. The polar “heads” are attracted by the polar material and the non-polar “tails” cover the surface. In that way, the surface becomes non-polar and as a result, no longer attracts water molecules (i.e. surface becomes hydrophobic) (see Figure 3-1) (Charola, 1995).

The intermolecular electrical forces between the negatively charged pore walls of the material with the positively charged end of water molecules induce a surface tension that creates a meniscus and a contact angle $\theta<90°$ which causes capillary rise (Figure 3-2a). When the water repellent molecules are attached to the pore wall, their non-polar tails render the surface of the material hydrophobic, an opposite meniscus is created and the contact angle becomes larger than 90° (Figure 3-2b). This means that instead of capillary suction, there is capillary depression and water is repelled (Møller 2003).

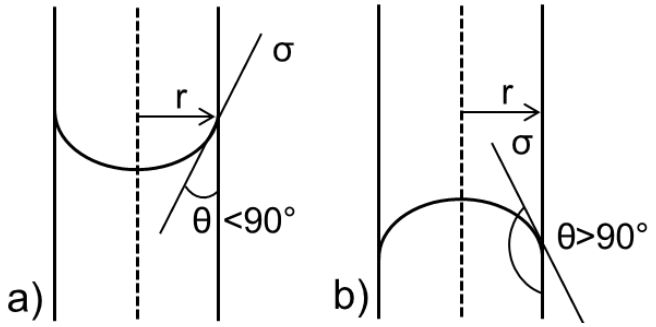

Figure 3-2: Simplified system with cylindrical pore a) Untreated pore - capillary rise with θ<90°. b) Impregnated pore - capillary depression with θ>90°. σ: surface tension, θ: contact angle, r: pore radius

3.3 Types of water repellent agents

Water repellent agents that are available on the market, are mainly based on the following types of materials: i) silicon-bearing compounds, ii) metal-bearing compounds and iii) organic materials (Charola, 1995). Although not widely available yet, water repellent products based on nano-technology claim to produce improved results compared to the more traditional products (Lubelli and van Hees, 2011; MacMullen et al., 2011). However, further studies are needed to conclude on the effectiveness and efficiency of these nano-technology based products.

3.3.1 Silicon-bearing compounds

Silicon-based systems are the most popular water repellents in use. Generally, all products that contain a Silicon-Oxygen backbone can be referred to as silicones, but their properties can vary significantly (Charola, 1995). The backbones can be modified by incorporating carbon-based side-groups, such as methyl (Mayer, 1998). When applied, the silicon-based systems form irreversible bonds with the mineral substrate and render the building material hydrophobized (Roos et al., 2008). A simple classification of silicon-based water repellent agents would include silanes, siloxanes and silicon resins.

3.3.2 Silanes

Silanes are monomeric low-weight molecules that contain one silicon atom which is connected to alkyl (-R) and alkoxy (-OR) groups (see Figure 3-3a). The alkoxy groups (-OR) permit the compound to polymerize and to link chemically to the hydroxylated surfaces of siliceous building materials (e.g. brick, concrete, granite, sandstone), providing an anchorage system between the hydrophobic film and the building substrate (Charola, 1995; Roos et al., 2008). The alkyl groups (-R) take no part in the polymerization but they provide the hydrophobic properties to the compound. The compound is polymerized through a two-step process that includes hydrolysis and condensation reaction. Hydrolysis requires water as a reactant and therefore moisture content in the material can play a significant role. Continuous polymerization leads to the production of longer chains or networks and increases the viscosity of the product. Simple silanes polymerize to siloxanes (between 1 and 5 repeating units) or oligomeric siloxanes (over 6 repeating units) and can be cross-linked to polymeric siloxanes (over 20 repeating units) or silicon resins (over 30 repeating units), as shown in Figure 3-3b (Charola, 1995; Selander, 2010).

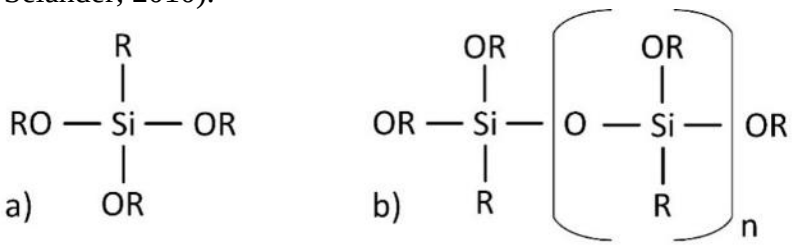

Figure 3-3. Alkyl trialkoxy silane (a) and siloxane (b). Si: Silicon, R: alcyl group (e.g. methyl), OR: reactive alkoxy group (e.g. methoxy). n=0: silane, 1≤n≤5: siloxane, n≥6: oligomeric siloxane, n≥20: polymeric siloxane, n≥30: silicone resin.

The low reactivity of silanes leads to high impregnation depths, even in alkaline substrates such as concrete. When the treated surfaces are neutral, the reaction may need the presence of a catalyst (Roos et al., 2008). Reactivity of silanes depends on alkoxy group (methoxy, ethoxy) and functionality (difunctional or trifunctional units). Ethoxy is longer and larger alkoxy group than methoxy and is easier to be linked chemically with the substrate. Difunctional units form the basis of higher-molecular chains and cyclic compounds, having two silicon-oxygen backbones, while trifunctional units cause the molecules to crosslink in three dimensions, having three silicon-oxygen backbones (Mayer, 1998). Therefore, reactivity of silanes can be increased with longer alkoxy groups and trifunctional functionality.

Silanes are highly volatile and therefore high concentrations of active content are required, according to the preferred use and performance (Syed & Donadio, 2013). Volatility of silanes depends on the molecular weight. Silanes with shorter alkyl groups like methyl (CH_3) have lower molecular weight than silanes with larger alkyl groups like iso-octyl (C_8H_{17}). Siloxanes are "pre-cured" silane material and therefore larger, which leads to a faster effect.

3.3.3 Siloxanes

Siloxanes are similar in nature to silanes, but their molecular structure is more complex, since they are oligomeric or polymeric molecules based on Si-O-Si chains. Due to this complexity, it is more difficult for siloxanes to migrate into the substrate, although their dimensions are

comparable to those of silanes (Syed & Donadio, 2013; Roos et al., 2008). The size of silanes is 0.4 to 1.5 nm and of siloxanes 3 to 30 nm (Sika AG, 2017). Siloxanes are more reactive compared to silanes and therefore there is no need for a catalyst. In fact, the fast curing process on highly alkaline substrates (e.g. concrete) does not permit the siloxane molecules to penetrate deep into the substrate. For that reason, they are mostly used in more porous and more neutral mineral substrates (e.g. brick, stones, and aged concrete) for façade treatment and protection against rising damp (Roos et al., 2008). However, due to their higher molecular weight, siloxanes are less volatile compared to silanes, and consequently the active content is usually no more than 10 to 15%. In addition, higher concentrations encompass the risk of darkening the surface (Syed & Donadio, 2013).

3.3.4 Silicone resins

Silicone resins are highly branched polysiloxanes with high molecular weight, whose backbone consists of silicon and oxygen atoms (Roos et al., 2008; Mayer, 1998). A silicone resin treatment is generally more stable than a silane treatment and presents less problems in practice, since the silicone resins are already polymerized and the evaporation of the solvent is the only process that takes place after application (Charola, 1995). However, silicone resins have poor solubility properties, can darken the surface and provide a beading effect, which is not always desirable (Roos et al., 2008; Charola, 1995). Silicon resins products should be diluted to 5-10% solids in solvents to achieve a better impregnation depth. Emulsified products are more difficult to penetrate to the substrate (Roos et al.,2008).

3.3.5 Metal-bearing compounds

Metal-bearing compounds are based on aluminum stearate, which is the most popular hydrophobization agent of this kind (although not effective for brick treatment), titanium stearate and butyl-ortho-titanate. All these metal-organic compounds are also used in mixtures with oligomeric siloxanes (Charola, 1995).

3.3.6 Organic materials

Hydrophobization agents that are based on organic materials include acrylics, polyurethanes and perfluoro-polyethers. Acrylic resins are mainly consolidants, but can provide some level of hydrophobicity to the treated material. Polyurethanes are polymers with usually long molecular chains that produce films through polymerization. They are also consolidants that have some hydrophobization properties (Charola, 1995). Perfluoro-polyethers are extremely stable to light, heat and chemicals, and also permeable to gases, transparent and colorless (Frediani et al., 1982). Waxes are also organic substances of either natural or synthetic origin and they are generally used for the conservation of materials such as marble and stone. Although waxes have good hydrophobic properties, they can easily suffer from mechanical damage and color variations (Charola, 1995; Szymura & Barnat-Hunek, 2013). Some organic materials are also used in combination with silicon bearing materials.

3.4 Product Identification

Silicon-based water repellent agents, which are the most popular in practice, can be identified through their active ingredient, the form, the type of diluent, the concentration of the active

ingredient, the alkyl group and the type of substrate that is recommended for application (see Table 3-1) (De Witte et al., 1996).

Table 3-1: Product identification.

Product characteristic	Description
Active ingredient	Silane - Siloxane - Silicone resins
Product form	Liquid or Cream
Used diluent	Organic solvent - Water emulsion - Water microemulsion
Agent concentration	1-100%, Undiluted* or Ready to use
Alkyl group	Octyl or iso-Octyl in commercial products
Intended substrate	Mineral substrate** - Masonry*** - Concrete

** Undiluted: contain no diluent and must not be diluted before application*
*** Mineral substrates: concrete, brick, natural stone, mortar, concrete blocks.*
**** Masonry: brick, mortar and natural stone, but not for concrete (or concrete blocks)*

3.4.1 Influence of the formulation and diluent

During the last decades, combination products of both silanes and siloxanes have been marketed as more broadly applicable water repellent agents. In order to be prepared as ready-to-use, these products have to be diluted with white spirits or alcohols, in various concentrations according to the product and the substrate type (Roos et al., 2008). However, volatile organic compounds (VOC) are released to the atmosphere when silanes, siloxanes and silicone resins are dissolved in organic solvent. For that reason, more environmentally friendly products based on water as diluent were developed (De Witte, 1996). Paste-like or cream products, developed since early 2000, provide alternative treatment methods, are easy to apply and show good water repellence characteristics (Roos et al., 2008; Charola, 2001; MacMullen et al., 2011).

Water based emulsions and creams contain emulsifiers to keep the reactive material stable in a water environment. These products perform better after rain exposure and solar radiation. Solar radiation increases the temperature and consequently the reactivity, while rain exposure “washes off” the emulsifiers that impede reactions with water. Micro-emulsions do not contain classical emulsifiers and can immediately demonstrate their performance. However, micro-emulsion products should be applied within 24 hours after dilution, so there would be no reactions between active ingredients and water (Hamont, 2017, personal comunication).

3.4.2 Influence of the concentration of the active ingredient

Concentration of the active ingredient is among the factors that are critical regarding the performance of the product. Lower concentrations generally decrease the effectiveness of the treatment but may result in faster drying (Charola, 2001; Engel et al., 2014). De Clercq & De Witte (2002) show that the influence of concentration on the effectiveness of the treatment becomes more important after ageing. Also, higher concentrations of active ingredient lead to larger impregnation depth (Ackermann, 2017, personal communication)

3.4.3 Influence of the composition of the active ingredient

As mentioned in section 3.3.2, the alkyl groups (-R) attached to silane, siloxane and silicone resin, take no part in the polymerization but provide the hydrophobic properties to the compound. The most popular alkyl groups found in commercial water repellent agents are shown in Figure 3-4. Some studies have shown that long alkyl groups are not more effective than methyl groups and that the nature of the substrate played a more significant role in the performance of the treatment (Charola, 1995). Field tests in stones with methyl silicones and methyl-octyl silicones confirm this proposition. DRIFT (Diffuse Reflectance Infra-red Fourier Transform Spectroscopy) has shown that hydrophobicity could be attributed only to the methyl group which is common to all alkyl groups.

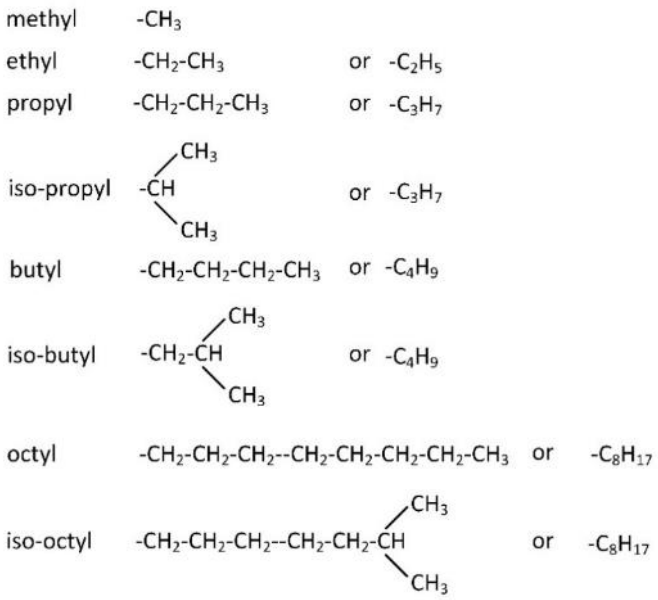

Figure 3-4. Common alkyl groups in commercial water repellent agents.

However, longer alkyl chains provide good resistance against alkalinity as they create a steric shield for the Si-O-Si bonds which are prone to hydrolysis (Roos et al., 2008). The chemical bond between the silane and the substrate is not completely stable in an alkaline environment like concrete. Alkyl groups which are responsible for the hydrophobic nature of the agent, keep water molecules away from the reactive OH-groups which are bonded to the pore wall of the material and thus, the chemical bond remains dry and stable. Longer and larger alkyl groups like octyl or iso-octyl (see figure 3-4) ensure that process and provide longer lifetime to the treatment, avoiding hydrolysis and deformation of the hydrophobic layer. If the hydrophobic compound is composed only of methyl groups, the alkaline stability may not be very strong. The influence of the alkyl group, in terms of alkali resistance, is more noticeable in cementitious substrates. For brick this influence may not be that important, because brick is a more neutral material than concrete. In masonry walls the length of the alkyl group may influence the treatment, since mortar is an alkaline material. However, most formulations nowadays contain longer alkyl groups so that the alkalinity of mortar cannot cause stability problems (Charola, 1995; Rewah ARTISIL B10, 2016; Dow Z-6689, 2017; Hamont, 2017).

3.4.4 Influence of the type of substrate

Compatibility between pore structure and polymer chain length can play an important role in the effectiveness of the hydrophobic treatment and the hygric behavior of the treated substrate. De Clercq & De Witte (2001) indicate that the polycondensation is governed primarily by the pore structure of the substrate. A polymer network is formed in the large and midsize pores, leaving the fine pores untreated. For that reason, the water repellent agents should be classified according to their polymer chain length in relation to the pore size of the substrate that will be treated (Carmeliet et al., 2002). Thus, different water repellent agents are suitable for different types of substrates.

3.5 Classification of commercial water repellent agents

There are several distributors of water repellent agents, and they all provide a spectrum of products that can be categorized according to several characteristics: type of active ingredient, formulation, concentration and type of substrate, explained in Section 3.1.3.3

Water repellent agents from thirteen distributing companies were classified, including five big silicon-producing companies: Wacker, Dow, BlueStar, Sika, and Momentive. The rest of the water repellent agents are selected from non-silicon-producing companies. These companies developed their own formulations using silicones from the above-mentioned silicon producing companies. In total 93 products suitable for mineral substrates were selected. However, only 77 products have sufficient information to be identified.

This study focuses on water repellent agents that are used as brick masonry impregnation against wind-driven rain. This means that products against rising damp, in-plant impregnations for cement, products used for wood and products that are used as admixtures in paints or coatings, are not included.

3.5.1 Silanes

Pure silane products, having small molecular size, aim to penetrate in the fine pores of the building materials and also to cover the larger pores by polymerizing into longer chains and networks. They have high alkali resistance and they recommended for both cementitious and mineral substrates.

Table 3-2 illustrates the pure-silane water repellent agents derived from different companies. Silane-based water repellent agents are mainly used in liquid form (Figure 3-5 (left)). Also, products with high concentrations of silanes are used for concrete applications, since silanes have lower molecular weight that results in higher volatility and therefore higher concentrations are needed.

Figure 3-5 (right) shows that pure silanes are used mainly for concrete (69% of the silane products) due to the compatibility of the small pores of cementitious materials with the small silane molecules and the high alkali resistance of silanes, which makes them more suitable for highly alkaline substrates, like concrete. Silane products that are also recommended for more neutral mineral substrates (like brick), may include a catalyst for faster reactions with the substrate and the creation of larger polymers.

Table 3-2 Silane water repellent agents.

No	Company	Product	Form	Diluent	Conc.	Substrate
1	WACKER	CREME C	cream	water	80%	concrete
2	WACKER	1701	liquid	undiluted	99%	concrete
3	WACKER	17040	liquid	water	40%	concrete
4	WACKER	16040	liquid	water	40%	concrete
5	SIKA	706 Thixo	cream	water	80%	concrete
6	SIKA	705 L	liquid	undiluted	99%	concrete
7	SIKA	740 W	liquid	water	40%	concrete
8	REMMERS	Funcosil IC	cream	water	80%	concrete
9	REYNCHEE	RC SILAN	liquid	solvent	98%	concrete
10	PEC	ENVIROSEAL 20	liquid	water	20%	concrete
11	REWAH	ARTISIL B10	liquid	solvent	10%	concrete
12	DOW	OFS-2306	liquid	solvent	96%	mineral substrates
13	DOW	IE 6682	liquid	water	52.5%	mineral substrates
14	REYNCHEE	RC 900	liquid	solvent	10%	mineral substrates
15	MOMENTIE	Silblock wms	liquid	water	40%	mineral substrates
16	REMMERS	Funcosil FC	cream	water	40%	masonry

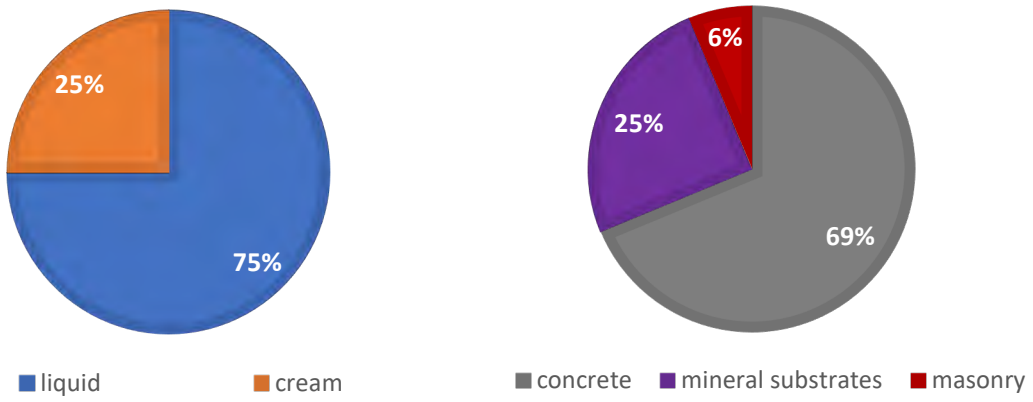

Figure 3-5. Form of silane products (left): cream (orange), liquid (blue). Type of substrate for silane products (right): concrete (grey), mineral substrates (purple), masonry (red).

All silane products from Wacker are a mixture of octyltriethoxysilanes isomers, with iso-octyltriethoxysilane as the main component (SILRES BS 1701, Wacker, 2017). DOW products and Artisil from REWAH, also contain octyltriethoxysilanes as an active ingredient (Dow Z-6689, 2017; Rewah ARTISIL B10, 2016). The other companies do not mention the chemical composition of the active ingredient. All agents suitable for concrete mention high alkali resistance which means that probably long alkyl groups are contained, to provide stability against the high alkalinity of cementitious substrates.

Funcosil FC, an emulsion silane cream contrary to conventional liquids products, can be applied in just one working operation. The active ingredient penetrates as deeply as possible and depending on the porosity of the substrate reacts and becomes polysiloxane. This is the main reason why it can efficiently treat the larger pores of brick materials although a silane.

However in order to illustrate the real performance it needs to be exposed for a long period in rain because it is a water emulsion product and the emulsifiers have to be washed off for the complete polymerization of the agent (Funcosil FC, Remmers, 2016). Wacker creme C may be used on any alkaline substrate that has been treated previously (SILRES BS Creme C, 2017).

Although RC 900 is recommended in general for mineral substrates, it is mentioned that it offers very good performance on substrates with small pores (like concrete) (RC 900, Reynchemie, 2017). Silblock wms from Momentive and SILRES® BS 17040 can be used both as an admixture of concrete and as a penetrating sealer. Moreover, Silblock wms showed excellent paintability on concrete (Silblock wms, Momentive, 2011; SILRES BS 17040, Wacker, 2014).

3.5.2 Mixture of silanes/siloxanes

Most of the products in the market consists of a mixture of silanes and siloxanes. This is to take advantage of the smaller size of silanes that can effectively penetrate in fine pores and to reach a sufficient impregnation depth, and the larger size of siloxanes that can effectively cover the larger pores and illustrate the desirable beading effect for the treatment to look effective.

There are many silane/siloxane products available in the market. Silane/siloxane products are predominantly available in liquid form and mainly for mineral substrates. Most of these products use water as diluent. Percentages of silane and siloxane in the mixture vary, as does the percentage of active ingredient.

SILRES® BS 39 is used for both water and oil repellency to inorganic substrates and it is mostly recommended for treatment in natural or synthetic stone, although there is a risk of discoloration. It is recommended to dilute the product in ratios of 1:3 to 1:6 (2.5% to 7% of active ingredient). The effect of the treatment starts to develop within the first day and is completed in one week (SILRES BS 39, Wacker, 2015). SILRES® BS 4004 has an excellent beading effect, it can be also used as an admixture. Along with SILRES® BS 1001, SILRES® BS 4004 is recommended to be diluted in the ratio 1:4 to 1:9 (12,5% to 5.6% active ingredient) (SILRES BS 4004, Wacker, 2016; SILRES BS 1001, Wacker, 2014). SILRES® BS 280 is particularly recommended for the conservation of monuments and the restoration of natural stone. It can be used on mineral substrates but it is specialized in limestone and gypsum. It should be diluted in a ratio of 1:11 (8.3% active ingredient) (SILRES BS 280, Wacker, 2014).

For BS 3003 and BS SMK 1311, dilutions of 1:5 to 1:11 (10% to 5% active ingredient) and 1:9 to 1:14 (10% to 6.7% active ingredient) are recommended respectively (SILRES BS 3003, Wacker, 2014; SILRES BS SMK 1311, Wacker, 2014). For application in concrete, SILRES® BS SMK 2101 is recommended to be diluted at ratios of 1:3 to 1:14 (25% to 6.7% active ingredient) (SILRES BS SMK 2101, Wacker, 2014). For BS SMK 2100 dilution of 1:9 (10% active ingredient) is recommended for water repellency and consolidating properties and a dilution of 1:14 (6.7% active ingredient) for water repellency and minimal consolidation (SILRES BS SMK 2100, Wacker, 2014).

Generally, the lowest concentrations of active ingredient are recommended for natural stone substrates due to the large pores and the risk of discoloration. For concrete, where the pores are much smaller, higher concentrations of the active ingredient are recommended to ensure that all pores of the substrate will be treated (Hamont, 2017).

Table 3-3 Silane/siloxane water repellent agents

No	Company	Product	form	diluent	concentration	Substrate
17	WACKER	SILRES®BS CREME N	cream	solvent	25%	mineral substrates
18	WACKER	SILRES® BS 280	liquid	solvent	100%	mineral substrates
19	WACKER	SILRES® BS 290	liquid	solvent	100%	mineral substrates
20	WACKER	SILRES® BS 39	liquid	water	25%	mineral substrates
21	WACKER	SILRES® BS 1001	liquid	water	50%	mineral substrates
22	WACKER	SILRES® BS 3003	liquid	water	60%	mineral substrates
23	WACKER	SILRES® BS 4004	liquid	water	50%	mineral substrates
24	WACKER	SILRES®BS SMK 1311	liquid	water	100%	mineral substrates
25	WACKER	SILRES®BS SMK 2100	liquid	water	100%	mineral substrates
26	WACKER	SILRES®BS SMK 2101	liquid	water	100%	concrete
27	DOW	Z-6689	liquid	solvent	98%	mineral substrates
28	DOW	IE 6683	liquid	water	40%	mineral substrates
29	DOW	520	liquid	water	40%	mineral substrates
30	DOW	IE 6694	liquid	water	60%	mineral substrates
31	Facabelle	Fassapearl-S	liquid	solvent	10%	mineral substrates
32	Facabelle	A104 TECHNIFUGE	liquid	solvent	10%	mineral substrates
33	Facabelle	Fassapearl-H	liquid	water	10%	mineral substrates
34	REYNCHEMIE	RC HYDROCRÈME III	cream	water	40%	mineral substrates
35	REYNCHEMIE	RC HYDROCRÈME IV	cream	water	40%	mineral substrates
36	REYNCHEMIE	RC 805 ECO	liquid	water	7.5%	mineral substrates
37	SIKA	Sikagard®-700 S	liquid	solvent	-	mineral substrates
38	SIKA	Sikagard® -704 S	liquid	solvent	-	concrete
39	SIKA	Sikagard®-703 W	liquid	water	-	mineral substrates
40	REMMERS	Funcosil C40	cream	water	40%	concrete
41	REMMERS	Funcosil WS	liquid	water	10%	mineral substrates
42	REWAH	GELIFUGE NEW	gel	solvent	25%	masonry
43	REWAH	STONEGEL	gel	water	25%	mineral substrates
44	Soudal	SOUDACLEAR FAÇADE S	liquid	solvent	8%	mineral substrates
45	Soudal	SOUDACLEAR FAÇADE	liquid	water	6.5%	mineral substrates
46	PEC	THORO® B	liquid	water	7%	masonry
47	SCALP	SCALPFUGE 35	liquid	water	-	masonry

Sikagard®-700 is used mainly for concrete but also for mineral substrates. However, in some stones a slight darkening of the surfaces may be observed (Sikagard 700, 2016). The same problem exists for STONEGEL, which, if applied to natural stone, it may cause the surface to become darker or discolored in places. Therefore, it is not recommended for natural stone. It can be applied onto a slightly moist substrate. Under the influence of the substrate moistness or the air humidity, STONEGEL polymerizes into a non-adhering polysiloxane. The full moisture-proof properties are obtained within a period up to four months after treatment (Stonegel, Rewah, 2016). GELIFUGE NEW is not recommended for natural stone. In brick walls, it can be applied in a single coat and becomes fully water repellent within four months of treatment. If efflorescent salts are present, treatment is not recommended (Gelifuge new, Rewah, 2016).

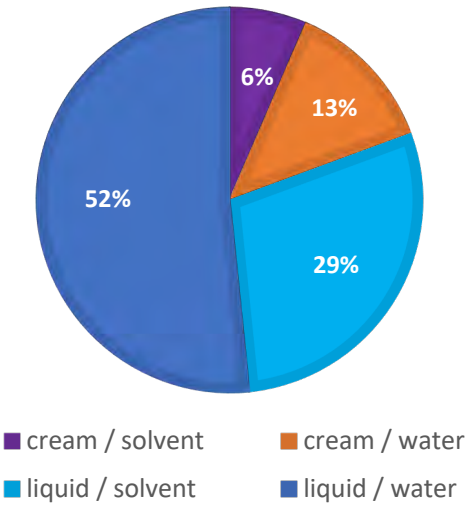

Figure 3-6. Form and dilution of silane/siloxane products: cream/solvent (purple), cream/water (orange), liquid/water (blue), liquid/solvent (light blue).

Dow Corning® Z-6689 can be used on both neutral and alkaline substrates, due to the presence of a catalyst (Dow Corning Z-6689, 2011).

3.5.3 Siloxanes, silicone resins

Siloxanes have larger size than silanes and aim to effectively cover the larger pores of building materials. Silicone resins are even larger networks. Siloxanes are responsible for the beading effect as they end to remain for longer on the surface of the substrate.

Table 3-4 Siloxane and silicone resins water repellent agents.

No	Company	Product	Type	Form	Diluent	Concentration	Substrate
48	Facabelle	Fassapearl-Gel	siloxane	cream	water	25%	mineral substrates
49	REMMERS	Funcosil SNL	siloxane	liquid	solvent	7%	mineral substrates
50	REYNCHEMIE	RC IP500	siloxane	liquid	solvent	10%	mineral substrates
51	DOW	1 _ 6184	siloxane	liquid	water	98%	masonry
52	REMMERS	Funcosil SL	siloxane	liquid	solvent	7%	masonry
53	BLUESTAR	WR 224	siloxane (oligomeric)	liquid	solvent	69%	mineral substrates
54	BLUESTAR	BP-9400	siloxane (oligomeric)	liquid	solvent	100%	mineral substrates
55	Facabelle	TECHNISIL	siloxane (oligomeric)	liquid	water	10%	mineral substrates
56	REYNCHEMIE	RC SILOX	siloxane (oligomeric)	liquid	solvent	100%	mineral substrates
57	REYNCHEMIE	RC 224	siloxane (oligomeric)	liquid	solvent	10%	mineral substrates
58	WACKER	SILRES®BS 66	siloxane (oligomeric)	liquid	solvent	100%	mineral substrates
59	REWAH	REDISIL S	siloxane (oligomeric)	liquid	solvent	10%	masonry
60	REWAH	AQUASIL RS 8	siloxane (oligomeric)	liquid	water	8%	masonry
61	BLUESTAR	BP 9710	siloxane (polymeric)	liquid	water	44%	mineral substrates
62	BLUESTAR	RES 4581	silicone resins	liquid	solvent	70%	mineral substrates
63	DOW	MR 2404	silicone resins	liquid	solvent	88%	mineral substrates
64	SCALP	AQUAFUGE18	silicone resins	liquid	water	-	mineral substrates

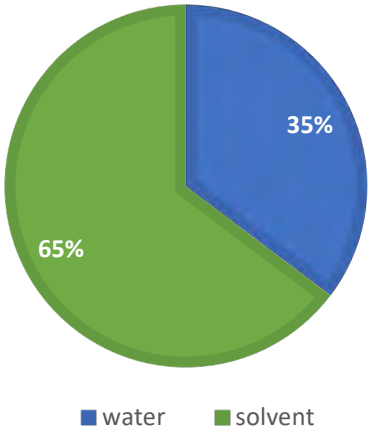

Figure 3-7. Diluent of siloxane and silicone resins products: solvent (green), water (blue).

Siloxane and silicone resin products are also predominantly available in liquid form. However, most products of this kind are diluted with solvents.

Remmers Funcosil SL was especially developed as a water repelling treatment for natural stone and limestone in particular (e.g. shell lime-stone). RC IP500 gives an excellent hydrophobic effect, especially for materials with large pores (RC IP500, Reynchemie, 2015). The recommended concentration of active ingredient for BLUESIL BP 9710 is between 4 and 8 % (Bluesil BP 9710, Bluestar, 2011). Aquafuge 18 is considered ideal for application in blue stone (Aquafuge 18, Scalp , 2017). Dow Corning® 1-6184 is specifically suitable for aged masonry (Dow Corning 1-6184, 2007).

3.5.4 *Miscellaneous water repellent agetns*

Some products contain organic materials in combination with silicon-based compounds, while other products contain only organic materials. The same pattern applies to metal bearing compounds, which are used either independently or in combination with silicon-based compounds. The products that contain organic or metal-bearing compounds are in liquid form. Products that contain organic compounds generally use water as diluent, whereas products with metal-bearing compounds use solvent as diluent. A specific product contains siliconates as the active ingredient, but it is recommended mainly for limestone substrates.

Table 3-5 Miscellaneous water repellent agents (organic, metal-bearing, siliconates)

No	Company	Product	Type	Form	Diluent	Concentration	Substrate
			Organic				
65	REMMERS	Funcosil OFS	Fluorinated acryl co-polymers	liquid	Water	-	mineral substrates
66	APP	ThefAPP	Fluorinated acryl co-polymers	liquid	Water	3.1%	mineral substrates
67	APP	APPHD	Fluorinated acryl co-polymers	liquid	Water	1.9%	concrete
68	REYNCHEMIE	RC 808	Fluorinated resins	liquid	Water	10%	mineral substrates
			Organic & Silicons				
69	Facabelle	TECHNISIL HYDRO PLUS	Silanes, oligomeric siloxanes, fluorinated and polyolefin resins	liquid	Water	10%	mineral substrates
70	REWAH	OLEOFUGE F	Silanes, siloxanes and fluorinated carbon bonds	liquid	Water	10%	mineral substrates
71	WACKER	SILRES® BS 38	Silane/siloxane and fluoropolymer	liquid	Solvent	46%	mineral substrates
72	REYNCHEMIE	RC 806 ECO	Silane/siloxane and acryl-fluorinated copolymers	liquid	Water	10%	mineral substrates
			Metal Bearing				
73	SCALP	SCALPFUGE OM 70	Metal bearing	liquid	Solvent	-	mineral substrates
			Silicons & Metal Bearing				
74	REWAH	ECONOSIL	Metal bearing, siloxanes	liquid	Solvent	10%	masonry
75	Facabelle	A101 TECHNISIL	Metal bearing compounds, silane/siloxane	liquid	Solvent	10%	mineral substrates
76	REWAH	REWASIL AVT	Organic metals, siloxane (oligomeric)	liquid	Solvent	8%	masonry
			Siliconates				
77	PEC	THORO®CLEAR SPECIAL	Siliconates	liquid	Water	5.5%	limestone

3.6 Conclusions

Table 3-6 compares the companies by presenting the characteristics of their available products according to the type of the active ingredient, the form of the agent and the type of substrate for which the products are recommended for application. All companies, excluding APP, use silicon bearing materials, while some of them also provide agents based on organic, or metal-bearing materials. All companies have products in liquid form, while most companies also provide products in cream form, mainly with water as diluent.

Table 3-6 Comparison of companies according to the characteristics of their products.

Company	Type of material					Form				Substrate		
	silicon bearing			Organic	Metal-bearing	Liqud		cream				
	Silane	Silane/ siloxane	Siloxane, silicon resins			Water	Solvent	water	Solvent	Concrete	Masonry	Mineral substrates
APP				●		●				●		●
ARCANE												
BLUESTAR			●			●	●			●		●
DOW	●	●	●			●	●				●	●
Facabelle		●	●		●			●	●			●
MOMENTIVE	●					●						●
PEC	●	●				●		●		●	●	●
PELICOAT												
REMMERS	●	●		●		●	●	●		●	●	●
REWAH	●	●	●	●	●	●	●	●		●	●	●
REYNCHEMIE	●	●	●			●	●	●		●		●
SCALP			●		●	●	●				●	●
SIKA	●	●				●	●	●	●	●		●
Soudal		●				●	●					●
WACKER	●	●		●		●	●	●	●	●		●

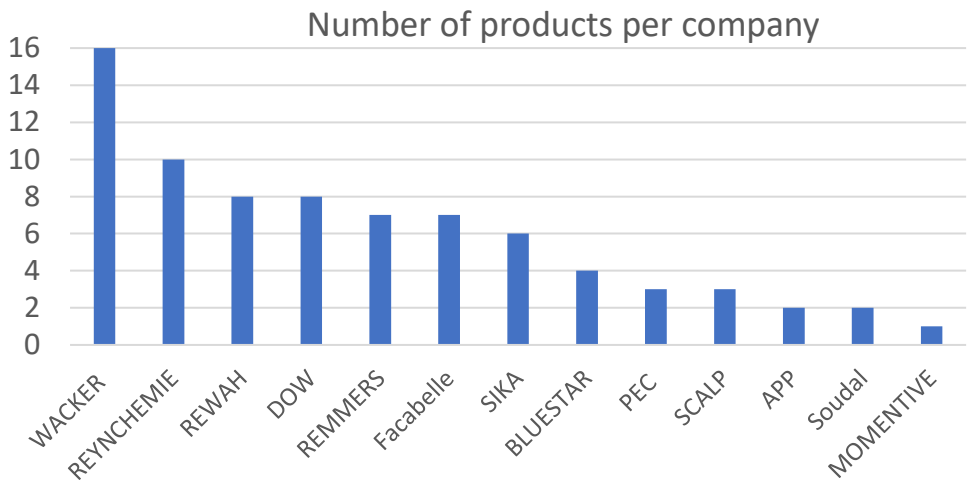

Figure 3-8. Number of water repellent products per company

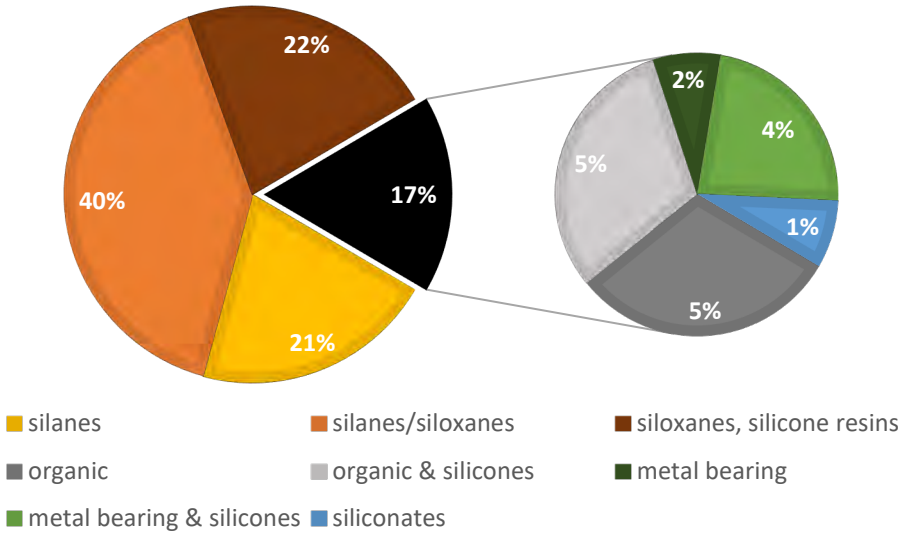

Figure 3-9. Types of water repellent agents: silanes (yellow), silanes/siloxanes (orange), siloxanes and silicone resins (brown), organic (grey), organic with silicones (light grey), metal bearing (green), metal bearing with silicones (light green), siliconates (blue)

The majority of water repellent agents are silicon-based. Some organic and metal-bearing agents, also contain silicones. Almost half of the the silicon-based products are mixtures of silanes and siloxanes.

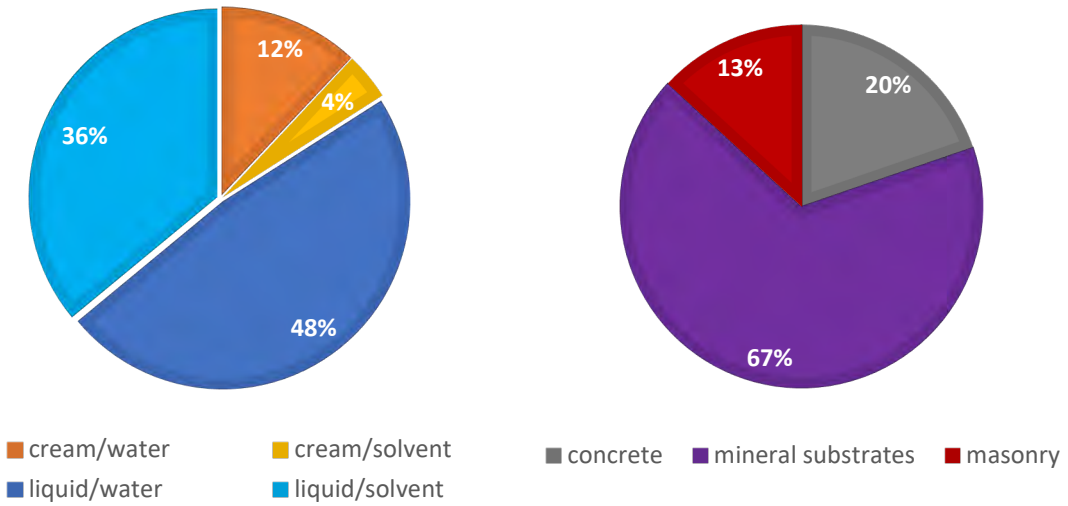

Figure 3-10. Form and diluent of water repellent agents (left): liquid/water (blue), liquid/solvent (light blue), cream/water (orange), cream/solvent (yellow). Type of substrate (right): mineral substrates (purple), concrete (grey), masonry (red).

The majority of water repellent agents are in liquid form. Most products use water as a diluent, especially if they are in cream form. Although some products are recommended only for application in concrete and cementitious materials, most products are recommended for mineral substrates in general.

Some water based products recommend to use deionized water for dilution and some other refer that tab water is suitable (Dow IE-6682, 2013; SILRES BS SMK 2101, Wacker, 2014).

Most water repellent agents are recommended to be applied wet-on-wet and from the top to the bottom of the wall. Some agents are recommended only for vertical surfaces or surfaces with a steep slope, while other agents are recommended for both horizontal and vertical surfaces. The application rate varies according to the product and the substrate. Two or three working operations are recommended for liquid products and one for cream products. For dense substrates a second application is recommended also for cream products. However, producers recommend to saturate the wall, (wet in wet). Higher active ingredient contents also cause higher impregnation depths in the treated substrate. Only in case of cost saving impregnation, it is recommended to use defined volumes/m^2, which corresponds to the minimum amount of agent should be applied for a strong hydrophobic layer formation.

If rain occurs during the application, it is recommended to stop the treatment and to cover the freshly impregnated areas. Especially in cream products, there is the risk of the cream to be washed and not enough time to be absorbed from the substrate. Strong wind and sunlight can accelerate the evaporation of the carrier agent which negatively influences impregnation depth. A Karsten pipe test is recommended by most companies, in order to check the performance of the treatment, after four to six weeks curing time, depending on the condensation procedure of each product.

It is mentioned for all water repellent agents that water vapor permeability remains possible and that pores or capillaries are not blocked. They refer no change in the water vapor permeability or change less than 10%.wo.

It is generally recommended to repair cracks, cracked joints, defective connections and rising damp and also to clean the surface before the treatment. Zhao & Meissener (2017) indicate that containment on the material surface has a negative impact on the hydrophobization and if the surface of the brick has been cleaned before the impregnation, the absorption coefficient is drastically reduced and the impregnation depth is increased.

The presence of salt crystals within pores in masonry is an obstacle for surface treatments (De Clercq, 2006). High concentrations of salts can cause severe damage to the building which cannot be prevented by a hydrophobizing impregnation (Funcosil WS, Remmers, 2016). Furthermore, water based impregnation agents may activate salts in the facade, causing efflorescence to form on the surface of the facade during the drying process. The treatment is usually not recommended when efflorescence salts are present.

The durability of water repellent treatments based on silicon-containing products has been estimated to last about 15 years, while after 5 years there is generally a drop in hydrophobicity. However, some water repellent treatments on brick masonry are performing well after 36 years. (Charola, 2001). Most water repellent products mention a durability of more than 10 to 15 years. The storage life of the product is usually one year after manufacturing, in the original packaging.

References

Aquafuge 18, Scalp . 2017. Scalp SAS. Technical data sheet.

Bluesil BP 9710, Bluestar. 2011. Bluestar Silicones. Technical data sheet.

Carmeliet J., Houvenaghel G., Van Schijndel J., Roels S. 2002. Moisture phenomena in hydrophobic porous building material Part 1: Measurements and physical interpretations. Restoration of Building and Monuments 8:165-183.

Charola A. 2001. Water Repellents and Other “Protective” Treatments: A Critical Review. In proccedings of 3rd International Conference on Surface Technology with Water Repellent Agents, Hydrophobe III, Philadelphia, USA.

Charola A.E. 1995. Water-repellent treatments for building stones: A practical overview. APT Bulletin 26:10-17.

De Clercq H. 2006. Performance of Selected Materials containing Different Mixtures of Salts after Water Repellent Treatment. Restoration of Buildings and Monuments 12: 25-34.

De Clercq H., De Witte E. 2002. Effestiveness of Comercial Silicon Based Water Repellents Applied under Different Conditions. Restoration of Buildings and Monuments 8: 149-164.

De Witte E., De Clerq H., De Bruyn R., Pien A. 1996. Systematic testing of water repellent agents. Royal Institute for Cultural Heritage. Belgian Building Research Institute.

Dow Z-6689. 2017. Dow Corning. Safety data sheet.

Dow Corning 1-6184. 2007. Dow Chemical company. Technical data sheet.

Dow Corning Z-6689. 2011. Dow Chemical company. Technical data sheet.

Dow IE-6682. 2013. Dow Chemical company. Technical data sheet.

Engel J., Heinze P., Plagge R. 2014. Adapting Hydrophobizing Impregnation Agents to the Object. Restoration of Building and Monuments. In proceedings of 7th International Conference on Water Repellent Treatment and Protective Surface Technology for Building Materials, Hydrophobe VII.

Frediani P., Manganelli Del Fa C., Matteoli U., Tiano P. 1982. Use of Perfluoropolyethers as Water Repellents: Study of Their Behaviour on PietraSerena, a Florentine Building Stone PietraSerena, a Florentine Building Stone. Studies in Conservation 27: 31-37.

Funcosil FC, Remmers. 2016. Remmers AG. Technical data sheet.

Funcosil WS, Remmers. 2016. Remmers AG. Technical data sheet.

Gelifuge new, Rewah. 2016. Rewah NV. Technical data sheet.

Lubelli B., van Hees R. 2011. Evaluation of the Effect of Nano-Coatings with Water Repellent Properties on the Absorption and Drying Behaviour of Brick. In proceedings of the 6th International Conference on Water Repellent Treatment of Building Materials, Delft.

MacMullen J., Zhang, Z., Rirsch E., Nath Dhakal H., and Bennett N. 2011. Brick and mortar treatment by cream emulsion for improved water repellence. Energy and Buildings, 43: 1560-1565.

Mayer H. 1998. Masonry protection with silanes, siloxanes and silicone resins. Surface Coatings International, 81: 89–93.

Møller E. B. 2003. Hygrothermal performance and soiling of exterior building surfaces. PhD theisis, DTU Civil engineering, Copenhagen, Denmark.

RC 900, Reynchemie. 2017. Reynchemie nv. Technical data sheet.

RC IP500, Reynchemie. 2015. Reynchemie nv. Technical data sheet

Rewah ARTISIL B10. 2016. Rewah NV. Technical data sheet.

Roos M., König F., Stadtmüller S., Weyershausen B. 2008. Evolution of Silicone Based Water Repellents for. In proceedings of the 5th International Conference on Water Repellent Treatment of Building Materials Hydrophobe V, Essen.

Selander A. 2010. Hydrophobic Impregnation of Concrete Structures- Effects on Concrete Properties. Phd Thesis, Royal Institute of Technology, Stockholm, Sweeden.

Sika AG. 2017. Refurbishment Sika technology and concepts for hydrophobic impregnations. Zurich.

Sikagard 700. 2016. Sika AG. Technical data sheet.

Silblock wms, Momentive. 2011. Silblock wms masonry water repellent. Technical data sheet.

SILRES BS 1001, Wacker. 2014. Wacker Chemie AG. Technical data sheet.

SILRES BS 1701, Wacker. 2017. Wacker Chemie AG. Technical data sheet.

SILRES BS 17040, Wacker. 2014.Wacker AG. Technical data sheet.

SILRES BS 280, Wacker. 2014. Wacker Chemie AG. Technical data sheet.

SILRES BS 3003, Wacker. 2014. Wacker Chemie AG. Technical data sheet.

SILRES BS 39, Wacker. 2015. Wacker Chemie AG . Technical data sheet.

SILRES BS 4004, Wacker. 2016. Wacker Chemie AG. Technical data sheet.

SILRES BS Creme C. 2017. Wacker AG. Technical data sheet.

SILRES BS SMK 1311, Wacker. 2014. Wacker Chemie AG. Technical data sheet.

SILRES BS SMK 2100, Wacker. 2014. Wacker Chemie AG. Technical data sheet.

SILRES BS SMK 2101, Wacker. 2014. Wacker Chemie AG. Technical data sheet.

Soulios V., Hansen E.J.D. P., Feng C., Janssen H., 2020. Hygric behavior of hydrophobized brick and mortar samples. Article in press, Building and Environment.

Stonegel, Rewah. 2016. Rewah NV. Technical data sheet.

Syed A., Donadio M. 2013. Silane sealers hydrophobic impregnation - The European perspective. International Concrete Repair Institute.

Szymura T., Barnat-Hunek D. 2013. Protection of Stone Building Structures Against Corrosion caused by Moisture. Lublin University of Technology, Lublin, Poland.

Zhao J., Meissener F. 2017. Experimental investigation of moisture properties of historic building material with hydrophobization treatment. In Proceedings of the 11th Nordic Symbosium on Building Physics. Trondheim.

4 Hygrothermal simulation campaign

(Vasileios Metavitsiadis, KUL[2])

4.1 Introduction

Masonry walls exposed to wind-driven rain exhibit elevated moisture contents (Zhao and Meissner, 2017), which can increase the risk of frost damage, mold growth, and/or wood decay in the facades (Fukui et al., 2017). The installation of internal insulation may exacerbate these dangers (Vereecken, 2013), because both inward drying and wall temperatures may be reduced (Kunzel and Kießl, 2014). A solution to these moisture-induced problems, caused by wind-driven rain, could be given through the practice of wall hydrophobization.

The main purpose of hydrophobization is to prevent liquid water from entering the treated surface (Carmeliet et al., 2002) and consequently, to minimize serious damage at the material and the component level. However, hydrophobization could slow down the drying speed of the facades (Finken et al., 2015), which may threaten the desired positive impacts. Therefore, the impact of hydrophobization on the hygrothermal performance of internally insulated walls is really to be examined.

This section presents simulations executed to assess the spectrum of impacts of hydrophobization on the moisture responses of solid facades with(out) internal insulation. The prime target is to investigate whether the balance between reduced wetting (due to less absorption of wind-driven rain) and reduced drying (due to less first-phase drying) can be manipulated by the strength of the hydrophobization (reduction of capillary absorption coefficient and/or increase of agent impregnation depth). If so, then the application of the water repellent agent could be tuned to the combined factors of facade material, geometry and moisture loads. This study focuses on the hygrothermal behavior of three solid facade configurations (uninsulated, and with two different internal insulation systems) with hydrophobic impregnations of various strengths and depths. The hygrothermal behavior of hydrophobized wall is examined via numerical simulations with Delphin, a coupled heat and moisture transfer simulation program (Nikolai and Grunewald, 2015).

Section 4.2 introduces the two methods applied to obtain a virtual hydrophobization, Section 4.3 then details the impact of the hydrophobization on the solid facades' hygrothermal responses and moisture damages. For the hygrothermal response, mainly the moisture contents' evolutions are analysed, for the moisture damages wood decay and mould growth are targeted.

4.2 Virtual hydrophobization

Hydrophobization leads to a dramatic alteration of the hygric properties of the brick. Moisture transport is reduced significantly, while the way that moisture storage changes is difficult to be defined. In order to represent a hydrophobized brick via a model that can be used for hygrothermal simulations two different methods have been implemented: scaling down the moisture retention curve ($w_{cap} \downarrow$) and reducing the absorption coefficient ($A_{cap} \downarrow$). Both methods result in the reduction of the absorption coefficient of the virtually hydrophobized brick. However, their main difference is that while moisture storage is reduced in the first method, it remains unchanged in the second. For both methods, the vapor permeability of virtually hydrophobized bricks remains unaffected.

[2] Activities performed while at KUL, currently no affiliation

The brick used for the virtual hydrophobization (*Brick 2*) was selected due to its relatively high capillary absorption coefficient value (0.46 kg/m²s$^{0.5}$), to obtain a broader spectrum of possible capillary absorption coefficents. The characteristics of *Brick 2* are shown in Table 4-1 (Vereecken et al., 2015).

Table 4-1: Brick 2 properties

Material property	Brick 2
Capillary absorption coefficient [kg/m^{2}s$^{0.5}$]	0.44
Bulk density [kg/m^3]	1786
Thermal capacity [J/kgK]	1000
Dry thermal conductivity (λdry) [W/mK]	1.08
Dry vapor resistance factor (μ) [-]	14.3
Capillary moisture content [kg/m^3]	206.7
Saturation moisture content [kg/m^3]	323

In what follows, the impact of the hydrophobization is always characterized with the resulting capillary absorption coefficient A_{cap}, which always carries the [kg/m²s$^{0.5}$] unit. For reasons of conciness in notation, this unit is assumed generally known, and is hence not included further on in text, in tables or in figures.

For the method of scaling down the moisture retention curve (w_{cap} ↓), the moisture retention curve of the initial (untreated) brick model is scaled down to four different levels, respectively 50 %, 25 %, 10 % and 2 % of the original moisture retention curve. This moisture storage reduction also results in a moisture transport reduction and consequently in different capillary absorption coefficients. For the method of reducing the absorption coefficient (A_{cap} ↓), the capillary absorption coefficient of the initial (untreated) brick is directly reduced to also four different levels, respectively by 80 %, 95 %, 99 % and 99.9 %. These alterations of the initial brick intend to represent a wide spectrum of impregnation strengths. The obtained capillary absorption coefficients are shown in Table 4-2.

Table 4-2: Resulting absorption coefficients (A_{cap})

w_{cap} ↓		A_{cap} ↓	
Percentage of the initial moisture retention curve	Resulting absorption coefficient (A_{cap})	Percentage of reduction of the initial A_{cap}	Resulting absorption coefficient (A_{cap})
50%	0.081	80%	0.088
25%	0.021	95%	0.022
10%	0.004	99%	0.0044
3%	0.0004	99.9%	0.0004

Figures 4-1 and 4-2 show the capillary absorption curves of the virtually hydrophobized bricks in comparison to that of the untreated brick, for the methods of scaling down the moisture retention curve (w_{cap} ↓) and reducing the absorption coefficient (A_{cap} ↓) respectively. The values of the capillary absorption coefficients, obtained after the hydrophobization, are 5 to 1000 times lower than the original value of the untreated brick.

The drying behavior of the virtually hydrophobized bricks is shown in Figures 4-3 and 4-4. The curves shown represent the drying of a composite, comprising 4 cm of untreated moisture-saturated brick at the bottom and 1 cm of hydrophobized dry brick at the top. The drying conditions at the top surface of the top layer are the same for both methods: 20 °C and 50 % RH, with the surface heat and vapour exchange coefficients 25 W/m^{2}K and $2 \cdot 10^{-7}$ s/m respectively.

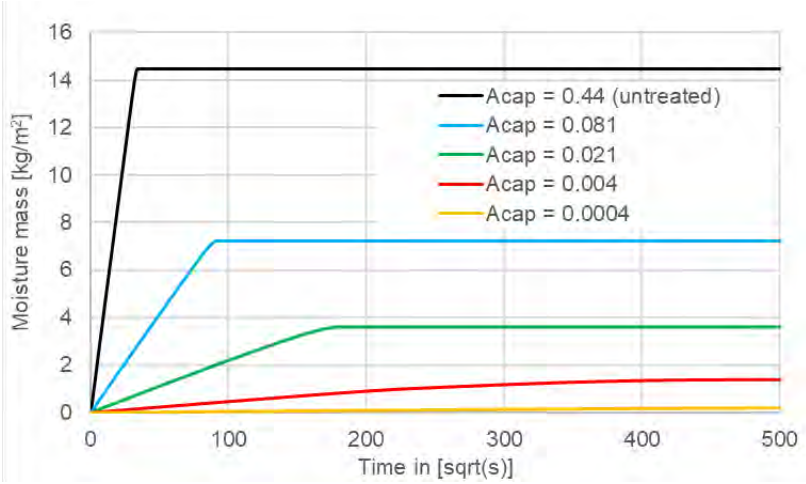

Figure 4-1: Water uptake curves for different impregnation strengths for the method of scaling down the moisture retention curve ($w_{cap}\downarrow$).

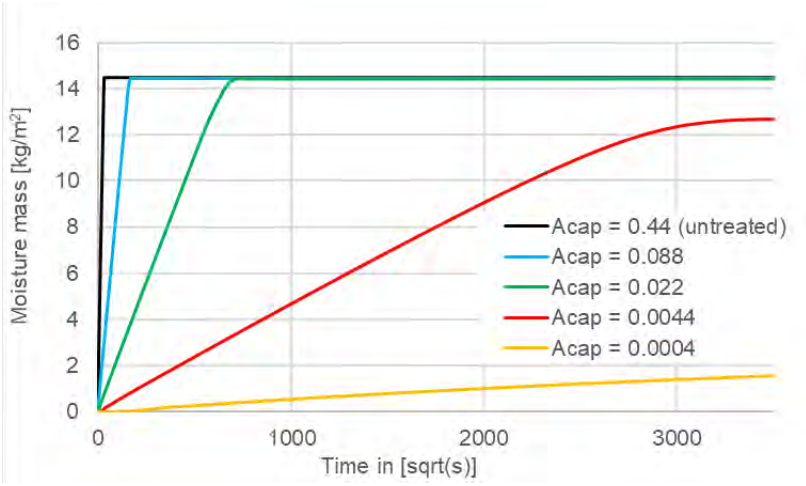

Figure 4-2: Water uptake curves for different impregnation strengths for the method of reducing the absorption coefficient ($A_{cap}\downarrow$).

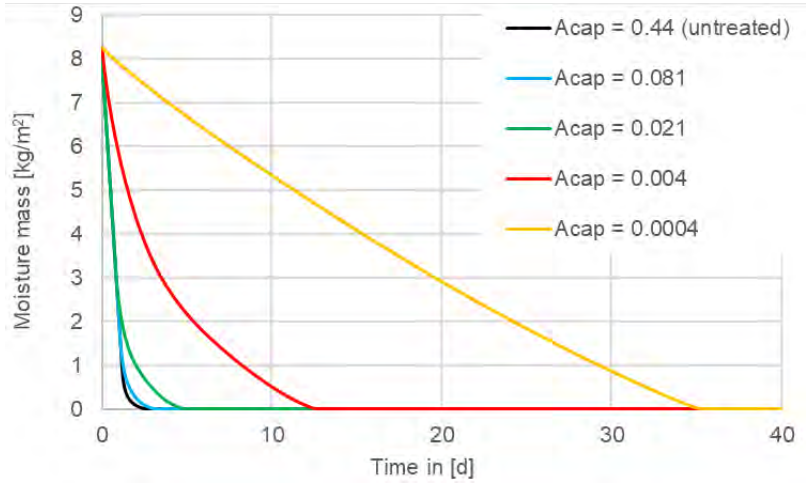

Figure 4-3: Drying test for different hydrophobization strengths, with a treated layer of 1 cm ($w_{cap}\downarrow$).

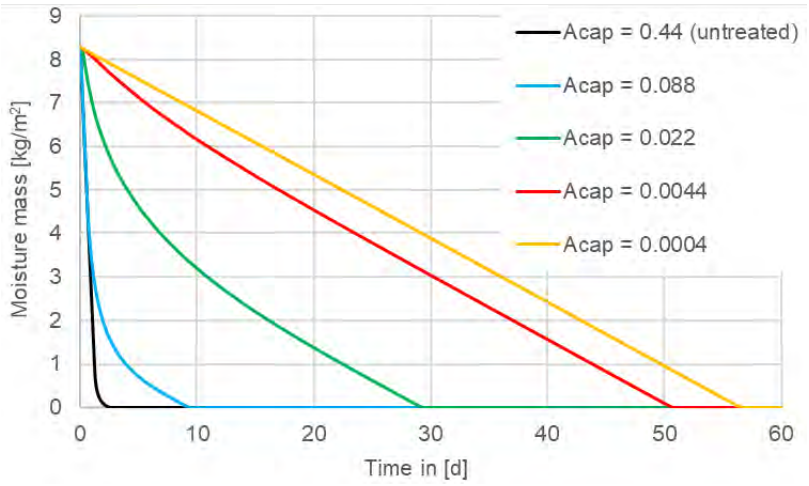

Figure 4-4: Drying test for different hydrophobization strengths, with a treated layer of 1 cm (A_{cap} ↓).

The strength and the depth of the impregnation affect the drying behavior of the bilayered composites for both methods. For the first method (moisture retention curve scaled down, w_{cap} ↓) the effect of hydrophobization is more evident when the strongest impregnations (1 % and 10 % of the initial moisture retention curve) are applied. For the second method (reduction of absorption coefficient, A_{cap} ↓) the effect of hydrophobization is apparent for all impregnation strengths, since the time that is needed for the bilayered composites to completely dry out is increased substantially.

The results of the simulated water uptake and drying tests suggest that the hydrophobized brick modes capture the basic characteristics of water repellency as described by recent studies (Engel et al., 2014; Zhao and Meissener, 2017; Fukui et al., 2017). The principal difference between the two methods (i.e. alteration of moisture storage) is the outcome of the limited experimental results regarding the actual hygric storage and transport properties of a hydrophobized brick. Since the hygric properties of hydrophobized materials have not been adequately measured, both methods only provide a rough estimation of the hygric behavior of a hydrophobized material. However, this approach can yield some interesting results regarding the possible risks of wall hydrophobization, in contrast to the simplistic and overly optimistic method of simulating hydrophobization via complete exclusion of the wind-driven rain loads (Hamid and Wallentén, 2017).

4.3 Hygrothermal performance of hydrophobized walls

This section covers the assessment of the hygrothermal performance of walls that combine internal insulation and hydrophobization, based on the virtual hydorophobization described in Section 4.3.

4.3.1 Overview and input parameters

The examination involves three solid wall configurations. The reference is an uninsulated masonry wall with a thickness of 30 cm. The two insulated configurations use i) a vapor-tight (XPS, extruded polystyrene) and ii) a vapor-open capillary active (CaSi, calcium silicate) internal insulation. For each of the latter: 6 cm and 14 cm. For all configurations, the impregnation strengths that are used lead to absorption coefficients of 0.081, 0.021, 0.004 and 0.0004 for the method of scaling down the moisture retention curve (w_{cap} ↓) and 0.088, 0.022, 0.0044 and 0.0004 for the method of reducing the absorption coefficient (A_{cap} ↓), as shown in Table 4-2. Also, three differrent impregnation depths are used: 0.5 cm, 1 cm and 4 cm.

For CaSi, a glue mortar of 4 mm is applied between insulation and masonry wall. As interior finishing, the reference and CaSi cases use a 1 cm plaster layer, while the XPS case applies a 1 cm gypsum board. Since all simulations are one-dimensional, some aspects of the construction, like the mortar joints and wooden beams, are neglected. The masonry wall is thus presumed to be composed of one (untreated walls) or two (treated walls) isotropic brick materials.

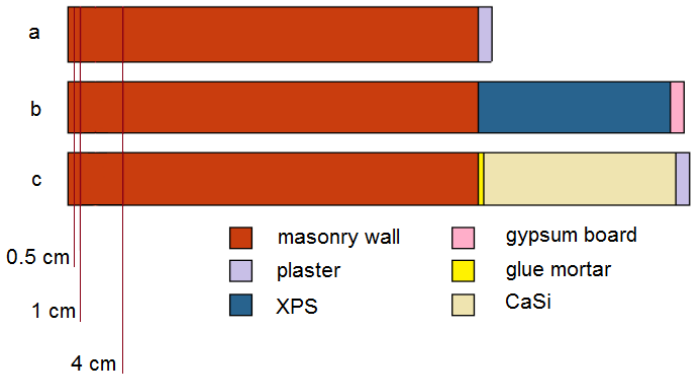

Figure 4-5: Wall composition: (a) non-insulated, (b) vapor tight (XPS), (c) capillary active (CaSi). The thickness of the internal insulation in the simulations is either 14 cm or 6 cm.

These wall configurations are subjected to a hygrothermal simulation under atmospheric excitation, wherein a South-West orientation and a temperate maritime climate (Essen, Germany) are applied. The exterior boundary conditions consist of convective heat exchange and long- and short-wave radiation on the thermal side, and of convective vapor exchange and wind-driven rain on the hygric side. The interior boundary conditions consist of convective heat exchange and long-wave radiation and convective vapor exchange for heat and moisture respectively, with constant indoor conditions (20 °C, 50 % RH). At the exterior and interior surface, standard values for the convective heat and vapor surface transfer coefficients are used. An overview of the most important input parameters regarding the boundary conditions of the simulations is given in Table 4-3. The simulations cover a simulation interval of five years, as it takes some time for the moisture conditions and damages to come to a sufficiently periodic response.

Table 4-3: Boundary conditions

Input parameter	Input value
Exterior surface	
Climatic conditions	Essen, Germany
Orientation	South-West
Exchange coefficient for heat convection	20 W/m^2K
Exchange coefficient for vapor diffusion	2 x 10^{-7} s/m
Long wave emissivity	0.9
Interior surface	
Exchange coefficient for heat convection & radiation	8 W/m^2K
Exchange coefficient for vapor diffusion	3 x 10^{-8} s/m
Temperature	20 °C
Relative humidity	50 %

The main goal of applying hydrophobization on the exterior of an internally insulated masonry wall, is the elimination or reduction of potential moisture damage of which the following are examined:

1) Wood decay of embedded beam ends due to overcritical relative humidities (and sufficiently moderate temperatures) in the wood material
2) Mold growth on the interior surface because of overcritical relative humidities (and sufficiently modest temperatures as well as a mold-sensitive finishing) at the surface.

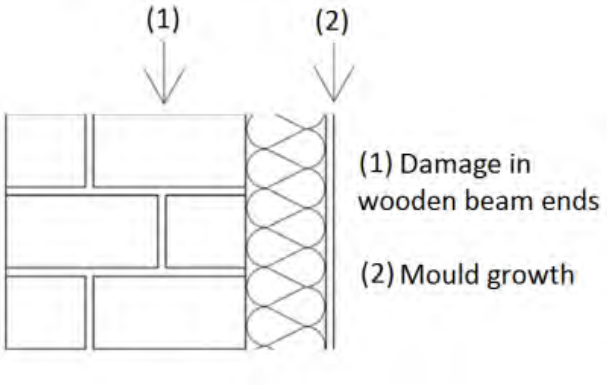

Figure 4-6: Potential damage planes for hygrothermal risks.

The risk of wood decay is quantified via the VTT-wood decay model (Viitanen et al., 2010), which is incorporated in Delphin. The model requires the temperatures and relative humidities that the wooden beam would be subjected to. Given that beams are not part of the current one-dimensional model, these are approximated with the conditions at a distance of 5 cm from the interior interface of the masonry wall. The mold growth risk is calculated with the VTT-mold growth model (Viitanen et al. 2011) which is an integrated part of Delphin as well and requires the values of temperature and relative humidity that occur at the interior surface. The potential damage planes for the examined hygrothermal risks are shown in Figure 4-6.

4.3.2 Average moisture content in masonry

This section focuses on the evolution of the average moisture content inside the masonry wall, during the last (5th) year of the simulation, for the uninsulated wall, the wall with CaSi insulation, and the wall with XPS insulation, each with the two different methods of virtual hydrophobization and the different impregnation strengths, depths and insulation thicknesses.

4.3.2.1 Virtual hydrophobization via moisture retention curve (w_{cap} ↓)

For the uninsulated wall (Figure 4-7), the moisture levels inside the masonry increase and decrease rapidly, in response to the wetting by wind-driven rain and drying via convective vapor exchange. For the two weaker impregnation strengths (A_{cap} 0.081 and 0.021), hydrophobization does not significantly affect the levels of moisture inside the masonry. For theimpregnation strength A_{cap} 0.004 (~100 times lower than that of the untreated brick), the effect of hydrophobization is more evident during the wetting periods, since moisture levels are lower. However, during drying periods the levels of moisture are slightly higher compared to the untreated wall or the weaker impregnation strengths, due to the reduced drying rate of the virtually hydrophobized layer. When the strongest impregnation is used (A_{cap} 0.0004) practically no water from wind-driven rain penetrates the hydrophobized layer.

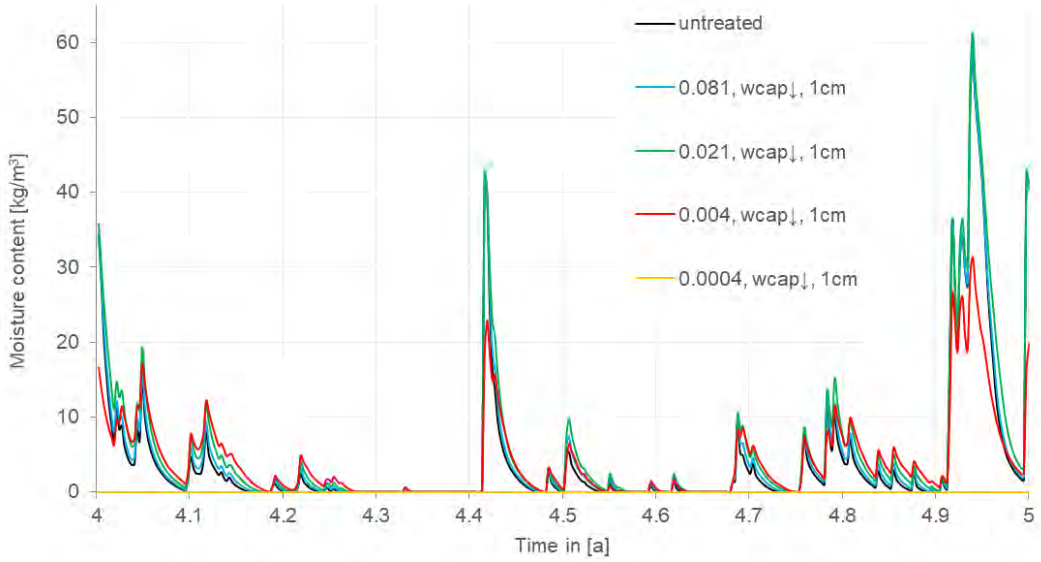

Figure 4-7: Average moisture content in the masonry for the uninsulated wall with impregnation depth of 1 cm.

For the XPS-insulated wall, the moisture levels are higher relative to the uninsulated wall configuration, due to the absence of inward drying and the lower wall temperature. The limited impact of the weak impregnations (A_{cap} 0.081 and 0.021) is also seen here, since only the strong impregnations significantly affect the moisture levels. For the impregnation strength A_{cap} 0.004, the moisture levels in the masonry wall remain high during drying periods, as shown by Figure 4-8. Although lower amounts of wind-driven rain enter the masonry wall, compared to the untreated wall or the weaker impregnations, it is more difficult for the wall to dry out due to the significantly reduced drying rate of the virtually hydrophobized layer. However, this is not the case with the strongest impregnation, for which the moisture levels in the masonry are negligible for the whole year.

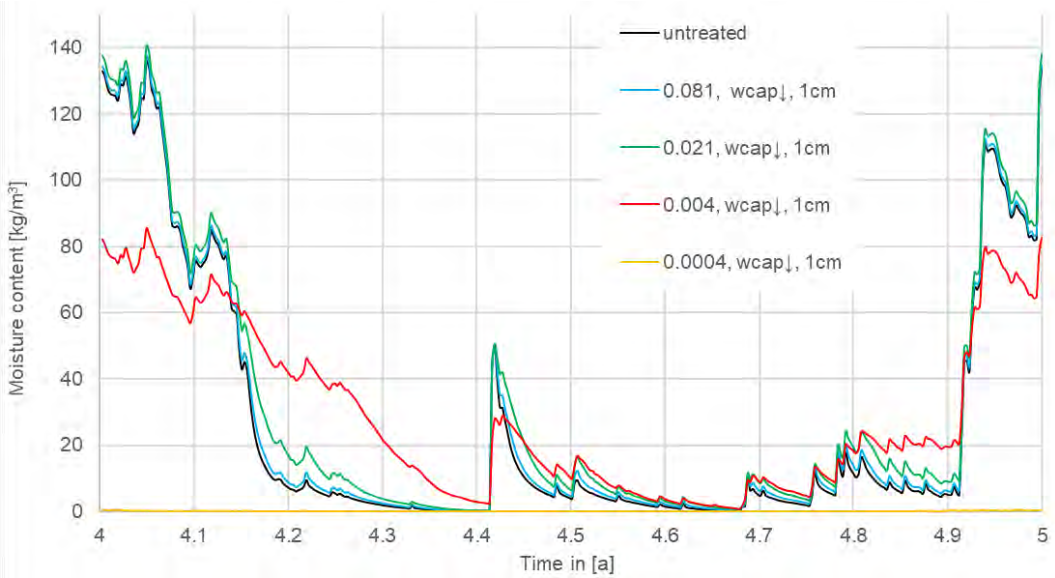

Figure 4-8: Average moisture contents in the masonry for the XPS-insulated wall with impregnation depth of 1 cm.

For the vapor-open capillary active (CaSi) internal insulation, the results are similar to those observed in the uninsulated wall. CaSi insulation showcases its capability for inward drying and therefore, avoids the typical increase of the moisture contents inside the masonry (Figure 4-9). Also, because of its higher thermal conductivity, compared to XPS, CaSi does not cause a substantial decrease in the temperature of the masonry.. Nevertheless this characteristic of the CaSi internal insulation has a negative impact on heat losses, when compared to the XPS internal insulation.

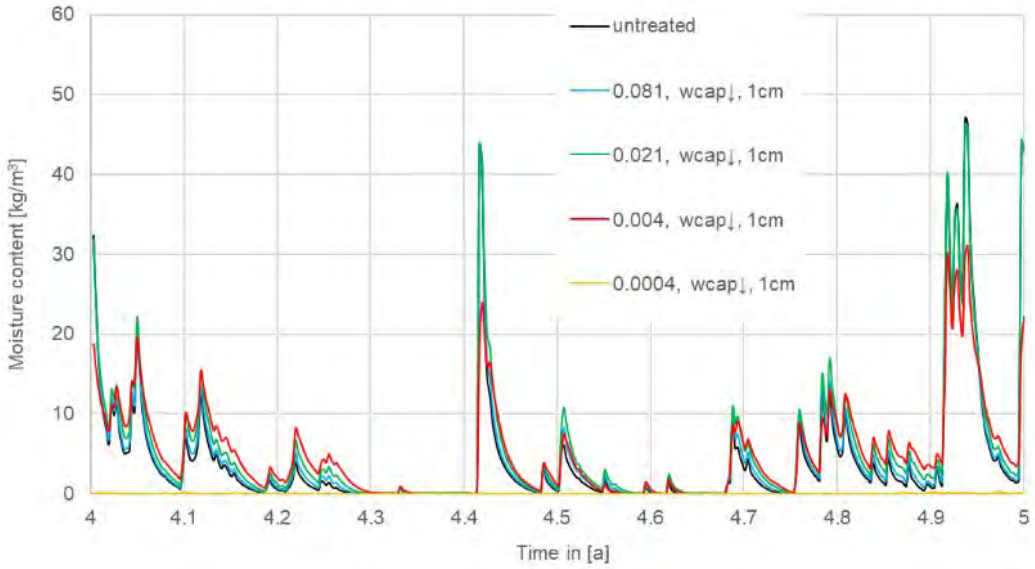

Figure 4-9: Average moisture contents in the masonry for the CaSi-insulated wall with impregnation depth of 1 cm.

4.3.2.2 Virtual hydrophobization method via absorption coefficient (A_{cap} ↓)

For the virtual hydrophobization method of reducing the absorption coefficient (A_{cap} ↓), the moisture levels inside the uninsulated wall (Figure 4-10) decrease rapidly, in response to the wetting by wind-driven rain. However, the rate of drying via convective vapor exchange is reduced compared to the method of of scaling down the moisture retention curve (w_{cap} ↓). Although hydrophobization does not affect significantly the levels of moisture inside the masonry, for the two weaker impregnation strengths (A_{cap} 0.088 and 0.022), the impregnation strength with 100 times lower absorption coefficient (A_{cap} 0.004) has an important impact on the levels of moisture. When the strongest impregnation is used (A_{cap} 0.0004), moisture remains at zero levels throughout the year, indicating that water from wind-driven rain does not penetrate the hydrophobized layer.

The situation changes dramatically for the XPS-insulated wall. When weak impregnation strengths are used, not only is water from wind-driven rain able to enter the masonry, but also it is much more difficult for the wall to dry out. This can be explained by the reduced drying rate of the hydrophobized layer, but also from the absence of inward drying and the lower wall temperatures of the XPS-insulated wall. Especially for the impregnated layer with A_{cap} 0.022, moisture inside the masonry remains at significantly high levels for the whole year. The elevated moisture content of the wall can increase the possibility of moisture-related damages and the level of heat losses. The completely reversed situation is experienced when stronger impregnations are taken into consideration, since moisture levels either remain relatively low for the whole year (A_{cap} 0.0044) or are totally eliminated (A_{cap} 0.0004).

Vapor open capillary active (CaSi) internal insulation, has the same behavior regarding the average moisture content, with that of the uninsulated wall, when hydrophobization is applied. In contrast to XPS insulation, CaSi insulation prevents the increase of the moisture contents inside masonry, due to its capacity for inward drying.

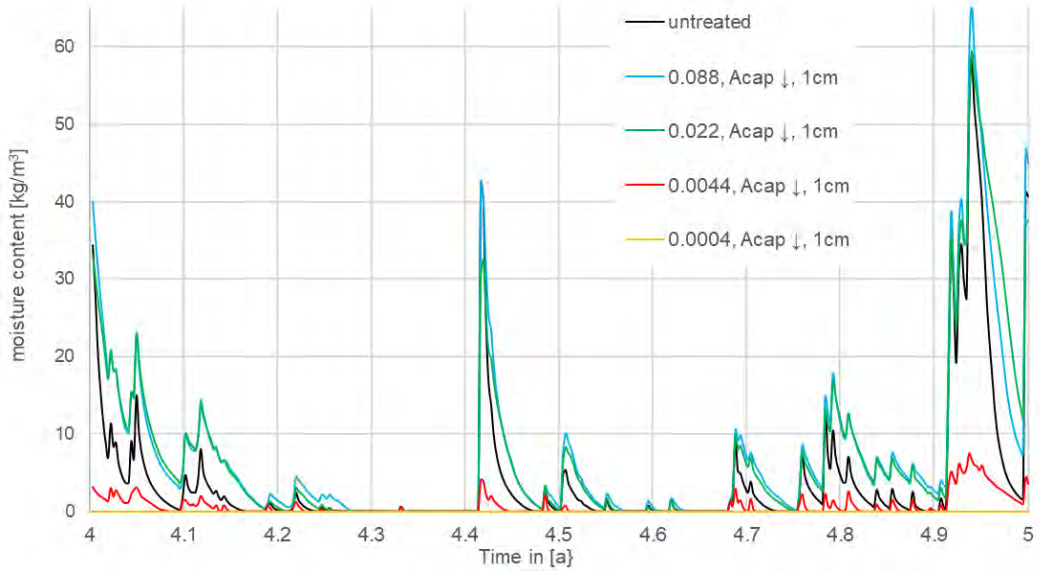

Figure 4-10: Average moisture content in the masonry for the uninsulated wall with impregnation depth of 1 cm.

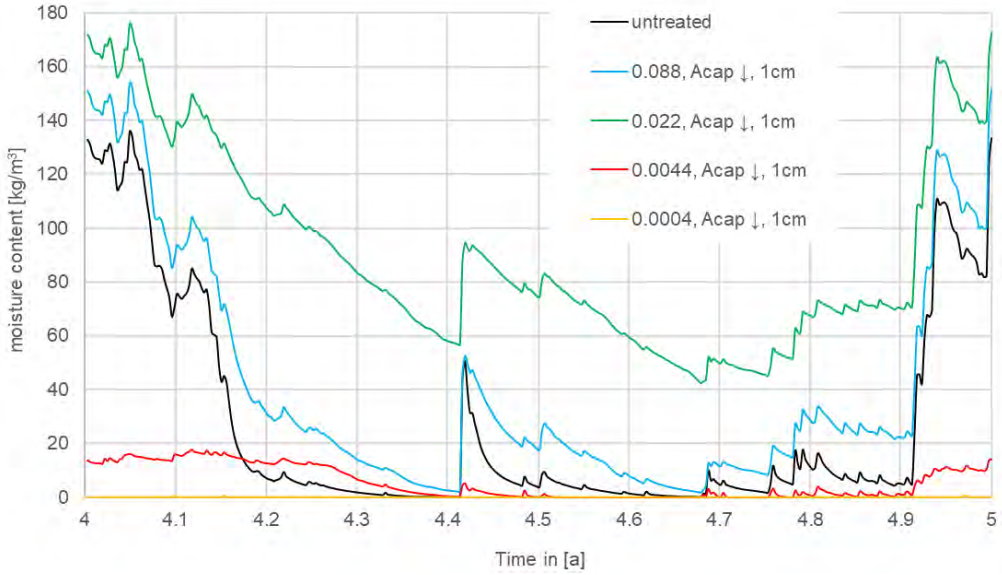

Figure 4-11: Average moisture contents in the masonry for the XPS-insulated wall with impregnation depth of 1 cm.

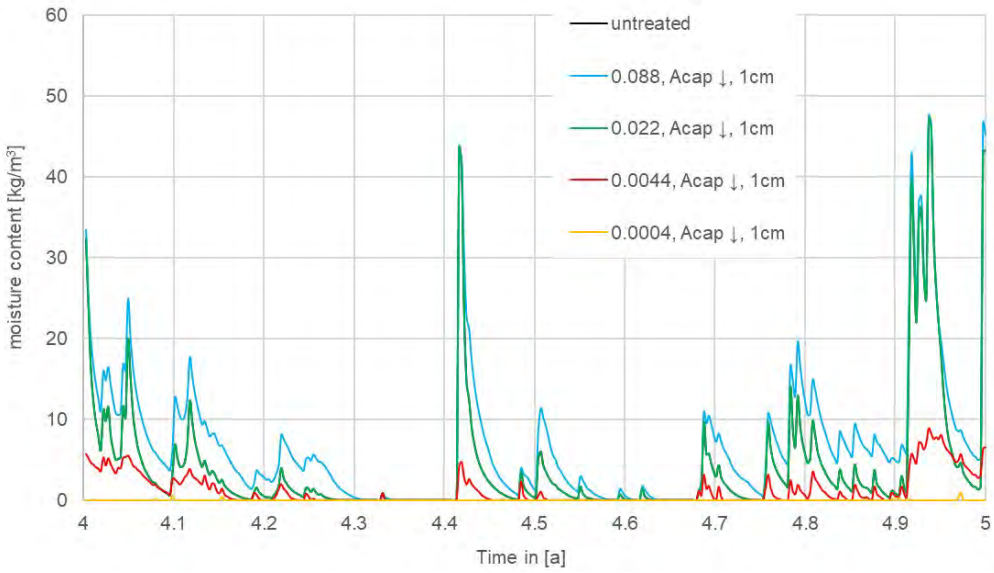

Figure 4-12: Average moisture contents in the masonry for the CaSi-insulated wall with impregnation depth of 1 cm.

4.3.2.3 Effect of impregnation depth on average moisture content

In this section, the effect of impregnation depth on the average moisture content of the masonry wall is examined, focusing on the impregnation strength that gives a capillary absorption coefficient about 100 times lower than that of the untreated brick (A_{cap}: 0.004 for w_{cap} ↓ & 0.0044 for A_{cap} ↓).

For the uninsulated wall (Figure 4-13), when the method of reducing the absorption coefficient (A_{cap} ↓) is considered, impregnation depth plays a minor role in the moisture content in the masonry, since for all the examined impregnation depths (0.5 cm, 1 cm, 4 cm) the levels of moisture content remain relatively low. For the method of scaling down the moisture retention curve (w_{cap} ↓) on the other hand, impregnation depth has a noticeable influence on the average moisture content of the wall. The average moisture content decreases when the impregnation depth increases, although for all impregnation depths the resulting moisture content remains on lower levels compared to the moisture content levels of the untreated wall. The same outcomes emerge as well in the case of the CaSi-insulated wall.

The influence of the impregnation depth is more evident in the case of the XPS-insulated wall (Figure 4-14). Higher impregnation depths seem to have a positive impact on the average moisture content of the hydrophobized wall when the method of reducing the absorption coefficient (A_{cap} ↓) is in question, as higher impregnation depths lead to higher reductions of the moisture content. However, for the method of scaling down the moisture retention curve (w_{cap} ↓), this pattern is reversed as higher impregnation depths lead to an increase of the average moisture content, resulting in a continuously high level of moisture content.

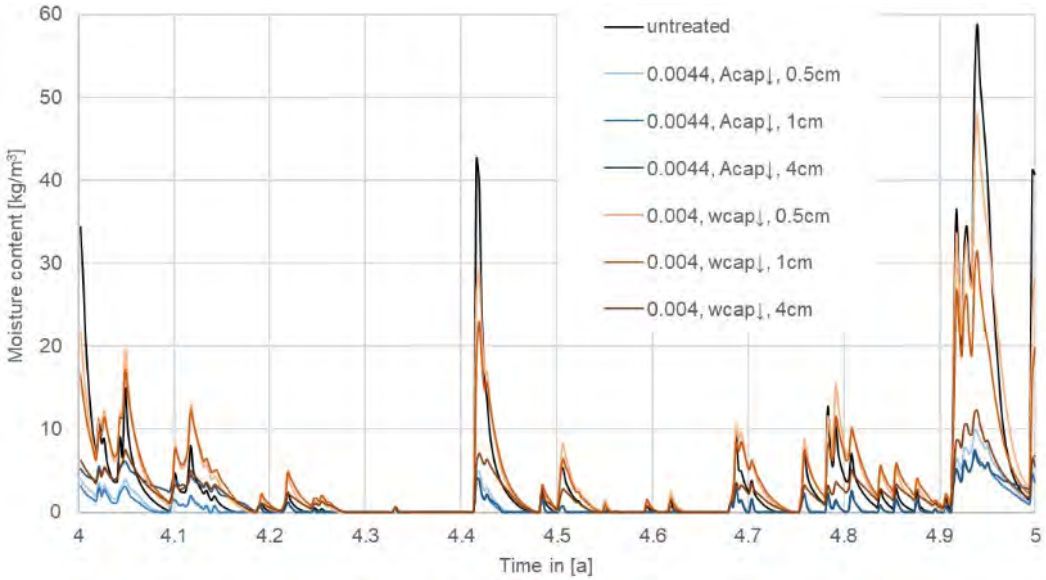

Figure 4-13: Average moisture contents in the masonry for the uninsulated wall, for all impregnation depths and both methods of virtual hydrophobization (A_{cap} 0.0044 and 0.004).

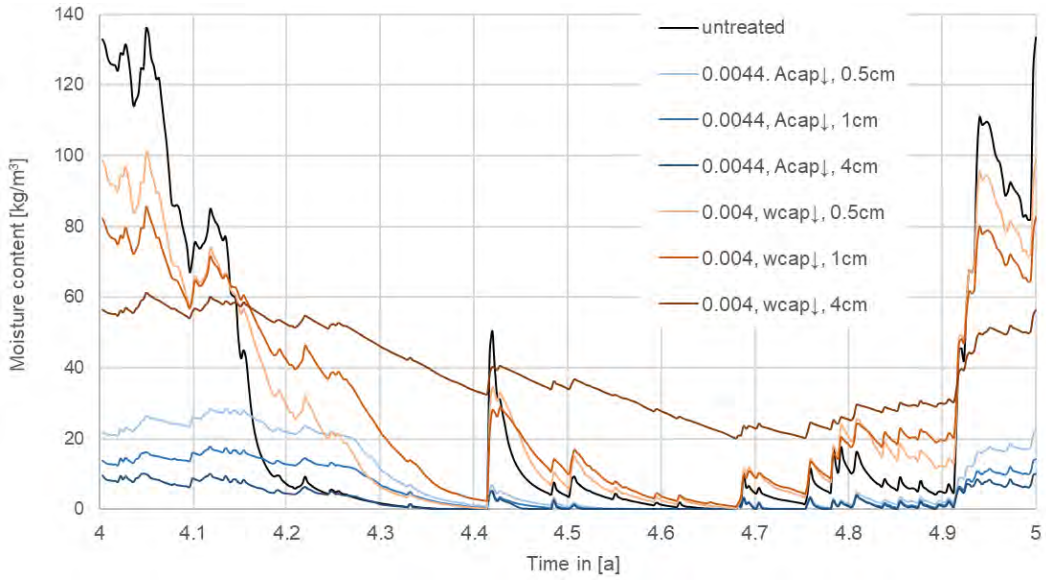

Figure 4-14: Average moisture contents in the masonry for the XPS-insulated wall, for all impregnation depths and both methods of virtual hydrophobization (A_{cap} 0.0044 & A_{cap} 0.004).

4.3.2.4 Effect of insulation thickness on average moisture content

Two different levels of insulation thickness are studied for both internal insulation solutions: 6 cm and 14 cm. For the XPS-insulated wall (Figure 4-15), the effect of the insulation thickness is more evident during the drying periods, the intervals during which the average moisture content goes down. The thin insulation (6 cm) leads to slightly lower levels of average moisture content in the masonry, compared to the thick one (14 cm). This difference does however remain small, even for the untreated wall and the wall with weak impregnation (A_{cap}: 0.088), and it moreover reduces further with stronger impregnations.

For the vapor open capillary active internal insulation (CaSi), the effect that the thickness of the insulation has on the average moisture content of the masonry wall, is practically insignificant, as shown in Figure 4-16. CaSi, being a vapor open capillary active material, provides the capacity for the wall to also dry out inwards. Although for the two examined levels of insulation thickness, the difference in the resulting moisture contents is negligible, the possibility that a greater insulation thickness could have a more noticeable effect cannot be rejected.

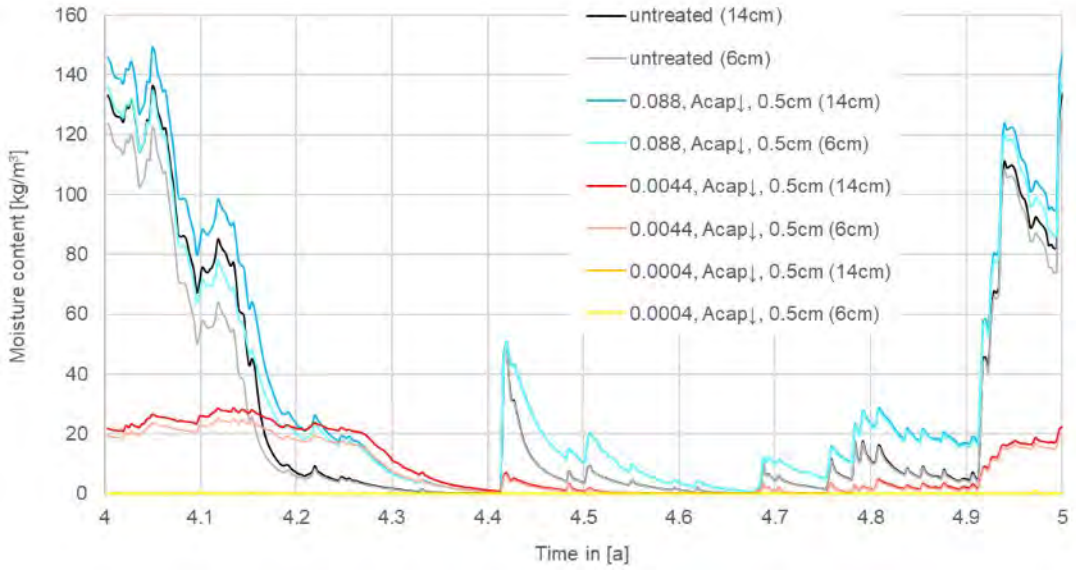

Figure 4-15: Average moisture contents in the masonry for the XPS-insulated wall.

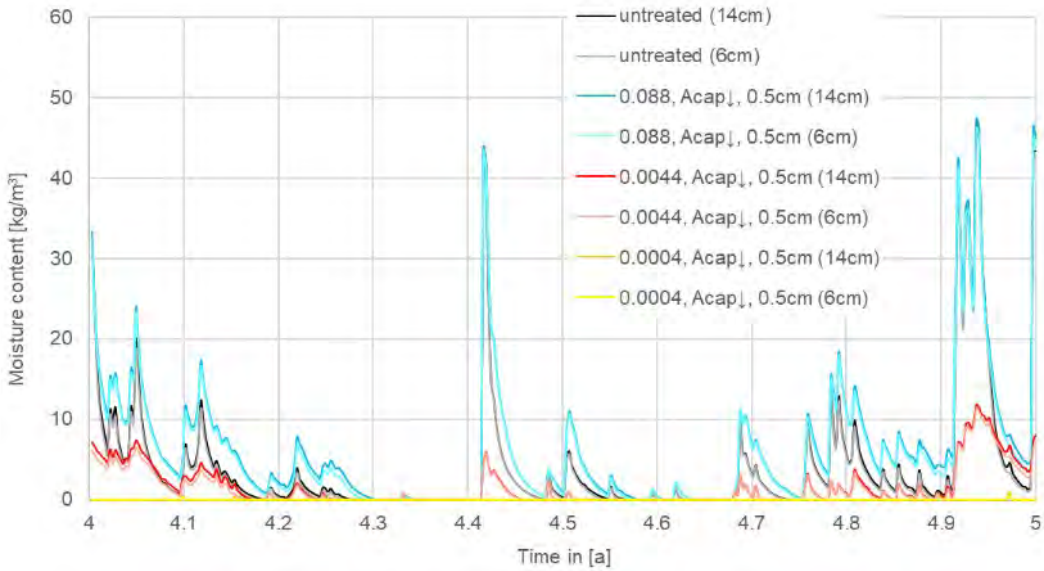

Figure 4-16: Average moisture contents in the masonry for the CaSi-insulated wall.

4.3.3 Moisture profiles

While the graphs containing the average moisture content display the temporal evolution of the moisture content inside the masonry wall, moisture profiles can provide information regarding the distribution of moisture inside the masonry wall at specific moments. For each case of masonry wall (uninsulated, XPS, CaSi), two different types of moisture profiles are presented: i) maximum moisture content profile, which refers to the day of the last simulation year with the maximum averge moisture content inside the masonry and ii) average moisture content profile, which depicts the annual average moisture content in the masonry for the last simulation year. Moisture inside the insulation systems and the interior layers (plaster, gypsum board) are neglected. The shown results are restricted to the 4 cm impregnation depth, as the findings for the other impregnation depths yield similar conclusions. It is worth mentioning that the difference in the moisture levels in the hydrophobized layer of the wall (4 cm deep from exterior surface) between both virtual hydrophobization methods (w_{cap} ↓ & A_{cap} ↓) is a direct consequence of their characteristic difference (alteration of the moisture storage or not).

For the uninsulated wall, strong impregnations (A_{cap}: 0.0044 for A_{cap} ↓ & 0.004 for w_{cap} ↓) yield lower levels of moisture content inside the masonry (with the exception of the hydrophobized layer for the method of A_{cap} ↓), compared to the untreated wall, both when maximum (Figure 4-17) and average (Figure 4-18) moisture contents are considered. Conversely, for weaker impregnations (A_{cap}: 0.088 for A_{cap} ↓ & 0.081 for w_{cap} ↓), moisture levels are slightly higher compared to the untreated wall, for both maximum and average moisture content profiles.

In the XPS-insulated wall, weak impregnations (A_{cap}: 0.088 for A_{cap} ↓ & 0.081 for w_{cap} ↓) give higher maximum values of moisture content, in comparison to the untreated wall, while strong impregnations (A_{cap}: 0.0044 for A_{cap} ↓ & 0.004 for w_{cap} ↓) give a significant reduction of maximum moisture content, especially for the method of absorption coefficient reduction (A_{cap} ↓). Regarding the average moisture content inside the masonry, all treatments cause higher average values compared to the untreated XPS-insulated wall, except for the strong impregnation in the case of reducing the absorption coefficient (0.0044, A_{cap} ↓). It is evident that all values of moisture content (maximum and average) of XPS are significantly higher than those of the uninsulated wall.

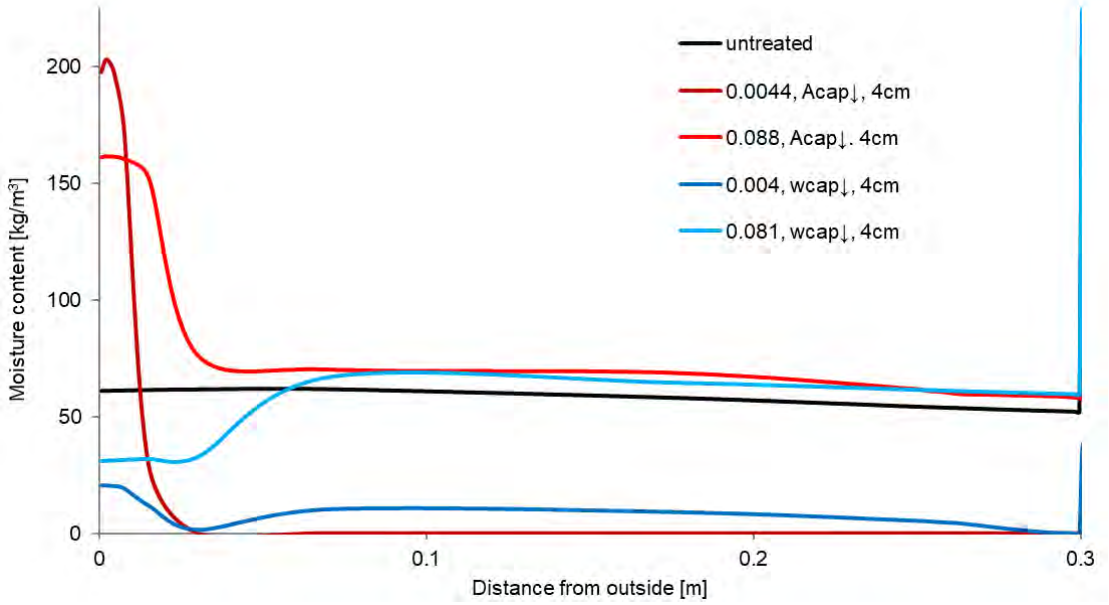

Figure 4-17: Maximum moisture content profile for the uninsulated wall.

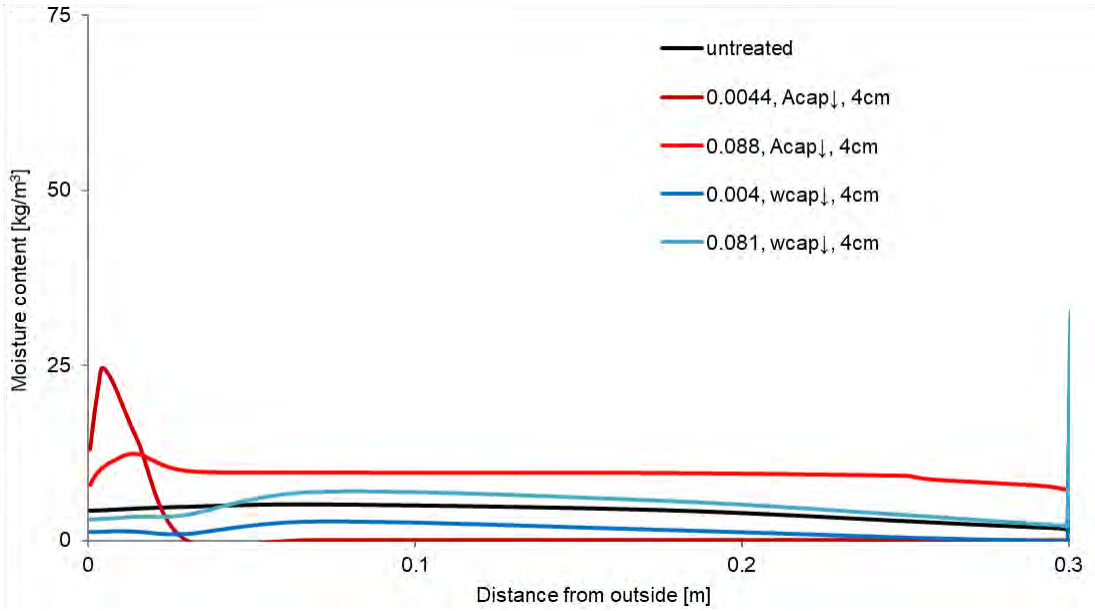

Figure 4-18: Average moisture content profile for the uninsulated wall.

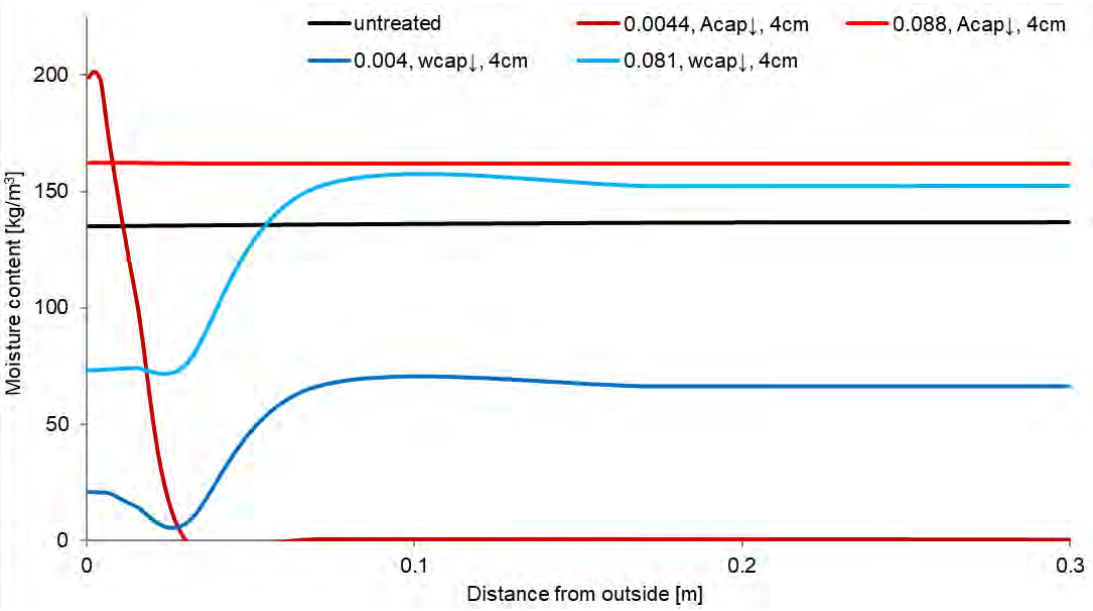

Figure 4-19: Maximum moisture content profile for the XPS-insulated wall.

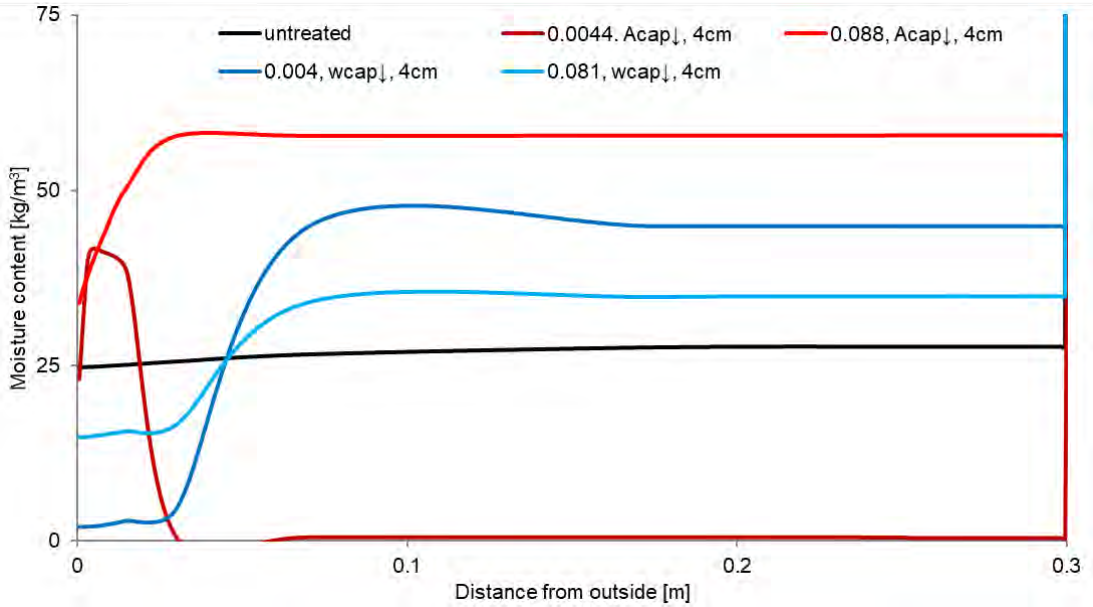

Figure 4-20: Average moisture content profile for the XPS-insulated wall.

The results of the CaSi-insulated wall are similar to those of the uninsulated wall, for which strong impregnations (A_{cap}: 0.0044 for A_{cap} ↓ & 0.004 for w_{cap} ↓) lead to lower maximum and average values of moisture content compared to the untreated wall and weak impregnations (A_{cap}: 0.088 for A_{cap} ↓ & 0.081 for w_{cap} ↓) result in values that are comparable to the moisture content levels in the untreated wall.

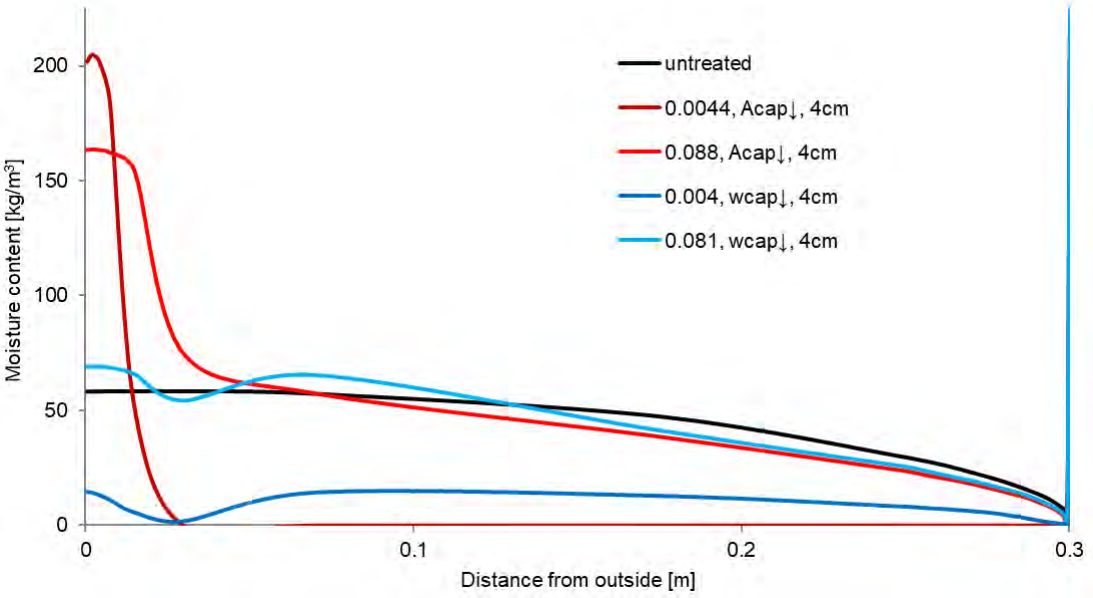

Figure 4-21: Maximum moisture content profile for the CaSi-insulated wall.

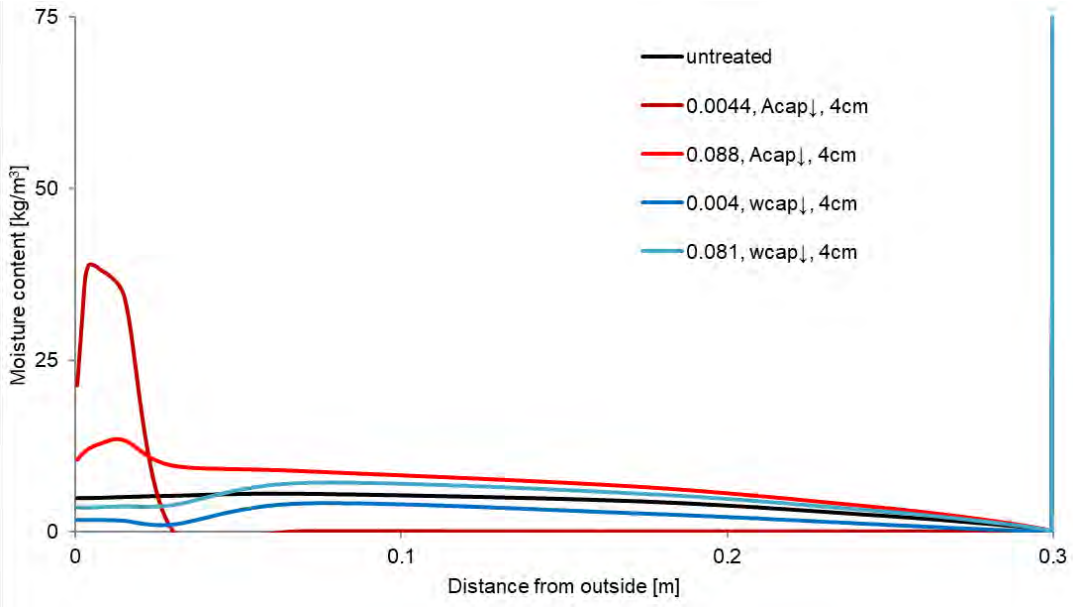

Figure 4-22: Average moisture content profile for the CaSi-insulated wall.

A pattern that is recognizable in all cases, is that for strong impregnations using the method of absorption coefficient reduction (A_{cap} ↓), average and maximum moisture contents in the masonry remain relatively lower, except for in the hydrophobized layer, inside which moisture levels are significantly higher. Since moisture storage of the virtually hydrophobized brick does not change when the method of absorption coefficient reduction is used, moisture that enters the wall due to wind-driven rain is stored in the hydrophobized layer and does not penetrate deeper into the masonry wall. This causes the moisture content inside the masonry wall to remain low, thus fulfilling the primary purpose of a hydrophobic treatment. However, the fact that the moisture content in the hydrophobized layer itself remains high throughout the year could potentially lead to problems caused by low temperature at the exterior surface of the wall (i.e. frost damage).

4.3.4 Wooden beam decay

For the uninsulated wall (Figure 4-23), weak impregnations (A_{cap}: 0.088 and 0.022 for A_{cap} ↓) impose a higher risk of wooden beam decay, compared to the untreated wall, regardless of the impregnation depth. On the contrary, stronger impregnations (A_{cap}: 0.0044 and 0.0004 for A_{cap} ↓), completely eliminate the risk of wooden beam decay, according to the VTT wood decay model.

For the XPS-insulated wall (Figure 4-24), the risk of wooden beam decay is generally higher, due to the elevated moisture levels inside the masonry wall. Weak impregnations lead to a slightly increased risk of wood decay, compared to the untreated XPS-insulated wall. Impregnation depth seems to be an important factor for the impregnation strength with a capillary absorption coefficient 100 times lower than that of the untreated brick (A_{cap}: 0.0044 for A_{cap} ↓), as an impregnation depth of 4 cm leads to a low risk of wood decay, while a depth of 0.5 cm does not have a signifficant effect. Furthermore, the strongest impregnation (A_{cap}: 0.0004 for A_{cap} ↓) again eliminates the risk of wooden beam decay.

In the CaSi-insulated wall (Figure 4-25), the results are once again similar to the results of the uninsulated wall: weak impregnations have a either a negative or a neutral impact, while strong impregnations eliminate the risk of wooden beam decay.

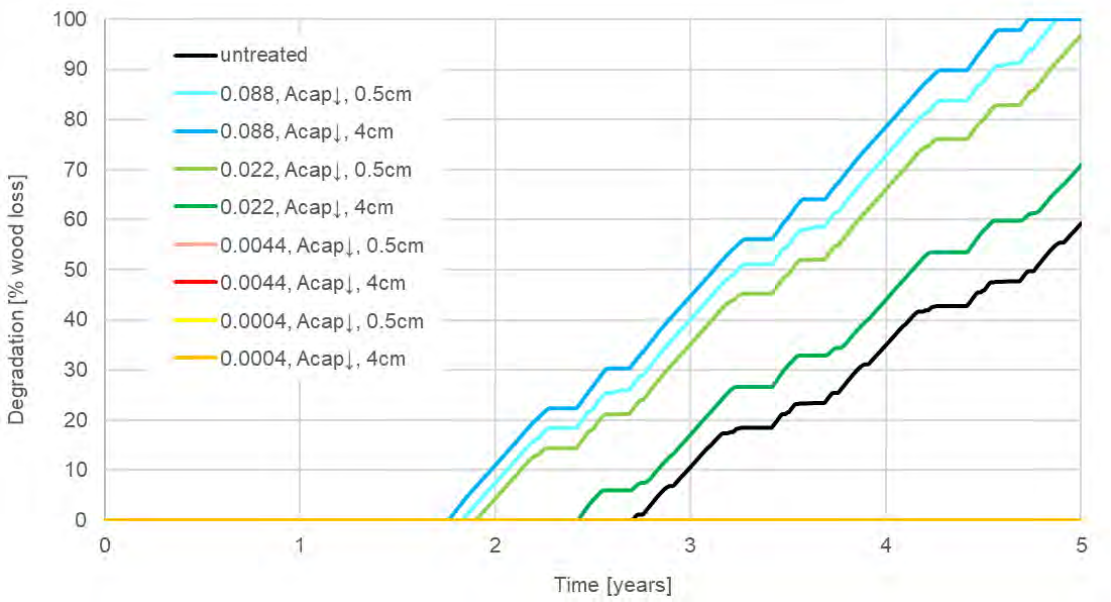

Figure 4-23: Wooden beam decay for uninsulated wall.

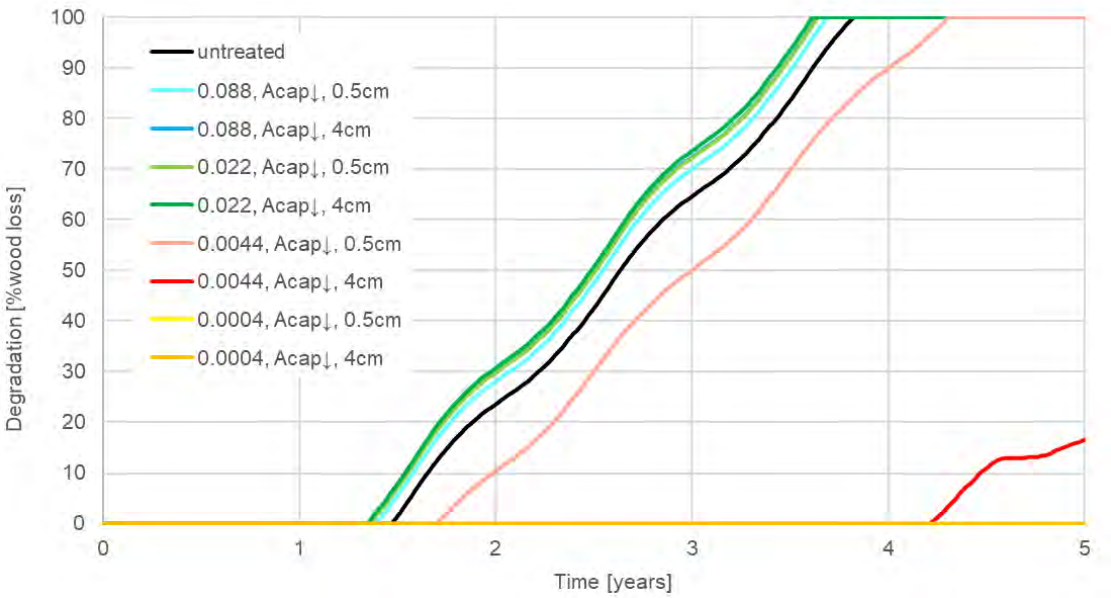

Figure 4-24: Wooden beam decay for XPS-insulated wall.

Regarding the effect of the thickness of the insulation on the risk of wooden beam decay, in the case of XPS-insulated wall, insulation thickness does not have a noteworthy impact. For the CaSi-insulated wall (Figure 4-27), a 6 cm-thick insulation has a positive but negligible effect on the risk of wood decay compared to the insulation with a thickness of 14 cm.

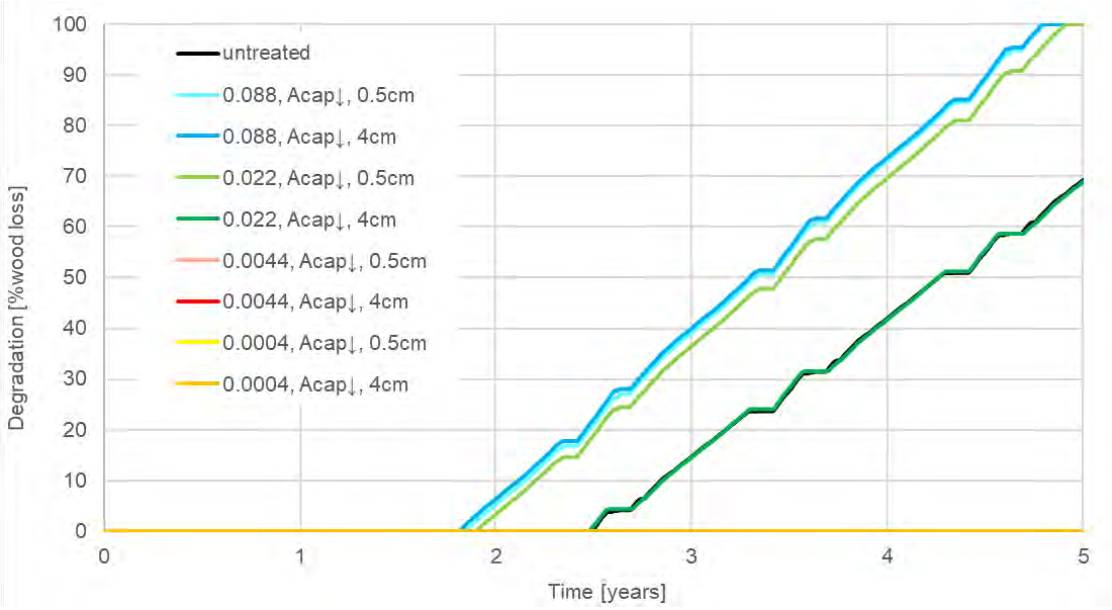

Figure 4-25: Wooden beam decay for CaSi-insulated wall.

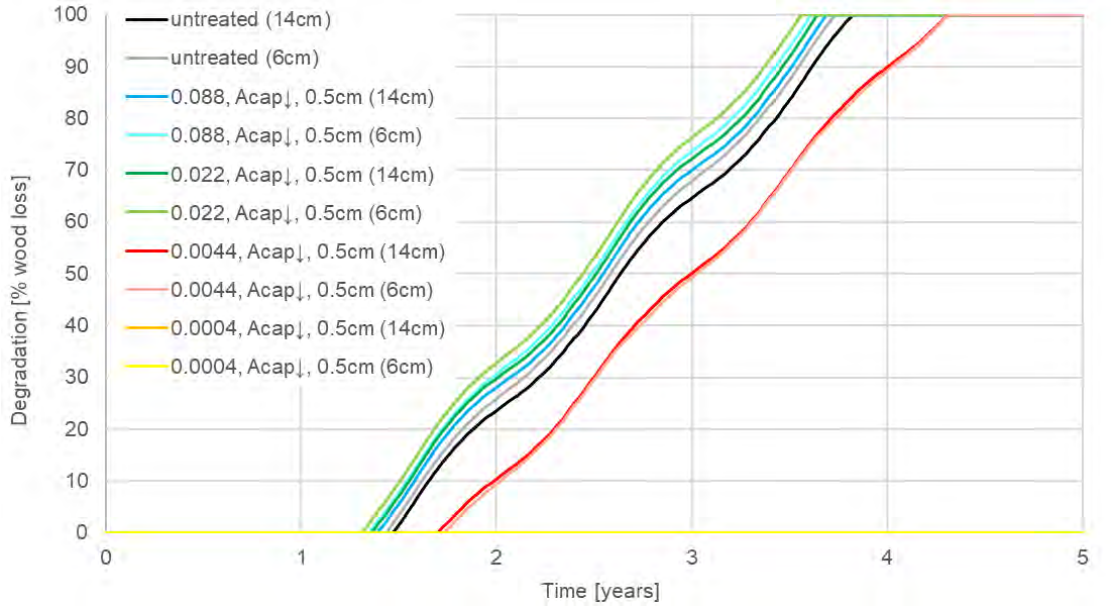

Figure 4-26: Effect of insulation thickness on wooden beam decay for XPS-insulated wall.

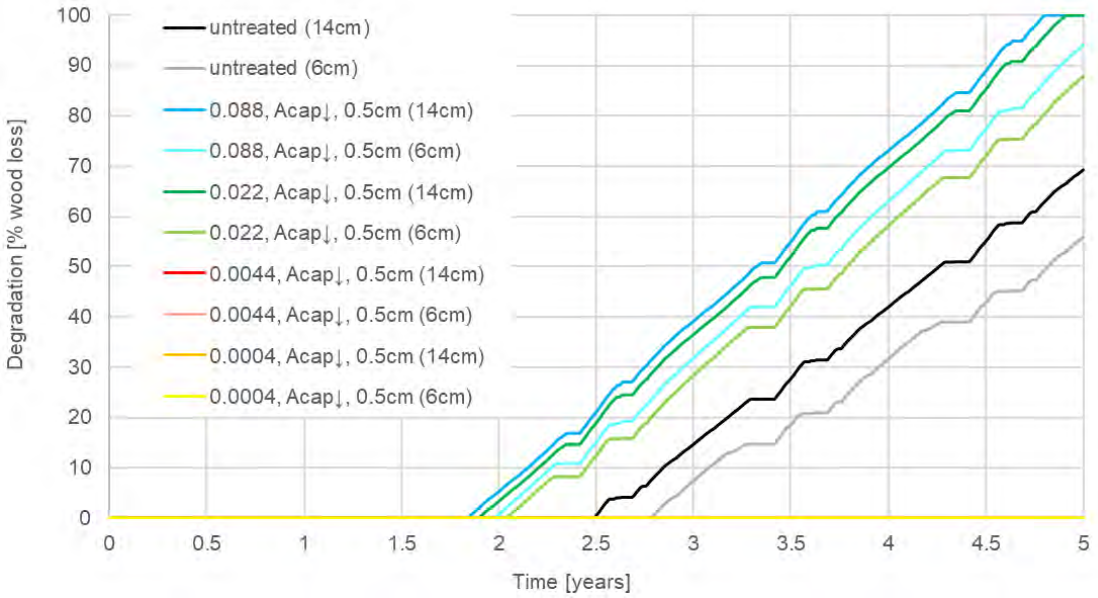

Figure 4-27: Effect of insulation thickness on wooden beam decay for CaSi-insulated wall.

4.3.5 Mold growth

XPS-insulated walls have, relatively seen, a very low risk for mold growth at the interior surface. The uninsulated wall and the CaSi-insulated wall with a thickness of 6 cm on the other hand demonstrate a higher risk regarding mold growth (CaSi-insulated walls with 14 cm insulation thickness behave in a way similar to XPS-insulated walls).

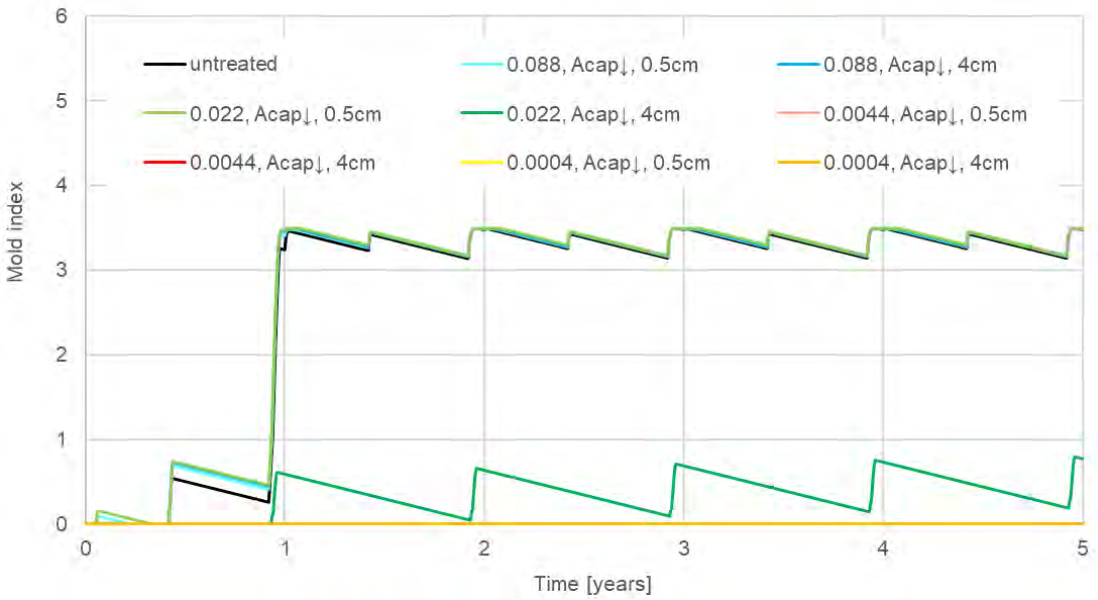

Figure 4-28: Mold growthfor uninsulated wall.

When the uninsulated wall is untreated, mold index rises rapidly at the end of the 1st year, and remains above 3 until the end of the simulation interval, implying that up to 10% of the surface area is visually affected by mold. Strong impregnations (A_{cap}: 0.0044 and 0.0004 for A_{cap} ↓) decrease the problem of mold growth in the uninsulated wall. When weak impregnations are applied (A_{cap}: 0.088 and 0.022 for A_{cap} ↓), mold growth remains practically unchanged compared to the untreated wall, regardless of

the impregnation depth, with the exception of the impregnation with A_{cap} 0.022 (for A_{cap} ↓) and impregnation depth of 4 cm, for which mold growth is significantly reduced but not eliminated. For the CaSi-insulated wall with an insulation thickness of 6 cm (Figure 4-29), mold growth occurs for the untreated wall and for all impregnation strengths, with the exception of the impregnations with A_{cap} 0.0004 (for A_{cap} ↓ & w_{cap} ↓) and the impregnation with A_{cap} 0.0044 (for A_{cap} ↓).

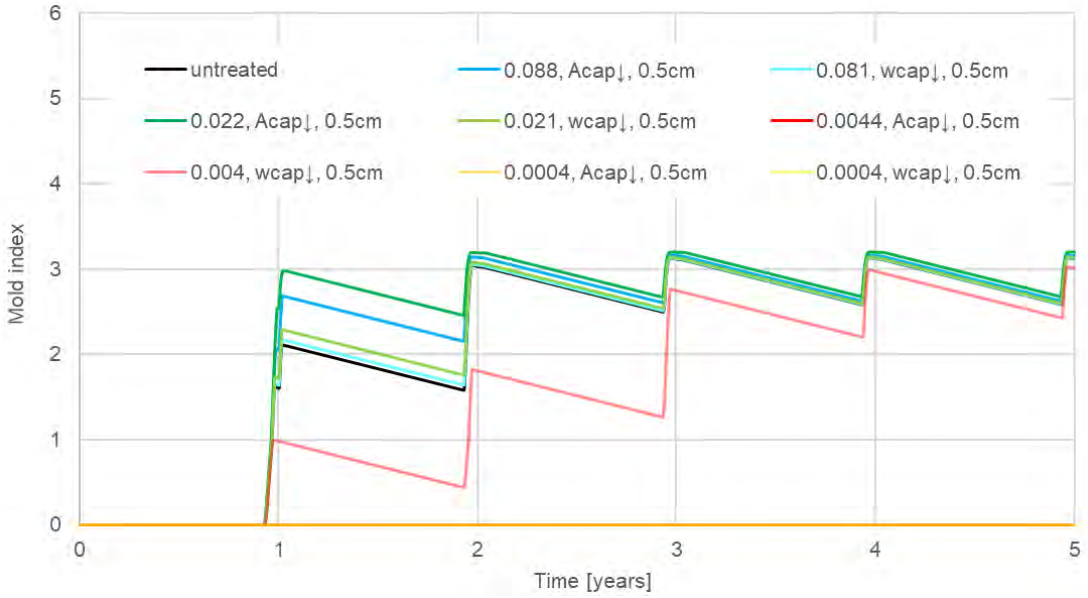

Figure 4-29: Mold growthfor CaSi-insulated wall (insulation thickness of 6 cm).

4.3.6 Heat loss

The total heat loss during the last heating season (October 1st – April 30th) is shown in Figure 4-30. It is apparent that type and thickness of the internal insulation system are the key factors when it comes to thermal behavior of the wall. Hydrophobization has the potential of further reducing the heat loss for both uninsulated and internally insulated walls. However, only strong impregnations (A_{cap}: 0.0044 and 0.0004 for A_{cap} ↓) are able to do so, since weak impregnations (A_{cap}: 0.088 and 0.022 for A_{cap} ↓) can increase, instead of reduce, the total heat loss. Even for strong impregnations, the effect of hydrophobization on the heat loss of the wall is small in the case of uninsulated wall and almost negligible in the case of the XPS-insulated wall, especially since for the latter, heat the loss is significantly reduced either with or without hydrophobization. Nevertheless, strong impregnations seem to have a largely positive impact when coupled with CaSi internal insulation and can further reduce the heat losses up to 57%, compared to the untreated CaSi-insulated wall (Figure 4-31).

The differences in heat loss between the vapor tight insulation system (XPS) and the capillary active system (CaSi) exist mainly due to the fact that the latter has higher thermal conductivity. In addition, capillary active systems have the capability of accumulating moisture inside the insulation and since strong impregnations reduce the moisture content of the masonry, hydrophobization (when applied succesfully) can increase the effectiveness of a capillary active system in terms of heat loss reduction. Therefore, a sufficiently hydrophobized wall in addition to a capillary active insulation can yield significant amounts of energy saving. Alternatively, a thin internal capillary active insulation (6 cm) coupled with hydrophobization can lead to the same amount of heat loss with those of a thick internal capillary active insulation (14 cm). In that way, the reduction of floor area will be smaller when an internal insulation system is installed, without experiencing greater heat losses.

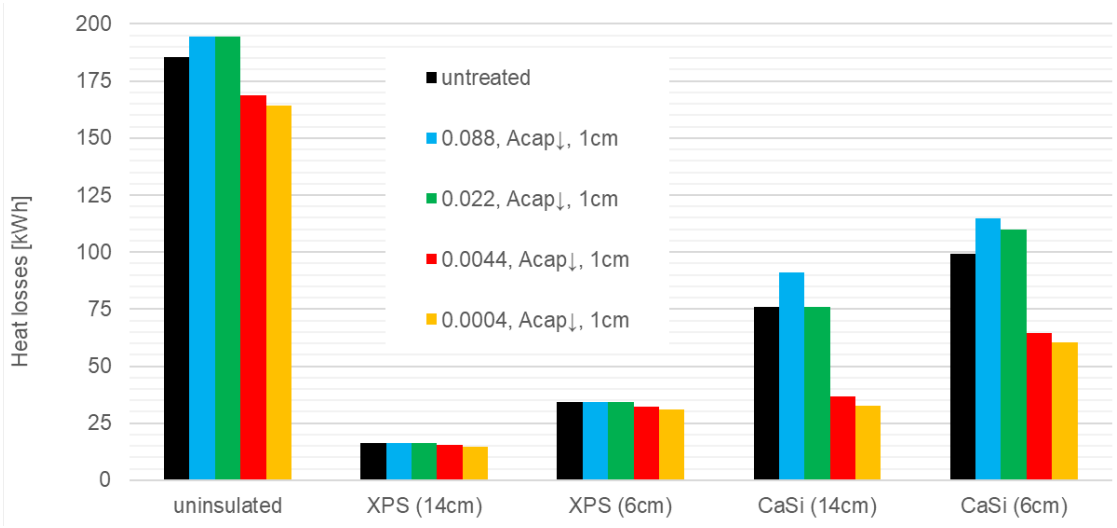

Figure 4-30: Total heat loss during the heating season (Oct 1st – Apr 30th).

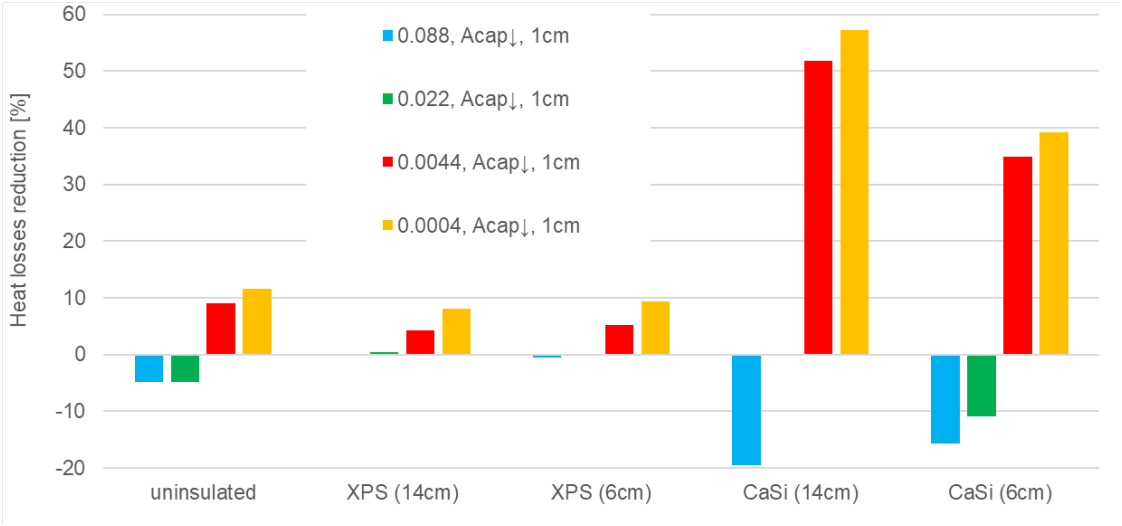

Figure 4-31: Percentage of heat losses reduction in comparison to the untreated wall, during the heating season (Oct 1st - Apr 30th).

4.4 Conclusions

This study focused on the impact of hydrophobization on the hygrothermal performance of masonry walls with internal insulation. For that purpose, numerical simulations were conducted with Delphin, a coupled heat and moisture transfer simulation program.

Initially, two methods of virtual hydrophobization were presented. Their main goal is the representation of a hydrophobized brick through a model that can be used for hygrothermal simulations. Both methods result in the reduction of the absorption coefficient of the virtually hydrophobized brick, while their main difference the modification of moisture storage of the brick. Then, the assessment of the hygrothermal performance of walls that combine internal insulation and hydrophobization takes place, based on the moisture content of the masonry walls, the risk of wood decay and mold growth and finally the heat loss of the wall during heating season.

A pattern that is persistent in most cases is that strong impregnations result in lower levels of moisture content inside the masonry, whereas weak impregnations can have a negative impact on the moisture content level, especially in XPS-insulated walls. The effect of impregnation depth is variable, according to the virtual hydrophobization method, the impregnation strength or the internal insulation type. In relation to wood decay and mold growth, strong impregnations generally lead to lower risks, while weak impregnations often increase the risk of moisture related damages. Regarding heat loss, hydrophobization is more effective when strong impregnations are combined with capillary active insulation systems. In general, it is shown that when hydrophobization succeeds in its main goal, preventing of liquid water from entering the masonry wall, there are many benefits for the hygrothermal performance of the wall. However, when there is water penetration due to wind-driven rain, the hygrothermal performance of the wall can deteriorate, resulting in increased risks for moisture-related damages.

References

Carmeliet J., Houvenaghel G., Van Schijndel J., Roels S. 2002. Moisture phenomena in hydrophobic porous building material Part 1: Measurements and physical interpretations. Restoration of Building and Monuments 8:165-183.

Engel J., Heinze P., Plagge R. 2014. Adapting hydrophobizing impregnation agents to the object. Restoration of Building and Monuments 20:1-8.

Finken G.R., Bjarlov S.P., Peuhkuri R.H. 2015. Effect of façade impregnation on feasibility of capillary active thermal internal insulation for a historic dormitory – A hygrothermal simulation study. Construction and Building Materials 113:202-214.

Fukui K., Iba C., Hokoi S. 2017. Moisture behavior inside building materials treated with silane water repellent. In proceedings of 11th Nordic Symposium on Building Physics, Trondheim, Norway.

Hamid A.A., Wallentén P. 2017. Hygrothermal assessment of internally added thermal insulation on external brick walls in Swedish multifamily buildings. Building and Environment 123:351-362.

Kunzel H.M., Kießl K. 2014. Drying of brick walls after impregnation. Bauinstandsetzen2:1-10.

Nikolai A., Grunewald J. 2015. User Manual and Program Reference Delphin 5.

Ojanen T., Viitanen H., Peuhkuri R., Lähdesmäki K., Vinha J., Salminen K. 2010. Mold growth modeling of building structures using sensitivity classes of materials. In proceedings of 11th Thermal Performance of the Exterior Envelopes of Buildings conference, December 5-9 2010, Clearwater Beach, United States.

Vereecken E. 2013. Hygrothermal analysis of internal insulation for renovation projects. Doctoral Thesis. KU Leuven.

Vereecken E., Van Gelder L., Janssen H., Roels S. 2015. Internal insulation for wall retrofitting – A probabilistic analysis of energy savings and hygrothermal risks. Energy and Buildings 89:231-244.

Viitanen H., Toratti T., Makkonen L., Peuhkuri R., Ojanen T., Ruokolainen L., Räisänen J. 2010. Towards modelling of decay risk of wooden materials. European Journal of Wood and Wood Products 68:303-313.

Viitanen H., Toratti T., Makkonen L., Thelandersson S., Isaksson T., Früwald E., Jermer J., Englund F., Suttie E. 2011. Modelling of service life and durability of wooden structures. In proceedings of 9th Nordic Symposium on Building Physics, May 29-June 2 2011, Tampere, Finland.

Zhao J., Meissner F. 2017. Experimental investigation of moisture properties of historic building material with hydrophobization treatment. In proceedings of 11th Nordic Symposium on Building Physics, Trondheim, Norway.

5 Hygric property measurements @ DTU

(Tessa Kvist Hansen, DTU[3])

5.1 General introduction

The following sections provides information on laboratory studies on hydrophobization performed at the Technical University of Denmark. The first study (Section 5.2), includes laboratory studies on hydrophobized samples of brick and air lime mortar. The study investigated the effect of 16 different hydrophobization agents on hygric properties such as water uptake, drying and vapor diffusion. Furthermore, the impregnation depth of each hydrophobization agent on both types of specimens was recorded.

The 2nd study (Section 5.3), describes an investigation of water migration through masonry in an experimental setup with masonry sections of the same types of brick and mortar as in Section 5.2. Nine 1½ brick thick masonry sections (~33x35cm), of which four were hydrophobized, had built-in temperature and relative humidity sensors, and different types of internal insulation. The wall sections were subjected to climate cycles with rain, radiation and cold climate, and the water migration through the masonry was studied.

The two studies focus on the efficiency and effect of various hydrophobization agents on historic masonry from a holistic point of view. The work has been published in the scientific journal Construction and Building Materials (Hansen et. al., 2018).

In terms of moisture safe internal insulation, hydrophobization may be a potential contributor to reducing moisture within masonry, by preventing ingress of liquid water (i.e. wind driven rain). For hydrophobization of masonry to be successful, it should firstly allow diffusion so that moisture does not get trapped in the walls, and secondly be able to reduce the water uptake over the entire area - both bricks and mortar joints. In Denmark, there has been a long tradition of the use of lime mortar, and up until 1960, lime mortars with 7-8% lime were the most commonly used (Teknologisk Institut, 2013). As lime does not contain silicates in itself, the silicone based hydrophobic agents maynot bind as well to lime mortar as to e.g. cement or brick. Some of the aggregates, e.g. sand, however may contain silicates, so some efficiency is assumed. Therefore, the effect of hygric properties on both brick and lime mortar samples was investigated with a variety of hydrophobization agents of all types; silane, siloxane, hybrid and nanotechnology. The study is presented in section 5.2: Hydrophobized brick and air lime mortar. A laboratory study of the efficiency of hydrophobization treatment of masonry with lime mortar and internal insulation holistically, is presented in section 5.3 Hydrophobized masonry sections – water migration. Furthermore, this experiment was made in order to study the performance of hydrophobization on masonry as a combination of siliceous brick and the less siliceous air lime mortar. The effect of hydrophobization was evaluated by monitoring water ingress during cycles of radiation, rain load, and cold climate.

[3] Activities performed while at DTU, currently at AAU

5.2 Hydrophobized brick and air lime mortar

5.2.1 Approach

As an initial investigation, 16 different hydrophobization agents were applied to specimens of brick and air lime mortar. The performance of each agent was evaluated based on water absorption, drying and impregnation depth. The initial investigation was performed to get an overview of the efficiency and differences between various types of agents. The investigation of the effect on vapor diffusion was performed with three different hydrophobization agents, that were chosen based on results from the initial investigation.

5.2.1.1 Materials

As the study refers to historic masonry, the experiments have been carried out on specimens of brick and lime mortar. Both the brick and mortar included in the study, were chosen to imitate historic building materials, and are used in larger scale studies of historic masonry at the Technical University of Denmark (Odgaard et al., 2018). The bricks were yellow soft-molded bricks from Helligsø Teglværk in Denmark, with a dry density of approximately 1677 kg/m^3. For the initial investigation, the mortar specimens provided were made of unspecified, carbonated lime mortar with open porosity between 0.26 (K-Q) -0.28 (A-J) m^3/m^3, and dry density of 1881 (A-J) – 1941 (K-Q) kg/m^3. The lime mortar used for the vapor diffusion experiments was a 7.7% lime mortar (air lime) with aggregates of 0-4 mm grain size with open porosity 0.33 m^3/m^3 and dry density 1752 kg/m^3.

For the initial investigation, 16 different hydrophobization agents were included; these are presented in Table 5-1. Most of the agents included in this study are based on silane or siloxane, or a hybrid of both. A few are based on nanotechnology.

5.2.1.2 Experimental methods

For the first three investigations (water uptake, drying, impregnation depth), the hydrophobization agents were applied to the specimens by two different methods. The liquid agents were applied to all sides of the specimens by shaking them in a plastic bag containing the agent for 10 seconds. The creamy products (I and J) were applied with a paint brush, in the amounts recommended by the manufacturer, see Table 5-1. The brick specimens were whole bricks, as it was desired to study the unbroken, external brick surface's susceptibility to the hydrophobization agents. Standard Danish brick dimensions are 228x108x54mm^3. The carbonated air lime mortar specimens were significantly smaller, and cut from a larger plate. The specimens were on average 93x40x30mm^3. One specimen of both brick and lime mortar was investigated for each hydrophobization treatment. The specimens were initially oven-dried at 105°C, and hereafter conditioned in room conditions before the application of hydrophobic treatment. The specimens were hydrophobized 14 days prior to the experimental execution.

Table 5-1: Hydrophobization agents included in the study, information as stated in technical data sheets of each agents.

	Active component (concentration of active component)	Liquid/ cream	Application method + coats	Consumption pr. coat [l/m^2 or g/m^2]
A	Siloxane and Fluoro Polymer (16%)	Liquid	Roll, paint brush, low-pressure sprayer or air-less sprayer, 1-2 coats	0.1-0.2 l/m^2
B	Copolymers (16%)	Liquid	Roll, paint brush, low-pressure sprayer or air-less sprayer, 1-2 coats	0.1-0.2 l/m^2
C	Various fluoric polymers (16%)	Liquid	Roll, paint brush, low-pressure sprayer or air-less sprayer, 1-2 coats	0.1-0.2 l/m^2
D	Silane, siloxane and Fluoro Polymer (16%)	Liquid	Roll, paint brush, low-pressure sprayer or air-less sprayer, 1-2 coats	0.1-0.2 l/m^2
E	Silane/siloxane (16%)	Liquid	Roll, paint brush, low-pressure sprayer or air-less sprayer, 1-2 coats	0.1-0.2 l/m^2
F	Siloxane copolymers and pefluorinated siloxane (16%)	Liquid	Roll, paint brush, low-pressure sprayer or air-less sprayer, 2-3 coats	0.1-0.2 l/m^2
G	Nanoparticle dispersion, isopropanol solvent (<13%wt)	Liquid	Airless standard low-pressure sprayer, roll or paint brush, min. 2 coats	0.062-0.075 l/m^2
H	Nanoparticle dispersion, isopropanol solvent (<3%wt)	Liquid	Roll, paint brush or air-less sprayer, 2 coats	0.1-0.125 l/m^2
I	Silane (80%)	Cream	Roll, paint brush or air-less sprayer, 1 coat	0.20-0.50 l/m^2
J	Silane (40%)	Cream	Roll, paint brush or air-less sprayer, 1 coat	0.15-0.20 l/m^2
K	*Unknown*	Liquid	Sponge, paint pad, cotton-cloth or sprayer, 2 coats	0.025-0.1 l/m^2
L	Chlorophyllane	Liquid	Roll, paint brush or low-pressure sprayer	0.08-0.17 l/ m^2
M	Flour-Acryl-Polymer and Alkyl-Acoxy Silane	Liquid	ND-sprayer with Viton seal, airless sprayer, roll, paint brush, 1-2 coats	90-170 g/m^2
N	Alkylalcoxysilane	Liquid	Brush or low-pressure sprayer, 1-3 coats	180-230 g/m^2
O	Silane >20%	Liquid	Low-pressure sprayer with Viton seal, 2-3 coats	2-300 g/m^2
P*	Silane/siloxane (100%)	Liquid	Roll, Paintbrush or sprayer, 2 coats	10-40 g/m^2 (110-440 g/m^2 diluted)
Q	Reference	-	-	-

* *Agent P is a 2-component hydrophobization agent, diluted 1:11 with organic solvent (e.g. mineral turpentine)*

The initial investigation of the 16 different hydrophobization agents presented in Table 5-1, section 5.2.2.2, consists of three different experimentations; water uptake by full immersion, drying, and impregnation depth. Based on the initial investigation, the agents were evaluated by means of a ranking system applied to the three parameters, for both brick and mortar. Impregnation depth was ranked according to percentage of half the specimen's thickness, specimens with full impregnation were thus given a score of 100%. The water uptake was ranked by the final mass% increase by the end of the experiment, as a percentage relative to the reference specimen. The drying was ranked by the percentage difference between the initial slopes of the drying graph for each treatment relative to the reference specimen. The final ranking score was the sum of the three scores for the three categories, and a higher score yielded an overall better performance of this agent. A combined score for brick and mortar consists of the sum of the final score for each material.

The formulas used for the ranking system, can be seen below in Equation 5-1 to Equation 5-5:

1) Impregnation depth	$\frac{registered\ penetration\ depth}{\frac{specimen\ thickness}{2}} \cdot 100$	[%]	**Equation 5-1**
2) Water uptake	$\frac{mass\ increase_{reference} - mass\ increasese_{specimen}}{mass\ increase_{reference}} \cdot 100$	[%]	**Equation 5-2**
2a) Mass increase	$\frac{mass_{end} - mass_{initial}}{mass_{initial}} \cdot 100$	[%]	**Equation 5-3**
3) Drying	$\frac{initial\ slope_{reference} - initial\ slope_{specimen}}{initial\ slope_{reference}} \cdot 100$	[%]	**Equation 5-4**
3a) Initial slope*	$\frac{y_2 - y_1}{x_2 - x_1}$	[-]	**Equation 5-5**

** The initial slope is calculated based on values from timestep 0 (x_1=0) to timestep 4020 minutes (x_2=4020)*

Specimens for vapor diffusion test

For the investigation of the influence of hydrophobization on vapor diffusion in specimens, three agents (J, N and P) were examined on three specimens with each agent, in addition to three reference specimens of both brick and mortar. Prior to the experiment, the specimens were cut into Ø80mm specimens and sealed in Ø100mm plastic rings designed for the cups. Mortar specimens were sealed in a plastic ring with silicone, and the brick specimens were sealed with epoxy, as seen in Figure 5-4. The specimens were hydrophobized on the top side faciung conditions in the climate, with the recommended application methods; the liquid agents, N and P, were applied with a sprayer with the number of layers specified in data sheets (N: 3 layers, P: 2 layers). The creamy agent, J, was applied in 1 layer, with specified amounts. Specimens were weighed before and after application of each layer, and the specific amounts are presented in Table 5-2.

Table 5-2: Applied hydrophobization agent on test specimens for water vapor diffusion experiment.

	Consumption of hydrophobization agent [g]						**Producer specified consumption pr. layer**
	Brick			**Mortar**			
	Layer 1	Layer 2*	Layer 3*	Layer 1	Layer 2*	Layer 3*	[g]
J1	1	-	-	1.3	-	-	
J2	0.9	-	-	1.5	-	-	~0.8
J3	1.1	-	-	1.5	-	-	
N1	1.1	1.2	1.2	1.3	0.9	1.2	
N2	1.3	1.1	1.3	1.1	1	1.6	~0.9-1.1
N3	1.2	1.2	1	1.2	1.2	1.3	
P1	1.3	1.3	-	1.1	0.9	-	
P2	1.3	1.1	-	1.4	0.9	-	~0.5-2.0
P3	1.2	1.1	-	1.1	1	-	

** Layers 2 and 3 were applied wet in wet*

Water uptake

The water uptake experiment was performed as full immersion experiments. The treated specimens were weighed and then placed on triangular spacers in a water tank, with a water level above the top of the specimen, as seen in Figure 5-1. The mass of the specimen was recorded before immersion, and after immersion at the following intervals; 2, 4, 8, 16, 30, 120, 180, 240, 300 minutes, as well as one final measurement 20-28 hours after immersion. At every weighing, each specimen was dried off with a damp cloth, to avoid hanging water affecting the results. The measurements were transformed into mass% increase, and plotted in a diagram over time; thus, the absorption of each specimen over time can be studied graphically.

Figure 5-1: Experimental setup of full immersion water absorption experiments on brick (left) and mortar (right).

Drying

After the water absorption experiment has finalized, all treated specimens and reference specimens were saturated by means of vacuum in desiccators (Figure 5-2) prior to initiating the drying experiment. For the vacuum saturation, boiled and cooled demineralized water was used. Hereafter, the specimens were placed on triangular spacers in a climate chamber of approximately 20°C and 85% relative humidity to dry. The initial drying was monitored with six weighings during the first hour, and hereafter one measurement per day or two days was carried out during the duration of six weeks for bricks and 17 days for mortar. The measurements were transformed into moisture content, which is illustrated graphically as a function of time.

Figure 5-2: Vacuum saturation of brick in desiccator (left), and drying in climate chamber of brick (middle) and mortar (right).

Impregnation depth

The specimens were broken in half with a hammer and chisel as seen in Figure 5-3, and the broken side sprayed with water to visually define the impregnation depth of the hydrophobization agents. The impregnation depth was measured at seven evenly distributed locations on both of the long sides, and one location on each short edge.

Figure 5-3: Halving of brick specimens with hammer and chisel (left), marking of 7 measuring locations on both sides (agent L), and example of visible impregnation depth, the lighter area around the brick (agent E).

Vapor diffusion

The experiment was carried out according to DS/EN ISO 12572 – Hygrothermal performance of building materials and products – Determination of water vapor transmission properties.

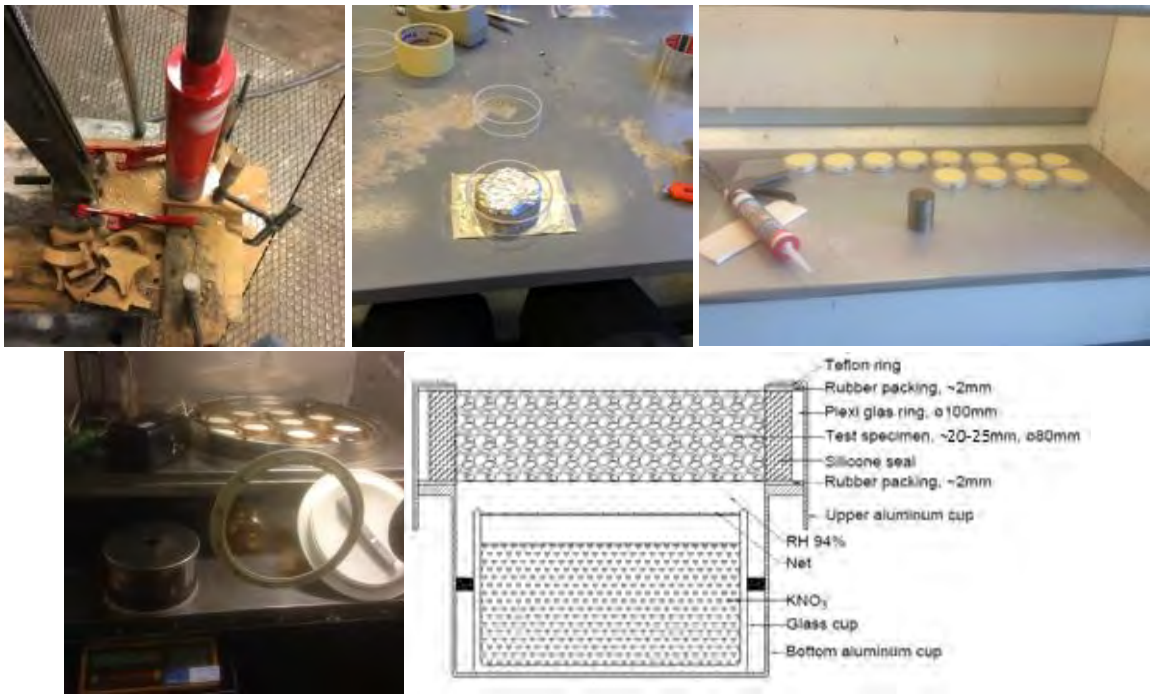

Figure 5-4: Top row: Preparation of specimens for cup experiment; brick cutting with a core drill, sealing lime mortar specimen in plexi glas rings with silicone, specimens in cups placed in climate chamber (right). Bottom: Illustration of the specimen in the specially designed cup.

The principle of the experiment is sealing a specimen in a cup containing an aqueous saturated solution, in this case KNO_3 (94% relative humidity). The cup was placed in a climate chamber with controlled temperature (23°C) and relative humidity (50%) conditions. Due to different partial vapor pressures on both sides of the specimen vapor flow occurs, and by daily weighings for a week, the rate of water vapor transmission in steady state can be determined, and further transformed into water vapor diffusion resistance factor, μ. Figure 5-4 illustrates the specimen preparation and experimentation.

5.2.2 Results

5.2.2.1 Water uptake

Results from the water uptake experiments are displayed in Figure 5-5 and Figure 5-6 for brick and mortar respectively. For the brick specimens, a large difference in water absorption was observed. After 300 minutes, agents A, B, C, D, K and L had reached saturation to the same degree as the reference specimen Q. Agents F and H followed closely with initial absorption, but took the durance of the experiment to reach saturation. Agents G and P are in the middle of the absorption range, and finally agents E, I, J, M, N and O have a mass increase of less than 2% during the duration of the experiment, and are thus deemed to be the most successful agents in regards to low water uptake.

For the mortar specimens, the results seem more random for the various agents. However, as can be seen in Figure 5-6, treatments N and O seem to have no effect on the mortar, as they quickly absorb the same amount of water as the reference specimen. Agents M and P gain less than 2% mass during the duration of the experiment, and agents E, G, H and K gain less than 5% mass during the experiment.

Figure 5-7 distinctly shows the effectiveness of the various hydrophobization agents, and it is clear that there is relatively no mass increase in brick specimens treated with E, I, J, M, N and O, all silane based except E which is a hybrid. For the mortar specimens, the largest effect of hydrophobization is seen from agents M and P, silane based and hybrid.

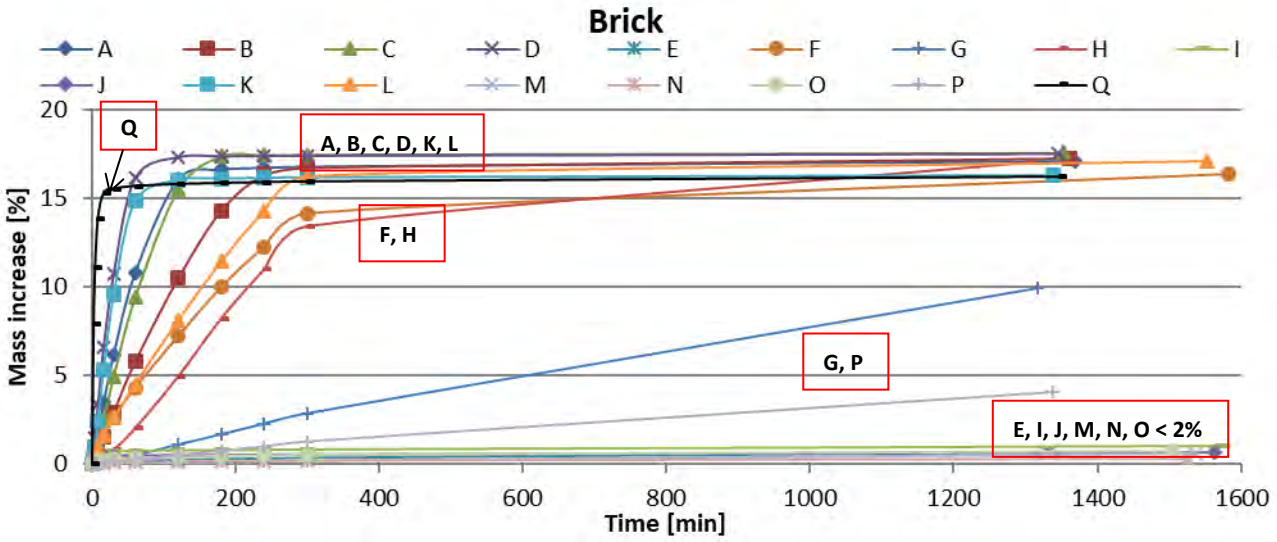

Figure 5-5: Mass increase by full immersion over time for brick specimens with hydrophobization agent A-P. Q is reference specimen.

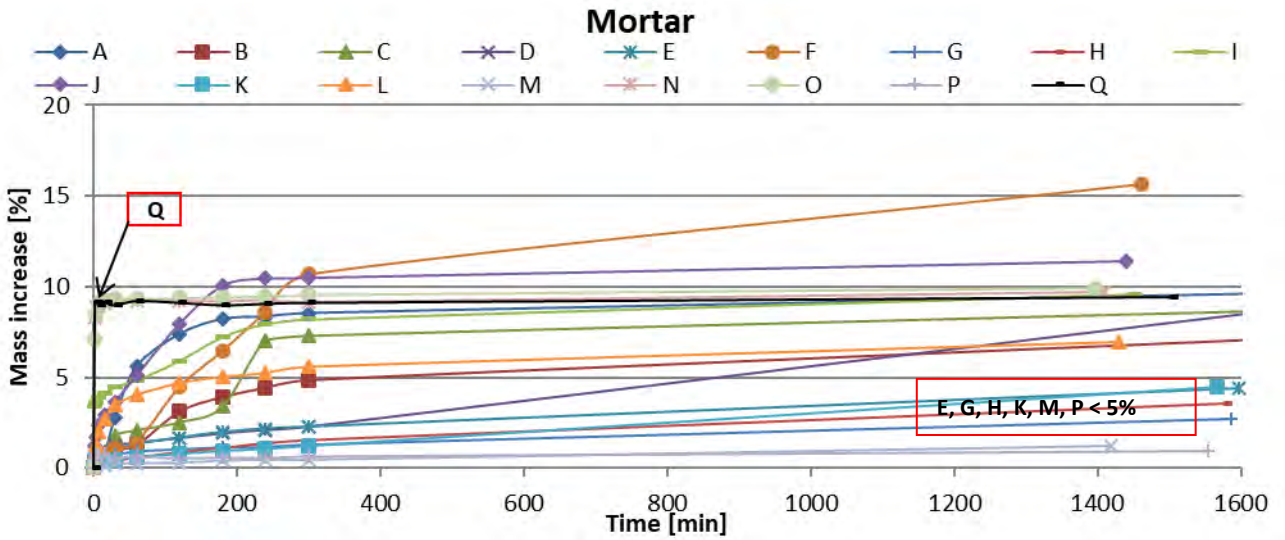

Figure 5-6: Mass increase by full immersion over time for mortar specimens with hydrophobization agent A-P. Q is reference specimen.

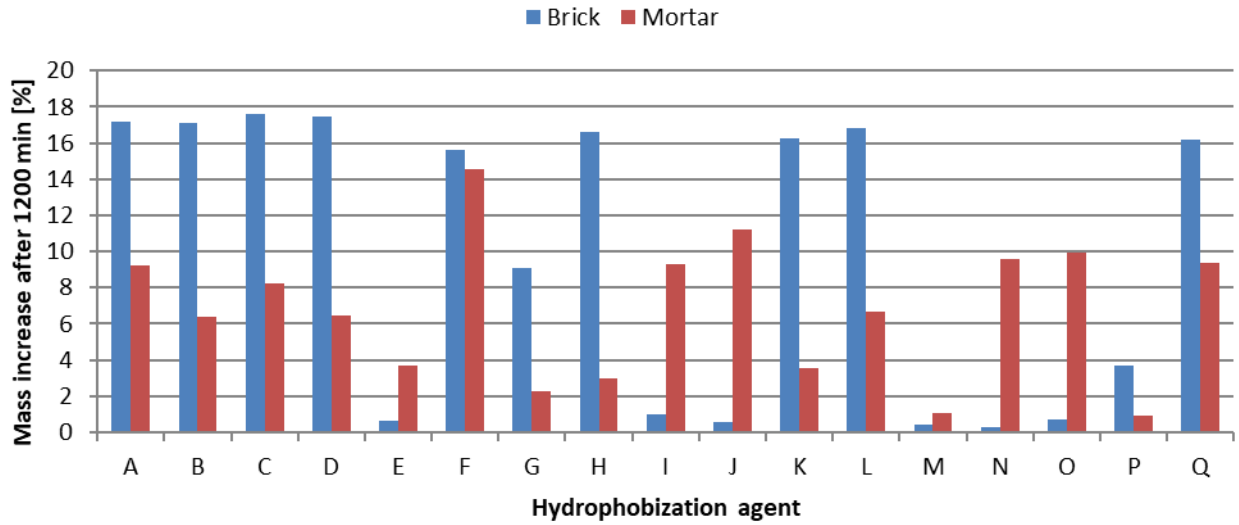

Figure 5-7: Bar chart of the mass increase of each specimen after 1200 minutes of full immersion. Q is reference specimen.

5.2.2.2 Drying

The results from the drying experiments are shown in Figure 5-8 and Figure 5-9 below. To the right, the initial drying period is shown as a section, where all the specimens' initial moisture content is adjusted, for a better visualization of the various slopes for different hydrophobization agents. The initial slopes of the drying curves are especially interesting, as this is where liquid transport to the surface occurs. Actual rain events are assumed not to yield vacuum saturated materials however. It can be seen that brick specimens, A, I, J, N, and O have the fastest initial drying, and several specimens showed a faster drying than the reference. In terms of long-term drying, brick specimens with agents A, B, C, D, F, H, K, M, N and O reach levels of relatively constant moisture content, and are all less than 1% moisture content. In regards to mortar specimens, the initial drying is most rapid in specimens with agents H, K, L, N and O.

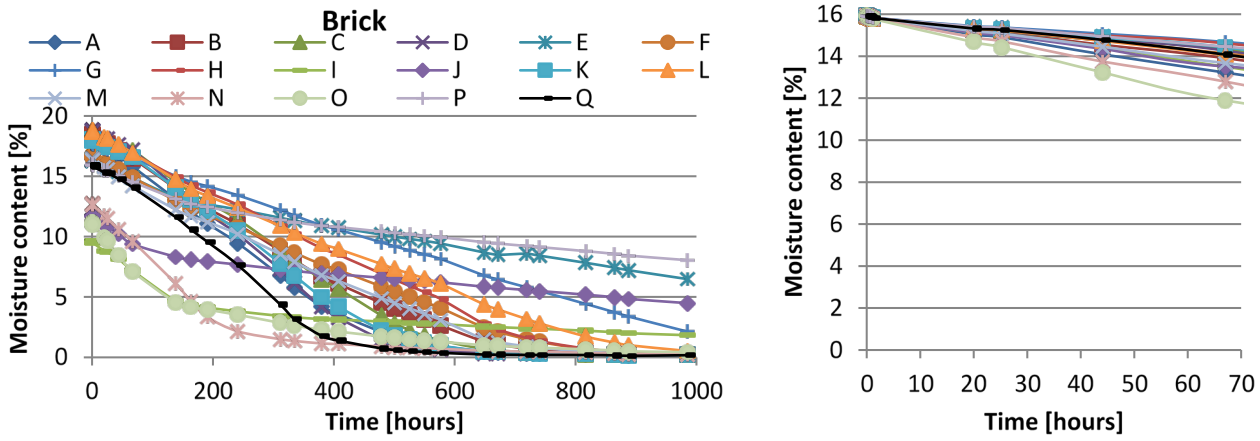

Figure 5-8: Moisture content reduction of brick during drying time in climate chamber. Right: All moisture contents are adjusted to the same initial moisture content.

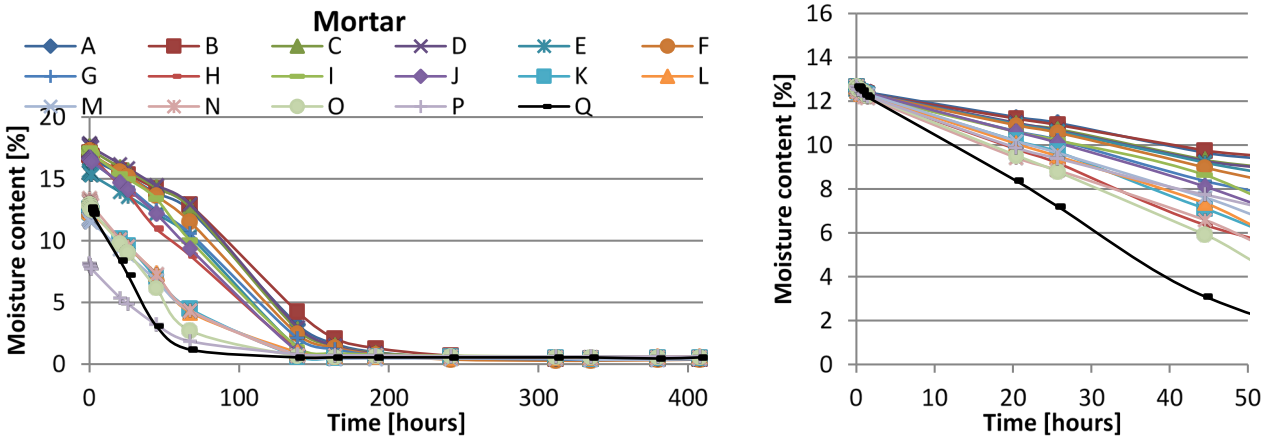

Figure 5-9: Moisture content reduction of mortar during drying time in climate chamber. Right: All moisture contents are adjusted to the same initial moisture content.

Table 5-3: Initial slopes of the various drying curves, generated for the first 67 hours of the experiment for brick, and 45 hours for mortar specimens.

Hydrophobization agent	Brick		Mortar	
	Initial slope	Relative to reference [%]	Initial slope	Relative to reference [%]
A	-0.0403	47	-0.0681	-68
B	-0.0301	9	-0.0658	-69
C	-0.0239	-13	-0.0755	-65
D	-0.0248	-10	-0.0767	-64
E	-0.0225	-18	-0.0783	-64
F	-0.0268	-3	-0.0833	-61
G	-0.0186	-32	-0.0972	-55
H	-0.0196	-29	-0.1421	-34
I	-0.0362	31	-0.0910	-58
J	-0.0361	31	-0.1028	-52
K	-0.0223	-19	-0.1254	-42
L	-0.0279	1	-0.1197	-44
M	-0.0336	22	-0.1141	-47

N	-0.0468	70	-0.1371	-36
O	-0.0602	118	-0.1520	-29
P	-0.0220	-20	-0.1111	-48
Q (ref)	-0.0276	-	-0.2154	-

In Table 5-3 an overview of the different initial slopes can be seen. The drying slopes for the mortar specimens are generally higher than those for the brick specimens. All the mortar specimens show slower drying compared to the reference, while there is much more variation in the drying velocity in brick specimens, as some bricks (A, B, I, J, L, M, N, O) exhibit faster initial drying than the reference, and the rest of the specimens show slightly slower initial drying.

5.2.2.3 Impregnation depth

The average impregnation depth of the hydrophobization agent is presented below, in Table 5-4 and in Figure 5-10 as a percentage of half the specimen thickness. It is seen that for both brick and mortar, agents I and J, which are both silane-based, creamy agents, have high impregnation depths. Furthermore, agents E, F, G, and L (hybrid, siloxane, nanotechnology and chlorophyllane) have high impregnation depths in the mortar samples. Brick specimens with agent N and O, both silane-based, leave an undefinable pattern of a dark/wet ring around the edges when compared to other samples, rather than being dry. However, no water absorption in the specimen yields the conclusion of almost full impregnation; see Figure 5-11-Figure 5-13.

Table 5-4: Impregnation depth [mm]

	Brick	Mortar
A	2,1	2,6
B	1,9	4,6
C	0,7	5,6
D	0,9	6,6
E	5,1	16,0
F	2,0	13,0
G	1,6	16,2
H	1,7	3,4
I	17,6	15,4
J	11,4	16,1
K	1,2	3,3
L	0,9	10,9
M	2,7	5,0
N	26,7	1,1
O	27,1	2,0
P	5,4	1,7
Q	0,0	0,0

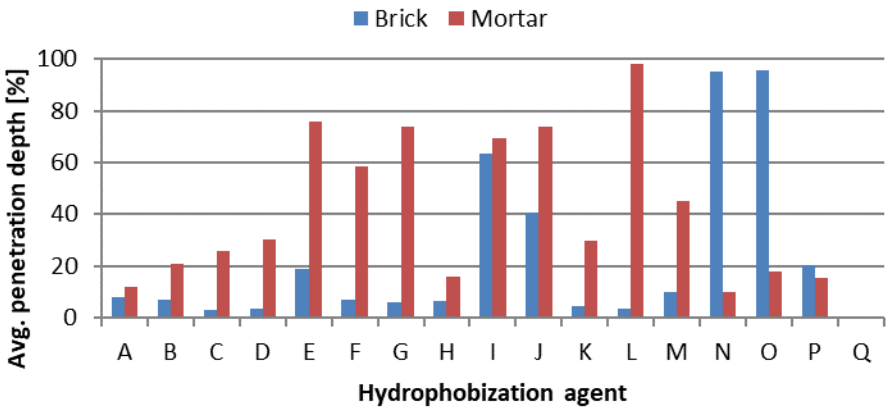

Figure 5-10: Impregnation depths, presented as percentage of ½ specimen thicknesses.

Figure 5-11, Figure 5-12, and Figure 5-13 illustrate three examples of impregnation depth in brick and mortar of agent I, F and O respectively. The difference in impregnation depth in the brick specimens was very apparent. For the brick specimen with agent F, there was only a thin, external line of dry material, whereas agent I was seen to penetrate deep into the brick. For mortars, agent I had fully penetrated the specimen, and water-drops lay on top of the specimen. The impregnation of agent F on the mortar sample was very uneven.


Figure 5-11: Impregnation depth of agent I on brick and mortar.


Figure 5-12: Impregnation depth of agent F on brick and mortar.


Figure 5-13: Impregnation depth of agent O on brick and mortar.

5.2.2.4 Vapor diffusion

Results from the water vapor diffusion experiment are seen in Table 5-5 and Figure 5-14 as averages and standard deviations pver the three specimens of each type. It can be seen that the diffusion resistance factor is not affected significantly by the three investigated hydrophobization treatments. There is however, a slight tendency of reduced water vapor diffusion resistance factor with the application of hydrophobization treatment. This tendency is attributed to uncertainties in the experiment.

Table 5-5: Average water vapor diffusion resistance factor and standard deviation

	μ [-]	**Standard deviation** [-]
Brick Q, ref	12.7	1.0
Mortar Q, ref	7.7	1.2
Brick J	12.2	2.8
Mortar J	7.7	1.1
Brick N	11.7	0.7
Mortar N	5.5	2.0
Brick P	11.5	1.3
Mortar P	6.7	0.9

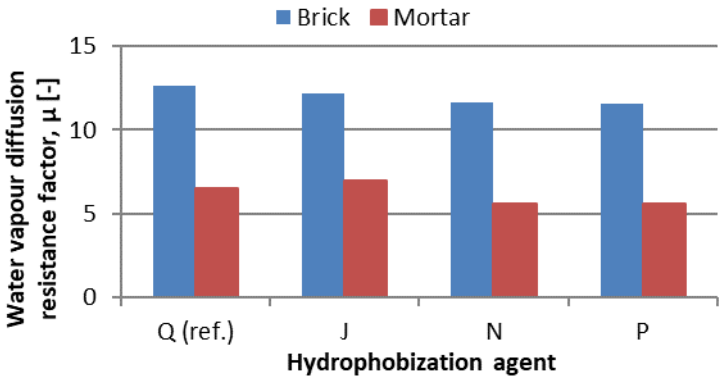

Figure 5-14: Graphical illustration of water vapor diffusion resistance factor on specimens with no treatment (Q) and treatments J, N and P.

5.2.3 Discussion

It should be noted, that for the initial investigation, agent P was not diluted, as this was unknown information at the time. Agent P was developed for calcareous materials; however, the erroneous application may be the reason for the less pronounced effect on lime mortar. As previously mentioned, specimens were vacuum saturated with hydrophobization agent on the drying surfaces prior to the drying experiment. As seen in Figure 5-8, brick specimens with agents I, J, N, and O did not reach the same saturation as other specimens. The vacuum saturation of these specimens was repeated to check for error in the saturation procedure. There was no error however, and the explanation was

found during the impregnation depth experiment. These silane-based agents simply penetrated the brick to such an extent that there was less room for water in the pores. It could also had been, that despite the vacuum, these agents blocked the saturation, as they all exhibited low water absorption (<2%) as well. The high impregnation depth and effectiveness exhibited by agents I and J, may be attributed to the application method, as these creamy agents were applied with a paint brush and in specified amounts, as opposed to the liquid agents which were applied to specimens by a 10 second exposure. For mortar specimens, it should be noted that specimens K, L, M, N, O, P, and Q had a slightly lower porosity, also giving these specimens a relatively lower degree of saturation.

The water uptake experiment took place for 24 hours, and naturally, it is not assumed that an actual rain event will strain a façade to the same degree, however, the experiment was conducted for the purpose of comparison between the different agents. Only one specimen of each agent, on brick and mortar, respectively, were investigated in the initial investigation, yielding the possibility of error, or erroneous results due to minor varieties in the samples. Also, a masonry wall will never undergo the same level of saturation as the vacuum saturated specimens prior to the drying experiment did. In reality, a wall would be much less saturated. The vacuum saturation was performed to achieve a similar moisture content basis.

For all of the experiments there are sources of error connected to measurement equipment and human error. For experiments with weight and dimension registration, the scale and caliper both have limitations. Scales used for the drying experiment were only ±0.1g, for the water uptake experiment the precision was ±0.01g, and for the investigation of influence on vapor diffusion, a ±0.001g scale was used. The caliper used for determination of specimen dimensions was 2 decimals. All specimens, especially mortar specimens, were irregular and the square (water uptake, drying and impregnation depth) and round shapes (vapor diffusion) were assumed for determination of dimensions. As the errors should be the same for all specimens in this comparative analysis, the effect of the errors is neglected. The sensors used in the investigation of water migration through masonry had an accuracy of ±1.8% RH and ±0.2°C.

For water absorption experiments on brick specimens, the best performances were seen in agents E, I, J, M, N, and O, which were primarily silane-based agents and one hybrid. For specimens of lime mortar, the effectiveness of the different agent types was not pronounced, as the best performers were a variety of types (silane, hybrid and nano). The drying experiment showed that brick specimens A, I, J, N, and O (primarily silane based) had the most rapid initial drying, whereas H, K, L, N, and O (a variety of types) exhibit fastest initial drying for mortar specimens. Brick specimens A, B, C, D, F, H, K, L, M, N, O, and Q reached constant levels of less than 1% after 1000 hours in the drying chamber, whereas all mortar specimens reached this level within 250 hours, but these specimens were also rather small.

As stated in the experiment description, the drying experiment was carried out in a climate chamber with a temperature of 20°C and 85 % RH. These conditions may not have been representative for real boundary conditions for a masonry wall, as it is also exposed to e.g. solar radiation and wind. However, for comparison purposes, these conditions were expected to give a correct picture of the influence of surface treatment on drying potential.

The ranking, performed as described in Section 5.2.2.2, of the various hydrophobization agents based on the initial investigation is seen in Table 5-6. The water uptake experiment distinctly showed the reduction in initial water uptake for most hydrophobization agents, as expected, due to the purpose of the surface treatment. This was also illustrated in (Kvist Hansen et al., 2016). It is evident that

hydrophobization treatments of silane rather than siloxane (O, N, I, J, and M) seemed to perform better overall, and especially on bricks. However, they seemed less efficient on the lime mortar. I and J performed better on the mortar, compared to O and N, which may be explained by the creamy consistency and application method. On the mortar, agents G, E, M, L and P seemed the most efficient; these are hybrids, silane and nanotechnology based.

Table 5-6: Ranking of the various hydrophobization treatments for brick and mortar altogether, and brick and mortar individually.

Brick and mortar	∑Score	Brick	∑Score	Mortar	∑Score
O	297	O	314	G	116
N	239	N	268	E	90
I	230	I	189	M	85
M	213	J	168	L	82
J	195	M	128	P	57
E	186	E	96	H	44
P	132	P	75	I	41
G	128	A	49	K	40
L	81	G	12	J	27
K	25	B	10	Q (ref)	0
H	17	F	4	O	-17
Q (ref)	0	Q (ref)	0	B	-24
A	-9	L	-1	D	-24
B	-14	D	-15	N	-29
D	-39	K	-15	C	-31
C	-50	C	-19	A	-58
F	-64	H	-27	F	-68

Overall, it was seen that brick generally is more responsive to hydrophobization treatment, and the effect is more pronounced in brick samples. The silane-based agents seemed to perform better in the initial investigation, and agent M was represented in top-5 of all the ranking lists.

A study from 2015 of masonry walls with severe wetting (Guizzardi et al., 2015) yielded information about migration of external water loads through masonry. The experiment revealed that interfaces posed as hydraulic resistances/barriers, and that the moisture transport occurred faster in the fine porous bricks than in mortar joints. This being the case, the lesser efficiency observed in hydrophobization of the lime mortar may not be crucial for the overall effect of hydrophobization on a masonry construction. In contrast, van Hees found that the mortar joints were the weakest part of hydrophobized masonry (Van Hees, 1998). He observed a difference in the efficiency of hydrophobization treatments on brick and mortar, yielding mortar joints a possible way for water ingress, which emphasized the need for hydrophobization efficiency of masonry in a holistic perspective.

Many historic façades have been renovated since the 1940's; thus, it can be expected that the external part of the joints in some cases has been replaced with a cementitious, siliceous mortar, and why the effect of hydrophobization on this type of mortar should be investigated. Macmullen *et al.* have investigated the efficiency of silane water repellent impregnation on cement-based mortars and concrete, and found that the capillary suction was significantly reduced (Macmullen et al., 2011). Slapø *et al.* have found, that fresh mortars with high water content improved masonry's resistance to WDR, as the mortar-brick interface becomes less porous (Slapø et al., 2017). Therefore, for renovation of façades, mortar with a high water content is recommended, thereby reducing the water ingress in itself, and enhancing the effect of a hydrophobization treatment.

The hydrophobization treatments examined did not seem to have a negative effect on the drying capability of specimens, nor the diffusion resistance. Engel *et al.* (Engel et al., 2014) have also performed a study on water absorption, drying and vapor diffusion of hydrophobized brick specimens. They examined five silane-based creams of different concentrations, and two fluid hybrid agents. They also found significant water absorption reduction, and with no influence on the vapor diffusion resistance. Their drying experiment showed that specimens hydrophobized with agents of lesser concentration of active ingredients, dried faster, thus an impregnation should be applied with the lowest, effective concentration. The present study did not show the same results in regards to concentrations and drying, as different agents were used, and not only various concentrations of an active component. An older study from 1995 by Charola found a reduction of 5-10 % in water vapor permeability with silicon-based hydrophobization treatments (Charola, 1995). Couto *et al.*, who investigated silicone-based water-repellents on ceramic brick, also found a reduction in vapor permeability of hydrophobized brick specimens in some water-repellent treatments (Couto et al., 2011). Van Hees (Van Hees, 1998) found a limited effect of hydrophobization on vapor diffusion as in the present study, however, he found the hydrophobization treatments to have a high impact on the drying process, as also found by Couto *et al.* (Couto et al., 2011) for most investigated treatments.

Lubelli *et al.* tested the efficiency of two nano-coatings on bricks, and found significantly reduced water absorption, and little effect on the drying, however, the impregnation depth was found to be much lower than traditional products (Lubelli et al., 2011). The nano-coating included in this study, namely G and H, performed well on mortar specimens in regards to water uptake and drying, however, the impregnation depth here was found to be similarly small.

5.2.4 Conclusions

The study concludes that a hydrophobization treatment had the desired effect of reduced rainwater penetration on historic masonry, however this effect was more pronounced in brick as compared to lime mortar. For specimens of ceramic brick, silane-based agents proved to have the best properties, however, for mortar a variety of active components were most efficient. Drying of treated specimens was not significantly influenced for brick; however, the drying of lime mortar was slightly impeded by the hydrophobic treatment. Furthermore, the investigation showed that the vapor diffusion, through both brick and mortar, was not influenced by the hydrophobization treatments.

5.3 Hydrophobized masonry sections – water migration

5.3.1 Approach

Nine masonry wall sections were constructed with built-in temperature and relative humidity sensors, and four of the walls were hydrophobized. The wall sections were subjected to cyclic climatic loads, including wind driven rain.

5.3.1.1 Materials

The experiment has been carried out on masonry sections constructed of the same type of brick, as presented in Section 5.2.2.1; the bricks were yellow soft-molded bricks from Helligsø Teglværk in Denmark, with a dry density of approximately 1677kg/m^3. The lime mortar was a 7.7% lime mortar (air lime) with aggregates of 0-4mm grain size with an open porosity of 0.33m^3/m^3 and dry density

of 1752kg/m^3. The hydrophobization agent applied to four of the nine wall sections, was a creamy, silane-based hydrophobization agent (agent J in Table 5-1, section 5.2.2.2). The internal insulation materials applied to the wall sections were a foam concrete developed at the Technical University of Denmark (Dysted et al., 2015), PUR insulation with CaSi channels, and aerated cellular concrete (ACC). Material parameters for the included insulation materials are included in Table 5-7.

Table 5-7: Material parameters of internal insulation systems applied to the wall sections

Insulation material	ρ_d [kg/m^3]	λ [W/(mK)]	A_{cap} [kg/(m^{2}s^{½})]	μ [-]
Foam concrete*	147	0.057-0.064	0.078	2
PUR with CaSi channels**	49	0.037	0.013	27
ACC**	99	0.042	0.006	7

* *Material parameters derived from the work by Dysted and Sandholdt (Dysted et al., 2015)*
** *Material parameters derived from material database of software Delphin 5.8.3 (Nicolai et al., 2006)*

5.3.1.2 Experimental setup

The experimental method was chosen with the purpose of monitoring the resulting hygrothermal behavior of solid masonry with and without hydrophobization, when exposed to typical climatic loads. To imitate the dynamics and the varying nature of the natural climate, a cyclic exposure was designed. The hydrophobization was applied with a paint brush and in amounts according to specifications. The investigation of water migration was performed to study the effect of hydrophobization within masonry walls rather than with the masonry components individually, as in Section 5.2.

The experiment was conducted on nine 1½ brick thick solid masonry wall sections of 330x348mm^2 built into the doors of three refrigerators, as seen in Figure 5-15 (left). Each wall section was surrounded by a vapor barrier tightly taped to the perimeter, to ensure adiabatic boundaries. Furthermore, the boundaries of the wall surface were sealed with silicone, to prevent water penetration through small airgaps at the perimeter. To prevent excess water influencing neighboring wall sections, gutters were incorporated for each wall section. 100 mm of the various insulation materials were applied to the internal side of the wall section, with the exception of the reference wall, which was uninsulated. Each wall section was built up as seen in Figure 5-15 (right).

For registration of the temperature and relative humidity in the wall sections as well as in the refrigerator itself (cold climate) HYT-221 sensors were used. The sensors were placed in drilled holes that were subsequently sealed with silicone. Each sensor was set for logging measurements every 5 minutes during the experiment, and the data was logged directly to a computer for data storage. The placements of each sensor are also seen in Figure 5-15 (right). The sensors logged temperature and relative humidity. As mentioned, there are 3 wall sections in each of the 3 refrigerator doors. Table 5-8 displays the setup of each wall section, with insulation types, as well as whether or not hydrophobization was applied. In the table, it is seen that each wall section is denoted with 1.1-1.3, 2.1-2.3, and 3.1-3.3, depending on the refrigerator door, and the height. Furthermore, the table states which sensor locations were in use for each wall section.

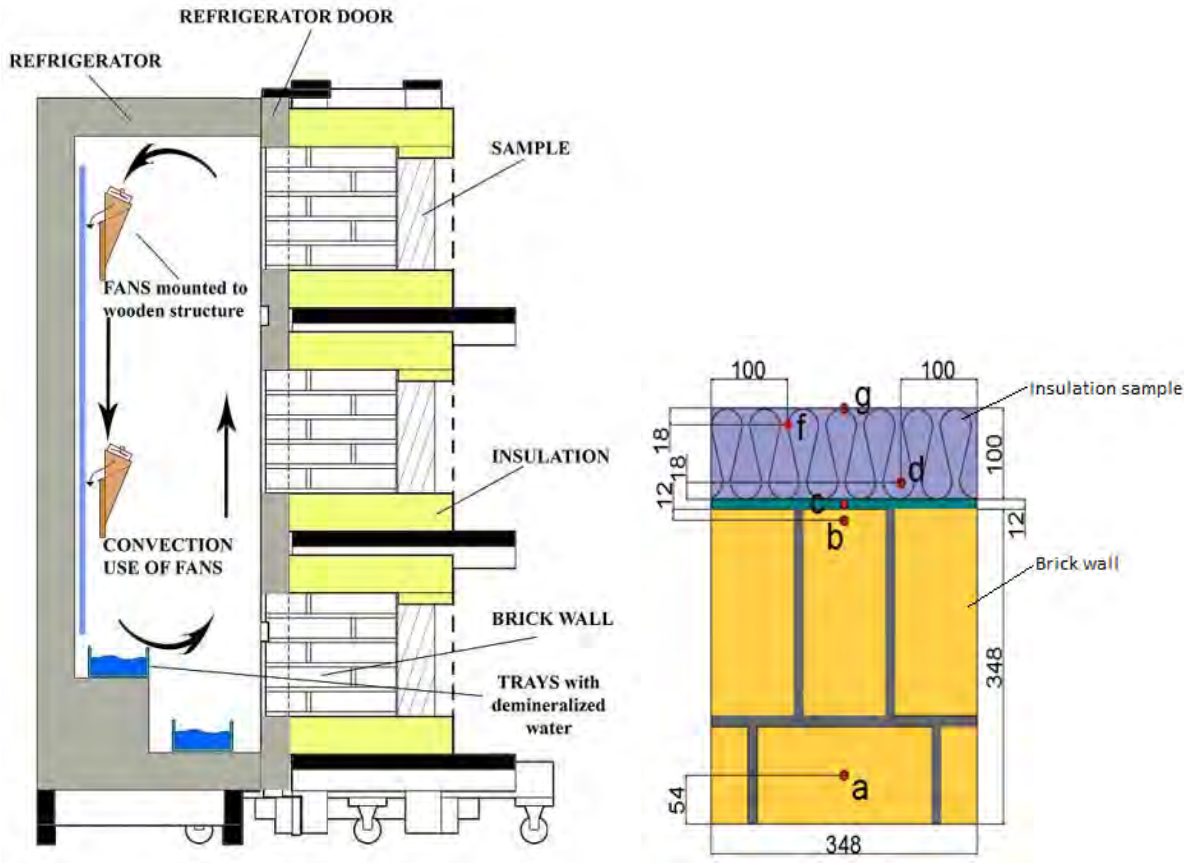

Figure 5-15: Left: Diagram of the experimental setup with the cooling chamber from Dysted et al., (2015). Right: Construction of each wall section, and sensor location. Dimensions are stated in [mm]. Sensor locations are denoted a, b, c, d, f, and g.

Boundary conditions

The experiment was conducted in a laboratory. Measurements from a sensor placed at the internal surface of a wall, represent the interior conditions that were found to be steady with a temperature of 22-23°C and relative humidity of 55-60%. The minor fluctuations in the internal hygrothermal conditions are not considered to impact the experimental results obtained. The experiment was conducted in 24-hour cycles. Each 24-hour cycle consisted of 30 minutes of rain, 2 hours of solar radiation, and 21½ hours of cold climate. This cycle was repeated five times.

The rain loads were applied to the wall sections by means of a purposely designed test stand, seen in Figure 5-16, C. A perforated (holes of Ø0.5mm pr. 50mm) 340mm long pipe in the length of each wall section was placed at the top, and provided a horizontal water load of 0.08-0.11 l/min. The water distribution was therefore more direct than actual rain, but the intention here was also to create severe climatic conditions. By Danish meteorological standards, a severe cloudburst rain storm is defined as a rain intensity of 15mm in 30 minutes or less (Hansen, 2015). This corresponds to 30mm/h, or 30 l/m^{2}h. The provided water load of approximately 0.1 l/min thus represents a severe cloudburst of 50mm/h, corresponding to each wall being subjected to 3 liters of water over 30 minutes.

Table 5-8: Overview of wall sections 1) insulation material, 2) with/without hydrophobization, 3) internal surface treatment, 4) sensors used in this wall section. Placements of the sensors are shown in Figure 5-15 (right)

1.1	**2.1**	**3.1**
1) Foam concrete	1) PUR with CaSi	1) ACC
2) Hydrophobization	2) Hydrophobization	2) No hydrophobization
3) Internal: Diffusion open paint*	3) Internal: No treatment	3) Internal: Diffusion open paint
4) a, b, c, d, f	4) a, b, c, g	4) a, b, c, d, f
1.2	**2.2**	**3.2**
1) No insulation (ref)	1) Foam concrete	1) ACC
2) No hydrophobization	2) No hydrophobization	2) Hydrophobization
3) Internal: No paint (ref)	3) Diffusion open paint	3) Internal: Diffusion open paint
4) a, b, c	4) a, b, c, d, f	4) a, b, c, d, f
1.3	**2.3**	**3.3**
1) Foam concrete	1) Foam concrete	1) PUR with CaSi
2) Hydrophobization	2) No hydrophobization	2) No hydrophobization
3) Internal: Ordinary paint	3) Internal: Ordinary paint	3) Internal: No treatment
4) a, b, c, d, f	4) a, b, c, d, f	4) a, b, c, g

*: The diffusion open paint system is a combination of a primer and a silicate-based paint (s_d<0.01m), whereas the ordinary paint used was a standard acrylic paint (s_d<0.18m).

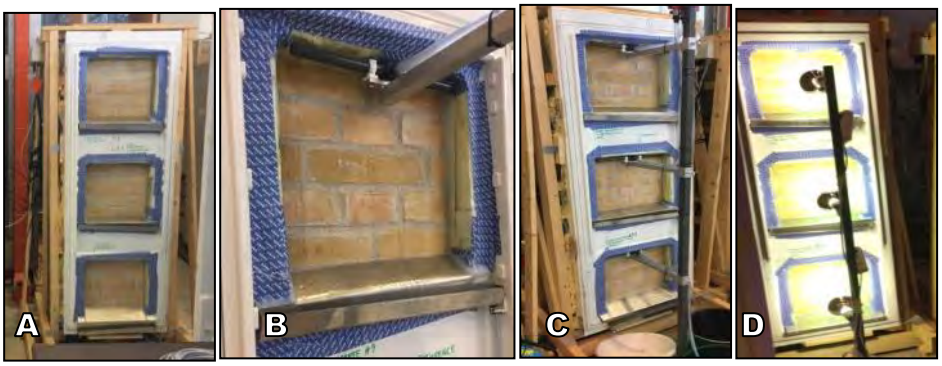

Figure 5-16: Experimental setup. A: Three wall sections in mounted in a refrigerator door. B: water loads applied horizontally to the top of the wall section, by perforated pipe. C: view of water loads applied to three wall sections. D: radiation loads on three wall sections.

The solar radiation loads were provided by Osram ULTRA-VITALUX 300W bulbs for simulation of heat and UV-radiation. These bulbs provide a radiation similar to natural sunlight, and are also used in climate simulators for accelerated aging (Kaaris, 2003). The bulbs were fixed in a stand as seen in Figure 5-16, D, with lightbulbs placed at 3 different heights, corresponding to the center of each wall section. The distance between the bulbs and the wall sections was determined by the so-called black panel temperature. In order to achieve a black panel temperature of 75±5°C, the distance between the wall and the bulb was set at 20cm, yielding an average black plate temperature of 78.1°C.

As mentioned, the wall sections were built into the doors of refrigerators, and these refrigerators provided the cold climate. The refrigerator doors with the wall sections were mounted on wooden rigs that were supplied with hinges. These hinges and the original rubber gaskets on the doors were utilized to ensure a tight fit to the original refrigerator. When the refrigerators/cold climate assimilators were not in use, the opening was covered with XPS plates to help maintain the cold climate conditions inside. The temperature in the refrigerators was controlled by a temperature regulated on/off switch, Sygonix® room thermostat, which was set to a temperature of 3°C, and set

to switch on at 3.2°C and off at 2.8°C. The original thermostat was moved outside of the refrigerator, to induce constant cooling until switching off by the Sygonix® (Dysted et al., 2015). The relative humidity was less controlled, however kept high by having a water bath inside the refrigerator. The conditions were monitored, and by the above mentioned means it was possible to keep the temperature at 4°C and the relative humidity at 80-85%, interrupted only when moving the refrigerators to provide water and radiation loads. The conditions in the refrigerator were kept steady and stratification avoided by mounting four fans inside each refrigerator for constant air circulation.

5.3.2 Results

Studying the relative humidity in points A, B, C, and D, presented in Table 5-9, the effects of hydrophobization was clear – especially in point A. The relative humidity in point A, for untreated masonry, reached 100%, and stayed at this level for the duration of the experiment, whereas for hydrophobized specimens, the relative humidity only exceeded 70% in short peaks when the water loads were applied. When studying the migration of moisture through the wall, it was seen that the relative humidity increased in all the sensor points during the experiment. In point D however, the relative humidity for all the cases seemed to reach individual maximum limits of 40-75% that were not further affected by the climatic loads.

Table 5-9: Relative humidity [%] measured in points A, B, C and D. Hydrophobized cases are presented with dashed lines

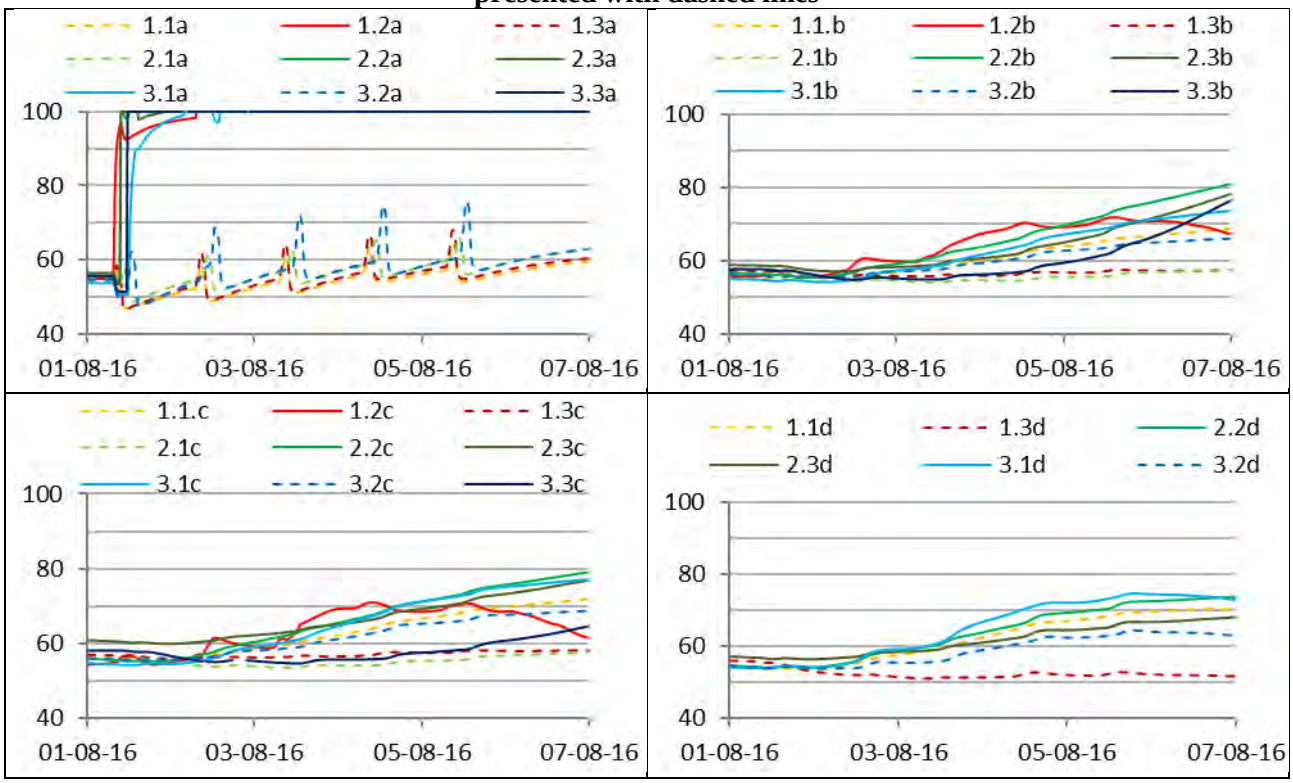

It was seen that the hydrophobized walls 1.3 and 2.1 had the lowest relative humidities monitored in points B, C and D (although the sensor D was missing for wall 2.1). In these points, the hydrophobized walls 1.1 and 3.2 had conditions resembling the untreated walls. These two walls both had diffusion open paint on the interior side, indicating more influence from interior conditions. Unfortunately, walls 2.1 and 3.3 did not have internal surface treatment. However, 1.3 had ordinary paint, which left it less susceptible to the indoor climate, and thus resulted in the lower relative humidity. Wall 2.2

with diffusion open paint, also exhibited higher RH in points B, C and D compared to 2.3 with ordinary paint. The same tendency applies to wall 3.1 that also had ordinary paint on the internal surface.

At the critical point C, the interface between internal insulation and masonry, the relative humidities seemed to be continually increasing, with the exception of the hydrophobized walls 1.3 and 2.1. The unhydrophobized wall 3.3 without internal surface treatment yielded a lower relative humidity, also when compared to the hydrophobized walls 1.1 and 3.2. Both the hydrophobized and unhydrophobized wall with insulation of PUR with capillary active channels (2.1 and 3.3), seemed to generate some of the lowest relative humidities at point C, likely due to the capillary active properties, despite the fact that the foam concrete exhibited both a higher water uptake coefficient and a lower vapor diffusion resistance factor.

5.3.3 Discussion

It was found that the hydrophobization treatment had the largest effect on the external part of the masonry, and to a lesser extent through the wall. Hydrophobization combined with ordinary paint on the internal side, however, seemed to generate the lowest relative humidities and moisture content in internal measuring points. Thus, the hydrophobization treatment on the masonry seemed to have the desired effect, despite the investigation presented in Section 5.2 showing less effect of hydrophobization on lime mortar. The moisture migrations in walls with foam concrete and ACC seemed to be unaffected by the insulation type, however, the walls insulated with PUR with integrated capillary active channels showed the best results in the interface between insulation and masonry, regardless of the hydrophobization treatment. The internal surface treatments seemed to be influential on the results, as the cases with ordinary paint (1.3 and 2.3) exhibit lower relative humidities compared to cases with diffusion open paint. Similarly, Finken *et al.* found, through a study of hydrophobization based on several hygrothermal simulations, that hydrophobization has a positive impact on the hygrothermal conditions within an internally insulated façade. In the simulation, the entire wall became dryer, compared to unhydrophobized cases (Finken et al., 2016). Slapø *et al.* performed a similar study on masonry panels, however, the water loads were provided with high pressure for 5 hours. They found the tested water repellents to be ineffective to high pressure driving rain after a few minutes of water loads; this inefficiency was attributed the extreme testing conditions (Slapø et al., 2017).

The 24-hour cycles implemented did not represent true nature, as the repeatability of the exact loads is highly unlikely. Despite this fact, the setup and the cycles represented realistic loads and gave results suitable for interpretation of WDR penetration of solid masonry, both with and without hydrophobization.

5.3.4 Conclusions

The investigation of moisture migration through masonry showed a distinctive effect of hydrophobization, especially in the external part of the wall, indicating a potential for protection from frost damages and biological growths. The hydrophobization treatment in general also yielded lower relative humidities throughout the wall in most cases; however, walls insulated with PUR with calcium silicate channels generally performed better in the critical interface, regardless of hydrophobization. The internal surface treatments also seemed to influence the results, and the two cases with ordinary paint show better results compared to their equivalents with diffusion open paint.

References

Blocken, B., Carmeliet, J. 2004. A review of wind-driven rain research in building science, Journal of wind engineering and industrial aerodynamics 92: 1079–1130.

Boostani, H., Modirrousta, S. 2016. Review of Nanocoatings for Building Application, International Conference on Sustainable Design, Engineering and Construction. 1541–1548.

Charola, E. 1995. Water-Repellent Treatments for Building Stones: A Practical Overview, The Journal of Preservation Technology 26(2/3): 10–17.

Couto, S., Goncalves, T. D., Lopes, J. M. G. 2011. Drying of Red Ceramic Brick. The effect of five Silicone-based Water-Repellent Treatments, in proceedings Hydrophobe VI. 6th International Conference on Water Repellent Treatment of Building Materials: 81–92.

DS/EN ISO 12572 Hygrothermal performance of building materials and products – Determination of water vapor transmission properties

Dysted, D., Sandholdt, H. 2015. Experimental and theoretical investigation of interior insulation of solid brick walls with foam concrete and another silicate based material. Master Thesis, Technical University of Denmark.

Engel, J., Heinze, P., Plagge, R. 2014. Adapting Hydrophobizing Impregnation Agents to the Object, Restoration of Buildings and Monuments 20(6): 1–8.

Finken, R. G., Bjarløv, S. P., Peuhkuri, R. 2016. Effect of façade impregnation on feasibility of capillary active thermal internal insulation for a historic dormitory – A hygrothermal simulation study, Construction and building materials 113: 202–214.

Guizzardi, M., Derome D., Vonbank, R., Carmeliet, J. 2015. Hygrothermal behavior of a massive wall with internal insulation during wetting, Building and Environment 89: pp. 59–71.

Hansen, T. K., Bjarløv, S. P., Peuhkuri, R. H., Harrestrup, M. 2018. Long term in situ measurements of hygrothermal conditions at critical points in four cases of internally insulated historic solid masonry walls, Energy and Buildings 172: 235–248.

Hansen, T. K, Bjarløv, S. P., Peuhkuri, R. H., Kielsgaard Hansen, K. 2018. Performance of hydrphobized historic solid masonry – experimental approach, Construction and Building Materials 188: 695-708.

Van Hees, R. P. J. 1998. The performance of surface treatments for the conservation of historic brick masonry, in proceedings: World Building Congress 1998 (CIB): 491-498.

Kaaris, H. 2003. Klimasimulatorer: Teknisk dokumentation for accelereret ældning, perioden 1994-2002, (Eng.: Climate simulators: Technical documentation for accelerated aging, the period 1994-2002). By og Byg Dokumentation 048.

Künzel, H. M. 1995. Simultaneous Heat and Moisture Transport in Building Components One- and two-dimensional calculation using simple parameters, IRB-Verlag.

Kvist Hansen, T., Bjarløv, S. P., Peuhkuri, R. 2016. Moisture transport properties of brick – comparison of exposed, impregnated and rendered brick, in proceedings International RILEM Conference - Materials, Systems and Structures in Civil Engineering 2016. Segment on Moisture in Materials and Structures, RILEM Publications S.A.R.L: 351–360.

Lubelli, B., Van Hees, R. P. J. 2011. Evaluation of the Effect of Nano-Coatings with Water Repellent Properties on the Absorption and Drying Behaviour of Brick, in proceedings Hydrophobe VI. 6th International Conference on Water Repellent Treatment of Building Materials: 125–135.

Macmullen, J., Zhang Z., Rirsch, E., Dhakal, H. M., Bennett, N. 2011. Brick and mortar treatment by cream emulsion for improved water repellence and thermal insulation, Energy & Buildings 43: 1560–1565.

Mayer, H. 1998. Masonry Protection with Silanes, Siloxanes and Silicone Resins, Surface Coatings International, 81(2): 89-93.

Nicolai, A., Grunewald, J. 2006. Delphin 5 version 5.2, User Manual and Program Reference: 1-113.

Hansen, N. 2015. Hvad kan du forvente, når DMI varsler skybrud? (Eng.: What to expect when DMI warns of cloudburst) https://www.dmi.dk/nyheder/2017/hvad-skal-du-forvente-naar-dmi-varsler-skybrud/ (accessed 21-01-2020).

Odgaard, T., Bjarløv, S. P., Rode, C. 2018. Influence of hydrophobation and deliberate thermal bridge on hygrothermal conditions of internally insulated historic solid masonry walls with built-in wood, Energy and Buildings 173: 530–546.

Slapø, F., Kvande, T., Bakken, N. Haugen, M., Lohne, J. 2017. Masonry's Resistance to Driving Rain: Mortar Water, Buildings 7(3): 70–86.

Teknologisk Institut, 2013. Mørtel – historie og typer (Eng.: Mortar - history and types). https://www.mur-tag.dk/fileadmin/user_upload/Editor/pdf/artikler/Moertel_historie-og-type.pdf (accessed 21-01-2020).

Vereecken, E., Van Gelder, L., Janssen, H., Roels, S. 2015[1]. Internal insulation for wall retrofitting - A probabilistic analysis of energy savings and hygrothermal risks, Energy and Buildings 89: 231–244.

Vereecken, E., Roels, S. 2015[2]. Capillary active internal insulation: do the advantages really offset potential disadvantages?, Materials and Structures 48(9): 3009–3021.

6 Hygric property measurements @ KUL

(Chi Feng, KUL[4]; Vasilis Soulios, KUL[5])

6.1 Hygric properties of hydrophobized brick and mortar

(Vasilis Soulios, KUL[5])

6.1.1 Introduction

The laboratory study of hygric material properties of hydrophobized brick and mortar samples was carried out by Vasilis Soulios and supervised by Hans Janssen and Ernst Jan de Place Hansen. The first section is a literature study on the hygric properties of hydrohpobized brick and mortar samples derivedderived from scientific papers and from the technical data sheets of the water repellent agents. Subsequent section describes the water repellent agents selected to be applied in order to test the hygric behavior of brick and mortar samples after treatment and illustrates the procedure for completely impregnated samples. Then an exploratory study which presented in CESBP 2019 in Prague of the impact of hydrophobization on wetting and drying is presented (Soulios et al., 2019)

6.1.2 Literature on hygric properties of hydrophobized brick and mortar

Water repellent agents alter the hygric behavior of hydrophobized building materials in such a way that liquid water transfer is impeded and vapor transfer remains possible. Table 6-1 illustrates the difference in some basic properties between treated and untreated brick and mortar samples with results deriving both from literature and industry.

Table 6-1: Hygric properties of hydrophobized brick and mortar samples

Reference	Type	Conc. (%)	Substrate	A_{cap} ↓ (%)	μ ↑ (%)	w_{cap} ↓ (%)
Pavlík et al. (2012)	siloxane	8.32	brick	98.1	-	-
Fukui et al. (2017)	silane	-	brick	-	0	4.9
Carmeliet et al. (2002)	silane	8.53	brick	99.7	140	28.0
Sadauskiene (2003)	silicon-based	-	brick	99.1	-	-
Sadauskiene (2003)	silicon-based	-	brick	13.7	-	-
Sadauskiene (2003)	silicon-based	-	mortar	0.4	-	-
Engel et al. (2014)	silane/siloxane	7	brick	98.6	-8.6	98.5
Engel et al. (2014)	silane/siloxane	10	brick	78.1	14.9	3.0
Engel et al. (2014)	silane	10	brick	88.8	-8.3	12.2
Engel et al. (2014)	silane	30	brick	98.9	-5.8	97.0
Engel et al. (2014)	silane	40	brick	97.3	-6.9	97.5
Engel et al. (2014)	silane	50	brick	83	-0.9	82.7
Engel et al. (2014)	silane	60	brick	98.6	-21.4	95.9
Zhao & Meissener (2017)	silicon based	60	brick	-	-12.9	98.8
Zhao & Meissener (2017)	silicon based	80	brick	-	-3.1	98.8

[4] Activities performed while at KUL, currently at Chongqing University, China
[5] Activities performed while at KUL, currently at AAU

Izaguirre (2009)	metal-bearing (adm.)*	-	lime mortar	75.4	-7.8	1.6
Izaguirre (2009)	metal-bearing (adm.)	-	lime mortar	97.5	-10.2	-1.2
Izaguirre 2009	metal-bearing (adm.)	-	lime mortar	32.6	25.3	-1.3
Izaguirre 2009	metal-bearing (adm.)	-	lime mortar	40.7	-5.4	-0.1
Klisińska (2012)	soap (adm.)	4.8	mortar	60.9	-	-0.1
Klisińska (2012)	silicon resin (adm.)	10	mortar	84.8	-	24.4
Klisińska (2012)	silane (adm.)	0.5	mortar	81.5	-	10.9
Momentive	silane	40	mortar	93	-	-
Wacker	silane/siloxane	25	brick	95.4	-	-
Wacker	silane/siloxane	-	mortar	90	-	-
Dow	siloxane	7	brick	95	-	-
Dow	siloxane	7	brick	92	-	-
Dow	siloxane	7	aged mortar	96	-	-
Dow	silane/siloxane	10	brick	98	-	-
Dow	silane/siloxane	10	mortar	76	-	-
Dow	silane/siloxane	15	mortar	81.6	-	-

* Adm.: admixture

6.1.2.1 Transport properties

Water repellent treatment prevents and reduces the moisture that penetrates into the material by altering the surface tension of the pore wall of the substrate (Zhao and Meissener, 2017). The reduction of water uptake is also considered an indirect index of cold resistance and durability of the brick masonry (Šadauskienė et al., 2003). However, when the liquid water transfer due to capillary forces in the hydrophobic layer is blocked, drying becomes possible only via water vapor transfer. Since vapor transfer is less effective than liquid transfer, the drying rate is significantly reduced.

Carmeliet *et al.* (2002), suggests that some pores can be completely blocked after hydrophobization. That could explain the 5 to 8 % reduction in vapor permeability indicated by Charola (1995). However, according to Mayer (1998), no clogging takes place in the pores after hydrophobization. Recent studies (Engel et al., 2014; Fukui et al., 2017; Zhao and Meissener, 2017) provide results showing that vapor permeability is practically unchanged after hydrophobization. This is also an indication that pores are not completely blocked when hydrophobization is applied.

6.1.2.2 Storage properties

The results presented in Table 6-1 about the moisture storage properties on hydrophobized brick and mortar samples refer to effective moisture content (in hydrophobized samples) derived from a lengthy water uptake test. An unchanged porosity, between treated and untreated samples, coming from the vacuum saturation test, is also needed, in order to build more confidence towards the claim that no clogging of pores takes place after hydrophobization. Also, similar results coming from mercury intrusion tests will confirm that the pore structure of the material is not affected by hydrophobization.

6.1.3 Agent selection

The vast majority of commercially available water repellent agents are silicon-bearing products. Silanes are mainly used for concrete impregnations, due to their low molecular size and high alkaline resistance. Siloxanes can create a positive effect faster than silanes, when applied in building materials with larger pores, due to their larger molecular size. Polymeric siloxanes and silicon resins have an even larger size and may cover efficiently the large pores of some building materials, such as brick. On the other hand, polymeric siloxanes and silicon resins can produce a beading effect on the treated façade, which although considered an advantage by most producers since it directly shows the effectiveness of hydrophobization, it is not always desirable in historic buildings. Beading is after all a surface effect and has a secondary role in the substrate protection. Also, silicon resins can darken the surface, something that is also undesirable, especially in historic buildings.

Most water repellent products are a mixture of silanes/siloxanes (see Figure 3-9). The combination of silanes and siloxanes can be beneficial in terms of effectiveness of the treatment, especially in the case of masonry walls, which consist of different pore size materials like brick and mortar. Silane/siloxane mixtures hence, can provide the advantages of both components.

Solvent based products release Volatile Organic Compounds (VOCs) into the atmosphere, negatively affecting the environment. In contrast, water emulsions are environmentally friendly and have been developing with increasing rate during the last years.

The current study thus, will initially focus on determining the performance of silane/siloxane water emulsion treatments in different concentrations.

Table 6-2 Product selection

No	Company	Product	Concentration
1	DOW	IE 6683	40%
2	DOW	520	40%
3	DOW	IE 6694	60%
4	Facabelle	Fassapearl-H	10%
5	PEC	THORO® ENVIROSEAL B	7%
6	REMMERS	Funcosil WS	10%
7	REYNCHEMIE	RC 805 ECO	7.5%
8	SCALP	SCALPFUGE 35	-
9	SIKA	Sikagard®-703 W	-
10	Soudal	SOUDACLEAR FAÇADE W	6.5%
11	WACKER	SILRES® BS 39	25%
12	WACKER	SILRES® BS 1001	50%
13	WACKER	SILRES® BS 3003	60%
14	WACKER	SILRES® BS 4004	50%
15	WACKER	SILRES® BS SMK 1311	100%
16	WACKER	SILRES® BS SMK 2100	100%
17	WACKER	SILRES® BS SMK 2101	100%

Eight companies provide products that have the desirable characteristics: silane/siloxane mixture in liquid form with water as diluent and appropriate for brick facades. However, only five of them have at least one product that combines the desirable characteristics: Dow, PEC, REMMERS, Soudal and WACKER. From these companies, WACKER provides a notable variety regarding the silane/siloxane products see Table 6-2. More specifically three silane/siloxane products with different ratios of silane and siloxane: SILRES® BS SMK 2101 (higher percentage of silanes), SILRES® BS SMK 2100 (more balanced silane/siloxane mixture) and SILRES® BS SMK 1311 (higher percentage of siloxanes), are going to be tested. Thus, the impact of both silanes and siloxanes will be evaluated. These products have 100% concentration of active ingredient, can be diluted with water and contain micro-emulsions which means that they can show their performance right away. In that way, various combinations of different concentrations can be examined in order to illustrate the influence of wetting and drying of impregnated samples in the material level. Also, another aspect that will have to be investigated is which combinations of silane/siloxane and which concentrations make the hydrophobic layer impermeable to liquid water and which of them leave liquid water to penetrate in order to measure the hygric properties.

Cream products are more difficult to be diluted to different concentrations of active ingredients, compared to liquid products, but can be ordered ready- to-use in different concentrations. After testing the influence of different percentages of silane/siloxane with liquid products, cream products will also be tested.

6.1.4 Laboratory test setup

Table 6-3 summarizes the test methods, building materials and water-repellent agents (liquid and cream products) used to investigate the impact of hydrophobic impregnation on open porosity (Φ), water absorption coefficient (A_{cap}) and vapor diffusion resistance factor (μ).

Table 6-3 Test plan.

Identification of material (No. of samples)	Product	Type	Form	Diluent	Conc.
Vacuum saturation test (Φ) (0.4x4x4 cm samples)					
R brick (5)	Wacker SMK 2100	Silane/siloxane	Liquid	Water	5 %
Capillary water uptake (A_{cap}) (8x4x4 cm samples)					
R brick (5)		Untreated			
R brick (9)	Wacker SMK 2101	90% silane	Liquid	Water	1 / 2.5 / 5 %
R brick (9)	Wacker SMK 1311	90% siloxane	Liquid	Water	1 / 2.5 / 5 %
R brick (9)	Wacker SMK 2100	Silane/siloxane	Liquid	Water	1 / 2.5 / 5 %
Cup test (μ) (8 cm diameter, 3 cm height samples)					
R brick, Y brick, H brick, L mortar (4)		Untreated			
R brick, Y brick, H brick, L mortar (4)	Remmers FC	Silane	Cream	Water	40 %
Drying test (μ-*eq*) (1x4x4 cm samples)					
R brick, Y brick, H brick, L mortar (3)	Wacker SMK 2100	Silane/siloxane	Liquid	Water	6 %
R brick, Y brick, H brick, L mortar (3)	Remmers FC	Silane	Cream	Water	40 %

R brick: Robusta Vandersanden Belgian brick, Y brick: Yellow soft molded Danish brick, H brick: Historic Danish brick from an old building in Copenhagen (1944), L mortar: carbonated lime mortar. *μ-eq*: equivalent μ value derives from drying test.

The impregnation process in the laboratory consisted of the following steps: the samples, prepared from regular bricks and casted mortar, were washed with deionized water to avoid absorption of extra salts and were carefully cleaned with a brush to remove dirt and dust. Afterwards, the samples were stored for drying in an oven (70 °C) for the absorbed moisture from the intense water exposure to evaporate. After reaching a stable mass (4-5 days), cooling in a desiccator took place, for the samples to reach room temperature and relative humidity. For impregnation with liquid products one surface of each sample was exposed to free agent uptake until the sample became fully impregnated (by visual observation of top surface becoming darker). The cream product was applied with a brush on the sample top surface with sufficient amount of agent for the sample to become fully impregnated. Finally, the samples were cured for one month in a climatic chamber (21 °C, 53.4% RH).

Vacuum saturation test was conducted according to (ASTM C1699-09, 2015), in order to determine open porosity (Φ), which is proportional to vacuum saturated moisture content wsat.

A free water uptake test was conducted to obtain the water absorption coefficient (A_{cap}) according to (ISO 15148, 2002). As impregnation significantly reduces the capillary water uptake, the test went on for three hours for impregnated samples compared to one hour for untreated samples. Measurement time intervals were: 10', 30', 1h, 1h 30', 2h, 3h. In addition, measurements were conducted after 18h and 30h, but it was not possible to define a second stage in the water uptake curve (Roels *et al.*, 2004). Therefore, the absorption coefficient was calculated, by taking all the points obtained from the water uptake test (3h) into account, since it was assumed that all points belonged to the first stage of the water uptake test.

The cup test was conducted along (ISO 12572, 2016), to calculate the water vapor diffusion resistance factor (μ). After pre-conditioning, each sample, enclosed in a lid, was attached to a cup containing a saturated salt solution (K_2SO_4, 97.3% RH) and placed in a climatic chamber (21 °C, 53.4% RH). The samples were weighed twice a week for four weeks. Further description of the procedures for the free water uptake, cup and vacuum saturation tests could be found in (Feng *et al.*, 2015).

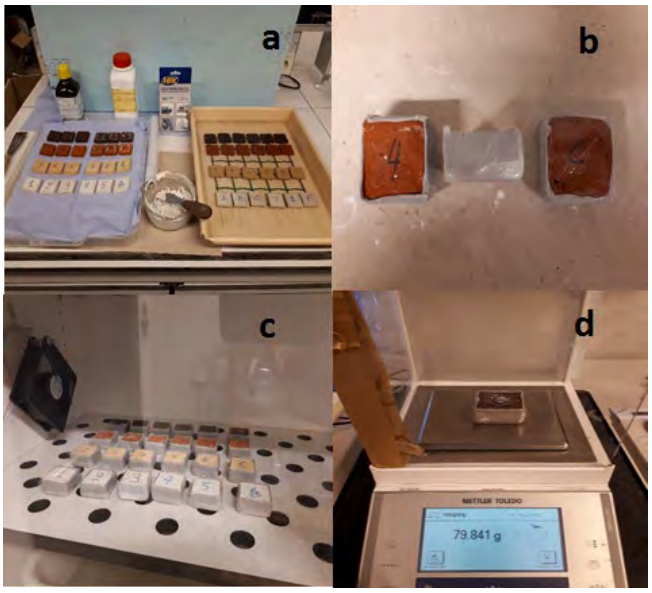

Figure 6-1 Drying set up of impregnated samples a) Fully impregnated samples (left) and water saturated samples (right), b) Impregnated and saturated sample attached with kaolin clay to ensurea hydraulic contact, seen from the top (impregnated), side and bottom surface (saturated). c) Left to dry out only from top surface in a climatic chamber (21ºC, 53.4 % RH). d) Weighing of samples.

In a drying test developed at KU Leuven, impregnated samples were attached with kaolin clay (50% hydrated aluminum silicate – 50% water) on top of water saturated samples, sealed and left to dry in a climatic chamber (21 °C, 53.4% RH) for 17 days with daily measurements of mass reduction (see Figure 6-1). The current drying set up can provide the drying curve of the impregnated samples, and this can be translated into an equivalent vapor permeability, from the section of the test with a constant drying rate.

6.1.5 Results and discussion

Open porosity (Φ) and vacuum saturation moisture content w_{sat} do not seem to be significantly influenced by hydrophobic impregnation (see Table 6-4). This is an indication that there is almost the same available pore volume space in the hydrophobized material that can be filled after submerging the sample and induce hydrostatic overpressure difference with the vacuum saturation test. The small reduction of the open porosity could be due to a limited extent of clogging in the finer pores of the brick (Carmeliet *et al.*, 2002).

The current study checks whether lower than recommended concentrations for brick samples, being 6 to 10% for SMK products (Wacker Chemie AG, 2014), still have a good water repellency performance, as expressed by a low A_{cap}. According to Table 6-5, even with concentrations between 1 and 5 %, A_{cap} is very low compared with the untreated material. Further, the effect of the different water-repellent agents is the same for a specific type of brick. Combining the results in Table 2 and 3, the reduction in A_{cap} is therefore not due to a reduction of the pore space but due to changes in the adhesion between water atoms and pore walls.

Table 6-4: Results of vacuum saturation test. Open porosity and moisture content.

R brick	**Untreated***	**Impregnated**
Open porosity Φ [%]	32.6 (0.4)	30.8 (0.01)
Vacuum saturation moisture content w_{sat} [kg/m^3]	326 (3.5)	307.9 (8.6)

* Values of untreated obtained from (Feng and Janssen, 2018), where the same brick type is used.

Figure 6-2 shows the drying curves of impregnated samples, indicating that “trapped” moisture behind the hydrophobic layer is able to dry out, with the vapor diffusion resistance of the impregnated sample as the dominant resistance.

The vapor diffusion resistance factor (μ) of the tested types of brick and mortar do not seem to be significantly influenced by hydrophobic impregnation (Table 6-6). Opposed to the cup test, in the drying test, liquid transfer between the water saturated and the impregnated sample could take place as A_{cap} of impregnated samples is not completely zero. This explains why the drying test results in lower μ-values. A small percentage of clogging in the fine pores of the impregnated materials (Carmeliet *et al.*, 2002) could possibly explain the increase in μ-value in impregnated samples using cup test where there is solely vapor transfer. Although, drying test can provide an estimation of the μ-value, by having solely vapor transfer cup test should be considered more reliable. Moreover, the comparison of the resulting μ-values between cup test and drying test indicates limited liquid transport in the hydrophobic layer in the drying test that can accelerate the drying speed.

Table 6-5: Water absorption coefficient of type R brick.

Agent	Untreated	SMK 2101			SMK 1311			SMK 2100		
Conc.		1%	2.5%	5%	1%	2.5%	5%	1%	2.5%	5%
A_{cap}[10^{-3} kg/m²√s]	607.3 (20.4)*	0.63 (0.3)	0.43 (0.2)	0.15 (0.1)	0.47 (0.2)	0.53 (0.2)	0.3 (0.2)	0.77 (0.3)	0.5 (0.2)	0.27 (0.1)

* The values in brackets corresponds to the standard deviation of the measurements.

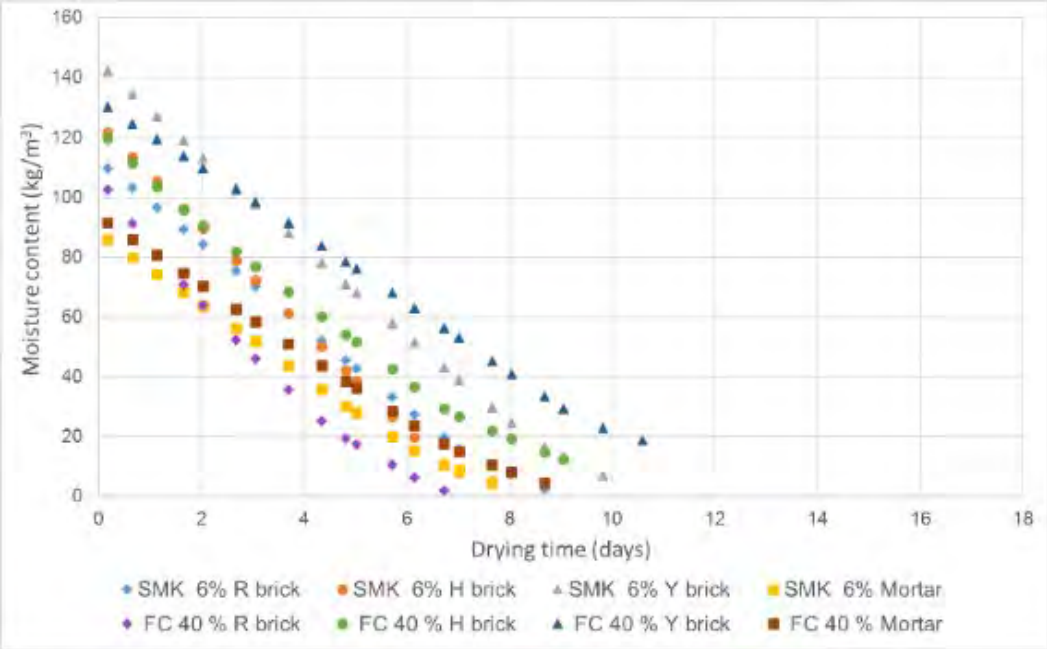

Figure 6-2: Drying curves, average of three tested samples for each water-repellent agent (SMK 2100 6% and FC 40%) and building material (brick and mortar types according to Table 6-3).

Table 6-6: Vapor permeability (δ_v) and vapor diffusion resistance factor (μ) of untreated and impregnated samples. Cup test and drying test for three types of brick and one type of mortar.

		R brick	H brick	Y brick	L mortar
Cup test, untreated	δ_v [10^{-11} kg/(msPa)]	1.8 (0.2)	2.3 (0.2)	1.7 (0.2)	2.5 (0.1)
	μ (53-97%)	11.3 (1.2)	8.7 (0.9)	11.9 (1.4)	8.0 (0.4)
Cup test, FC 40%	δ_v [10^{-11} kg/(msPa)]	1 (0.8)	2 (0.2)	1 (0.2)	2 (0.1)
	μ (53-97%)	15.1 (0.9)	9.7 (1)	13.7 (2)	9.7 (0.7)
Drying test, SMK 6%	δ_v [10^{-11} kg/(msPa)]	3 (0.4)	3.4 (0.3)	3.5 (0.5)	2.9 (0.8)
	μ-eq (53-≈100%)	6.7 (0.9)	5.8 (0.6)	5.8 (0.8)	7.1 (1.8)
Drying test, FC 40%	δ_v [10^{-11} kg/(msPa)]	5.1 (2)	3.6 (2)	2.3 (0.8)	2.5 (0.5)
	μ-eq (53-≈100%)	4.1 (1.1)	6.4 (3.1)	9.4 (3.1)	8.0 (1.5)

The values in brackets correspond to the standard deviations of the measurements.

6.1.6 Conclusions

The slightly reduced open porosity between untreated and hydrophobic impregnated brick indicates only a minimal change in the pore structure of impregnated brick.

According to the transport properties of the hydrophobic impregnated brick tested, the absorption coefficient is significantly reduced compared to the untreated regardless of the percentage of silane/siloxane, even with lower concentrations than recommended. On the other hand, the vapour diffusion resistance factor (μ-value) does not seem to significantly change after hydrophobic impregnation, neither in bricks or mortar.

Drying set up can provide an estimation of the vapour diffusion resistance factor (μ-value) of the impregnated materials, but cup test could be considered as a more accurate method as the samples are not in contact and there is no liquid transfer. However, the slightly lower μ-value derived from drying tests indicate limited liquid transport in the hydrophobic layer that accelerates the drying speed.

6.2 Hygric behaviour of hydrophobized brick and mortar samples *(Vasilis Soulios, KUL[6])*

6.2.1 Introduction

Apart from the hygric properties of the treated materials, also the impregnation depth of the agent is an important factor in the performance of hydrophobization. For that reason, a series of experiments on the impregnation depth of various agents, has been executed. The results are part of a scientific paper (Soulios et al., 2020).

6.2.2 Materials and methods

6.2.2.1 Building materials

The current study looks into ceramic brick and carbonated lime mortar (one type), described in Table 6-7. Lime mortar placed in a carbonation chamber (4.7% CO2 exposure) for 2 weeks in order to represent an carbonated historic mortar (Cizer et al., 2012). The mortar samples were tested with phenolphthalein in order to check if they were fully carbonated.

Table 6-7 Building material used in the current study. Properties of untreated samples.

Name	Description	A_{cap}* [kg/m²√s]	w_{cap}* [kg/m³]	μ*
R brick	Robusta Vandersanden Belgian Brick	0.607	208	11.3
L mortar	Carbonated lime mortar	0.258	227	8.00

* A_{cap} and w_{cap} are estimated from water uptake test, μ from wet cup test [RH 53.2 – 97.4%]

6.2.2.2 Water repellent agents

The SMK products from Wacker (SILRES BS) are micro-emulsion water-based mixtures of silane/siloxane (see Table 6-8). SMK 2101 has a high percentage of silane (Wacker Chemie AG, 2014). SMK 1311 has a high percentage of siloxane and SMK 2100 has a balanced mixture of silane/siloxane. SMK products are available with 100% concentration and they can be diluted with tap water (preferably deionized) to produce any concentration (Wacker Chemie AG, 2014)

[6] Activities performed while at KUL, currently at AAU

Table 6-8: Water repellent agents used in the current study.

Product	Company	Type	Form	Diluent	Concentration	Substrate
SMK 2101	Wacker	90% silane	Liquid	Water	6 / 10 / 25** %	Concrete
SMK 1311	Wacker	90% siloxane	Liquid	Water	6 / 10 / 25** %	Mineral
SMK 2100	Wacker	Silane/siloxane	Liquid	Water	/ 6 / 10 / 25** %	Mineral

Information derived from the technical data sheets of the products.

6.2.2.3 Hydrophobization treatment

The samples were washed with deionized water to avoid absorption of extra salts and were carefully cleaned with a brush to remove dirt and dust (Rewah NV, 2016). Afterwards, the samples were stored for drying in an oven (70 °C) for the absorbed moisture from the intense water exposure to evaporate. After reaching a stable mass (4-5 days), the samples were cooled in order to obtain room T and RH.

The impregnation with liquid products followed the test practice of Wacker where samples are dipped for five minutes in the liquid agent. According to Wacker this represents two to three working operations. In the current study, one surface of each sample was exposed to free agent uptake for five minutes (contact time).

Finally, the samples were stored in a climatic chamber (21 °C, 53% RH) for one month of curing.

6.2.2.4 Laboratory experiments

The impregnation depth of impregnated samples was initially measured by visual inspection (i.e. measuring the length of the surface that becomes darker after impregnation), right after the impregnation and one month later. In addition, water uptake tests were conducted from the impregnated and the non-impregnated side of the samples to illustrate the redistribution and the extent of spreading of the water repellent agent in the samples.

6.2.3 Results and discussion

A sufficient impregnation depth of the hydrophobic treatment is vital, since a thin hydrophobic layer may pose a risk for water penetration in the case of cracks at the exterior surface. Initially in this study the impregnation depth of impregnated samples was measured by visual inspection right after as well as one month after the impregnation process. The visual inspection indicates impregnation depths of approximately 25 mm on bricks and of 5 to 10 mm on mortar, right after impregnation with various liquid water repellent agents (see figure 6-3).

The redistribution of the agent after one month is visible mainly in R brick where the impregnation depth is around 30 mm. After one month, the hydrophobized layer is not visible in most of the cases in L mortar. The ratio of silane/siloxane and the percentage of the active ingredient concentration do not seem to influence the impregnation depth

In order to thoroughly investigate the partially hydrophobized volume, water uptake tests from the impregnated and not-impregnated sides were conducted. Table 6-3 gives an indication of the strength and depth of the partly hydrophobized volume by comparing the water absorption coefficient of samples from the impregnated side and the not impregnated side. The impregnated samples show water repellency even at the not-impregnated side, as the water volume absorbed by the not-impregnated side is significantly reduced compared to the untreated material. Figure 6-4 also

illustrates that the redistribution of the agent leads to much larger impregnation depths than the ones measured by visual inspection or referred in the technical data sheets of the water repellent agents. After the hydrophobization procedure, the active ingredient spreads further into the material, leading to a major raise of the impregnation depth.

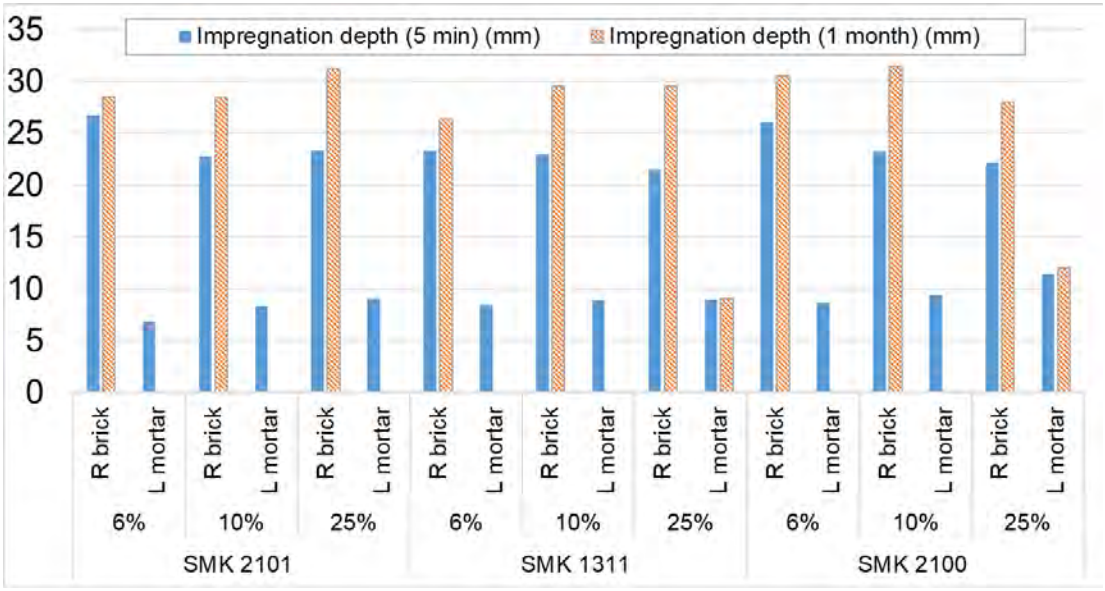

Figure 6-3 Impregnation depth with visual inspection of R brick and L mortar impregnated with liquid water repellent agents, right after impregnation and after 1-month curing.

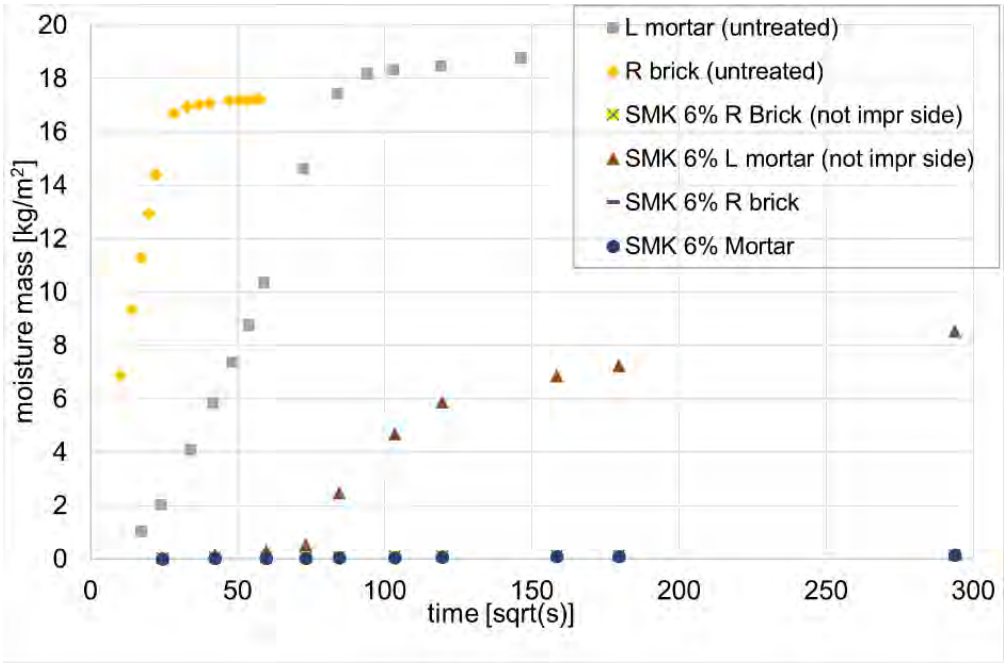

Figure 6-4 Water uptake of R brick and L mortar, comparison between untreated, impregnated and not impregnated side with SMK 2100 sIlane/siloxane 6%.

6.2.4 Conclusions

After the evaluation of hydrophobized samples with capillary absorption tests, it is shown that the water repellent agents penetrate deep into the materials, successfully blocking capillary effects. Moreover, the water repellent agent appears to spread in the material for a long time after the hydrophobic treatment.

6.3 Development of new methods for measuring hygric properties *(Chi Feng, KUL[7])*

6.3.1 Introduction

The experimental determination of the hygric properties of porous building materials is crucial, as they are indispensable for the hygrothermal analysis of buildings and built environment (D'Orazio and Maracchini, 2019; Feng et al., 2019; Yan et al., 2019; Zhang et al., 2017). Currently many different experimental methods are available, but the full-range material characterization is still impossible. For instance, the desiccator test measures the storage property in the hygroscopic range for both adsorption and desorption processes (the sorption isotherms, (Feng et al., 2013)), while the pressure plate/membrane method measures the storage property in the over-hygroscopic range for the desorption process only (the moisture retention curve, (Feng et al., 2015)). Thus, their combination fails to investigate the adsorption process in the over-hygroscopic range. For measuring transport properties similar challenges also exist. Consequently, it is significant to develop new methods to extend the measurable humidity range and transfer process.

For the measurements on the moisture storage properties, the psychrometer method, the semi-permeable membrane method, the adsorption pressure plate method and the hanging water column method have been innovated. The first two methods enable both adsorption and desorption measurements in the over-hygroscopic range; the adsorption pressure plate is modified from the traditional pressure plate for the application on the adsorption process in the over-hygroscopic range; the hanging water column provides precise results in the capillary pressure (p_c, Pa) range close to 0.

For the measurements on the moisture transport properties, the water head method, the semi-permeable membrane method and the tension infiltrometer method have been designed. The water head test can measure the liquid permeability (K_l, $kg \cdot m^{-1}s^{-1}Pa^{-1}$) close to saturation (between saturated and capillary moisture content, w_{sat} and w_{cap}, $kg \cdot m^{-3}$); the other two methods aim for a lower moisture content (w, $kg \cdot m^{-3}$) but are still under development.

These newly developed experiments are utilized to measure the hygric properties of porous building materials, before and after hydrophobization treatment (Section 6.4).

[7] Activities performed while at KUL, currently at Chongqing University, China

6.3.2 Methods for storage property measurements

6.3.2.1 Psychrometer method

The psychrometer method is a suction control method. During the test, the sample is conditioned to an arbitrary moisture content first, and the p_c in the sample is then obtained by holding the sample in a sealed chamber and measuring the air humidity caused by the water evaporation from the sample. In the over-hygroscopic range, the resultant air humidity is very close to saturation. Consequently, the widely used RH sensors are no longer reliable because they are mainly designed for applications at a lower humidity, while psychrometers specifically designed for the high humidity range become a much better choice instead.

There are different types of psychrometers, such as the transistor psychrometer and the chilled-mirror dew-point psychrometer. Many factors – such as temperature, hysteresis, calibration and equilibrium time – all have an impact on the accuracy. After comprehensive comparisons, Cardoso et al. (2007) recommended the chilled-mirror dew-point psychrometer. In this project, we follow their recommendation and adopt the chilled-mirror dew-point psychrometer for the humidity measurement. The adopted model is WP4C (Figure 6-5), produced by Decagon Devices Inc. According to the manufacturer, this psychrometer has an accuracy of $\pm 5 \cdot 10^4$ Pa in the p_c range of 0 ~ $-5 \cdot 10^6$ Pa and ±1% for $-5 \cdot 10^6$ ~ $-3 \cdot 10^8$ Pa. More info about this psychrometer can be found in (Leong et al., 2003).

Psychrometers have been widely used in soil science, geology and other disciplines to determine the moisture retention curves for a long time (Leong et al., 2003; Lu et al., 2017; Madsen et al., 1986). However, the function of a psychrometer is measuring, rather than controlling the moisture potential. Consequently, the sample conditioning protocols and the adsorption/desorption processes can differ significantly. Here we propose a method that is optimal for most porous building materials. It is based on a chilled-mirror dew-point psychrometer (model: WP4C). Figure 6-5 shows its appearance and the sample cups, as well as its internal structure.

For adsorption measurements, samples are first pre-conditioned at an ambient RH of 97% controlled by saturated K_2SO_4 solution (Figure 6-6 a). Next, samples are placed above pure water in desiccators placed in an insulated chamber for better temperature stability (Figure 6-6 b and c). From time to time, the adsorption process is interrupted by sealing samples into small sample cups (Figure 6-6 d). After a standing period, the profiles of moisture content and potential in the sealed samples are assumed equilibrated. The w and p_c of samples are then measured by the balance and by the WP4C psychrometer, respectively. Resultantly, the adsorption curve starting from the dry state in the over-hygroscopic range is determined. For small-pore materials such as calcium silicate and autoclaved aerated concrete, the adsorption progresses very slowly when the humidity is extremely high, while for large-pore materials such as ceramic brick the adsorption directly from air can hardly result in an observable change in moisture content. For those cases, we apply some tiny water drops directly on the samples for acceleration.

Reversibly, desorption curves can be obtained. For desorption measurements, samples are first pre-conditioned to w_{sat} or w_{cap} and then exposed to 97% or 94% ambient RH (controlled by saturated K_2SO_4/KNO_3 solutions). With a similar process, the w and p_c can be measured, and the desorption curves are hence available.

a. A photo

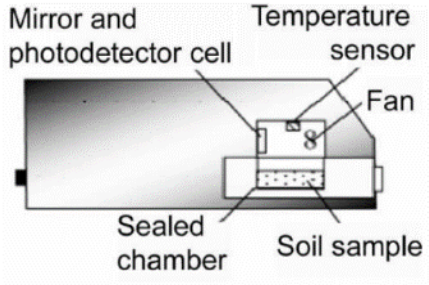

b. A schematic (Leong et al., 2003)

Figure 6-5: The chilled-mirror dew-point psychrometer (model: WP4C).

a. Samples under pre-conditioning

b. Samples in the insulation chamber

c. A close look of samples in the test

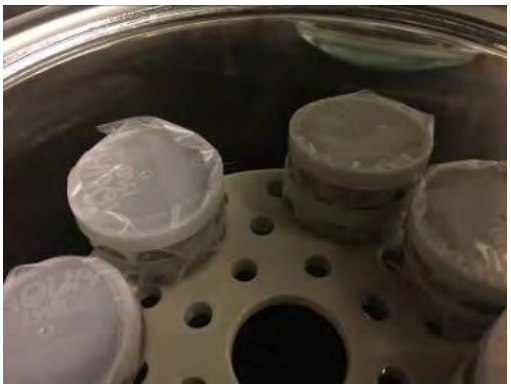

d. Samples sealed in cups

Figure 6-6: The psychrometer method for measuring moisture storage curves.

It should be noted that in the psychrometer test we always weigh the sample first and then measure its p_c, and the working principle of the chilled-mirror dew-point psychrometer subsequently makes an underestimation of the original sample p_c (or an equivalent overestimation of w), inevitable due to the evaporation. However, the total volume of the sealed chamber can be estimated as 50 ml. A simple calculation reveals that under our experimental conditions 1.1 mg water vapor could yield 100% ambient RH in such a volume. The sample size is roughly $3.5 \cdot 10^{-6}$ m^3, corresponding to an overestimation of w around 0.3 $kg \cdot m^{-3}$, which is completely negligible in most cases.

It should also be mentioned that the purpose of pre-conditioning samples at 97% RH in the adsorption tests is to slow down the moisture absorption process when samples are exposed above pure water, so that the p_c and w profiles inside the sample are more uniform. For the same reason, the desorption tests are carried out at relatively high RHs. In our trial measurements, the p_c evolutions of some samples are monitored after their sealing. It is observed that during the initial hours there are still some p_c changes, which should be mainly attributed to the moisture content re-distribution within the sample. After several hours, equilibrium has almost been reached and the measured p_c only shows minor fluctuations. For this reason, it's recommended to carry out the p_c measurements on samples having been standing overnight.

6.3.2.2 Semi-permeable membrane method (for storage)

The semi-permeable membrane method can be deemed as a derivative of the desiccator test (ISO 12571, 2013; Feng et al., 2013): while saturated salt solutions are often used in the hygroscopic range for humidity control, unsaturated salt solutions can be similarly utilized for maintaining desired moisture potentials in the over-hygroscopic range. By exposing samples to such an environment, the over-hygroscopic equivalent of the desiccator test can be achieved.

There are, however, two critical issues concerning the use of unsaturated salt solutions in the over-hygroscopic range. First, it is liquid, rather than vapor, that dominates the moisture transfer in the over-hygroscopic range. Consequently, the surface transfer resistance of vapor diffusion will result in an enormous amount of time for the sample to reach equilibrium if directly exposed to humid air (in the psychrometer test, for instance). Moreover, a slight temperature fluctuation can cause a large shift in the air humidity in the over-hygroscopic range due to the limited thermal inertia and moisture capacity of air.

To solve these two problems, we keep samples in close contact with the salt solution, with a piece of semi-permeable membrane in between. Thanks to the osmosis effect (Figure 6-7), the moisture transport is allowed but the salt penetration is blocked. The salt solution can also effectively buffer the fluctuations of temperature and moisture potential. When equilibrium is reached, samples should have the same p_c as the solution. This is the basic principle of the semi-permeable membrane method for measuring moisture storage curves (Figure 6-8). This method is obviously applicable to a wide moisture content range for both adsorption and desorption processes.

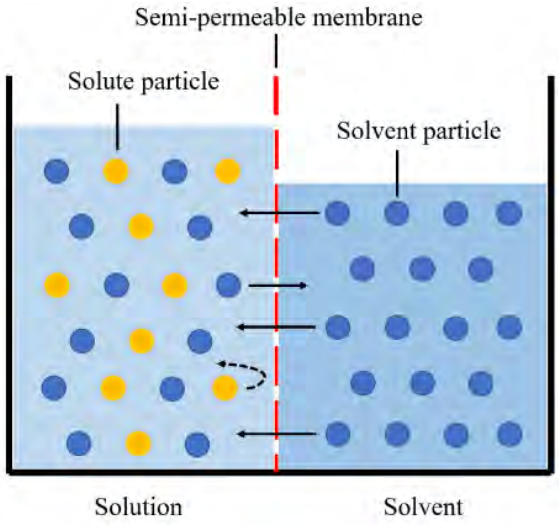

Figure 6-7: The osmosis effect with a semi-permeable membrane.

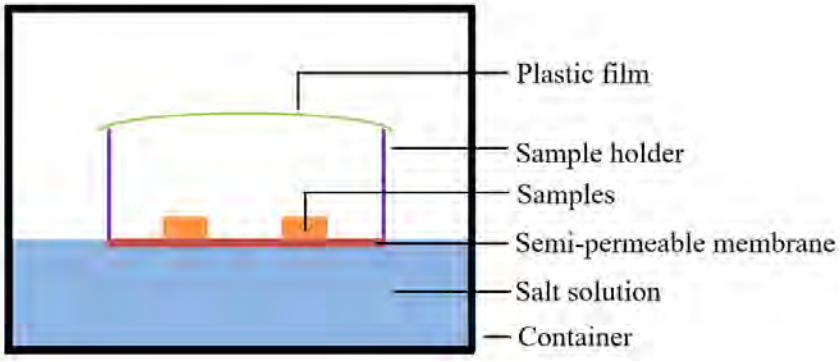

Figure 6-8: A schematic of the semi-permeable membrane setup.

a. Samples lying on the semi-permeable membrane

b. Samples in desiccators with salt solutions

Figure 6-9: The semi-permeable membrane method for measuring moisture storage curves.

During the test, samples are pre-conditioned to a desired initial moisture content (dry state, w_{sat} or w_{cap}) and then laid in a sample holder whose bottom surface is a semi-permeable membrane (Figure 6-9 a). The top of the sample holder is covered by a piece of plastic film to minimize the impact of condensation caused by temperature fluctuations. Next, multiple sample holders with samples inside are placed into desiccators, floating on unsaturated K_2SO_4 solutions of different concentrations (Figure 6-9 b). When the mass of samples no longer changes (after approximately 3~4 weeks), the final wet mass is recorded for the moisture content determination. Due to the moisture transfer across the semi-permeable membrane, the concentrations of K_2SO_4 solutions will slightly deviate from the original values, and the p_c will change accordingly. We use a WP4C psychrometer (explained in Section 6.3.2.1) to measure the final p_c.

Ideally, no salt could cross the semi-permeable membrane, while in practice a tiny amount of salt may still penetrate. The membrane used in this study is an industrial-level reverse osmosis membrane (Filmtech® Flat Sheet BW30) with a NaCl rejection capability as high as 99.5%. The salt used in our test is K_2SO_4. Since K^+ is larger than Na^+ in size, and SO_4^{2-} is larger than Cl^- in both size and charge amount, it is more difficult for K_2SO_4 to pass through the membrane. The impact of salt transport can thus be reasonably neglected.

Semi-permeable membranes have previously been used for determining the moisture storage curves of porous materials (Bannour et al., 2014; Delage et al., 1992). However, our protocol is very simple and efficient, with the capability to test multiple samples at the same time in easily-available setups.

6.3.2.3 Adsorption pressure plate method

The pressure plate method can be utilized to determine the moisture retention curve in the over-hygroscopic range (ASTM C1699, 2015; ISO 11274, 2019; Feng et al., 2015). During the test, a piece of porous ceramic plate is pre-saturated and placed in a pressure vessel. Wet kaolin is laid on the plate for maintaining hydraulic contact and a piece of pre-saturated cellulose film (or filter paper, silk cloth, etc.) is used as the separating material, upon which samples (usually pre-conditioned to either w_{sat} or w_{cap}) are placed. After sealing the pressure vessel, compressed air – in correspondence with p_c – is supplied into the vessel and the water in the samples is driven through the porous ceramic plate, draining from the outlet. The equilibrium moisture content of the samples can be then determined gravimetrically. More details can be found in the ISO and ASTM standards (ASTM C1699, 2015; ASTM D6836 2016; ISO 11274, 2019).

From the operational procedures it is clear that the traditional pressure plate method only suits the desorption process. Recently Fredriksson and Johansson (2016) modified the traditional pressure plate and successfully applied it to the adsorption of brick and spruce. However, their setup is very complicated (Figure 6-10) and is only applicable in the p_c range between 0 and $-4 \cdot 10^5$ Pa. To resolve such problems, we modified the traditional pressure plate for the adsorption process in another way. The setup and operational procedures are only slightly changed but the applicable p_c range is as wide as the traditional pressure plate, typically between 0 and $-15 \cdot 10^5$ Pa.

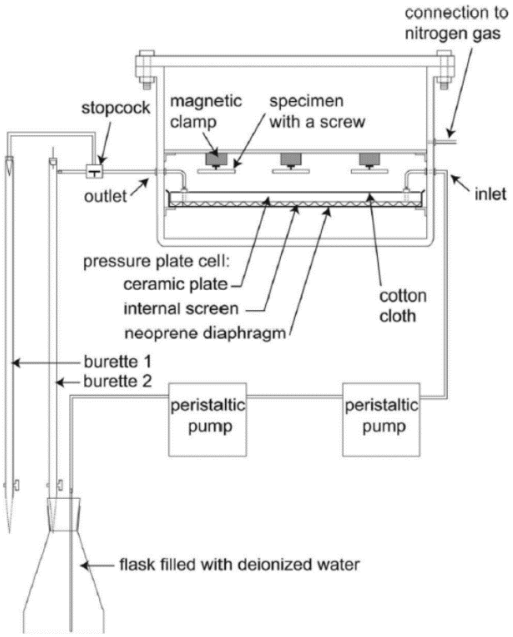

Figure 6-10: The modified pressure plate developed by Fredriksson and Johansson (2016) for adsorption measurements.

For our novel adsorption pressure plate, the porous ceramic plate is pre-saturated and placed in the pressure vessel as usual. However, on the plate a piece of moderately moist filter paper is laid directly, without kaolin. Above the filter paper lie the (relatively) dry samples for the test (Figure 6-11 a). If needed, non-hygroscopic and non-capillary weight (such as plastics) can be laid on the samples to ensure good hydraulic contact. Next, the pressure vessel is sealed as usual but the outlet is kept in direct contact with pure water (Figure 6-11 b), unlike in the traditional setup where a burette is used to measure the water outflow.

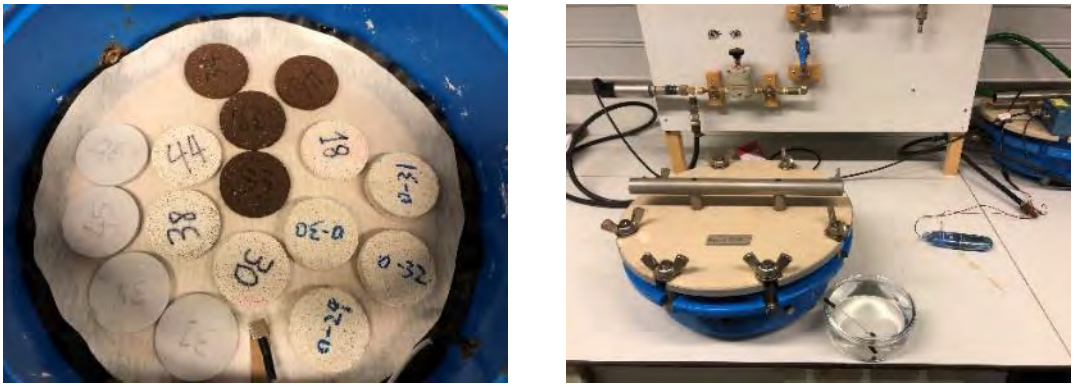

a. Samples in the pressure vessel b. Overview of the setup

Figure 6-11: The adsorption pressure plate for measuring moisture storage curves.

During the test, compressed air is first supplied into the vessel at a pressure 1~2 $\cdot 10^5$ Pa higher than the target value. At this stage, the water in the filter paper and in the porous ceramic plate slowly flows out of the vessel into the container with pure water, creating an uninterrupted hydraulic continuity in the system. After 1~2 hours, when the pressure equilibrium has been fully realized, the air pressure in the vessel is slowly decreased to the target value, causing a suction from the water outlet into the pressure vessel. Now the samples can absorb moisture at this target pressure while the suction ensures a continuous water supply from the container. After reaching equilibrium, the moisture content of the samples can be gravimetrically determined, the same as in the traditional pressure plate test.

It should be noted that when the samples are laid on the filter paper before the compressed air is exerted, it is possible for them to absorb moisture from the moist filter paper and the pre-saturated porous ceramic plate freely. That's the reason why the filter paper should only be moderately moist and the compressed air should be exerted as soon as possible, in order to avoid the situation that samples quickly reach a moisture content higher than the value corresponding to the aimed p_c. For the ceramic plate it typically has very fine pores, so without external air/suction pressure the moisture transport between the samples and the plate would be negligibly slow.

It should also be mentioned that without a burette it is difficult to determine the equilibrium state during the test. Thus, the adsorption is interrupted from time to time to check the moisture content of the samples. The time needed for reaching equilibrium differs by different materials, but in most cases 2~3 weeks would suffice. In the future, we will make further modifications to the setup by integrating a burette into the water supply system, in order to facilitate the observation of equilibrium.

6.3.2.4 Hanging water column method

Theoretically, the traditional and adsorption pressure plates have an application p_c range between 0 Pa and -15$\cdot 10^5$ Pa. However, when the target p_c is very close to 0 (-5000 Pa, for instance), it becomes difficult to control the pressure very accurately, since any minor fluctuations in temperature, leakage condition and other factors could have a great impact on the applied air pressure and hence the p_c. To resolve this problem, the hanging water column is designed specifically for the close-to-0 p_c range. Figure 6-12 illustrates the schematic and Figure 6-13 are the photos of different parts.

Similar to the pressure plate, the hanging water column also has a pressure vessel. Since only moderate pressure is involved, there is no need to use very rigid metal but a plastic container can suffice. A porous ceramic plate is also fixed in the container, separating it into two parts and acting as the axis translation accessory for pressure regulation. However, unlike the pressure plate, the target pressure here is no longer controlled by the compressed air exerted above the porous ceramic plate but by a water column hanging below. By adjusting the height of the negative water head, an accurate suction could be maintained.

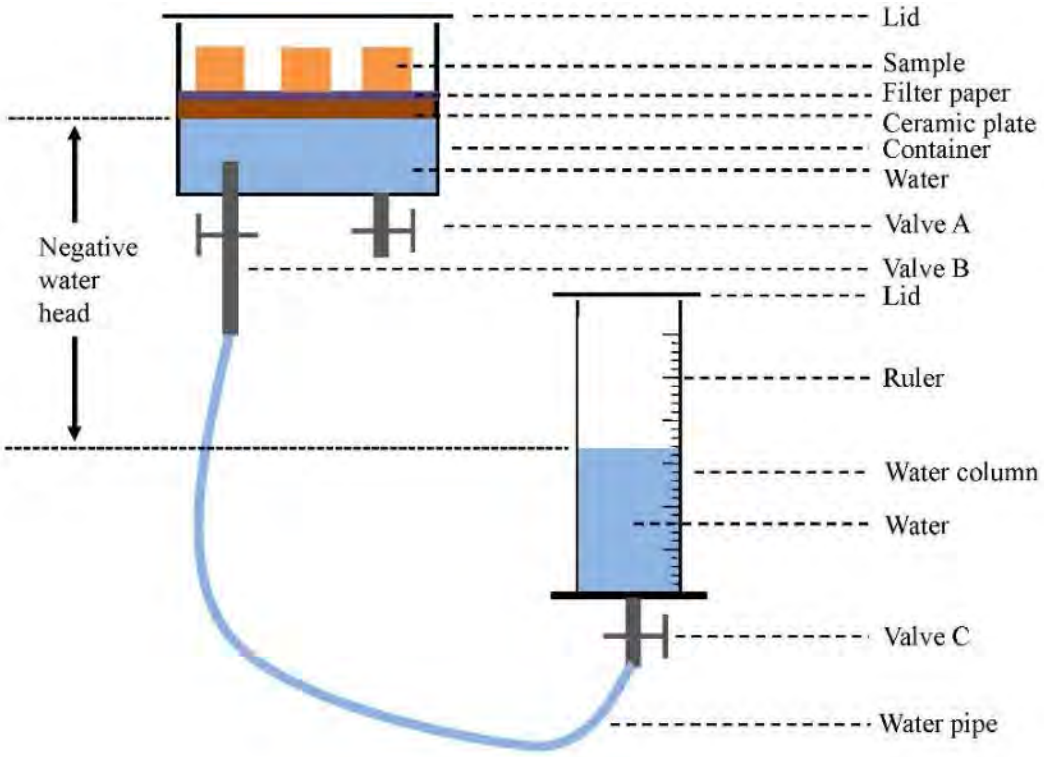

Figure 6-12: A schematic of the hanging water column setup.

Before the test, the container is turned upside down and the water column is filled with water. By opening valves A, B and C, water in the column flows into the container and expels the air inside. When all air has been evacuated, Valve A is closed and the container is turned around back to its normal direction. Now the water head could be adjusted to the target. After that, a piece of moist filter paper is placed on the porous ceramic plate to ensure good hydraulic contact, and the samples are laid above. To avoid evaporation, both the container and the water column are covered with lids. When equilibrium has been reached, the moisture content of the samples could be determined gravimetrically.

From the operational procedures it is clear that the hanging water column method suits both adsorption and desorption processes. In theory, the negative water head could be as large as wanted as long as the suction remains within the air penetration pressure of the porous ceramic plate and no cavitation phenomenon occurs. In practice, however, it is most convenient to keep a water column within 2 m, generating a p_c greater than -20000 Pa. In the future, we will try to combine the water column with a vacuum pump system to broaden the application pressure range.

a. Overview of the setup

b. Samples on the ceramic plate

c. Control valves

d. Water column for pressure control

Figure 6-13: Photos of the hanging water column for measuring moisture storage curves.

6.3.3 Methods for transport property measurements

6.3.3.1 Water head method

When a material is (almost) saturated, the moisture transport is dominated by liquid and the vapor transport can be neglected. Consequently, if a water head is exerted upon a sample, by measuring the liquid flux, the permeability can be determined according to Darcy's law. Water head setups can differ in many details but the basic principle remains the same. According to whether the water head remains steady or is changing, setups can be generally classified into the constant head (Nijp et al., 2017) and the falling head (Pedescoll et al., 2011) categories. The constant head method produces a steady flow and is therefore simple in the calculation, but the setup is more complicated to ensure a constant water head. On the contrary, the falling head method involves transient flow, causing more complex in the calculation. However, its setup can be simpler.

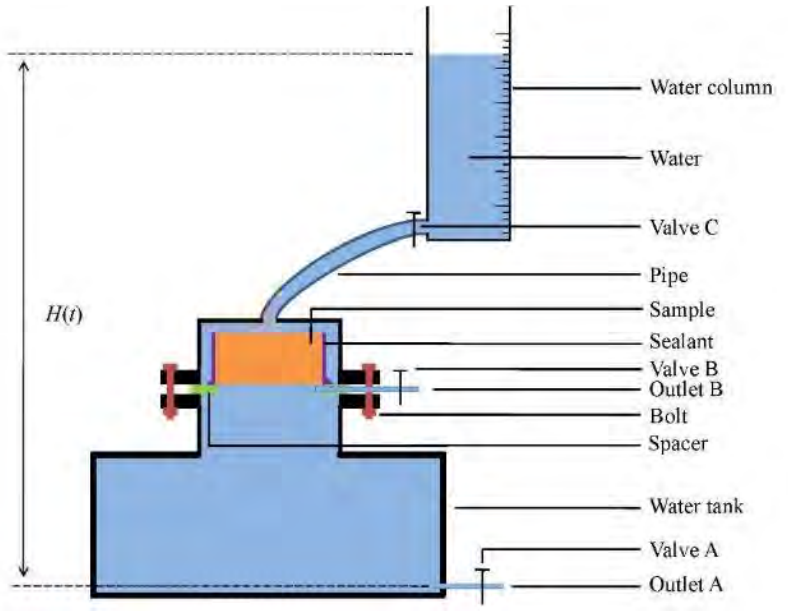

Figure 6-14: A schematic of the water head setup.

a. Overview of the setup

b. The water column

Figure 6-15: Photos of the water head setup for measuring liquid permeability.

In this project, we use the falling head. Figure 6-14 illustrates the schematic and Figure 6-15 shows the photos of the setup. During the test, a laterally sealed sample is first mounted into the setup and then the water tank is filled with water. All air inside the water tank can be evacuated by properly opening/closing valves, similar to the hanging water column (Section 6.3.2.4). After that either Outlet A or Outlet B can be used and the water column acts as the water supply. The instant water head $H(t)$ (m) is recorded regularly during the measurement.

To derive the liquid permeability, we define vertical upward as the positive direction. Assume the water column with a constant intersection area S (m^2), then within time interval dt (s), the total flow volume dV (m^3) is:

$$\boldsymbol{dV = -S \cdot dH(t)} \quad \textbf{Equation 6-1}$$

The mass flow rate $\dot{G}$ ($kg \cdot s^{-1}$) is therefore:

$$\boldsymbol{\dot{G} = \rho_{water} \cdot \frac{dV}{dt} = -\rho_{water} \cdot S \cdot \frac{dH(t)}{dt}} \quad \textbf{Equation 6-2}$$

where ρ_{water} is the water density, $kg \cdot m^{-3}$. The sample's surface area is A (m^2), its thickness is T (m). According to Darcy's law, the water flux $\dot{g}$ ($kg \cdot m^{-2}s^{-1}$) through the sample can be written as:

$$\boldsymbol{\dot{g} = K_l \cdot \frac{\Delta p_l}{T} = K_l \cdot \frac{\rho_{water} \cdot g \cdot H(t)}{T}} \quad \textbf{Equation 6-3}$$

where Δp_l is the liquid pressure difference, Pa; g the gravitational acceleration, $m \cdot s^{-2}$.

The water flow $\dot{G}$ ($kg \cdot s^{-1}$) through the sample is therefore:

$$\boldsymbol{\dot{G} = \dot{g} \cdot A = K_l \cdot \frac{A \cdot \rho_{water} \cdot g}{T} \cdot H(t)} \quad \textbf{Equation 6-4}$$

Equating Eq.(6-2) and (6-4) yields:

$$\boldsymbol{-\rho_{water} \cdot S \cdot \frac{dH(t)}{dt} = K_l \cdot \frac{A \cdot \rho_{water} \cdot g}{T} \cdot H(t)} \quad \textbf{Equation 6-5}$$

which finally gives the solution:

$$\boldsymbol{ln\big(H(t)\big) = -K_l \cdot \frac{A \cdot g}{S \cdot T} \cdot t + lnH_{t=0}} \quad \textbf{Equation 6-6}$$

The permeability K_l can thus be obtained.

6.3.3.2 Semi-permeable membrane method (for transport)

As explained in Section 6.3.2.2, the semi-permeable membrane can be used for osmotic/capillary pressure control. It is, therefore, possible to use saturated salt solutions to exert a constant driving force for liquid water flowing through a sample, with semi-permeable membranes to protect the sample against salts' interference. The liquid permeability can thus be derived from the water flux and the pressure difference. By altering the saturated salt solutions, the capillary pressure difference over and the moisture content in the sample can be controlled.

Based on this idea, a simple experimental setup is designed and constructed (Figure 6-16 and 6-17 a). In this setup, a sample of known size is laterally sealed with epoxy to obtain a 1-D liquid flow. The top of the sample is in direct contact with pure water (p_c=0 Pa). The sample bottom sits on a semi-permeable membrane in contact with a saturated K_2SO_4 solution with an RH of 97% at 22±1°C, corresponding to a p_c of $-3.6 \cdot 10^6$ Pa. The additional water head difference on both sides of the sample, originating from different water levels in the container and burette, is negligibly small relative to the used p_c difference ($\Delta p_c = 3.6 \cdot 10^6$ Pa). Consequently, the capillary pressure difference is assumed as the only driving force for the water flow through the sample.

When the flow is ongoing, the pure water in the water tank passes through the sample and the semi-permeable membrane, entering the solution tank, where undissolved salt exists and a magnetic stirring system is installed to keep the solution saturated all the time. In this way, a constant Δp_c can be maintained and a steady flow can be reached after an initial period. The volumetric flow rate (G, $m^3 \cdot s^{-1}$) can be easily measured by reading the burette regularly. Given that the burette is part of the container with the saturated solution, the volumetric flow rate thus relates to the inflowing pure water and the additionally dissolved salt.

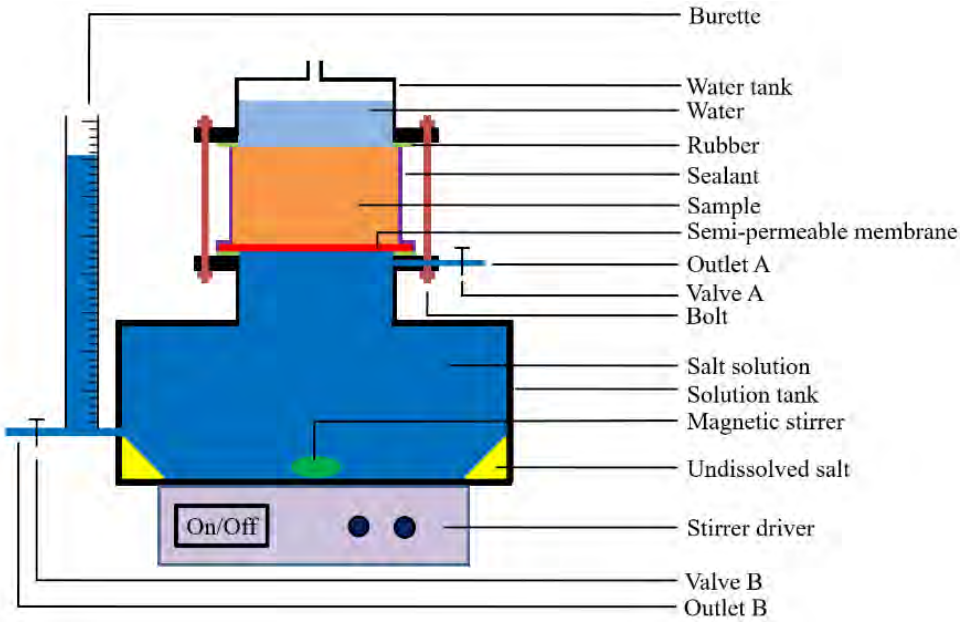

Figure 6-16: A schematic of the semi-permeable membrane setup.

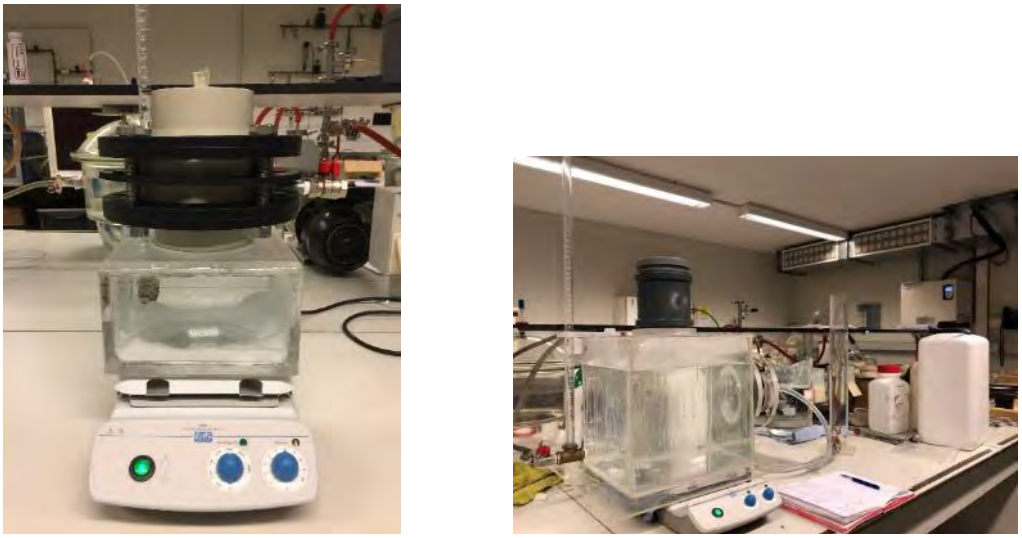

a. The vertical version b. The horizontal version

Figure 6-17: The semi-permeable membrane setup for measuring liquid permeability.

Assuming a certain amount of pure water (Δm_{water}, kg) passes through the sample and the membrane into the solution tank. The K_2SO_4 dissolved by it (Δm_{K2SO4}, kg) amounts to $s \cdot \Delta m_{water}$, where s is the solubility of K_2SO_4, kg(K_2SO_4)·kg(water)$^{-1}$. Consequently, in the solution tank the increased saturated K_2SO_4 solution ($\Delta m_{solution}$, kg) occupies a volume of $\Delta V_{solution}$ (m^3):

$$\Delta V_{solution} = \frac{\Delta m_{solution}}{\rho_{solution}} = \frac{\Delta m_{water} + \Delta m_{K2SO4}}{\rho_{solution}} = \frac{\Delta m_{water} + S \cdot \Delta m_{water}}{\rho_{solution}} \quad \textbf{Equation 6-7}$$

where $\rho_{solution}$ is the density of saturated K_2SO_4 solution, kg·m^{-3}.

Since previously undissolved K_2SO_4 is now dissolved, its volume (ΔV_{K2SO4}, m^3) should therefore be accounted for when calculating the net volume change (ΔV_{net}, m^3) in the solution tank:

$$\Delta V_{net} = \Delta V_{solution} - \Delta V_{K2SO4} = \frac{\Delta m_{water} + S \cdot \Delta m_{water}}{\rho_{solution}} - \frac{S \cdot \Delta m_{water}}{\rho_{K2SO4}} \quad \textbf{Equation 6-8}$$

where ρ_{K2SO4} is the density of K_2SO_4, $kg \cdot m^{-3}$. Now we define a coefficient c ($kg \cdot m^{-3}$) by:

$$c = \frac{\Delta m_{water}}{\Delta V_{net}} = \frac{1}{\frac{1+s}{\rho_{solution}} - \frac{s}{\rho_{K2SO4}}} \quad \textbf{Equation 6-9}$$

At 22°C it can be obtained that c=1009 $kg \cdot m^{-3}$, meaning that 1 m^3 increase in the net volume of the solution tank (indicated by the burette) reflects 1009 kg of inflowing pure water. With the help of the known c, the mass balance of the transport process can be described by:

$$G \cdot c = \frac{\Delta p_c}{R_{total}} \cdot A \quad \textbf{Equation 6-10}$$

where R_{total} is the total liquid transport resistance, $m^2 sPa \cdot kg^{-1}$. R_{total} is the sum of the membrane's resistance $R_{membrane}$ ($m^2 sPa \cdot kg^{-1}$) and the sample's resistance R_{sample} ($m^2 sPa \cdot kg^{-1}$):

$$R_{total} = R_{membrane} + R_{sample} = R_{membrane} + \frac{T}{K_l} \quad \textbf{Equation 6-11}$$

Combining Equation 6-10 and Equation 6-11, the liquid permeability of the sample can be finally derived:

$$K_l = \frac{T}{\frac{\Delta p_c \cdot A}{G \cdot c} - R_{membrane}} \quad \textbf{Equation 6-12}$$

After finishing the test, the moisture content of the sample can be obtained gravimetrically, while $R_{membrane}$ can be obtained from similar measurements without installing the sample in the setup.

To completely fulfill the measurements in a wide moisture content range, a double-membrane setup with two semi-permeable membranes separating two different saturated salt solutions on both sides of the sample is needed. At the trial stage, we simplify the setup to the single-membrane system described above. This setup restricts the applicable moisture content range to near saturation but is adequate for preliminary validation. Its success will call for a slightly more complicated double-membrane setup.

To validate and utilize this method, trial measurements are performed on two representative porous building materials: calcium silicate and autoclaved aerated concrete. As a reference, falling head water column tests (Section 6.3.3.1) are also performed for comparison. Figure 6-18 illustrates the experimental results. As is clearly shown, for both calcium silicate and autoclaved aerated concrete, the measured K_l reflects an expected moisture content dependence – the higher the w is, the larger the K_l is. However, it is very noticeable that the measured K_l values from the two methods differ about 4 orders of magnitude. Our water column measurements on other materials agree nicely with other data sources. Thus, the water column results should be trustworthy and the semi-permeable membrane approach underestimates K_l. This underestimation is far beyond what common experimental errors can explain, and more profound reasons must exist.

The first explanation for the underestimation could be that the transport area of the sample should be corrected for the masked sample edge in the setup. However, in our trial measurements the total diameter of the sample is 10 cm while the unmasked diameter is roughly 9 cm. Simple estimation reveals that the underestimation of K_l caused by the masked edge should be less than $1-(9/10)^2 \approx 20\%$, while from Figure 6-18 we should focus on the difference amounting to 4 orders of magnitude. Consequently, the masked edge is not a primary reason for the underestimation.

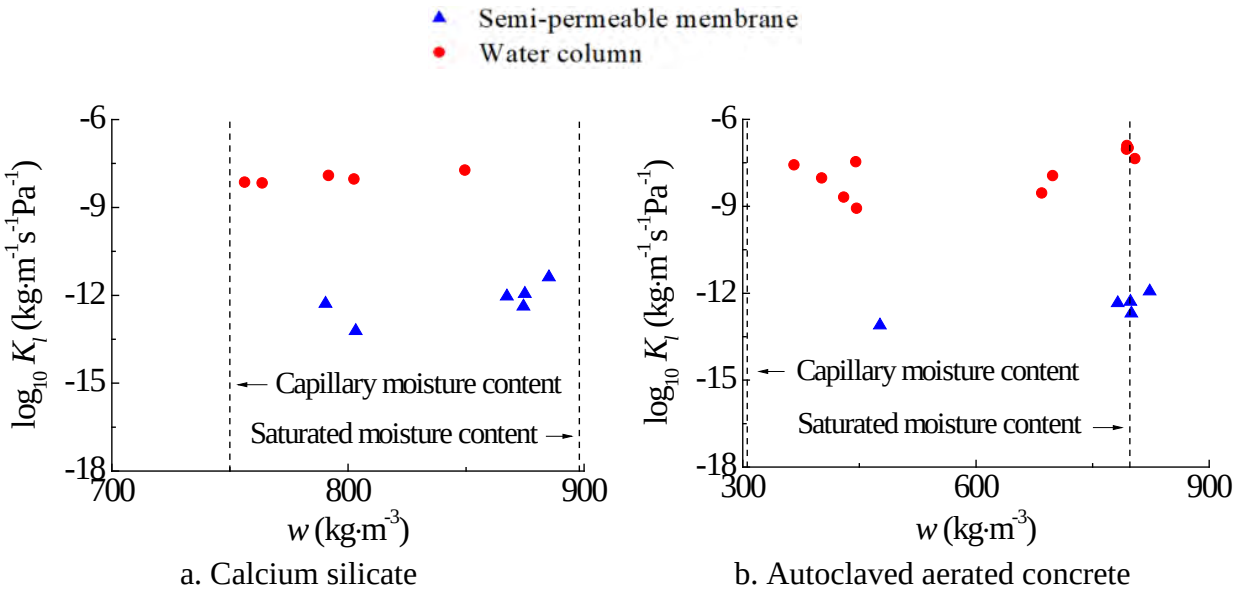

a. Calcium silicate b. Autoclaved aerated concrete

Figure 6-18: Experimental results of the semi-permeable membrane and water head tests.

Another possibility is the change in driving force. Ideally no salt can pass the semi-permeable membrane, while in practice a small amount of salt may still penetrate through the membrane. If salt gets through the membrane and the sample, thus entering the tank for pure water, the real driving force will decrease and subsequently an underestimation of the final K_l will occur. However, reducing the Δp_c to $1/10^4$ of the assumed original value ($3.6 \cdot 10^6$ Pa) means that the pure water tank above the sample should almost get saturated with K_2SO_4. The membrane used in this study is also Filmtech® Flat Sheet BW30 (the same one as in Section 6.3.2.2) with a very high salt rejection rate. Consequently, it is unimaginable to assume an almost saturated solution in the upper tank due to the negligible salt transfer through the membrane. Direct measurements of the capillary pressure and electrical conductivity in both tanks also provide support.

A third plausible reason is that the overall transport resistance is underestimated due to the existence of air layers in the setup. A key to the success of the semi-permeable membrane test is that perfect hydraulic continuity must be ensured throughout the whole system. In reality, however, there can be very thin air layers on both sides of the membrane, acting as an additional transport resistance. For the lower side of the membrane, Valve A and Outlet A may not work perfectly to realize their intended function to remove the air below the membrane during the setup assembling process. For the upper side of the membrane, the sample may not be in perfect hydraulic contact with the membrane and air may be trapped in between. To check this hypothesis and completely remove the air in the system, we re-designed and built the semi-permeable membrane setup, turning the vertical system into a horizontal one (Figure 6-17 b). That should allow a proper elimination of the air layers around the membrane. Unfortunately, this horizontal setup also fails to produce reasonable results, and hence invalidate this hypothesis.

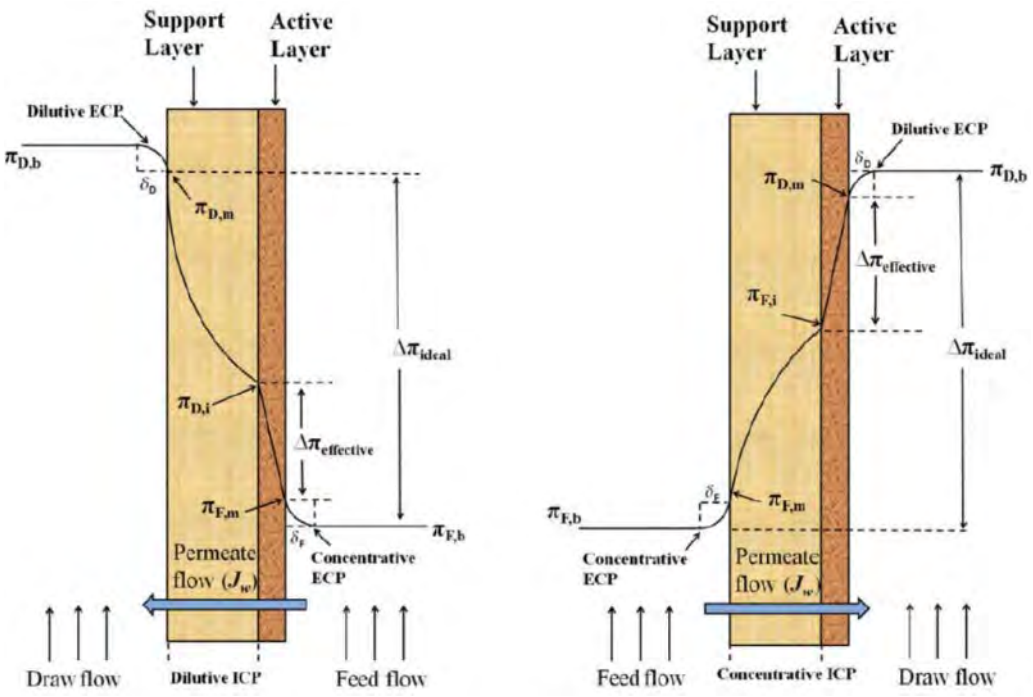

Figure 6-19: The concentration polarization of the semi-permeable membrane (Bhinder et al, 2017).

The last clue we are looking at is called concentration polarization, which is a common phenomenon for the transport with a semi-permeable membrane. It can be classified as external concentration polarization (ECP) and internal concentration polarization (ICP), both including dilutive and concentrative effects (Figure 6-19). Details of this phenomenon can be found in (Bhinder et al., 2017) and many other references. In short, it is the support layer of the semi-permeable membrane that causes sharp decrease in the driving force across the membrane and hence reduces the water flux significantly. To solve this problem, we removed the support layer of our semi-permeable membrane (Figure 6-20) and used the active layer only. Trial tests show that after peeling off the support layer, the resistances of the membrane determined by the semi-permeable membrane setup and by the water head setup are very close to each other, both agreeing nicely with literature values. It is, therefore, most likely that our previous failure should be (mainly) attributed to the concentration polarization phenomenon. However, the active layer of the semi-permeable membrane is very thin and fragile, so using the membrane without the support layer requires modifications to the setup to test porous building materials, which is our ongoing effort.

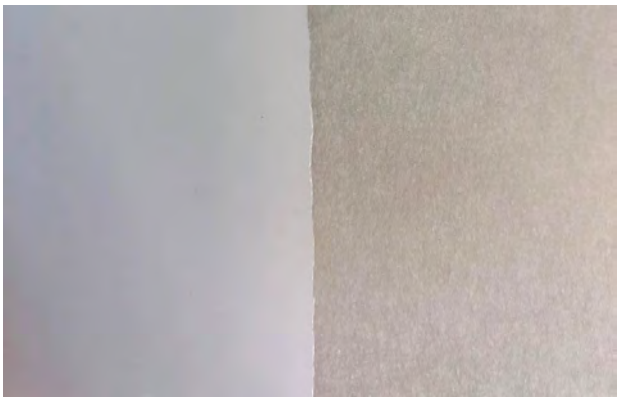

Figure 6-20: The semi-permeable membrane (left: active layer; right: support layer).

6.3.3.3 Tension infiltrometer method

Besides the semi-permeable membrane method, we also designed new setups to measure the liquid permeability of porous building materials at a moisture content below w_{cap}. Given the success of the water head method, we are trying to make a modification to it.

In the water head setup described in Section 6.3.3.1, a positive water head is put upon the sample. Thus, its moisture content can never go below w_{cap}. However, by placing the sample up and keep the inflow/outflow water columns down, a suction pressure can be exerted on both sides of the sample, reducing its moisture content. This negative water head method has the same principle as the tension infiltrometer used in soil science (Figure 6-21, (Moret-Fernández et al., 2012)), but can differ in the details of the setup.

While trying to design a simple tension infiltrometer (or negative water head setup) for our purpose, we encountered some practical difficulties. The most important two are the applicable p_c range and the moisture content determination. As explained in Section 6.3.2.4, a common water column in a lab is within a couple of meters, unable to produce a very low p_c. Consequently, the sample's moisture content may not reach a value much lower than w_{cap}, limiting the application value of this setup. Moreover, with a negative water head, a suction pressure is applied to the sample, keeping its moisture content below w_{cap}. However, to get the sample out of the setup for moisture content determination, the system must be restored to atmospheric pressure. Once the pressure is recovered, the sample can immediately absorb water and raise its moisture content. Currently we are trying to find solutions to these problems.

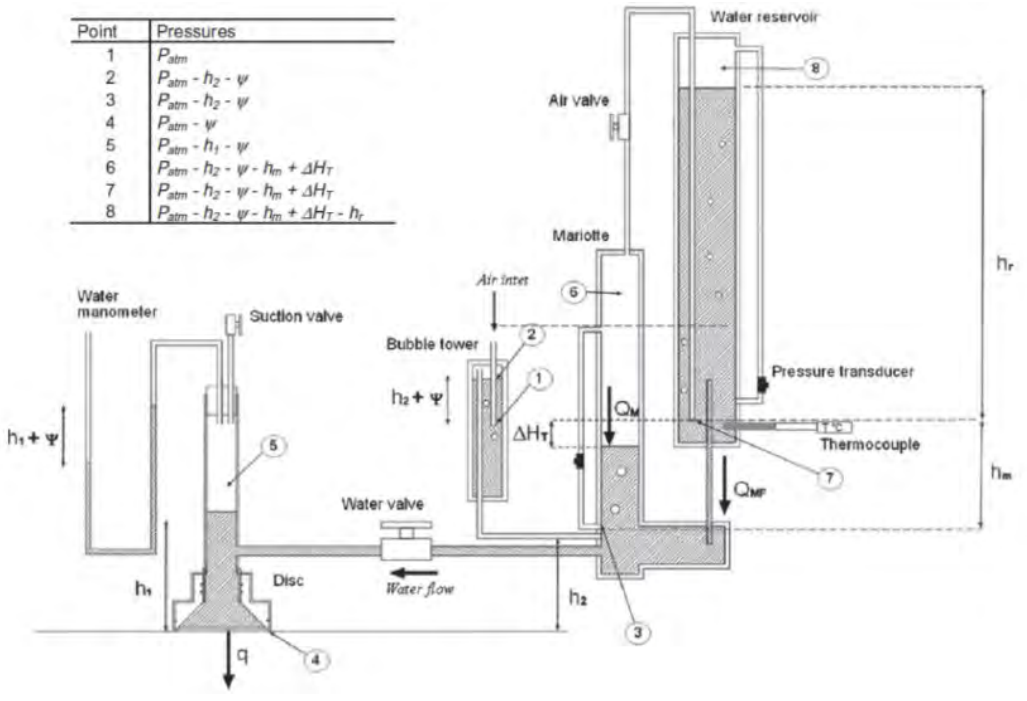

Figure 6-21: The schematic of a tension infiltrometer (Moret-Fernández et al., 2012).

6.3.4 Conclusions

In this section, we introduce several novel experimental methods to determine the hygric properties of porous building materials. Specifically, the psychrometer method, semi-permeable membrane method (for storage), adsorption pressure plate method and hanging water column method are innovated for measuring the moisture storage properties, while the water head method, semi-permeable membrane method (for transport) and tension infiltrometer test are designed for moisture transport properties. These methods enable the measurements in the full humidity range for both adsorption and desorption processes, on samples either untreated or hydrophobized.

6.4 Hygric properties of (not) hydrophobized building materials *(Chi Feng, KUL[8])*

6.4.1 Introduciton

With standardized and newly developed experimental protocols, we have tried to determine the hygric properties of Robusta ceramic brick and lime mortar as completely as possible. The brick is an industrial product widely used in Europe with good homogeneity. The mortar is on the other hand home-made, composed at the ratio of 10 liters of water, 12.5 kg of lime and 50 kg of sand, with a moisture curing period of two months and an accelerated carbonation period of one month. These two materials compose many building facades and are therefore representative. Sintered glass – even if not a building material – is also included as a reference for additional information due to its superb homogeneity. These materials (Figure 6-22) are tested both with and without hydrophobization treatment. For the hydrophobization treatment, the Wacker SMK 2100 agent (Figure 6-23 a) is used. Samples first absorb the diluted agent (10%, 0.1% or 0.01% by volume) to w_{cap} (Figure 6-23 b), then are exposed to 100% RH for two weeks and 54% RH for one week. After that, samples are dried in a ventilated oven at 70 °C for the dry mass determination. All measurements are carried out at lab temperature.

In the following sections, we first introduce the results from the vacuum saturation test and the mercury intrusion porosimetry (MIP), which characterize the basic information of the material. Next, the results from transport measurements – the capillary absorption test, the water head test, the cup test, and the drying test – are presented. Finally, the moisture storage functions – the sorption isotherms in the hygroscopic range and the retention curves in the over-hygroscopic range are reported.

a. Robusta ceramic brick

b. Lime mortar

c. Sintered glass

Figure 6-22 Target materials.

[8] Activities performed while at KUL, currently at Chongqing University, China

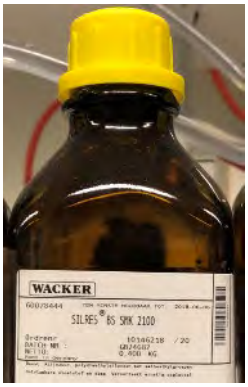

a. The SMK 2100 hydrophobization agent

b. Samples absorbing the diluted agent

Figure 6-23: The hydrophobization treatment.

6.4.2 Basic measurements

6.4.2.1 Vacuum saturation test

The vacuum saturation test (Figure 6-24) provides information on the bulk density (ρ_{bulk}, kg·m^{-3}), open porosity (ϕ) and saturated moisture content of materials. Detailed operational procedures can be found in (ISO 10545-3, 2018; Feng et al., 2015), and are not repeated here. Figure 6-25 - Figure 6-27 illustrate the experimental results, with error bars representing the standard deviations for multiple samples. It has been clearly revealed for all three materials that as the concentration of the hydrophobization agent increases, the bulk density increases while the open porosity and saturated moisture content decrease, with only minor exceptions due to experimental uncertainties. This common trend should be attributed to the fixation of the hydrophobization agent on the pore surfaces of materials and the subsequent decrease in the accessible pore volume. But in general these changes are not significant.

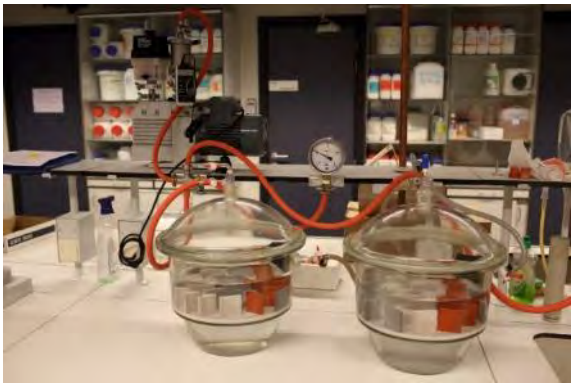

a. The vacuum saturation system

b. The underwater weighing system

Figure 6-24: The vacuum saturation setup.

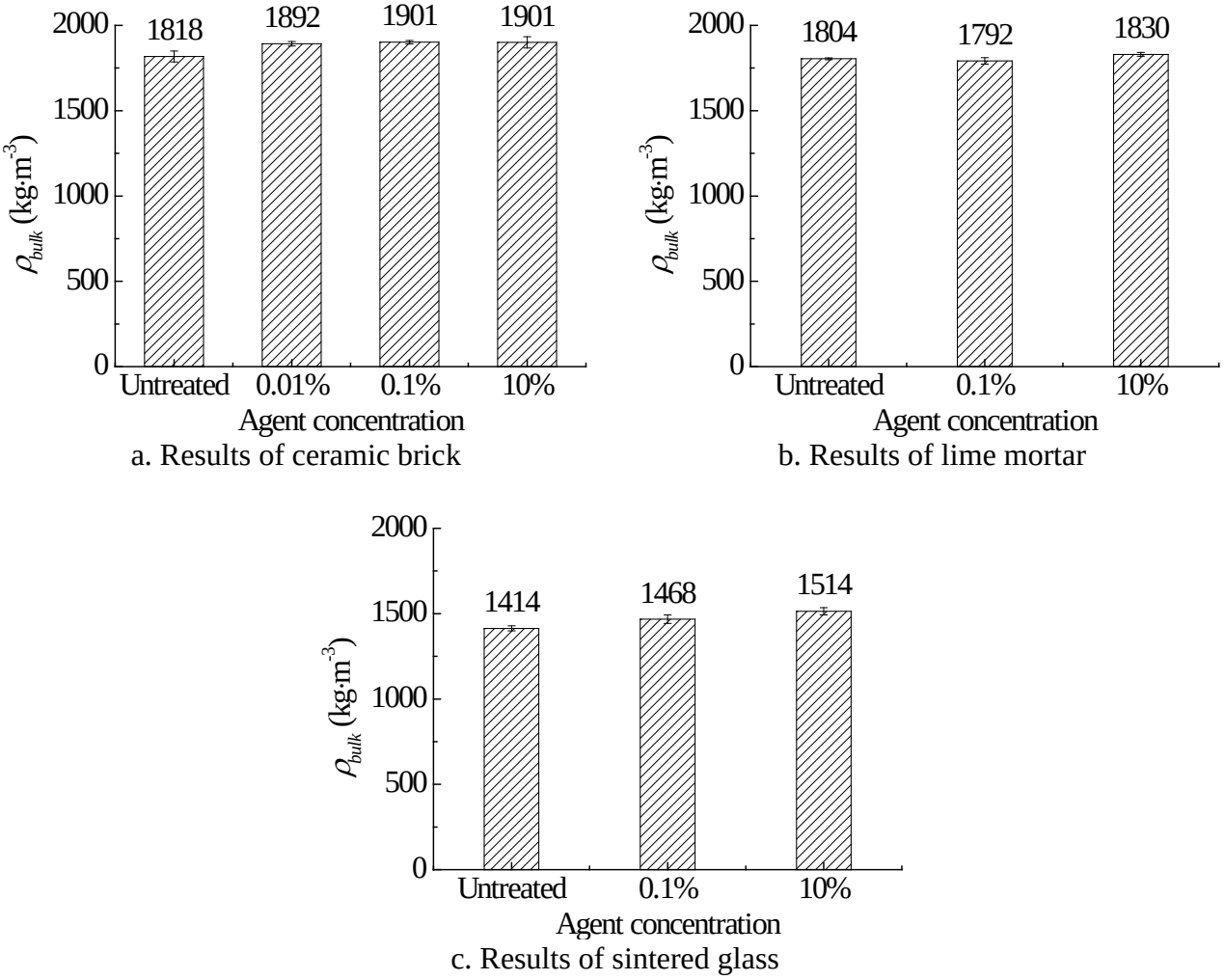

Figure 6-25: Bulk density obtained from the vacuum saturation test.

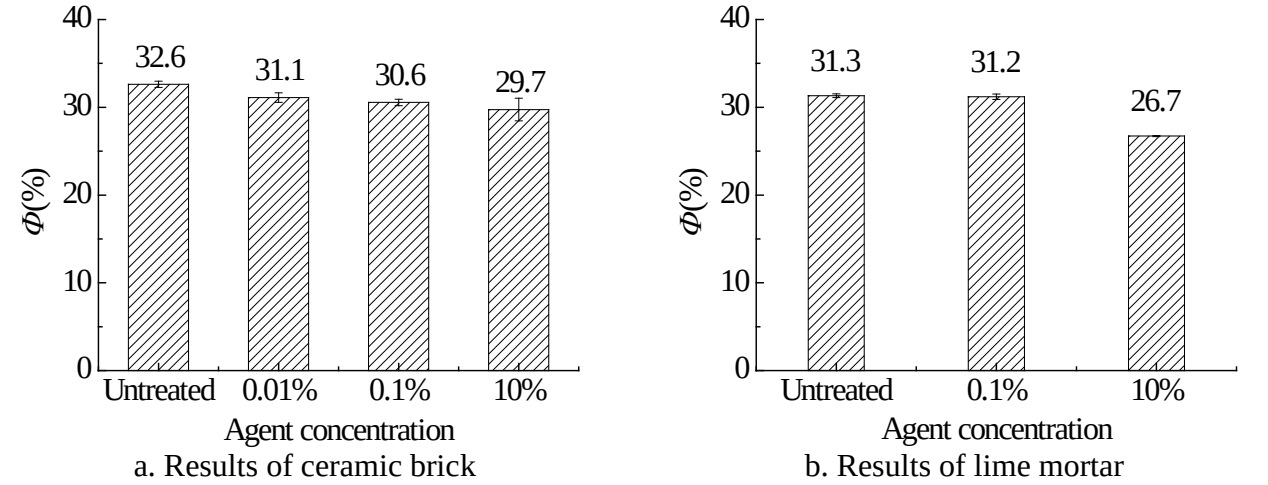

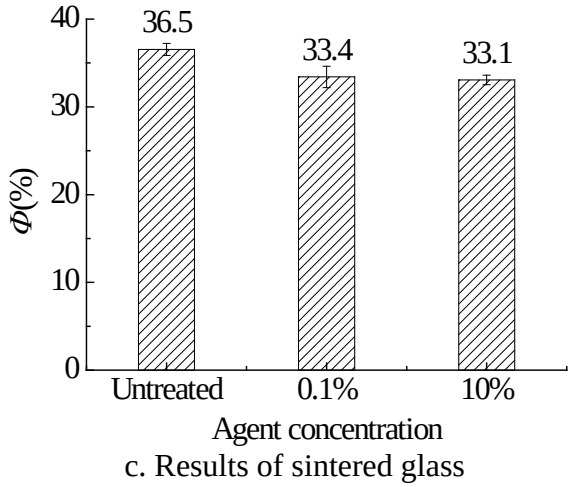

c. Results of sintered glass

Figure 6-26: Open porosity obtained from the vacuum saturation test.

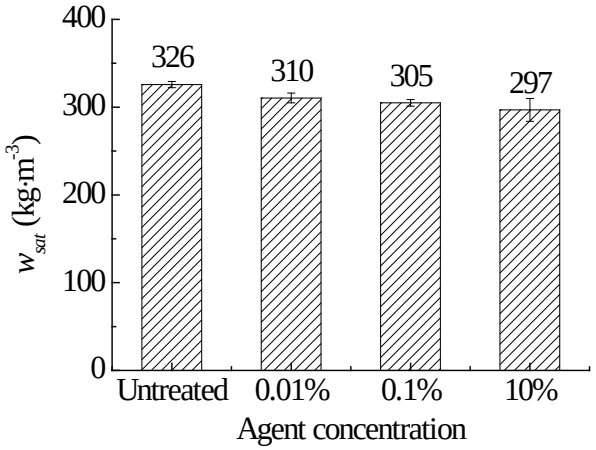

a. Results of ceramic brick

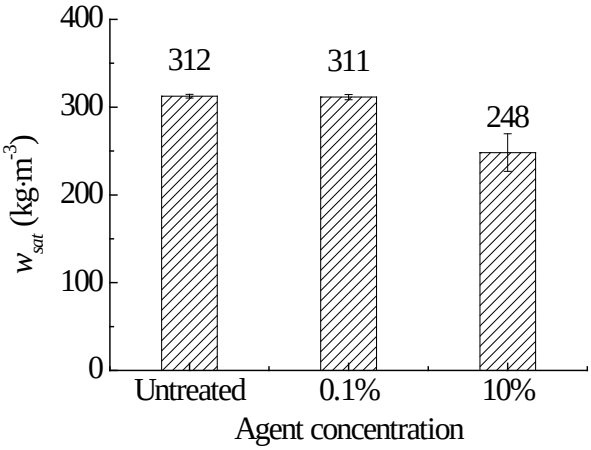

b. Results of lime mortar

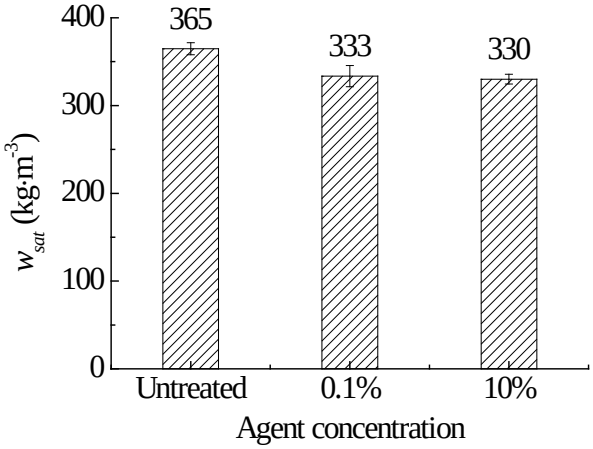

c. Results of sintered glass

Figure 6-27: Saturated moisture content obtained from the vacuum saturation test.

6.4.2.2 Mercury intrusion porosimetry (MIP)

The MIP test (Figure 6-28 a) is widely used to determine the pore volume distributions of porous materials (ASTM D4404, 2018; Roels et al., 2001). Albeit not perfectly accurate, it still serves as a very informative reference. The results of ceramic brick, lime mortar and sintered glass obtained from this method are illustrated in Figure 6-28.

It is clear that for all three materials the hydrophobization treatment has very limited impact on the pore radius (r, m) where the peak locates. For ceramic brick, the peak values seem to be changed significantly, but this is mainly due to our calibration. To process the raw mercury intrusion data, we shift the intrusion curves based on the open porosity and the desorption isotherm. Affected by the accumulated experimental errors from various sources, it is difficult to guarantee that all curves have been calibrated to the same extent. Consequently, a relative comparison could be informative while the absolute results from the mercury intrusion may not be highly dependable.

a. The MIP setup

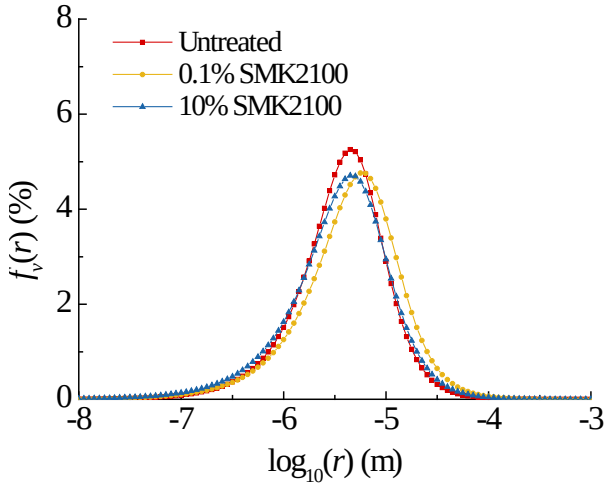

b. Results of ceramic brick

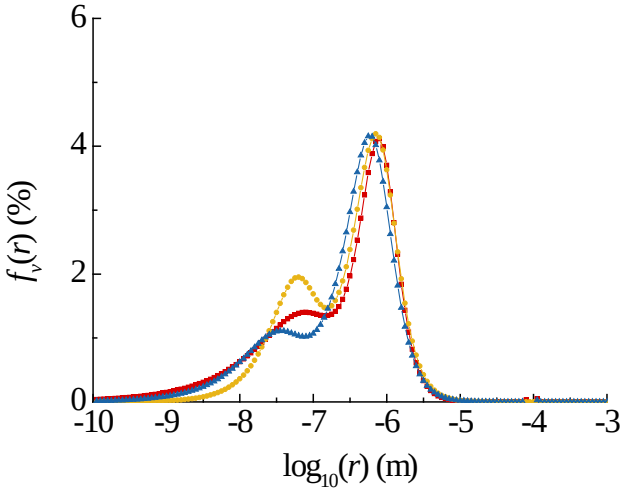

c. Results of lime mortar

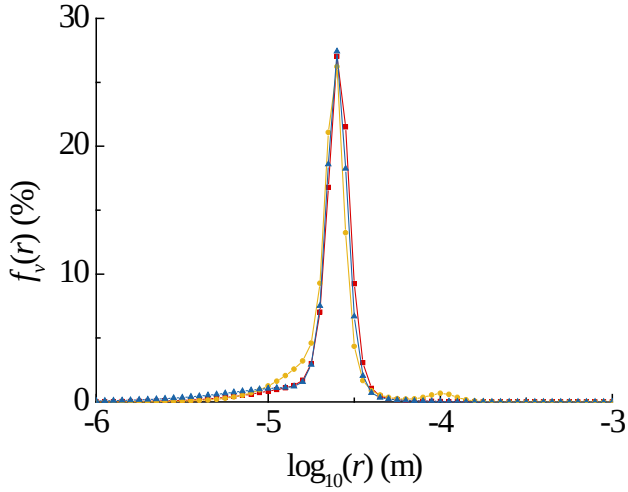

d. Results of sintered glass

Figure 6-28: The MIP setup and the retention curves.

6.4.3 Measurements on transport properties

6.4.3.1 Capillary absorption test

The capillary absorption test (Figure 6-29 a) is a popular and standardized method to measure a material's capillary absorption coefficient (A_{cap}, kg·m^{-2}s$^{-0.5}$) and capillary moisture content (ISO 15148, 2002; ASTM C1794, 2015; Feng and Janssen, 2018). The capillary absorption coefficients of ceramic brick, lime mortar and sintered glass obtained from this method are illustrated in Figure 6-29. It is clear that the hydrophobization treatment has a negative impact: the higher the agent concentration is, the lower the A_{cap} value becomes. There seems to be a critical agent concentration, beyond which a sharp decrease in A_{cap} occurs. However, this critical concentration varies with materials and has not been accurately determined in this project, which remains as a future task.

For the capillary moisture content, the value cannot always be determined if the capillary absorption coefficient becomes too small after hydrophobization (hence the waterfront cannot reach the sample's top). For the possible cases, the w_{cap} values are listed in Table 6-9. Clearly, unlike the capillary absorption coefficient that suffers from a decrease, the capillary moisture content remains almost unaffected.

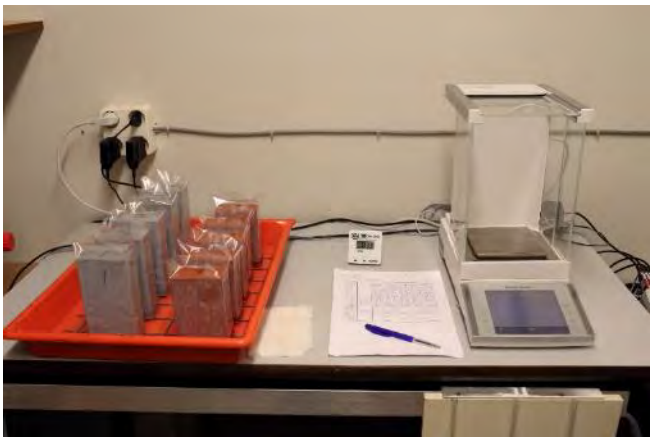

a. The capillary absorption setup

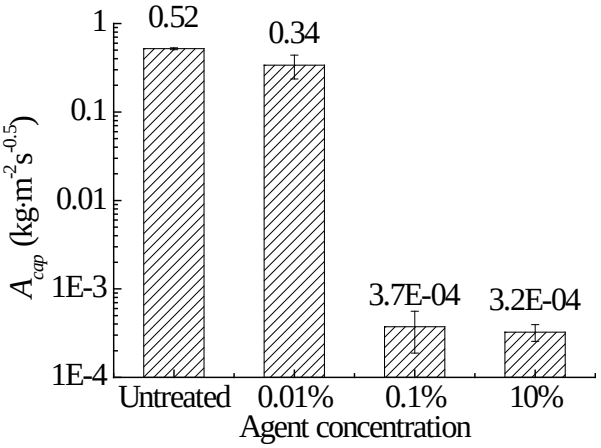

b. Results of ceramic brick

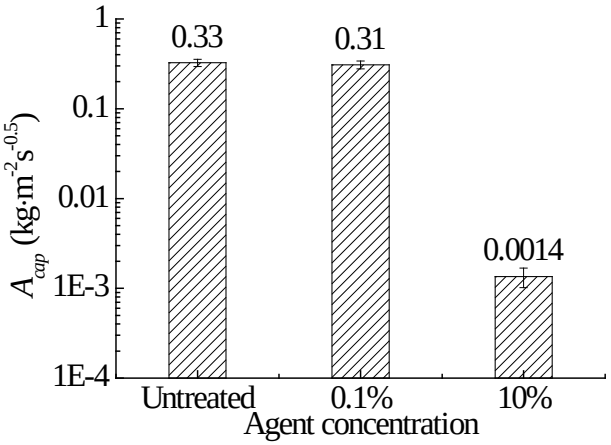

c. Results of lime mortar

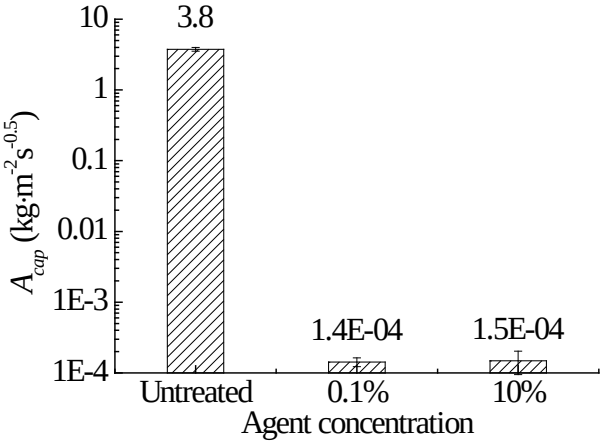

d. Results of sintered glass

Figure 6-29: The capillary absorption setup and the capillary absorption coefficients.

Table 6-9 Capillary moisture content obtained from the capillary absorption test

Material	Agent concentration	w_{cap} (kg·m^{-3})	
		Average	Standard deviation
Ceramic brick	Untreated	197	7
	0.01%	199	8
Lime mortar	Untreated	268	5
	0.1%	262	5
Sintered glass	Untreated	272	3

6.4.3.2 Liquid permeability from water head test

As explained in Section 6.3.3.1, the water head test can be used to measure the liquid permeability around capillary moisture content or above. The results for the target materials are illustrated in Figure 6-30. As references, the saturated and capillary moisture content of untreated materials are indicated. It can be generalized that liquid permeability (K_l) increases with moisture content, and the hydrophobization treatment reduces the K_l values. These are reasonable phenomena, and one plausible explanation is that the hydrophobization agent fixed on the pore surfaces of the material blocks the pathway of water. Consequently, the higher the agent concentration, the greater the K_l value decreases.

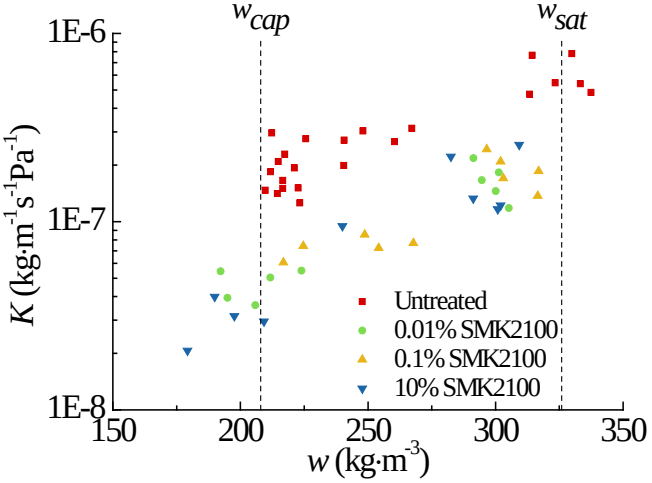

a. Results of ceramic brick

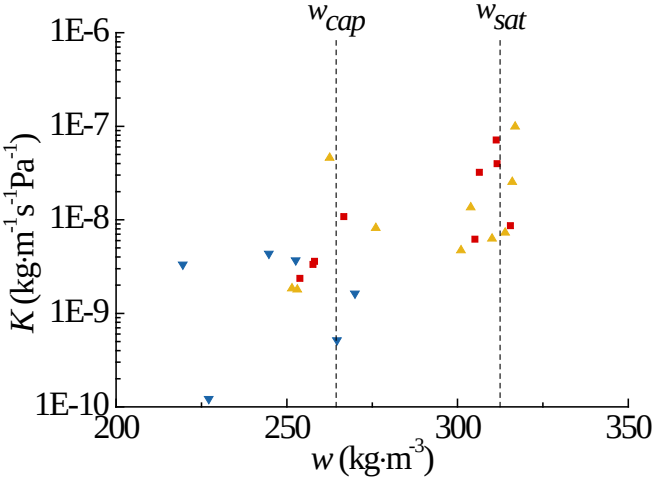

b. Results of lime mortar

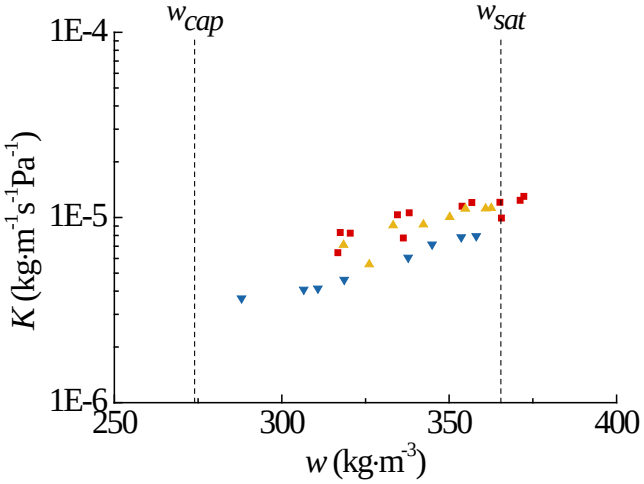

c. Results of sintered glass

Figure 6-30: The liquid permeabilities obtained from the water head test.

6.4.3.3 Vapor permeability from cup test

The cup test is the most frequently adopted method to measure the vapor permeability of porous building materials. It has been standardized world widely, e.g. by the ISO 12572 (2016) and the ASTM E96 (2016) standards. Tests are performed on all three target materials at different RH conditions, and the results are expressed in terms of the vapor resistance factors (the μ values). Figure 6-31 illustrates the results for ceramic brick and lime mortar, and two obvious trends can be concluded. First, the μ value decreases as the RH increases. This can be expected mainly due to the enhanced vapor condensation and its contribution. For ceramic brick this effect is not as significant as the lime mortar, because of its larger pore size and hence the weaker hygroscopicity. Moreover, the μ value increases with the concentration of the hydrophobization agent, and the effect on ceramic brick is again less obvious than lime mortar. This can also be attributed to the differences in the hygroscopicity. For the ceramic brick we also tested the untreated samples at RH 53.5%~84.7%, obtaining a μ value of 11.1 ± 1.0. For treated ceramic brick the measurements at this RH are not performed, as the results could be expected to lie between the tested cases, without much added value.

a. Samples sealed on the cups

b. The diffusion chamber

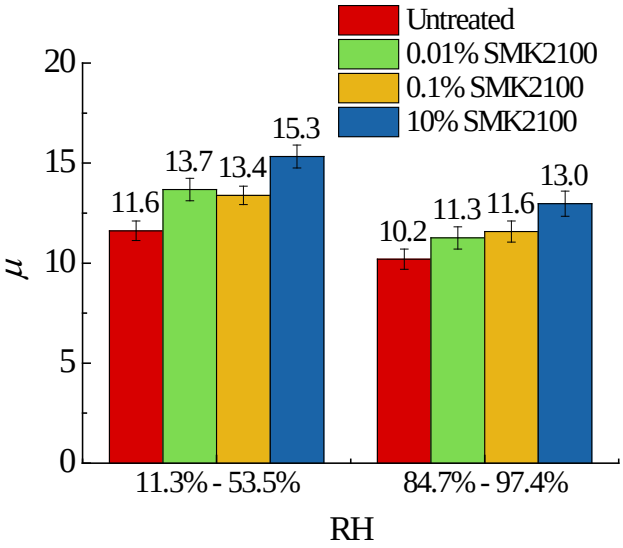

c. Results of ceramic brick

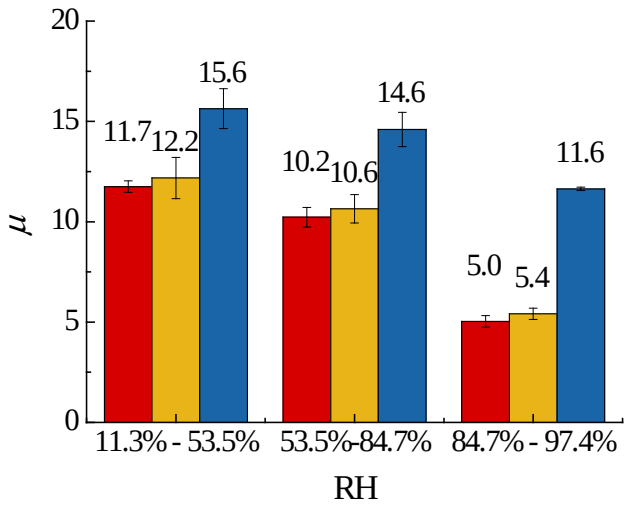

d. Results of lime mortar

Figure 6-31: The cup test setup and the vapor resistance factors.

Sintered glass has a larger pore size than ceramic brick, and is hence even less hygroscopic. Consequently, the hydrophobization treatment should have a very limited effect on vapor transfer and the measurements on treated sintered glass samples are subsequently not carried out. The μ values of untreated sintered glass at RH 11.3%~53.5%, 53.5%~84.7% and 84.7%~97.4% are 5.5, 5.4 and 4.7, respectively, with standard deviations of around 0.1.

6.4.3.4 Moisture permeability from drying test

To check the moisture permeability of treated and untreated materials, a modified drying test is also performed. Figure 6-32 illustrates the procedures. First, an untreated sample is conditioned to w_{sat}, with a thin layer of kaolin on top of it. Next, another sample of the same size, either untreated or treated, is laid above the kaolin. After that, the bottom and the lateral sides are sealed. Finally, the samples are placed in a climate chamber for drying. The bottom of the upper sample is assumed to have an RH of 100%, while the RH in the climate chamber is known. By checking the drying rate, the equivalent moisture resistance factor of the upper sample can be derived, with the help of the sample's dimension. The drying tests are performed on ceramic brick and lime mortar.

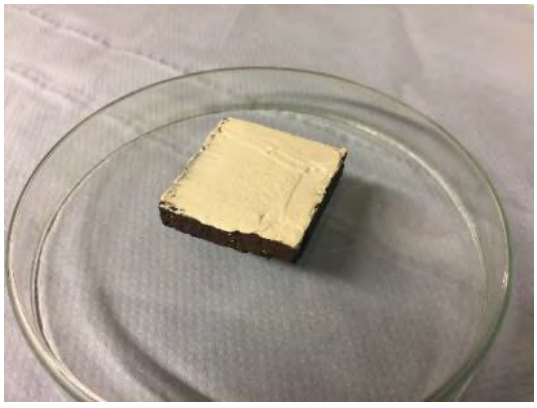

a. Kaolin and saturated sample

b. (Un)treated sample above the kaolin

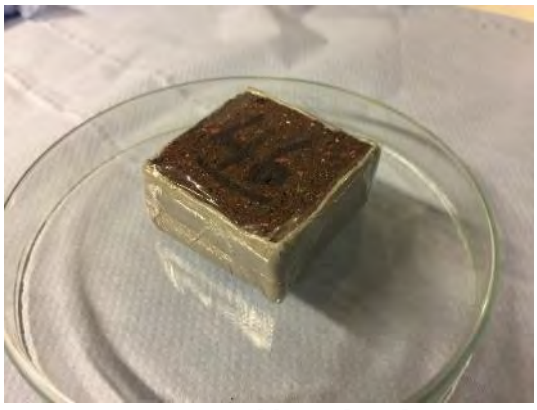

c. Bottom and lateral sealing

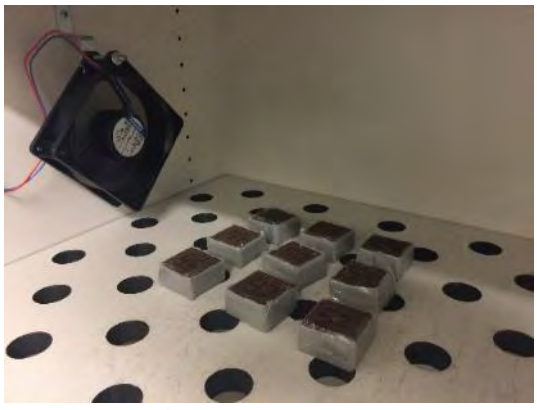

d. Drying process

Figure 6-32: The procedures of the drying test.

Results from the drying test are illustrated in Figure 6-33, with the dry cup and wet cup vapor resistance factors indicated as references. Clearly, when the samples are untreated or treated at a very low agent concentration, the μ values measured from the drying test are much lower than the values from the cup test. Actually, these μ values from the drying test are even smaller than 1, meaning that

the resistance is smaller than stagnant air. This is impossible for pure vapor diffusion, hence the liquid transport must play a role here. On the contrary, when the samples are treated at a higher agent concentration, the μ values measured from the drying test become comparable with the values from the cup test. This indicates that liquid transport no longer plays a significant role, and now it is the vapor diffusion that dominates.

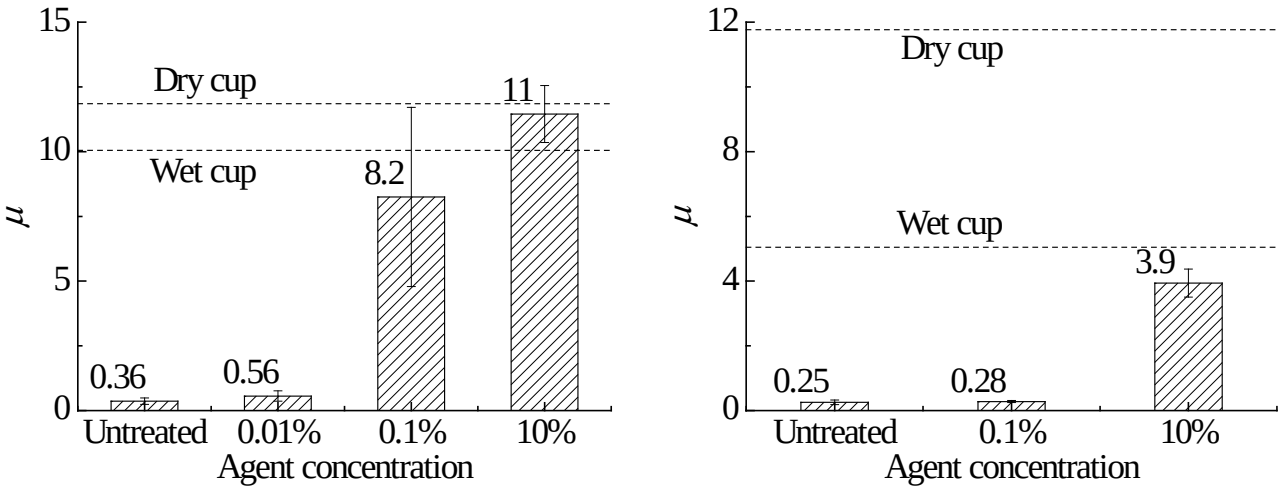

a. Results of ceramic brick b. Results of lime mortar

Figure 6-33: The moisture resistance factors obtained from the drying test.

6.4.4 Measurements on storage properties

6.4.4.1 Sorption isotherms in the hygroscopic range

Sorption isotherms reflect the moisture storage capacity of a material in the hygroscopic range. They can be measured either manually (e.g. the desiccator method (ISO 12571, 2013; Feng et al., 2013)) or automatically (e.g. the DVS method (Garbalińska et al., 2017)). In this project we resort to the desiccator method (Figure 6-34 a and b), which is simple and accurate.

For ceramic brick, trial measurements are first performed on untreated samples for both adsorption and desorption from w_{sat}. However, due to the material's weak hygroscopicity, the experimental uncertainties are too high so that the results are not reliable (Figure 6-34 c). It is therefore also meaningless to measure hydrophobized samples. As explained before, sintered glass is even less hygroscopic. Consequently, it is not tested for the sorption isotherms for either treated or untreated samples.

For lime mortar, the sorption isotherms for adsorption and desorption from w_{sat}/w_{cap} have been successfully obtained for untreated samples. For treated samples, the desorption curves starting from w_{sat} are also obtained. As is clearly demonstrated by Figure 6-34 d, lime mortar does not have an obvious hysteresis phenomenon, and the hydrophobization treatment causes a decrease in the material's hygroscopicity but only to a very limited extent.

a. Glass desiccators

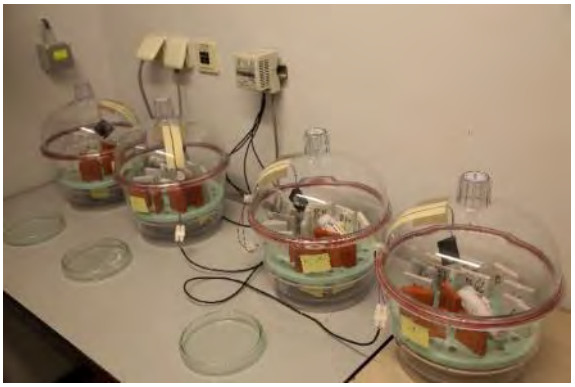

b. Plastic desiccators

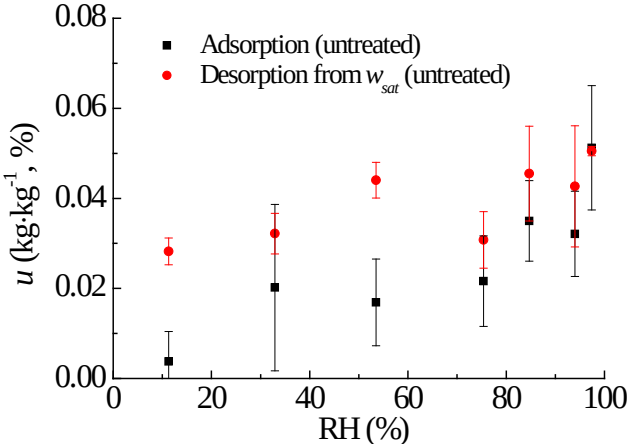

c. Results of ceramic brick

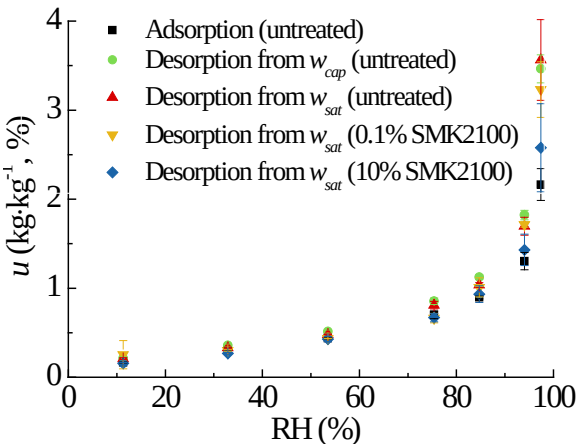

d. Results of lime mortar

Figure 6-34: The desiccator setup and the sorption isotherms.

6.4.4.2 Retention curves in the over-hygroscopic range

Retention curves characterize the moisture storage capacity of a material in the over-hygroscopic range. For the desorption process of untreated materials, pressure plate tests (ASTM C1699, 2015; ISO 11274, 2019) are performed and results are illustrated in Figure 6-35. Clearly, the retention curves of lime mortar decline slowly with p_c, while ceramic brick and sintered glass have their curves rapidly decreased in the low p_c range. These can be expected due to the respective pore sizes of different materials.

Limited by the accuracy of the pressure plate method for p_c>-1·10^5 Pa (Bittelli and Flury, 2009), the retention curves of ceramic brick and sintered glass there may not be reliable. To gather more trustworthy information, the hanging water column method described in Section 6.3.2.4 is used. Results are shown in Figure 6-36, in comparison with the pressure plate and MIP results. Clearly, the hanging water column tends to be a promising choice in this range (especially for sintered glass), although some uncertainties still exist.

a. The pressure plate setup

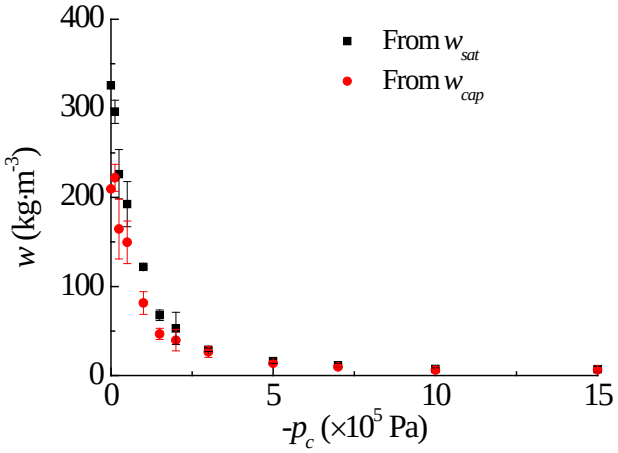

b. Results of ceramic brick

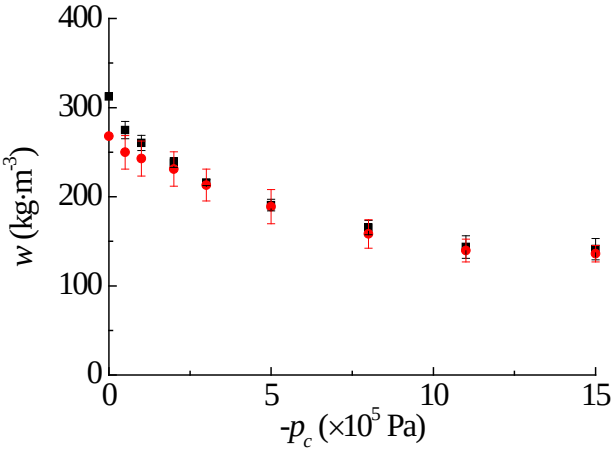

c. Results of lime mortar

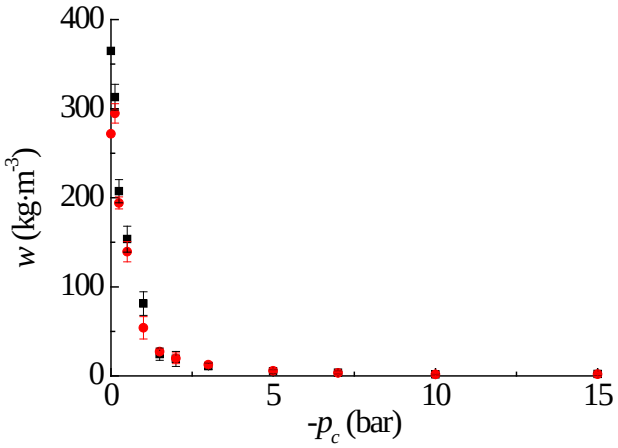

d. Results of sintered glass

Figure 6-35: The pressure plate setup and the desorption curves of untreated materials.

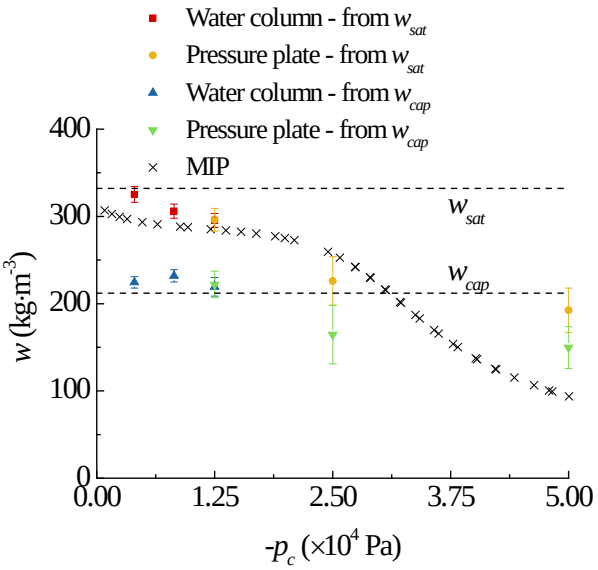

a. Results of ceramic brick

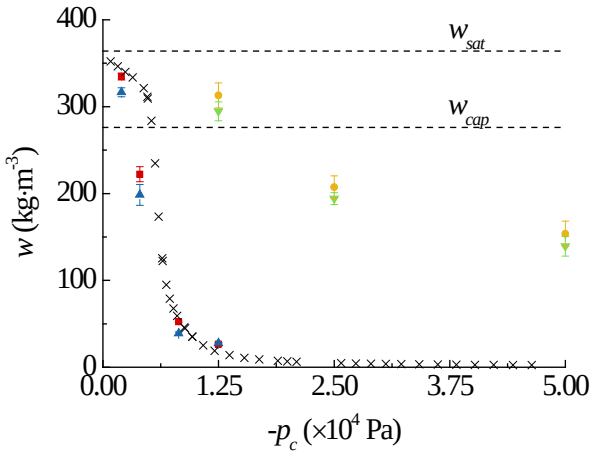

b. Results of sintered glass

Figure 6-36: The desorption retention curves of untreated materials close to p_c=0.

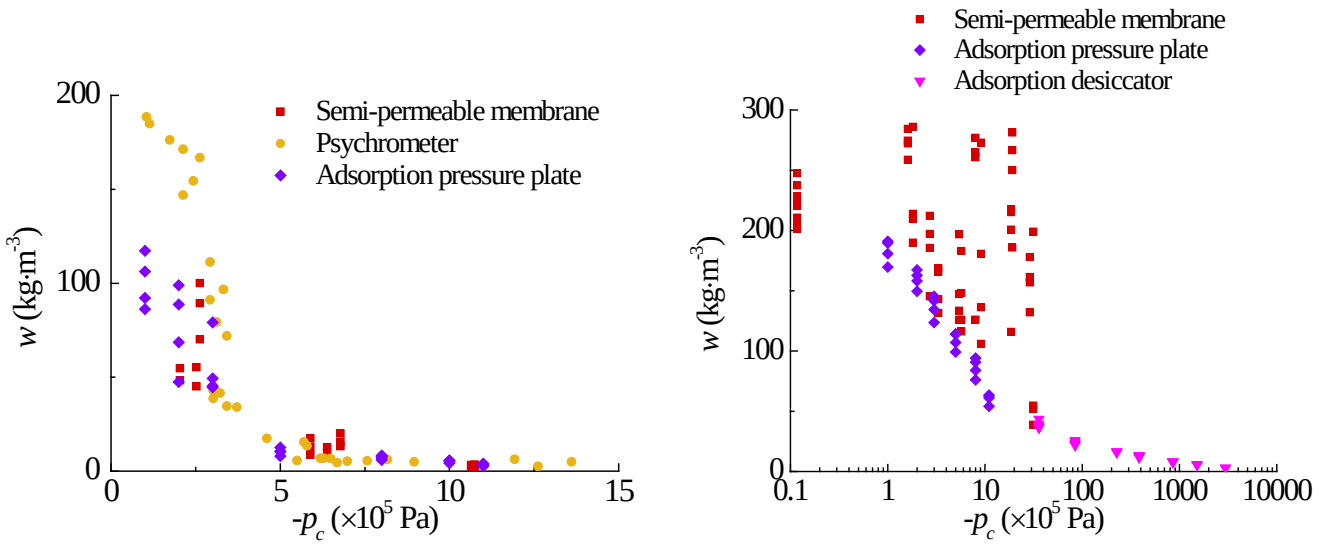

a. Results of ceramic brick

b. Results of lime mortar

Figure 6-37: The adsorption retention curves of untreated materials.

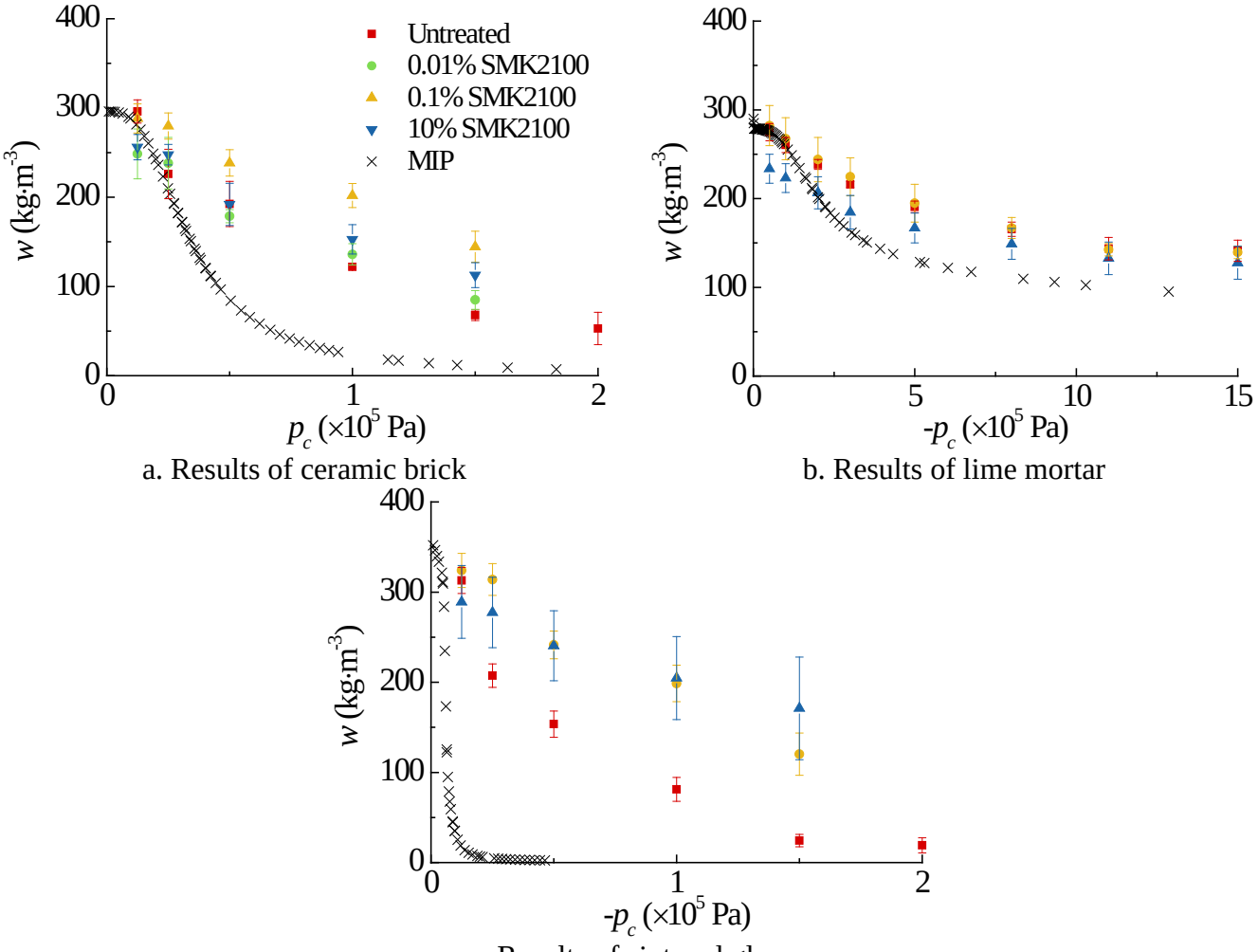

a. Results of ceramic brick

b. Results of lime mortar

c. Results of sintered glass

Figure 6-38: The desorption retention curves from pressure plate tests for treated materials (starting from w_{sat}, in comparison with untreated materials and the MIP results).

For the adsorption retention curves of untreated materials, the psychrometer method (Section 6.3.2.1), the semi-permeable membrane method (Section 6.3.2.2) and the adsorption pressure plate method (Section 6.3.2.3) are combined. Measurements are done on ceramic brick and lime mortar, and results are shown in Figure 6-37. For ceramic brick the large scatters for p_c close to 0 indicate that none of these methods is reliable there, but for the rest range results from different methods agree nicely. For lime mortar the semi-permeable membrane test always gives significant scatters. This may be because of the poor hydraulic contact between the sample surface and the membrane, as well as the large inhomogeneity of small samples for the semi-permeable membrane test. Fortunately, the adsorption results from the desiccator test provide external support to the reliability of the adsorption pressure plate. For sintered glass its adsorption retention curve can be expected to lie beyond the applicable range of these methods (due to its large pores), and is hence not tested.

For the desorption retention curves of treated samples, the pressure plate test fails to produce reliable results (Figure 6-38). For ceramic brick and sintered glass, the retention curves of treated samples are even above the ones for untreated, which is absolutely unreasonable. The main reason should be that after hydrophobization the hydraulic contact can no longer be nicely maintained in the pressure plate system. Consequently, external air pressure cannot drive the water in the samples out. Due to the same reason, the results of lime mortar are not highly reliable, either.

As an alternative, the hanging water column test is performed on the treated brick and mortar samples for the desorption process. The results in Figure 6-39 seem logical, but information within such a limited range is far from adequate. Thus further investigation into the treated samples are needed.

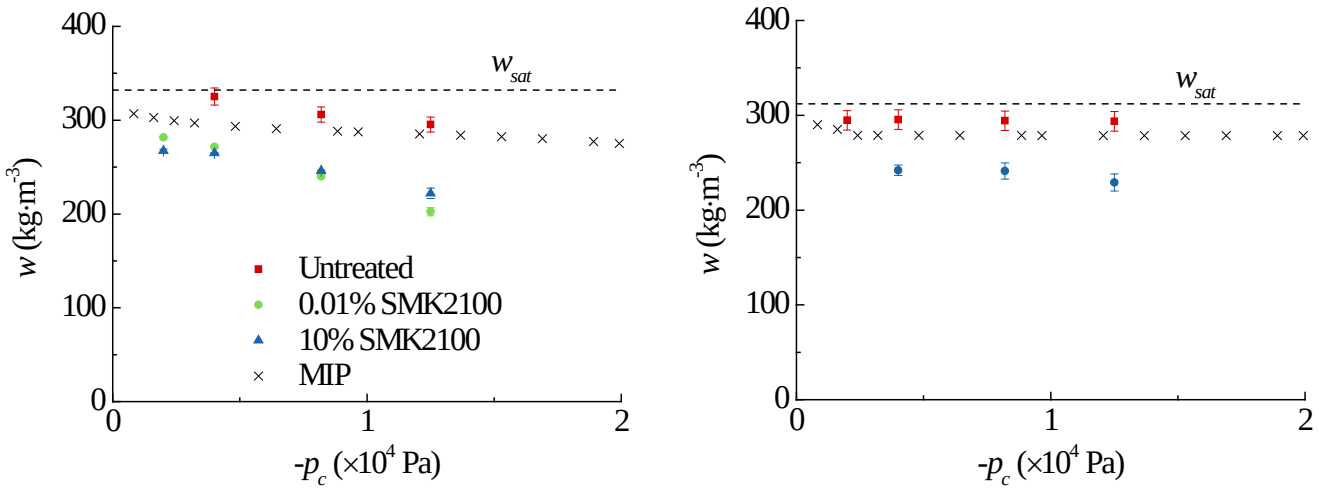

a. Results of ceramic brick b. Results of lime mortar

Figure 6-39: The desorption retention curves from hanging water column tests for treated materials (starting from w_{sat}, in comparison with untreated materials and the MIP results).

6.4.5 Conclusions

In this section, we measure the moisture storage and transport properties of ceramic brick, lime mortar and sintered glass. Tested samples are either untreated or hydrophobized. Results show that hydrophobization has a limited impact on a material's bulk density, open porosity and pore size distribution, although small pores may get partially blocked. The effectiveness of hydrophobization depends on materials' pore sizes and the imposed agent amounts. There is a material-dependent critical concentration of the water repellent agent, beyond which the impact of hydrophobization

becomes clear. When a material is treated above the critical agent concentration, its capillarity is significantly influenced, while its hygroscopicity is moderately reduced.

References

For section 6.1

ASTM C1699. 2009 (Reapproved 2015). Standard test method for moisture retention curves of porous building materials using pressure plates.

Carmeliet J., Houvenaghel G., Van Schijndel J., Roels S. 2002. Moisture phenomena in hydrophobic porous building material Part 1: Measurements and physical interpretations. Restoration of Building and Monuments 8:165-183.

Charola A.E. 1995. Water-repellent treatments for building stones: A practical overview. APT Bulletin 26:10-17.

Dow Z-6689. 2017. Dow Corning. Safety data sheet.

Engel J., Heinze P., Plagge R. 2014. Adapting Hydrophobizing Impregnation Agents to the Object. Restoration of Building and Monuments. In proceedings of 7th International Conference on Water Repellent Treatment and Protective Surface Technology for Building Materials, Hydrophobe VII.

Feng C., Janssen H., Feng Y., Meng Q. 2015. Hygric properties of porous building materials:Analysis of measurement repeatability and reproducibility. Building and Environment 85:160-172.

Feng C., Janssen H. 2018. Hygric properties of porous building materials (III): Impact factors and data processing methods of the capillary absorption test. Building and Environment 134: 21-34.

Fukui K., Iba C., Hokoi, S. 2017. Moisture behavior inside building materials treated with silane water repellent. Energy Procedia 132: 735–740.

ISO 12572:2016 (E). Hygrothermal performance of building materials and products - Determination of water vapor transmission properties - Cup method.

ISO 15148:2002 (E). Hygrothermal performance of building materials and products -determination of water absorption coefficient by partial immersion.

Izaguirre A., Lanas J. Álvarez J. I. 2009. Effect of water-repellent admixtures on the behaviour of aerial lime-based mortars. Cement and Concrete Research 39:1095–1104.

Klisińska-Kopacz A. Tilova R. 2012. Effect of hydrophobization treatment on the hydration of repair Roman cement mortars, Construction and Building Materials 35: 735–740.

Mayer H. 1998. Masonry protection with silanes, siloxanes and silicone resins. Surface Coatings International, 81: 89–93.

Momentive, Silblock wms, 2011. Technical data sheet. Albany, NY, USA.

Pavlík Z., Keppert M., Pavlíková M., Černý R. 2012. Investigation of the Effectiveness of Siloxane Hydrophobic Injection for Renovation of Damp Brick Masonry. International Journal of Chemical, Molecular, Nuclear, Materials and Metallurgical Engineering 6: 123–126.

Roels S., Carmeliet J., Hens H., Adan O., Brocken H., Cerny R., Pavlik Z., Kumaran, K., Pel, L., Plagge, R. 2004. Interlaboratory Comparison of Hygric Properties of Porous Building Materials. Journal of Thermal enviroment and building science 27: 307-325.

Šadauskienė J., Ramanauskas J., Stankevičius V. 2003. Effect of Hydrophobic Materials on Water

Impermeability and Drying of Finish Brick Masonry. Materials Science 9: 94-98.

Soulios V., Hansen E.J. D.P, Janssen H. 2019. Hygric properties of hydrophobized building materials. In proceedings of Central European symposium on Building Physics. Prague.

SILRES BS SMK 1311, Wacker. 2014. Wacker Chemie AG. Technical data sheet.

SILRES BS SMK 2100, Wacker. 2014. Wacker Chemie AG. Technical data sheet.

SILRES BS SMK 2101, Wacker. 2014. Wacker Chemie AG. Technical data sheet.

Zhao, J. Meissener F. 2017. Experimental investigation of moisture properties of historic building material with hydrophobization treatment. Energy Procedia 132: 261–266.

For section 6.2

Cizer Ö., Van Balen K., Jan E., Van Gemert D. 2012. Real-time investigation of reaction rate and mineral phase modifications of lime carbonation. Construction and Building Materials 35: 741–751.

Rewah NV. 2016. Gelifuge new, Technical data sheet.

Soulios V., Hansen E.J.D. P., Feng C., Janssen H., 2020. Hygric behavior of hydrophobized brick and mortar samples. Article in press, Building and Environment.

SILRES BS SMK 1311, Wacker. 2014. Wacker Chemie AG. Technical data sheet.

SILRES BS SMK 2100, Wacker. 2014. Wacker Chemie AG. Technical data sheet.

SILRES BS SMK 2101, Wacker. 2014. Wacker Chemie AG. Technical data sheet.

For section 6.3 and 6.4

ASTM C1699. 2009 (Reapproved 2015). Standard test method for moisture retention curves of porous building materials using pressure plates.

ASTM C1794. 2015. Standard test methods for determination of the water absorption coefficient by partial immersion.

ASTM D6836. 2016. Standard test method for determination of the soil water characteristic curve for desorption using hanging column, pressure extractor, chilled mirror hygrometer, or centrifuge.

ASTM E96 / E96M. 2016. Standard test methods for water vapor transmission of materials.

ASTM D4404. 2018. Standard test method for determination of pore volume and pore volume distribution of soil and rock by mercury intrusion porosimetry.

Bannour H., Stoltz G., Delage P., Touze-Foltz, N. 2014. Effect of stress on water retention of needlepunched geosynthetic clay liners. Geotextiles and Geomembranes 42(6):629-640.

Bhinder A., Shabani S., Sadrzadeh M. 2017. Effect of internal and external concentration polarizations on the performance of forward osmosis process. Osmotically Driven Membrane Processes:Approach, Development and Current Status.

Bittelli M., Flury, M. 2009. Errors in water retention curves determined with pressure plates. Soil Science Society of America Journal 73(5):1453-1460.

D'Orazio M., Maracchini G. 2019. An experimental investigation on the indoor hygrothermal environment of a reinforced-EPS based temporary housing solution. Energy and Buildings 204:109500.

Delage P., Suraj de Silva G. P. R., Vicol T. 1992. Suction controlled testing of non saturated soils with an osmotic consolidometer. In Proceedings of the 7th International Conference on Expansive Soils, August 3-5 1992, Dallas, USA.

Feng C., Feng Y., Meng Q., Janssen H. 2015. Best choice of the separating material for pressure plate tests. Energy Procedia 78:1389-1394.

Feng C., Janssen H. 2018. Hygric properties of porous building materials (III):Impact factors and data processing methods of the capillary absorption test. Building and Environment 134:21-34.

Feng C., Janssen H., Feng Y., Meng Q. 2015. Hygric properties of porous building materials:Analysis of measurement repeatability and reproducibility. Building and Environment 85:160-172.

Feng C., Janssen H., Wu C., Feng Y., Meng Q. 2013. Validating various measures to accelerate the static gravimetric sorption isotherm determination. Building and Environment 69:64-71.

Feng C., Roels S., Janssen H. 2019. Towards a more representative assessment of frost damage to porous building materials. Building and Environment 164:106343.

Fredriksson M., Johansson P. 2016. A Method for Determination of Absorption Isotherms at High Relative Humidity Levels:Measurements on Lime-Silica Brick and Norway Spruce (Picea abies (L.) Karst.). Drying Technology 34(1):132-141.

Garbalińska H., Bochenek M., Malorny W., von Werder J. 2017. Comparative analysis of the dynamic vapor sorption (DVS) technique and the traditional method for sorption isotherms determination - Exemplified at autoclaved aerated concrete samples of four density classes. Cement and Concrete Research 91:97-105.

ISO 10545-3:2018 (E). Ceramic tiles - Part 3:Determination of water absorption, apparent porosity, apparent relative density and bulk density.

ISO 11274:2019 (E). Soil quality - Determination of the water-retention characteristic - Laboratory methods.

ISO 12571:2013 (E). Hygrothermal performance of building materials and products - Determination of hygroscopic sorption properties.

ISO 12572:2016 (E). Hygrothermal performance of building materials and products - Determination of water vapor transmission properties - Cup method.

ISO 15148:2002 (E). Hygrothermal performance of building materials and products -determination of water absorption coefficient by partial immersion.

Leong E.C., Tripathy S., Rahardjo H. 2003. Total suction measurement of unsaturated soils with a device using the chilled-mirror dew-point technique. Géotechnique 53(2):173-182.

Lu Y., Abuel-Naga H., Bouazza, A. 2017. Water retention curve of GCLs using a modified sample holder in a chilled-mirror dew-point device. Geotextiles and Geomembranes 45(1):23-28.

Madsen H.B., Jensen C.R., Boysen T. 1986. A comparison of the thermocouple psychrometer and the pressure plate methods for determination of soil water characteristic curves. Journal of Soil Science 37(3):357-362.

Moret-Fernández D., González-Cebollada C., Latorre B. 2012. Microflowmeter-tension disc infiltrometer - Part I:Measurement of the transient infiltration rate. Journal of Hydrology 466-467:151-158.

Nijp J.J., Metselaar K., Limpens J., Gooren H.P.A., van der Zee S.E.A.T.M. 2017. A modification of the constant-head permeameter to measure saturated hydraulic conductivity of highly permeable media. MethodsX 4:134-142.

Pedescoll A., Samsó R., Romero E., Puigagut J., García J. 2011. Reliability, repeatability and accuracy of the falling head method for hydraulic conductivity measurements under laboratory conditions. Ecological Engineering 37(5):754-757.

Roels S., Elsen J., Carmeliet J., Hens H. 2001. Characterisation of pore structure by combining mercury porosimetry and micrography. Materials and Structures 34(2):76-82.

Yan T., Sun Z., Xu X., Wan H., Huang G. 2019. Development of a simplified dynamic moisture transfer model of building wall layer of hygroscopic material. Energy 183:1278-1294.

Zhang H., Yoshino H., Hasegawa K., Liu J., Zhang W., Xuan, H. 2017. Practical moisture buffering effect of three hygroscopic materials in real-world conditions. Energy and Buildings 139:214-223.

7 Laboratory experiments on impact of cracks

(Daan Deckers, KUL)

7.1 Introduction

Recently, hydrophobizing a facade has become a more popular way of reducing the wind-driven rain absorption (Abdul Hamid & Wallentén, 2017; Soulios et al., 2019). This is especially the case for buildings with preservation-worthy facades since they are in need of such invisible solutions. Most of these (historical) preservation-worthy facades are relatively old and weathered down and consequently cracks are guaranteed. To investigate whether or not these cracks render the application of a hydrophobic agent ineffective, a master thesis was dedicated to this subject at the KU Leuven under the supervision of Hans Janssen, Staf Roels and Chi Feng (Vanspeybrouck, 2019). The results shown in this report concisely summarise the most important conclusions of the research. For additional results and a more detailed description of the study, the reader is referred to Vanspeybrouck (2019).

In the first part of this written report, the overpressure required for water penetration into a hydrophobized crack (i.e. the breakthrough pressure) is measured experimentally and calculated with the help of contact angle measurements. Subsequently, the occurring external pressure on a facade is quantified. Finally, the breakthrough pressure and the occurring external pressures are compared in order to qualitatively describe water penetration in hydrophobized cracks.

7.2 Determination of the breakthrough pressure

7.2.1 Test samples

The test samples are made of Vandersanden Robusta bricks (Vandersanden, 2020) which are hydrophobized by capillary absorbing a water repellent agent/water emulsion with a volume concentration of 10% water repellent agent (Silres BS SMK 2100 (Wacker Chemie AG, 2014)). After hydrophobization, the samples are stored in an environment at room temperature (ca. 20-21°C) with a relative humidity (RH) of close to 100% for two weeks. Subsequently, they are moved to a climate chamber with 53% RH and 23°C for one week. These three weeks of conditioning guarantee the completion of the polymerisation reactions of the water repellent agent (van Besien et al., 2003). Finally, prior to the measurements, the samples are dried in an oven at 70 °C and 12% RH for a period of one week.

To represent a wide spectrum of cracks, following parameters are of interest during the preparation of the test samples:

- Moment of hydrophobization: Samples are either hydrophobized before or after they are cracked.
- Method of cracking: A distinction is made between broken cracks with a rough inner surface (e.g. cracks in bricks caused by internal stresses) and sawn cracks with a smooth inner surface (e.g. cracks between mortar joints and bricks). Either way, the crack extends over the entire height of the sample as shown by Figure 7-1.
- Crack width: Several prior studies have been dedicated to quantifying the maximum allowable crack width in hydrophobized building materials. Sandin (1999) spoke of a maximum allowable crack width of 0.3 mm in a hydrophobized masonry wall, a figure which is readily used by manufacturers as well. Lunk and Wittmann (1998) stated 0.4 mm as the maximum allowable crack width above which hydrophobized concrete lost its hydrophobic properties.

Based on the literature review, the maximum crack width was limited to an extreme value of 1 mm. The crack width is realised by placing a number of plastic foil sheets in between the two parts of the brick as shown by Figure 7-1. Limited by the thickness of an individual sheet, crack widths of 0.063 mm, 0.147 mm, 0.3 mm, 0.5 mm and 1 mm are realised by respectively using one, two, four, six and twelve sheets of plastic foil.

- Penetration depth of the hydrophobic agent: Test samples are hydrophobized by capillary absorbing water repellent agent/water emulsion until the visible wet front of the emulsion reaches a certain height in the sample (1 cm, 2 cm or 4 cm). It should be noted that the water repellent agent is redistributed in the sample, which makes its influence measurable beyond the penetration depth of the emulsion (van Besien et al., 2003).

7.2.2 Direct measurement of the breakthrough pressure

To measure the breakthrough pressure, a plexiglass measuring tube is placed on top of the cracked brick and the contact between the tube and the sample is sealed with butyl tape. The tube is slowly filled with water using a squeeze bottle to make sure that water is forced into the crack by the hydrostatic water pressure instead of the impact of falling water. At the moment water penetrates the crack, the breakthrough pressure is calculated from the height of the water column ($p = \rho gh$). Figure 7-1 shows the experimental set-up of one such measurement. At least three different samples are tested for every type of crack and the mean values and standard deviations are shown in this report.

Initial measurements showed that the penetration depth of the water repellent agent does not have a pronounced effect on the breakthrough pressure, which is in accordance with the results of van Besien et al. (2003). Therefore, to compare the other parameters (moment of hydrophobization, method of cracking and crack width) only the results recorded for the samples with a penetration depth of 2 cm are shown in Figure 7-2 as well as the breakthrough pressure calculated with the help of contact angle measurements as explained in section 7.2.3 (”Contact angle estimation” in Figure 7-2). The entries in the legend below the graph note the moment of hydrophobization (e.g. Sawn-hydrophobized = the cracks are first sawn and afterwards hydrophobized). Results for samples with a crack width of 1 mm are not shown due to the lack of accuracy of the measurements caused by the small breakthrough pressure. It should be noted that the experiments belonging to a crack width of 0.147 mm were only executed for samples that were first hydrophobized and cracked afterwards.

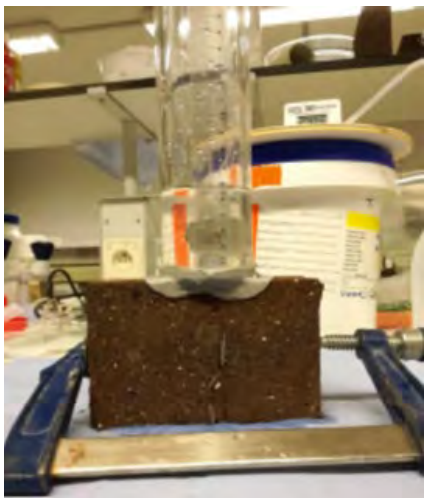

Figure 7-1: Test set-up to measure the breackthrough pressure.

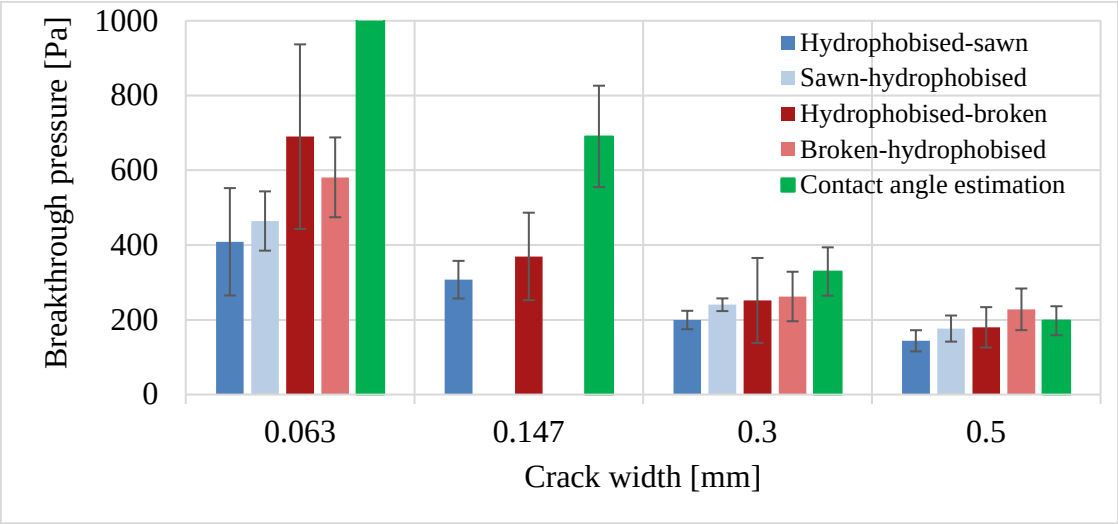

Figure 7-2: Results of the breakthrough pressure measurements.

As expected, smaller crack widths can withstand larger external pressures before water penetration occurs. Additionally, hydrophobizing a sample after cracking seems to increase the breakthrough pressure, but only by a very limited amount. The results also indicate that by breaking the samples rather than sawing them, the rough inner surface of the crack increases the breakthrough pressure. It should be noted that these last two conclusions are rather uncertain due to the large experimental variation of the results (see error bars in Figure 7-2).

7.2.3 Calculation of the breakthrough pressure

The effect of a water repellent agent on a material is readily quantified by the contact angle between the hydrophobized material's surface and a water drop. In this report, the contact angle is measured with the help of the optical sessile method, in which imaging software measures the contact angle of a drop of water on the surface of a hydrophobized material every second for a total period of 40 seconds. All of the 40 contact angle measurements (1 for each second) are subsequently averaged to obtain one contact angle per droplet of water. This is performed using 10 drops for each of the three different samples, all of which were hydrophobized with a 2 cm penetration depth.

The contact angle was measured on droplets deposited on the surface of the hydrophobized brick next to the existing cracks. Therefore, the properties of the crack itself do not influence the contact angle, which means that a single value of the contact angle, applicable to all samples, could be obtained. The test set-up and an example of the outcome of the imaging software are shown in Figure 7-3. Once the contact angle (θ) is known, the breakthrough pressure (p) can be estimated with the help of Equation 7-1 (Mayer & Stowe, 1965) for crack width (r) and surface tension σ = 0.0725 N/m.

$$p = \frac{-2\sigma cos(\theta)}{r}$$ **Equation 7-1**

The contact angle measurements gave a mean value of 133.7° and a standard deviation of about 10°. This large standard deviation can be partially explained by static wetting hysteresis (Dussan, 1979). However, due to the extent of the variation between measurements, other possible reasons such as the evaporation of water from the droplet, which is encompanied by a decrease of the contact angle over time, and possibly some inaccurate measurements, could have influenced the results as well.

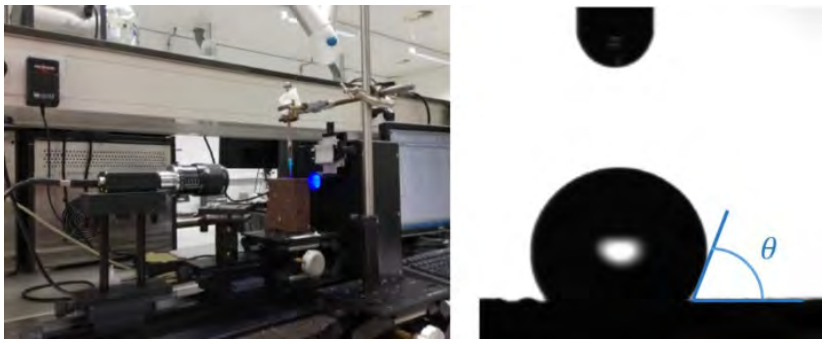

Figure 7-3: Test set-up for the contact angle measurement (left) and an outcome of the imaging software (right).

Besides the contact angle uncertainty, Equation 7-1 is only capable of providing an estimate of the breakthrough pressure through a crack since this equation is only fully applicable for a cylindrical capillary (Mayer & Stowe, 1965). In addition, it has been proven in literature that the contact angle of a drop, deposited on the surface of a material, significantly differs from the contact angle of water in this material's pores (Li et al., 2014) and therefore from the contact angle in a crack as well. Nevertheless, the breakthrough pressure, calculated using Equation 7-1, is shown in Figure 7-2. Due to the numerous simplifications this equation presupposes, a large discrepancy between the calculated and directly measured breakthrough pressure is noted, especially for small crack widths. Therefore, in the remaining part of this report, only the (more correct) measured breackthrough pressure will be of interest.

7.3 Occuring external pressure on a hydrophobized facade

To properly quantify water penetration in cracks, the breakthrough pressure needs to be compared to the occurring external pressures on the facade. Besides the obvious wind pressure, a second possible pressure source might be present in the case of a hydrophobized facade. Due to the limited water absorption of the hydrophobic masonry, runoff water forms a thin waterfilm on the facade. The pressure distribution within such a film may force water into the cracks. Therefore in this section, the presence of such external pressures in the liquid water film are first experimentally determined. Afterwards, the magnitude of the wind pressure is estimated with the help of the European norm EN 1991-1-4 (European committee for standardization, 2015).

7.3.1 Pressure in the water film

The presence of an external pressure on the wall, provided by the water film, is tested with the help of the experimental set-up shown in Figure 7-4. By opening the bottom valve of the test set-up, a water film flows from the reservoir down plexiglass plate B. The thickness of this water film is limited by reducing the distance between the two plexiglass plates with the help of aluminium strips taped to plexiglass plate A. Next, the three valves on the right hand side of the sketch are opened to bring the water film in contact with the water in the three tubes. If the water film exerts no (or only a negligible) pressure on the water in the tubes and by extent on plate B, the tubes will be emptied. The results from this experiment are shown in Table 7-1 for film thicknesses from 0.1 mm to 1 mm. The water level in the table represents the height indicated by h in the sketch of the test set-up (Figure 7-4). At the start of the test, the water level in tube 1, tube 2 and tube 3 was respectively equal to 25 cm, 35 cm and 45 cm.

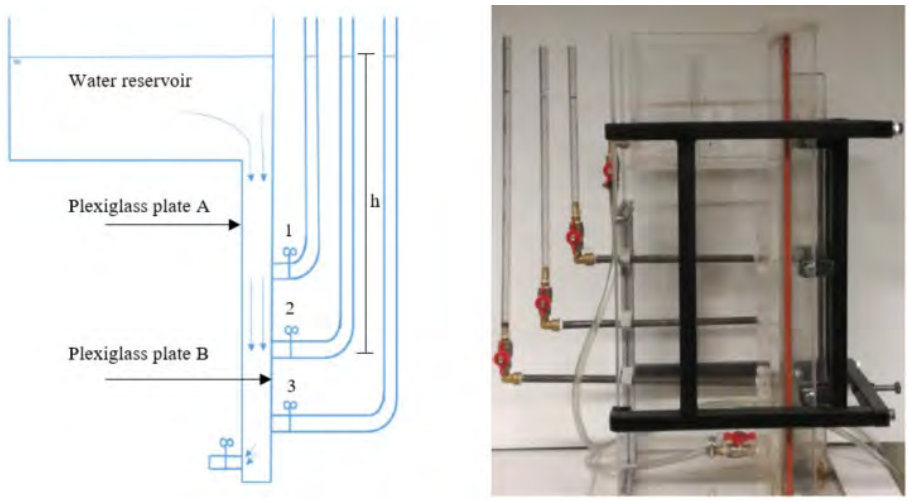

Figure 7-4: A sketch (left) and a photo of the test set-up (right) used to investigate the pressure exerted by a water film on a wall.

The water film seems to exert no pressure on the plexiglass plate for thin water films, which results in all tubes being emptied after opening the valves. Only for a film thicker than 0.9 mm, an external pressure is measured. However, this external pressure is probably caused by the limited flow rate allowed through the exit hole in the bottom of plexiglass plate A (Vanspeybrouck, 2019). Furthermore, simulations in Vanspeybrouck (2019) have shown that the thickness of a water film rarely exceeds 0.06 mm, making the presence of a pressure in the water film very unlikely. For a numerical confirmation of this conclusion, the reader is referred to Vanspeybrouck (2019).

Table 7-1: Results from the test to measure pressure in the water film.

	Water level after opening of the valves (h in Figure 7.4) [cm]		
Film thickness [mm]	**Tube 1**	**Tube 2**	**Tube 3**
0.1	Emptied	Emptied	Emptied
0.2	Emptied	Emptied	Emptied
0.3	Emptied	Emptied	Emptied
0.4	Emptied	Emptied	Emptied
0.5	Emptied	Emptied	Emptied
0.6	Emptied	Emptied	Emptied
0.7	Emptied	Emptied	Emptied
0.8	Emptied	Emptied	Emptied
0.9	3	9	15.5
1	5	11	18

7.3.2 Wind pressure

In this section, the wind pressure caused by the peak wind velocity on a facade is calculated according to the European norm EN 1991-1-4 (European committee for standardization, 2015). Because an order of magnitude of the wind pressure suffices in this report, only one type of building is regarded. This building has a flat roof at a height of 20 m and a cross-section of 10 m by 10 m. The calculation is done for a terrain category II and a fundamental basic wind velocity of 25 m/s, which is in accordance to the value for central Belgium (European committee for standardization, 2015). For the complete calculation method, the reader is referred to the European norm EN 1991-1-4 (European committee for standardization, 2015).

These peak wind velocities only occur sporadically, which is why the wind pressure is also calculated for more common wind velocities (1 m/s to 10 m/s) using Equation 7-2 (Gullbrekken et al., 2018).

$$p_{wind} = \frac{1}{2} c_p \, \rho_a v_{wind}^2 \qquad \textbf{Equation 7-2}$$

In this equation ρ_a is the density of air, v_{wind} is the wind velocity and c_p is the pressure coefficient, which is equal to 0.8 for this type of building (European committee for standardization, 2015). The peak velocity pressure and the more common wind pressures, calculated using Equation 7-2, are shown in Table 7-2.

Table 7-2: Wind induced pressure

Wind velocity [m/s]	Wind pressure [Pa]
1	0.5
5	12.5
10	50
Peak wind velocity	1200

7.4 Conclusions

As shown in section 7.3, the wind pressure is the only driving force behind water penetration in cracks. Therefore, this wind pressure, albeit the peak velocity pressure of 1200 Pa or the common wind pressure with a maximum of about 50 Pa, has to be greater than the breakthrough pressure of a crack for water penetration to occur. Cracks with a width smaller than 0.5 mm require at least an external pressure of 100 Pa to 150 Pa for water to enter. Therefore, the common wind pressures are insufficient to force water into the cracks. If the crack width exceeds 0.5 mm, regular water penetration, driven by the wind pressure, becomes more likely, which emphasizes the maximum allowable crack width in the papers of Sandin (1999) and Lunk and Wittmann (1998), respectively equal to 0.3 mm and 0.4 mm.

During storms, the peak velocity pressure is capable of forcing water into all cracks regardless of their width. However, these storms and the corresponding water penetration only occur sporadically, making the peak wind pressure less relevant for design. However, van Besien et al. (2003) have shown that regardless of the external pressure exerted on a wall, a supply of water (e.g. a rain event) is absorbed immediately by water-filled cracks. Therefore, future work could focus on the drying behaviour of water-filled cracks to investigate whether or not the water has time to evaporate before the next rain event.

References

Abdul Hamid A., Wallentén P. 2017. Hygrothermal assessment of internally added thermal insulation on external brick walls in Swedish multifamily buildings. Building and Environment, 123: 351–362.

Dussan E. B. 1979. On the Spreading of Liquids on Solid Surfaces: Static and Dynamic Contact Lines. Annual Review of Fluid Mechanics 11(1): 371–400.

European committee for standardization. 2015. Eurocode 1: Actions on structures - Part 1-4: General actions - Wind actions (EN 1991-1-4:2005+A).

Gullbrekken L., Uvsløkk S., Kvande T., Pettersson K., Time B. 2018. Wind pressure coefficients for roof ventilation purposes. Journal of Wind Engineering and Industrial Aerodynamics, 175: 144–152.

Li X., Fan X., Brandani S. 2014. Difference in pore contact angle and the contact angle measured on a flat surface and in an open space. Chemical Engineering Science 117: 137–145.

Lunk P., Wittmann H. 1998. The Behaviour of Cracks in Water Repellent Concrete Structures with Respect to Capillary Water Transport. Proceedings of Hydrophobe II: 63–76.

Mayer R. P., Stowe R. A. 1965. Mercury porosimetry—breakthrough pressure for penetration between packed spheres. Journal of Colloid Science 20(8): 893–911.

Sandin K. 1999. Influence of cracks on moisture conditions in facades with water-repellent treatments/ Einfluss von Rissen auf den Feuchtigkeitshaushalt hydrophobierter Fassaden. Internationale Zeitschrift Für Bauinstandsetzen Und Baudenkmalpflege 5(5): 499–521.

Soulios V., de Place Hansen E. J., Peuhkuri R. 2019. Hygrothermal simulation assessment of internal insulation systems for retrofitting a historic Danish building. MATEC Web of Conferences 282: 02049.

van Besien T., Roels S., Carmeliet J. 2003. A laboratory study of the efficiency of a hydrophobic treatment of cracked porous building materials. 2nd International Conference on Building Physics: 1–7.

Vandersanden. 2020. Vandersanden Robusta brick: Technical specifications. Available at: https://www.vandersandengroup.be/bricks/nl-be/gevelsteen-steenstrip/robusta

Vanspeybrouck G. 2019. De invloed van scheuren op de waterpenetratie in gehydrofobeerd metselwerk. Master Thesis, Catholic University of Leuven, Leuven, Belgium.

Wacker Chemie AG. 2014. Silres ® bs smk 2100, Technical data sheet. pp.1-2

8 In-situ assessment @ Klitgaarden, Denmark

(Tessa Kvist Hansen, DTU[9])

8.1 General information

In connection with refurbishment of this old farm house, both internal insulation and hydrophobization were applied. The Technical University of Denmark and the Technological Institute of Denmark performed measurements in connection with research. The RIBuild partner from Intro Flex provided the contact, as this case was insulated with Remmers' IQ-Therm, and hydrophobized with Remmers' Funcosil. The owner of the house made a complete renovation of the old house, both inside and outside.

8.2 Introduction

Klitgaarden is a free-standing single-family house from 1875, as seen in Figure 8-1. The house has two stories, and a total of 221m^2. The house is located by the sea, on the coast of northern Zealand, in Denmark, as seen in Figure 8-2. The facades and gables are solid masonry: east and west facades have three layers of brick (37 cm), and north and south gables have two layers of brick (25 cm).

Figure 8-1: View of the case building. Left: southern gable after renovation; Middle: eastern façade before renovation; Right: northern gable after renovation.

Figure 8-2: Location of the case building. Left: Map of Denmark, and indication of the location of the test house on the northern coast of Zealand. Right: the case building is less than 100 m from the coastline.

[9] Activities performed while at DTU, currently at AAU

The house is built on a foundation of granite boulders on top of a stone foundation. During 2016 the house underwent an extensive renovation, including internal insulation with 80 mm of PUR foam with capillary active calcium silicate channels (IQ-therm). The exterior surfaces of the building were sandblasted during renovation, and plastered with a thin layer of bank sand mortar. Some test fields on the facades were treated with Funcosil, a silane based, creamy hydrophobization agent, and Karsten tube measurements were performed. In September 2018, all external facades and gables were hydrophobized with Funcosil FC.

Prior to the renovation, the former farmhouse had been unused for 20 years, and significant renovation was needed. Besides internal insulation and hydrophobization, the extensive renovation also included new ground floor and floor heating, window replacements, new domestic hot water system, roof insulation, installation of ground heat pump, drain around the house, plastering of the façade, and waterproofing the foundation.

8.3 Hydrophobization

As the case building is located less than 100 m from the coast, the building owner had noticed wetting of the exterior façade, especially on the north west corner in connection with wind-driven rain and sea mist. Furthermore, it had been observed, that the roof overhang prevented façade wetting at heights above 1.6 m. During the application of internal insulation in 2016, smaller test areas on the facades and gables, were treated with hydrophobization. In Figure 8-3 the test areas are clearly seen. During rain (Figure 8-3, middle) it is clearly seen, that the hydrophobized area does not absorb the rainwater. In Figure 8-3, right, water was sprayed on the façade on both the treated test area, and the area adjacent to this. The immediate effect of hydrophobization of the light plastered façade is obviuous, and on the treated part, the water droplets are repelled and not absorbed into the wall.

Figure 8-3: Test fields with hydrophobization in 2016. Left: southern gable with 1 m^2 hydrophobized in the left corner; Middle: close up of the hydrophobized test field during rain; Right: water sprayed on the border between hydrophobized and not hydrophobized area of the façade.

In September 2018, after giving the glue mortar time to dry after installation of internal insulation, the entire exterior surface of the building was hydrophobized. The hydrophobization treatment Funcosil FC was provided by Remmers. The product is developed for porous, mineral building materials such as brick, clinker, lime sandstone, silicate natural stone, and mineral plaster. The product is based on silane, with a 40% concentration of active ingredients. It is a milky white, creamy product, and applied with paint roller in the specified amounts of 0.15-0.20 l/m^2. The product is marketed with feasible properties such as being able to reduce the water uptake and also being

diffusion open and having a significant impregnation depth. Furthermore it should have optimal resistance towards alkalis, and high protection towards frost and salt loads (Remmers, 2016).

8.4 Measurements

8.4.1 Hygrothermal performance

The hygrothermal performance of the internal insulation system, was monitored with temperature and relative humidity sensors placed at interfaces between the insulation and existing wall. At least one sensor was placed in each orientation, and on north and east facades, sensors were placed at two heights, namely 50 cm above the floor, and 50 cm below the ceiling. Furthermore, the indoor climate was monitored in two rooms (temperature and relative humidity). The outdoor climate by the north gable (temperature and relative humidity) was also monitored. The locations of sensors are depicted in Figure 8-4.

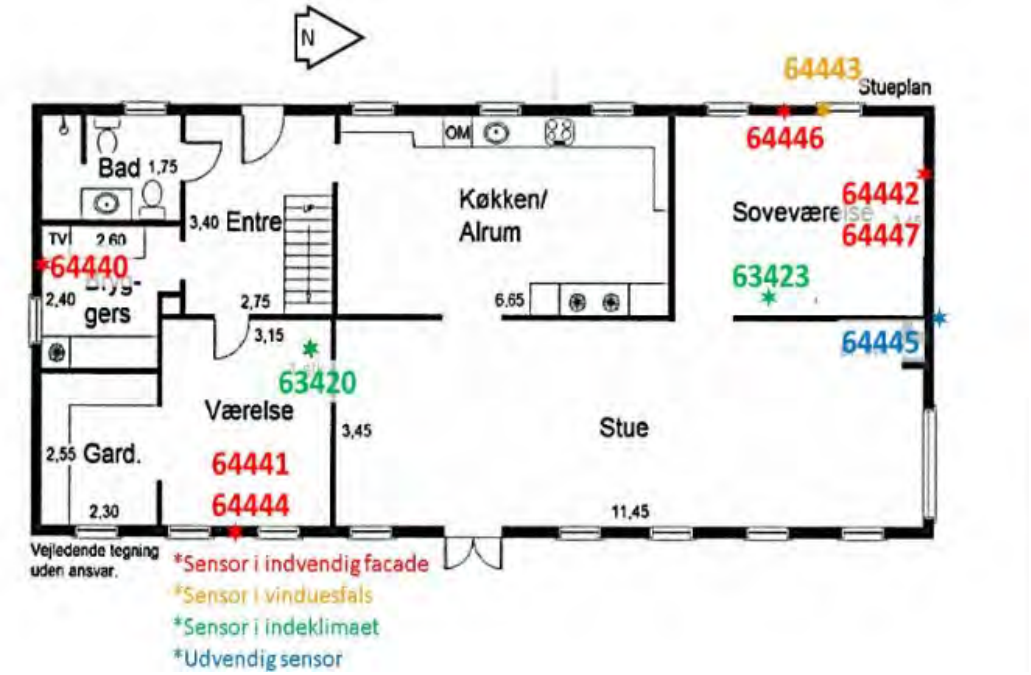

Figure 8-4: Sensor locations in Klitgaarden. Red color denotes sensor located at the interface between internal insulation and the existing wall. The yellow sensor is located in the window rebate. Green sensors monitor indoor climate, and the blue sensor monitors the outdoor climate.

The temperature and relative humidity conditions were monitored every half hour since the summer of 2016, and the equipment is still measuring (November 2019). The data is stored on a server provided by fugtlog.dk, and can be downloaded from a distance. The built-in sensors are climaSpot sensors, and the sensors monitoring indoor and outdoor climate are Tramex Hygro-i. Specifications on accuracy are given in Table 8-1.

Table 8-1: Accuracy of the sensor types used in Klitgaarden measurements

	Temperature	Relative humidity
ClimaSpot	±0.3% for 10-40°C	±1.8% for 10-90%
	±1% for -10-10°C and 40-55°C	±4% for 0-10% and 90-100%
Tramex Hygro-i	±0.3°C	±1.8% for 10-90% at 25°C

In addition to the continuous temperature and relative humidity measurements, several measurements were performed during the renovation, including Troxler and HF measurements. These will however not be references here, and the reader is referred to Case Study Documentation, WP3.

8.4.2 Karsten tube

The Karsten tube is a simple and non-destructive way for measuring water absorption in porous, inorganic materials on-site. The principle of the test method is fixation of a small tube or pipe with a measuring scale, to a wall or desired test specimen as seen in Figure 8-5. The pipe is filled with water to the mark of 5 ml, and the amount of water absorbed into the wall within 30 minutes, is recorded every 5 minutes. After measurement, the pipe is removed, and the area of the water contact can be established, as this will vary according to the fixation putty. Based on the volume of water removed from the pipe during the specific time for the measuring period and the area of water contact, the capillary water uptake can be estimated.

Figure 8-5: Karsten tube fixed on mortar joint

In the summer of 2016, Karsten tube measurements were performed on both eastern and western facades of Klitgaarden. The measurements were performed on both test areas with hydrophobization, and untreated areas of the surface. Furthermore, it was sought to measure the uptake on both brick and mortar joints, however the surface treatment of a thin layer of bank sand mortar (mortar wash) made it difficult to distinguish between brick and joint, and furthermore may also have influenced results in the same direction.

8.5 Results

8.5.1 Hygrothermal performance

The results from the hygrothermal monitoring is presented in Figure 8-6. Temperature registrations are presented in blue/gray colors, while measurements of relative humidity are represented by green/brown/orange nuances. There are a few fall outs in measurements, however tendencies of the conditions appear quite clear.

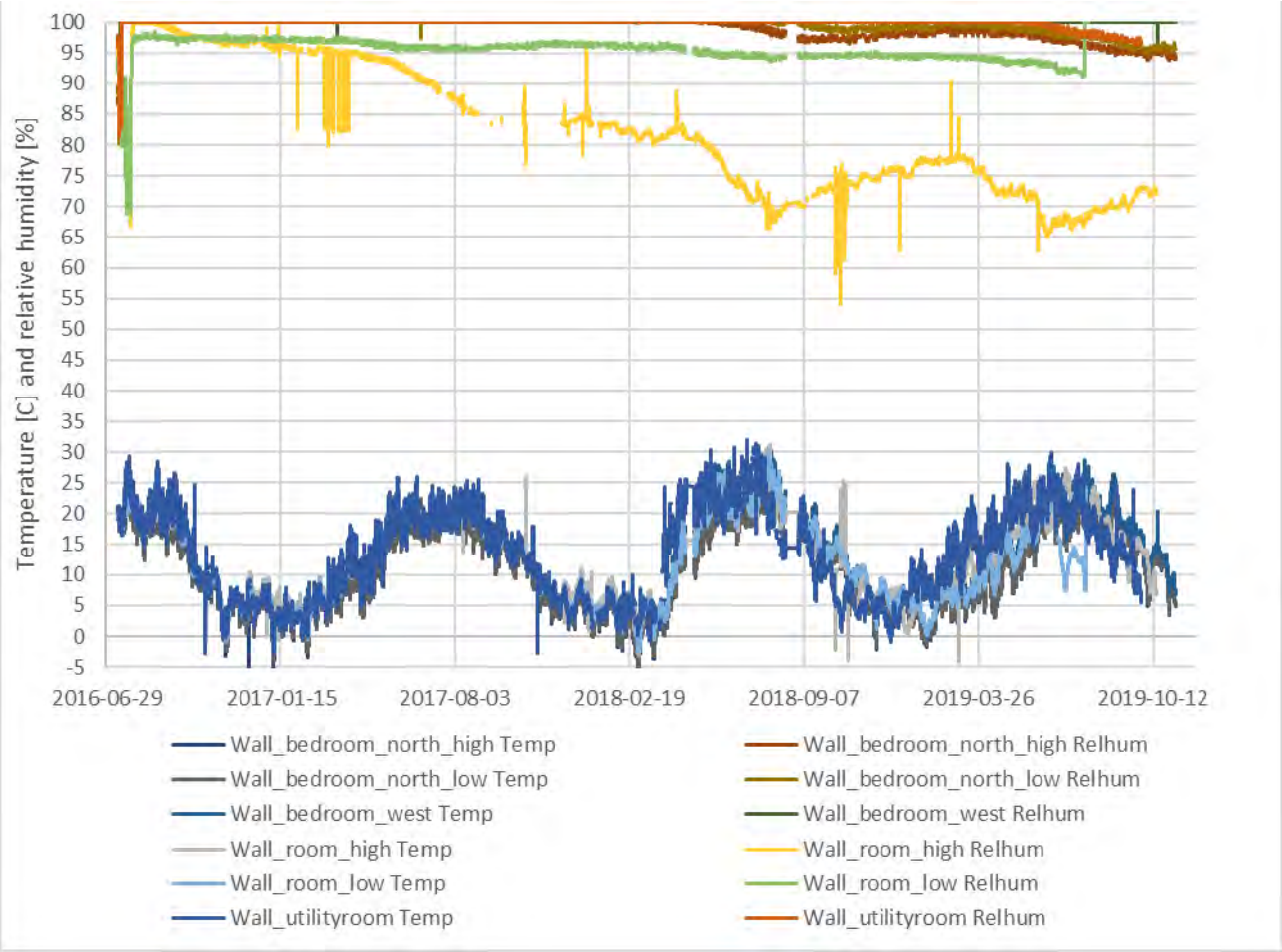

Figure 8-6: Results from the hygrothermal monitoring at the interface between internal insulation and the existing masonry.

8.5.2 Karsten tube

Images from the Karsten tube measurements performed in Klitgaarden are presented in Figure 8-7. In the 4th image, the Karsten tubes are placed on a hydrophobized test area, and the difference in the wet circles around the tubes is evident.

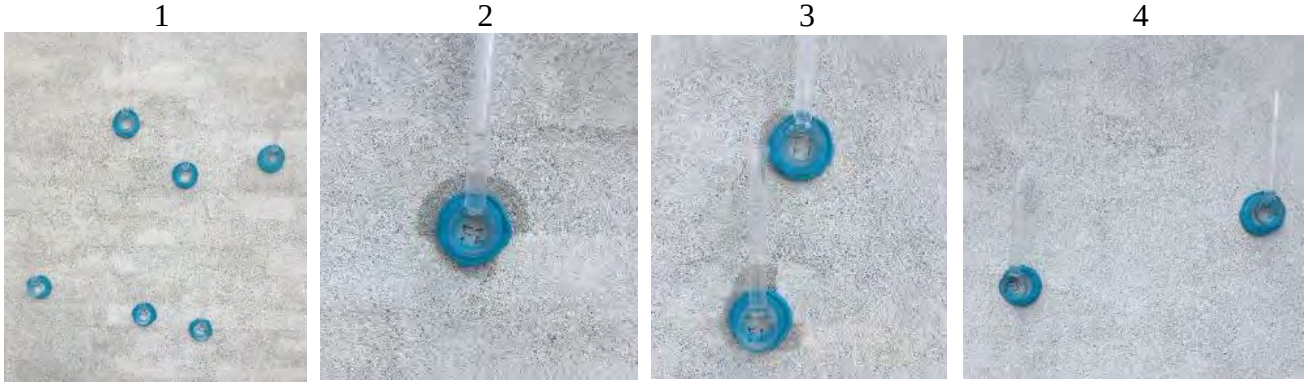

Figure 8-7: Karsten tube measurements on Klitgården. 1) Placement of Karsten tubes over both brick and mortar joints. 2) Karsten tube placed on mortar joint, and the brick outline is clear. 3) The top tube is placed on brick, and the bottom on mortar joint. 4) Karsten tubes placed on hydrophobized test area.

Results from Karsten tube measurements on brick is seen in Figure 8-8, and results of measurements performed on joints are seen in Figure 8-9. It should be noted that there is a factor 10 difference in the y-axis of the two charts, and thus it appears the mortar joints have higher water uptake than bricks.

Figure 8-8: Karsten tube measurements on bricks. Red lines represent hydrophobized bricks, while the blue nuanced lines represent untreated brick.

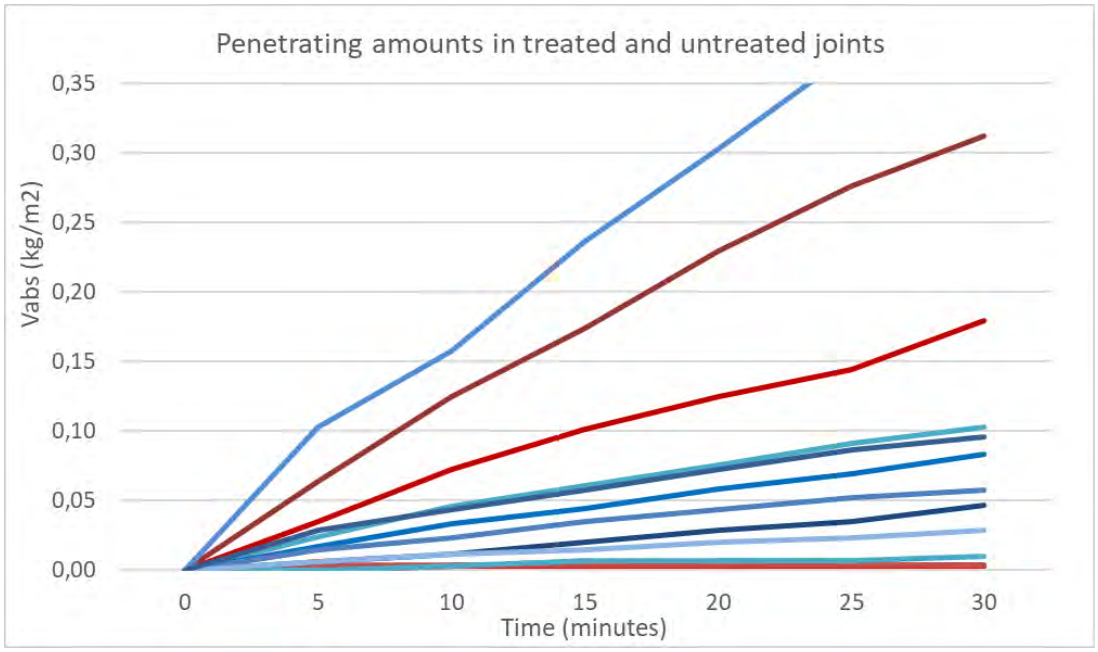

Figure 8-9: Karsten tube measurements on mortar joints. Red lines represent hydrophobized brick, while the blue nuanced lines represent untreated brick.

8.6 Conclusions

The monitoring of hygrothermal conditions at the interface between internal insulation and the existing wall, does not give definite answers to the questions about the efficiency of the hydrophobization. Nevertheless, it is seen that the relative humidity appears very high for the duration of measurements in all sensors, with the exception of the one in the room in high position. This is the only sensor that indicates drying of the glue mortar, and acceptable humidity conditions with regard to mold growth. The remaining sensors, exhibit very high relative humidities since the beginning of measurements and application of insulation in summer of 2016. By late summer of 2018 most of these sensors do exhibit slight, and slow, decline in relative humidity. Seasonal variation causes the relative humidity to increase slightly in the 2018-2019 winter, but in summer of 2019, the humidity conditions appear to be at the lowest level yet. It cannot surely be attributed to the hydrophobization, however the reduction in relative humidity seems to happen simultaneously to the hydrophobization of all external facades.

By the Karsten tube measurements, the effect of hydrophobization is clearly seen. Although some measurements from the untreated sections of brick and mortar have similarly low water uptakes, it is clear that the hydrophobization treatment reduces the water uptake from the external surface. There is a large variety in the brick types within the masonry of historic buildings, and this is not an exception, which is clearly seen in the results. Most of the untreated brick measurements were in the same area of water absorption, ending at 0.025-0.035kg/m^2 after 30 minutes. Some measurements from the joints also show large variety, however most measurements also end up in the same vicinity – up to 0.10kg/m^2 after 30 minutes.

References

Remmers. 2016, Funcosil FC - Impregnation cream in emulsion form on a siloxane base. Technical Information Sheet, Article No. 0711, Remmers (UK) Limited Crawley: GB 0711 - 04.08.doc: pp. 1–3. http://in.remmers.com/fileadmin/doc/tm/TM1_0711_IN.pdf (accessed 21-01-2020)

9 In-situ assessment @ Copenhagen, Denmark

(Angela Vanek, DTU)

9.1 Introduction

An ongoing project is located in the Bispebjerg area in the northwestern part of Copenhagen, Denmark. This involves five apartments in a large residential area, built around 1940, provided by AKB (housing organization). Four apartments are test apartments and one is used as reference. In collaboration DTU, Xella Denmark and Introflex, and partly financed by Realdania, four gable walls, two facing north and two facing south, were refurbished with a 10 cm internal insulation system (Multipor). Two gable walls, one facing each orientation, were additionally hydrophobized by applying Remmers Funcosil FC. As part of this collaboration project, the hydrophobization, application and the product itself, was financed by RIBuild.

9.2 Set up

The five apartments are currently monitored for a year and will be for at least six more months. The different cases can be seen in Table 9-1.

Figure 9-1 illustrates the location and the appearance of the case buildings.

Table 9-1: Cases, including the time of the set up

Apartment	Floor	Orientation	Hydrophobization (incl. refurbishment)	Internal insulation system
1	2nd floor	N	Yes (mid Sept-18)	Yes (start/mid Oct-18)
2	1st floor	S	Yes (mid Oct-18)	Yes (start Oct-18)
3	3rd floor	N	No	Yes (mid Sept-18)
4	4th floor	S	No	Yes (start Nov-18)
Reference	1st floor	S	No	No

Figure 9-1: Pictures of all four gable walls with the test apartment highlighted

Figure 9-2: Geographical location of the test apartments with indication

9.2.1 Materials

As part of this project, solely the gable walls were refurbished. These gable walls have a thickness of 1½ brick (348 mm). However, the thickness of the wall at the spandrel is only 1 brick thick (228 mm). All walls were blank on the exterior, had an interior plaster as well as wallpaper.

9.2.1.1 Hydrophobization

To prepare the two gable walls that were hydrophobized, the external walls were fully renovated before the hydrophobization product, Funcosil FC by Remmers, was applied. The renovation included exchanging broken or cracked bricks, grinding the bricks to smoothen the surface as well as scraping out all joints and replacing them with new ones, see Figure 9-3 and Figure 9-4. After a drying period of two weeks, the hydrophobization product was applied, following the producer's instructions, as one layer using a roll brush.

Figure 9-3: Refurbishment of the gable walls at apartment 1 and 2 and hydrophobization of these

Figure 9-4: Before (left) and after (right) refurbishment and hydrophobization

9.2.1.2 Internal insulation system

After removing the existing wallpaper, existing plaster and chemically cleaning the wall from eventually existing mould and organic compounds an insulation system from Xella Denmark was applied in all four apartments, see Figure 9-5. This application consisted of Multipor's lightweight mortar, 100 mm Multipor mineral insulation board, reinforcement mesh including lightweight mortar and a finishing plaster using Multipor's lightweight plaster. After a drying period, the wall was finished up with a diffusion open paint.

At the window spandrel, the applied Multipor insulation system had a thickness of 220 mm.

Figure 9-5: Removing of wallpaper and plaster, chemically cleaning the interior bricks'bricks surface from possible (?) mould, application of the Multipor insulation system

9.2.1.3 Material parameters

Material parameters of brick and mortar of the existing wall were determined in the lab at DTU according to Table 9-2, based on two samples each. The bricks used for the refurbishment were typical Danish "yellow bricks". The mortar joints that were scraped out were replaced with a lime-cement mortar (KC 50/50/700, 0-2 mm). Table 9-2 also states the material parameters of the Multipor insulation system, based on data sheets. Multipor insulation boards are made of low density aerated lightweight concrete, considered to be capillary active and diffusion open.

Table 9-2: Material parameters of the tested existing bricks and mortar, according to DTUs experimental tests and of the Multipor insulation system, according to Multipors data sheet (Ytong, 2017)

Material parameter	Existing brick	Existing mortar	Multipor mineral insulation board	Multipor light-weight mortar
Dry density [kg/m^3]	1774	1783	85 - 95	Approx. 770
Open porosity [m^3/m^3]	0.363	0.329	-	-
Thermal conductivity [W/mK]	0.761	0.839	0.042	0.18
Volumetric heat capacity [J/m^{3}K]*10^6	1.52	0.948	-	-
Water vapor diffusion resistance factor μ	-	-	2	≤10
Water absorption coefficient [kg/m^{2}s$^{0.5}$]	0.199	-	-	-

9.2.2 On-site measurement sensors

To document the relative humidity and temperature at the intersection between the existing gable wall and the internal insulation system, three Rotronic sensors (HL-RC-B with HC2A-S) where placed. The position of these sensors can be seen in Figure 9-6. These sensors measured with an interval of one hour and have an accuracy of ±0.1°C and ±0.8% RH (Rotronic, 2019). The reference apartment was equipped with one Rotronic logger mounted in a non-destructive way in a cavity at the inside of the exterior wall in the living room to measure the relative humidity of the walls surface.

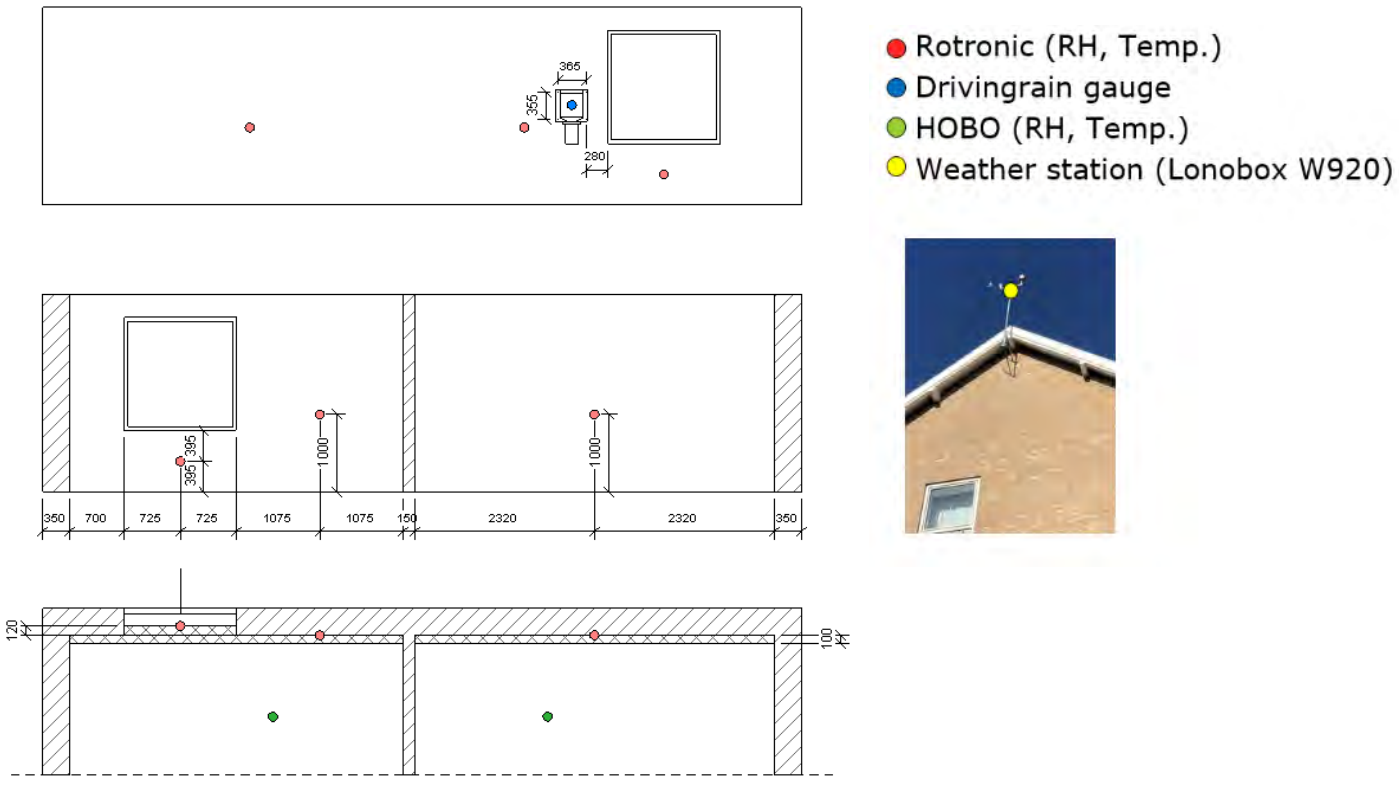

Figure 9-6: Position of measurement equipment - Rotronic (red), Driving rain gauge (blue), HOBO (green) – either hung on the wall or placed on a shelf, and Lonobox W920 (yellow)

9.2.3 Interior and exterior climate conditions

Further, both interior and exterior climate conditions were measured. The interior climate (relative humidity and temperature) was determined as the mean of measurements from two HOBO data logger (U12-012) placed in the living room and the bedroom, though only in the living room in the reference apartment. The logging interval is one hour and the accuracy of the HOBO data logger is ±0.35°C and ±2.5% RH (Onset, 2020b).

The logging of the exterior climate conditions consists of a weather station, Lonobox W920, and two driving rain gauges. The weather station includes an anemometer and a vertical rain gauge that were placed at the top of Apartment 2, exceeding the gable wall by approx. two meters. The logger of the relative humidity and temperature were placed under the roof sill, protected from solar radiation. In a previous project DTU developed a driving rain gauge that measured the amount of horizontal rain meeting the surface of the wall. Two driving rain gauges, one per orientation, were mounted to the gable walls next to the windows at apartment 1 (north faced) and 2 (south faced), respectively. The logging interval was 15 minutes for the weather station and one hour for the driving rain gauge. The driving rain gauge had an accuracy ±1.0% (Onset, 2020a).

9.3 Results and discussion

In this section, the results of the measurements over a period of one year are presented.

9.3.1 Intersection between insulation and existing wall

Figure 9-7 - Figure 9-12 show the RH and the temperature in the interface in the living room, bedroom and at the spandrel in the living room, organised by the orientation of the façade of the gable walls, of all test apartments over a period of one year.

The insulation material was not installed at the same time on all four gables and the drying out phase had therefore different offsets. However, when looking at Sep 19 – Dec 19 (see red box at Figure Figure 9-7 - Figure 9-12), it is clearly seen that hydrophobization has a positive effect on the gable wall facing north but no or a negative effect on the gable wall facing south.

9.3.1.1 South faced façade

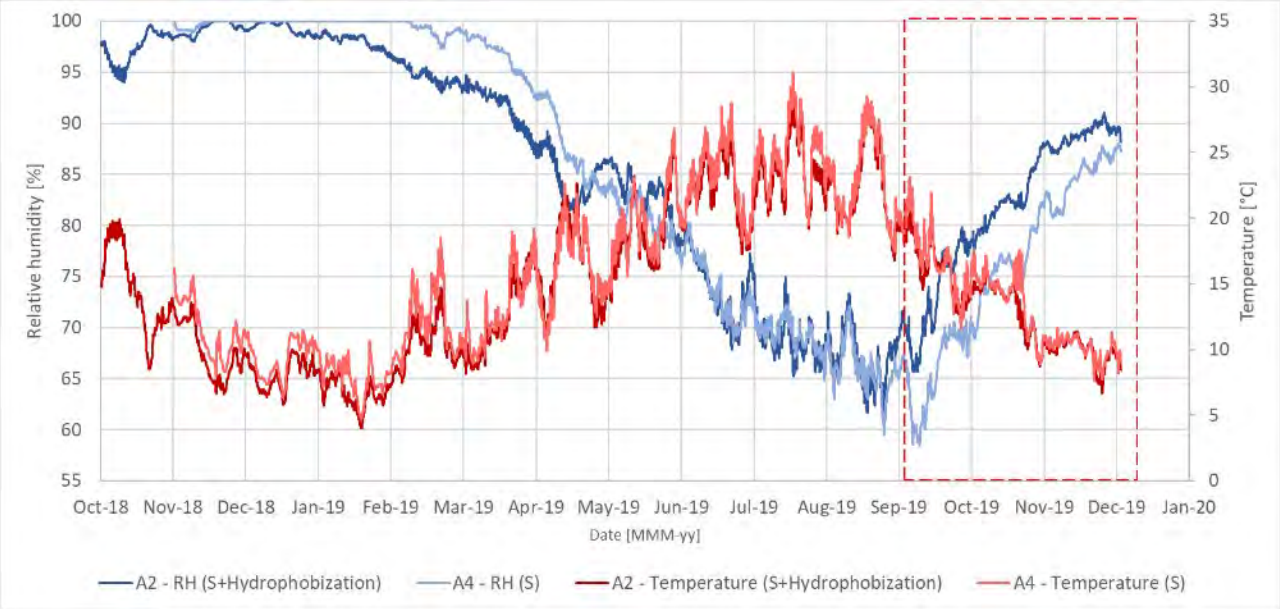

Figure 9-7: RH and temperature in the interface, living room, southern faced façade. The installation was offset by approx. one month, therefore only the period Sep-19 to Dec-19 (red box) is investigated.

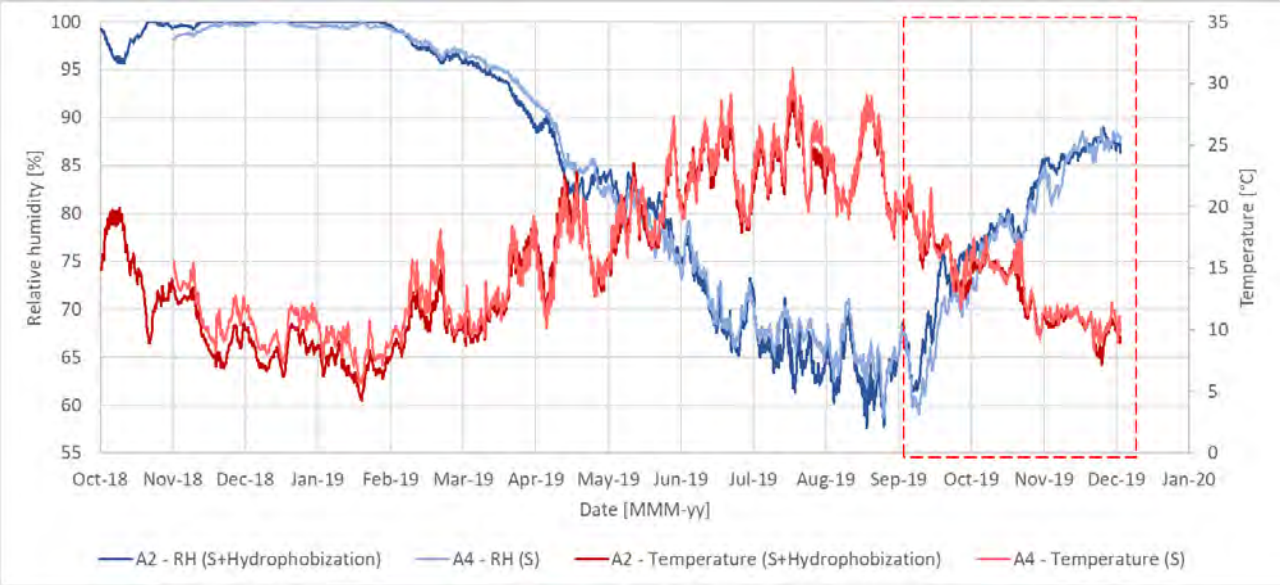

Figure 9-8: RH and Temperature in the interface, sleeping room, southern faced façade. The installation was offset by approx. one month, therefore only the period Sept-19 to Dec-19 (red box) is investigated.

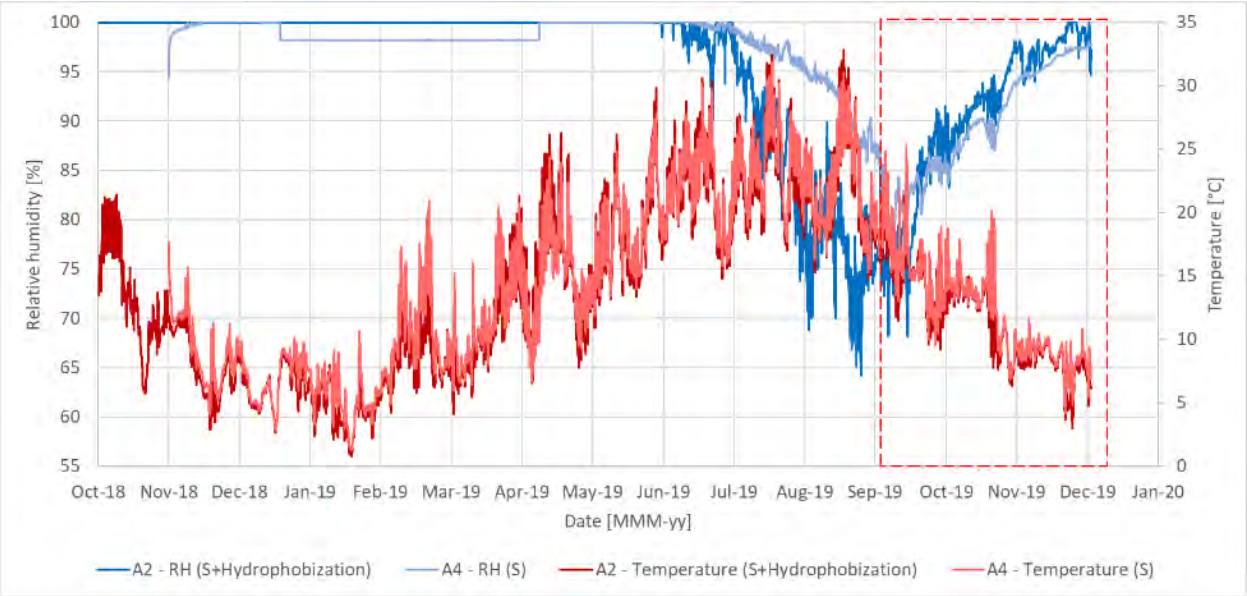

Figure 9-9: RH and Temperature in the interface, spandrel (living room), southern faced façade. The installation was offset by approx. one month, therefore only the period Sept-19 to Dec-19 (red box) is investigated.

9.3.1.2 North faced façade

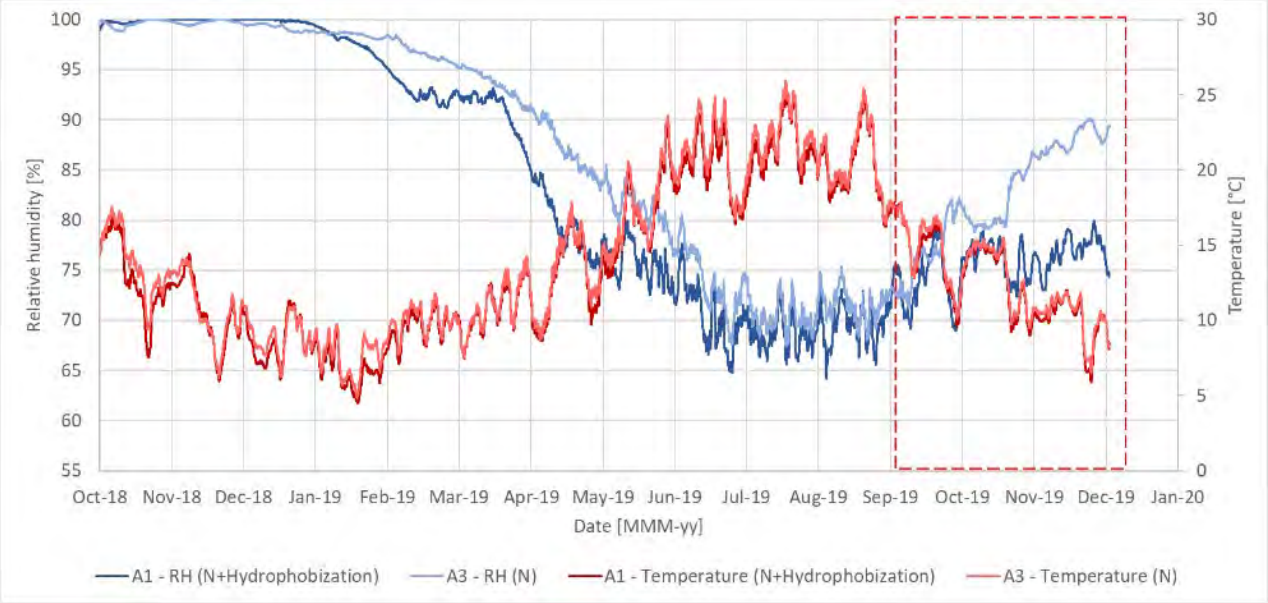

Figure 9-10: RH and Temperature in the interface, living room, northern faced façade. The installation was offset by approx. one month, therefore only the period Sept-19 to Dec-19 (red box) is investigated.

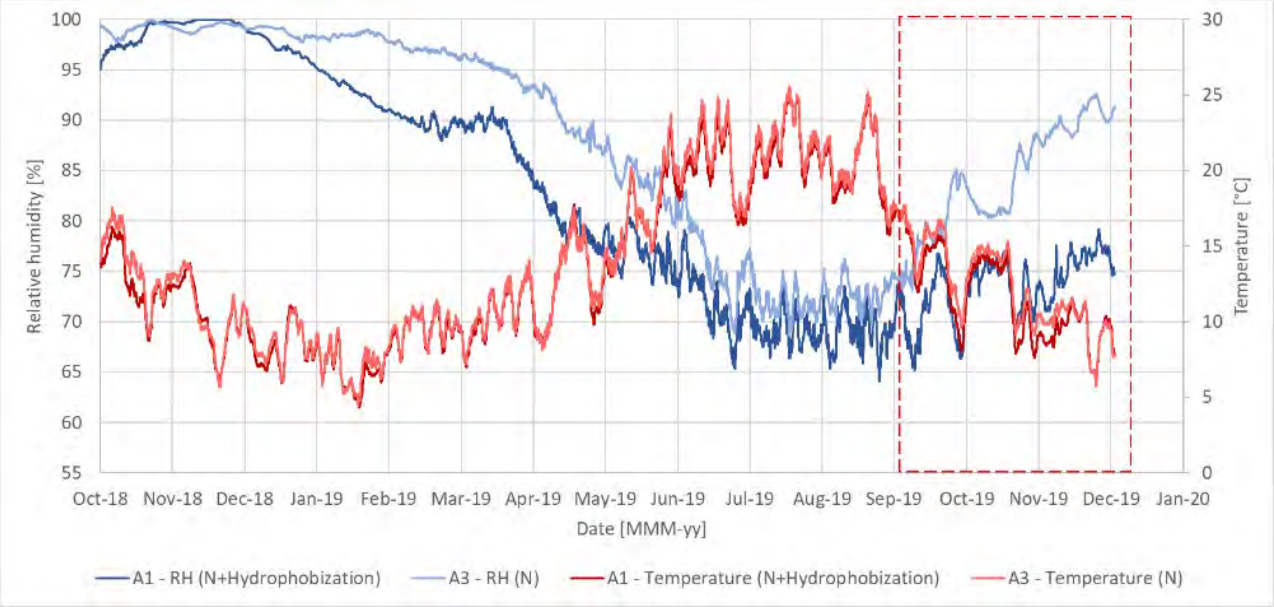

Figure 9-11: RH and Temperature in the interface, sleeping room, northern faced façade. The installation was offset by approx. one month, therefore only the period Sept-19 to Dec-19 (red box) is investigated.

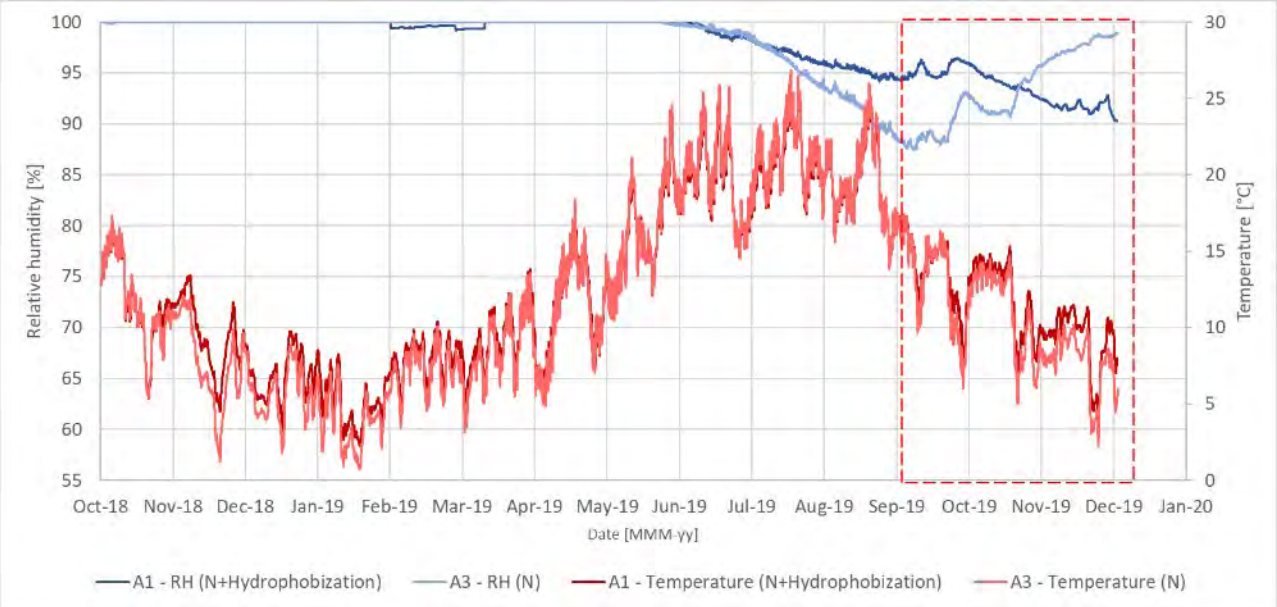

Figure 9-12: RH and Temperature in the intersection, spandrel (living room), northern faced façade. The installation was offset by approx. one month, therefore only the period Sept-19 to Dec-19 (red box) is investigated.

9.3.2 Interior climate conditions

Figure 9-13 and Figure 9-14 show the water vapor density for the living room, the bedroom and the exterior conditions. During the last winter period, both rooms in the apartments without hydrophobization have a higher water vapor density than in those with. It has to be mentioned, that there was a data loss from apartment 3 in the period July to October 2019.

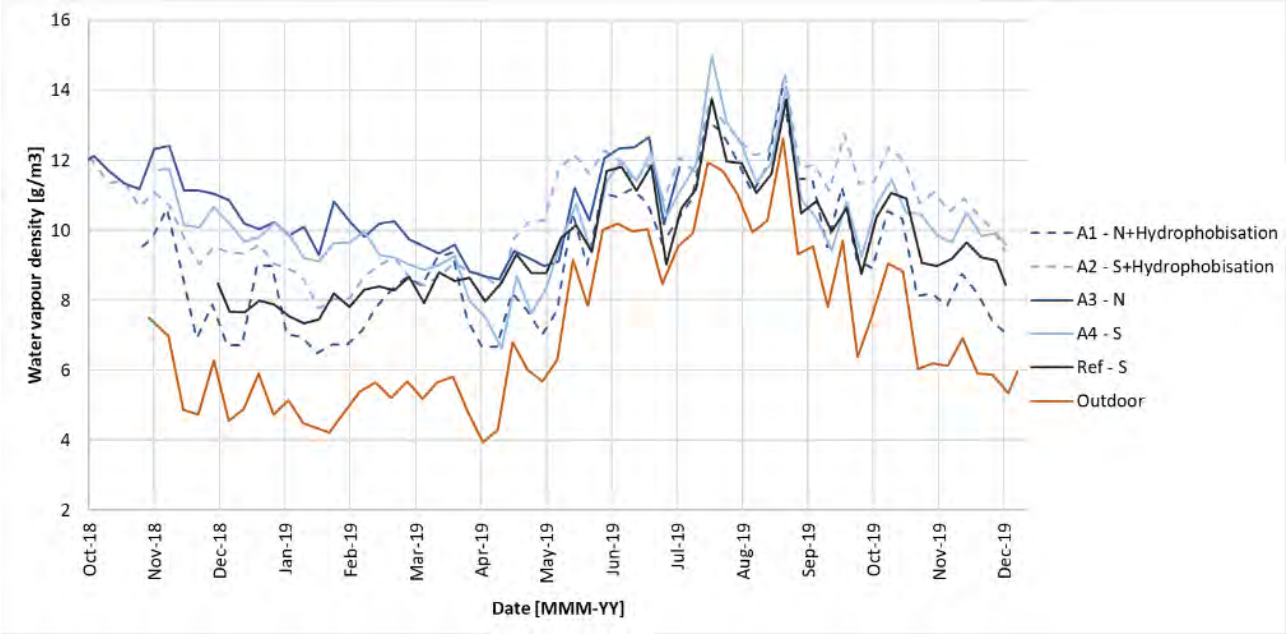

Figure 9-13: Water vapor density of all living rooms and of the exterior (weekly average)

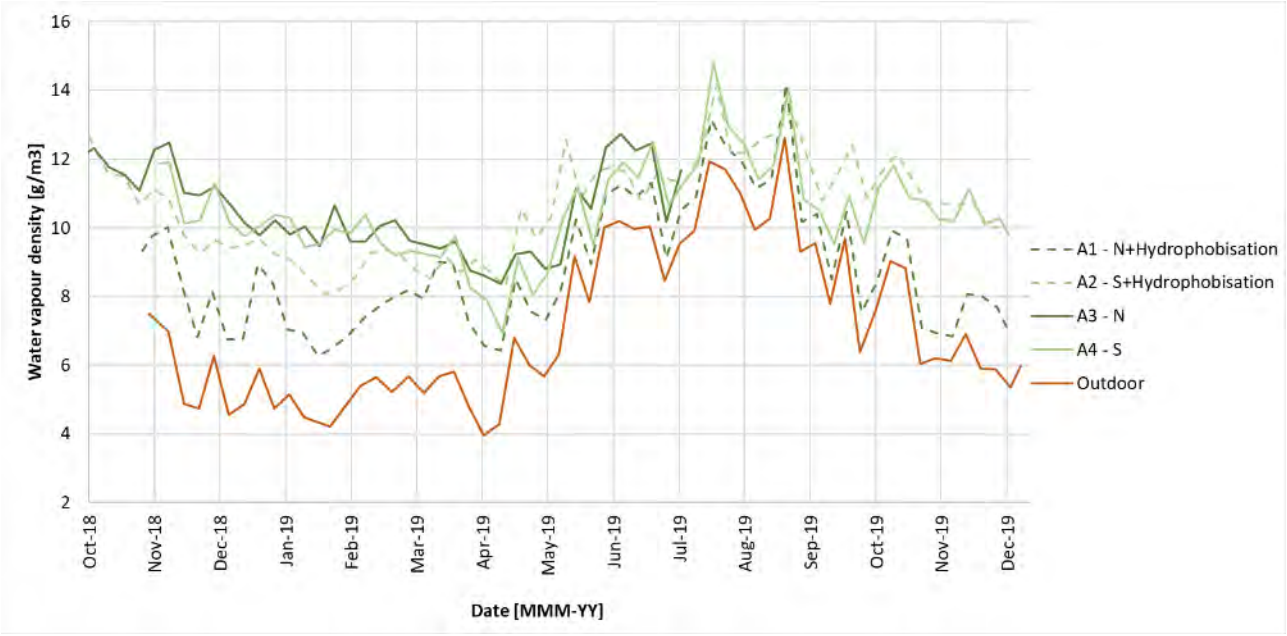

Figure 9-14: Water vapor density of all bedrooms and of the exterior (weekly average)

9.3.3 Exterior climate conditions

9.3.3.1 Driving rain

Figure 9-15 shows the amount of driving rain as an event of mm per hour as well as a total count in mm over the period of a year. From this count, it is seen that the amount of driving rain reaching the surface of the southern faced wall is 3½-4 times higher compared to the northern faced wall. It is therefore surprising that the effect of hydrophobization on the relative humidity at the interface is only visible for the north facing gables.

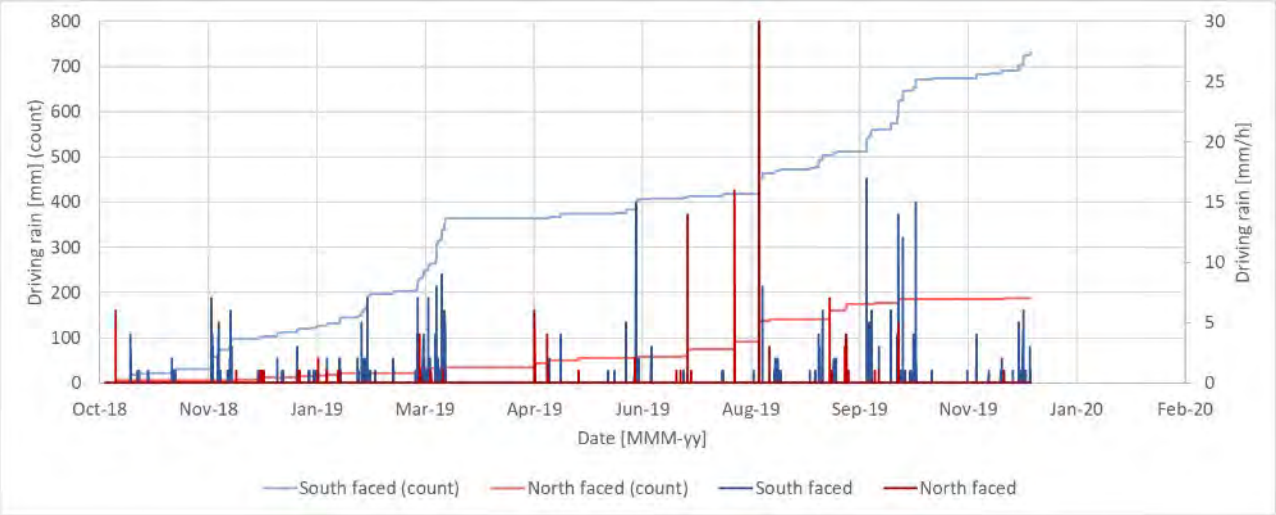

Figure 9-15: Driving rain, measured on the façades facing north and south

Figure 9-16 shows the exterior relative humidity and temperature over the period of a year.

Figure 9-16: Exterior relative humidity and temperature (weekly average), measured by Lonobox W920

9.4 Conclusion and further work

The first winter period (2018-2019) was the period of drying out the built-in moisture, followed by a summer period. It is therefore crucial to measure during a second winter period (2019-2020) to draw a conclusion on the effect of hydrophobization in addition to internal insulation of gable walls at this location. The preliminary findings indicate, that hydrophobization only has an impact of the relative humidity in the interface between insulation and existing wall on the north facing wall, although the driving rain on this gable is 4 times smaller than on the south facing wall. This could be a result of following factors:

- Difference in interior moisture level. The southfacing A2 has a higher moisture level to begin with than the northfacing A3. Drying is hampered by hydrophobisation and maybe the moisture level in A2 was too high and the drying too slow to make it possible to notice any effect of the hydrophobisation within the measuring periode
- 1st to 4th floor differences. The driving rain is higher in A4, which is on the 4th floor but has no hydrophobization as in A2, which is located on the first floor and was hydrophobized. The expectation would therefore be that the difference should be bigger in these southfacing gables. However, the gables were refurbished and driving rain may therefore be of less importance than the ron off, which is higher in the 1st floor apartment A2 (no hydrophobization), but run off higher in A2 (hydrophobization)

It is therefore important to evaluate the results after the next winter period.

References

Onset 2020a. HOBO RG3-M Data Logger data sheet, available at:

https://www.onsetcomp.com/datasheet/RG3-M

Onset 2020b. HOBO U12-012 Data Logger data sheet, available at:

https://www.onsetcomp.com/datasheet/U12-012

Rotronic 2019. HC2A Data sheet, available at: https://www.rotronic.com/en-ch/hc2a-s.html

Ytong 2017. Multipor Technical data sheet, available at:
https://www.ytong.dk/dk/docs/279243_DB_Multipor_WI_0717.pdf

10 In-situ assessment @ Heverlee, Belgium

(Evy Vereecken, KUL)

10.1 Introduction

This section describes the setup and the preliminary results of an ongoing in-situ experiment at the VLIET-test building of KU Leuven, Heverlee (Belgium). In the field study, the hygrothermal performance of hydrophobized masonry walls, provided with vapor tight or capillary active internal insulation are analysed. As a reference, also non-hydrophobized and non-insulated walls are analysed. To study the hygric performance, apart from traditional relative humidity sensors, in-house made moisture pins are embedded in the walls and are shown to yield valuable information in the high moisture range. Attention is given to a.o. the hygric performance of wooden beam ends, the impact of wind-driven rain on the moisture conditions in the masonry wall, as well as to the impregnation depth of the water repellent agent. For the latter, the field study is supplemented with X-ray and liquid droplet measurements on a small semi-duplicate test wall.

The section is an extended version of a conference paper accepted for DBMC2020 (Vereecken et al., 2020) and is organised as follows. Section 10.2 first describes the field test setup with inclusion of the applied measurement techniques. Next, in Section 10.3 a selection of the logged data is presented and analysed. In Section 10.4, a special focus is put on the impregnation depth in the masonry. Finally, in Section 10.5 the main conclusions are drawn.

10.2 Field test setup

10.2.1 Test walls

To study the impact of hydrophobization on internally insulated walls, six 1½ stone thick masonry test walls, approximately 32 cm thick, 0.6 m wide and 2.7 m high were constructed in two south-west oriented wall frames of the VLIET test building of KU Leuven (Figure 10-1a). The masonry assemblies were masoned by use of Vandersanden Robusta bricks ($A_{cap} \approx 0.61$ kg/(m^2.s$^{0.5}$)) and lime mortar (ratio: 12.5 kg Saint-Astier NHL3.5, 50 kg River sand 0/2, 10 litres water; $A_{cap} \approx 0.26$ kg/(m^2.s$^{0.5}$) for mold cured mortar). Between the different test walls, a barrier was provided, such that the hygrothermal behaviour of the test walls was not affected by the adjacent test walls. The construction of the test walls was finalised by the end of August 2017, after which a drying period took place.

On October 23th 2018, three of the six test walls (Figure 10-1a,c) were hydrophobized by use of Silres® SMK2100 from Wacker Chemie AG. An impregnation depth of 3 cm in the bricks was pursued, for which per m^2 wall 6.9 litres of a 10 vol% hydrophobic agent solution was applied by spraying. During the application of the hydrophobization, the other test walls were protected, as shown in Figure 10-1b.

The rain load on the test setup was initially measured via two wall-mounted WDR gauges positioned inbetween the hydrophobized and non-hydrophobized test walls. In December 2019, two additional wall-mounted WDR gauges were positioned at half heigt of the test wall (Figure 10-1c,d). The four WDR gauges had a collection area of 0.2 m x 0.2 m, as used by Blocken and Carmeliet (2006). To ease a comparison between the wall's hygrothermal performance and the WDR, the WDR load measured by the top WDR gauge is shown together with the results (Figure 10-7a).

Figure 10-1: Outside view of the field test setup: (a) south-west oriented side of the VLIET-test building, (b) spraying of the hydrophobic agent solution, (c) hydrophobized and non-hydrophobized masonry test walls with (d) wind-driven rain gauges.

On the inside, two test walls were provided with a vapor tight XPS internal insulation system, while two other test walls had a capillary active calcium silicate (CaSi) internal insulation system. Both systems were built up of a 10 cm thick insulation board which was fully adhered to the masonry by use of a glue mortar. As an interior finish, the XPS-system and the CaSi-system were provided with a gypsum board and plaster layer, respectively. The application of the internal insulation systems was performed in the second half of December 2018. The remaining two test walls had no internal insulation system, and thus acted as reference walls. An overview of the six test cases is given in Table 10-1.

In each of the test walls, two wooden beam ends were embedded in the masonry (Figure 10-2). The upper wooden beam ends were in contact with a mortar layer, whereas for the lower wooden beam ends an air gap was present at all sides except for the bottom of the wooden beam end. At the room side, the end of the wooden beams were covered with bituminous paint, avoiding vapor diffusion via the longitudinal wood direction. To prevent convective moisture transport, as discussed in (Vereecken and Roels, 2018), the gap between the wooden beam and the insulation system was sprayed up with flexible PUR-foam and the connection with the interior surface was sealed with an airtight tape. After all, also in hygrothermal studies including a wind-driven rain exposure (Kopecký et al., 2019) an airtight sealing of the beam junction has been put forward.

The indoor climate during the first measured winter period (2018-2019) could be classified as indoor climate class 1 (Figure 10-3), which was attributed to a malfunctioning of the humidifier. In the second (still ongoing) winter period of the measurement campaign (2019-2020), the indoor moisture load could be higher resulting in an indoor climate class 3.

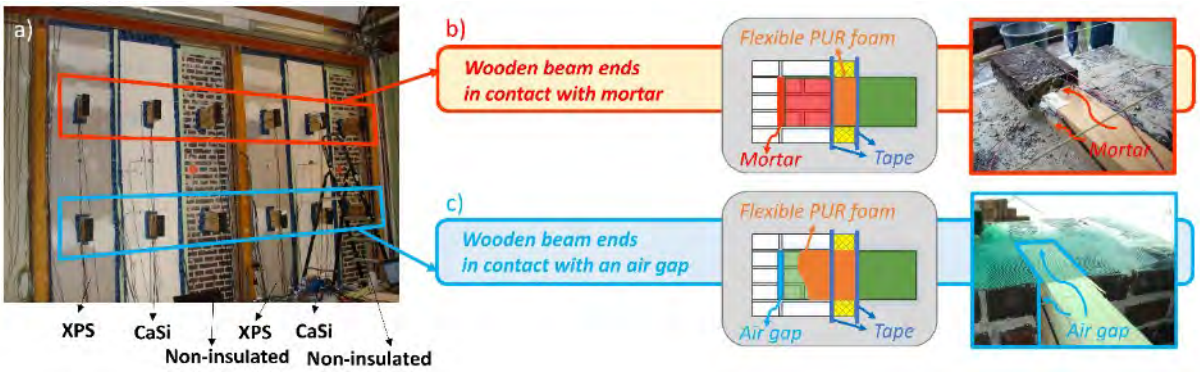

Figure 10-2: Inside view of the test walls: (a) global overview of the internally insulated and non-insulated test walls with embedded wooden beam ends, (b) wooden beam end in contact with mortar and (c) wooden beam end in contact with an air gap.

Table 10-1: Overview of the test walls

Label	Hydrophobization?	Internal insulation system
NH-XPS	No	XPS
NH-CaSi	No	CaSi
NH-Non	No	Non-insulated
H-XPS	Yes	XPS
H-CaSi	Yes	CaSi
H-Non	Yes	Non-insulated

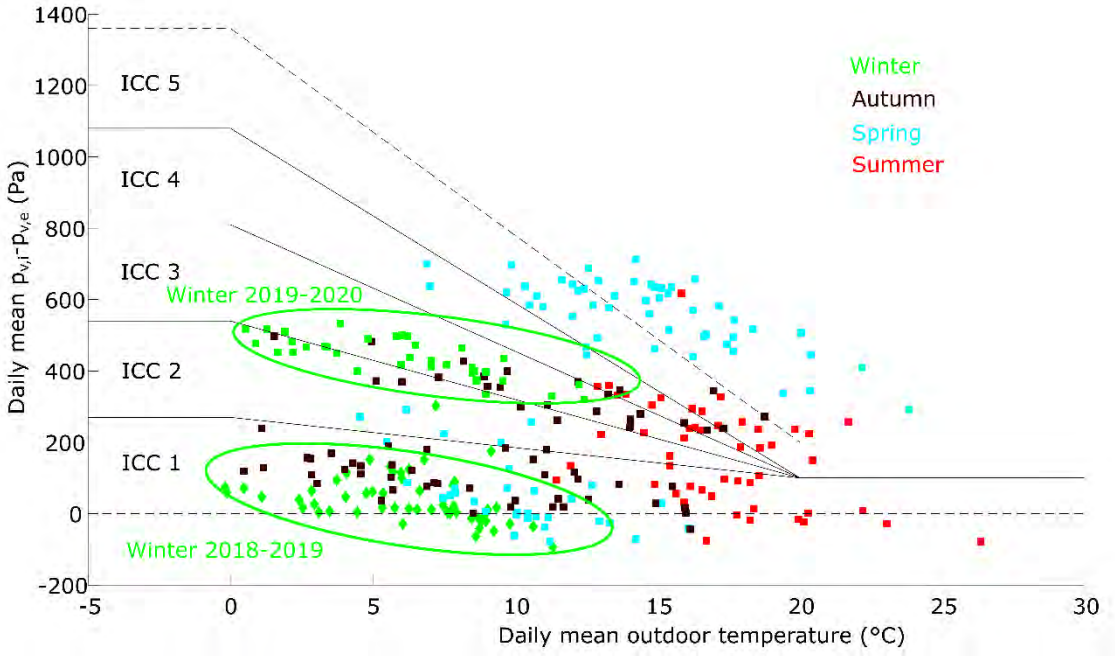

Figure 10-3: Daily mean difference in indoor and outdoor vapor pressure as a function of the daily mean outdoor temperature as an indication of the indoor climate class (ISO 13788, 2012) in the test setup.

10.2.2 Measurement techniques

The temperature and the relative humidity in the test walls were measured by use of in-house calibrated Thermo Electric Type T (class 1) thermocouples and Honeywell HIH-4021 humidity sensors, with an accuracy of +/- 0.2°C and +/- 2% RH. To limit the risk on a malfunctioning of the humidity sensors when embedding them in the masonry, the RH-sensors that were planned to be positioned in a mortar layer were protected by use of nylon and/or wrapped with the respective (glue) mortar. By putting the sensors in contact with mortar before embedding them in the test wall, sensors that showed already some malfunctioning after this first contact could still be replaced. In addition to the thermocouples and humidity sensors, in-house made moisture pins, measuring the electrical resistance, were used to analyse the moisture conditions at the back of the wooden beam ends, in the mortar in the masonry, in the glue mortar and in the calcium silicate.

It is well known that the electrical resistance of a material depends on the material's moisture content, as moisture is a good electrical conductor. The lower the electrical resistance measured in a material, the higher the moisture content of the material. For a more in depth description on the electrical resistance method, the reader is referred to (Otten et al., 2017). The moisture pins in the wooden beam ends were non-insulated nails: this way the moisture pins measured the highest moisture content along the length of the moisture pins, which gives the worst-case scenario when assessing the risk of wood rot. Over the nail heads, thus at the surface of the wooden beam end, a small tape was glued in order to avoid measuring the electrical resistance over the mortar layer in contact with the wooden beam.

For the moisture pins embedded in the mortar, two types were applied. A first type, in what follows reffered to as 'surrogate' mortar moisture pin, was prepared in advance. For this type, two electrical wires were positioned at a fixed width. Next, mortar with the same composition as applied in the test walls was used to make a mortar sample in which the wires were positioned (Figure 10-4a). Additional surrogate mortar moisture pins were prepared for calibration measurements. For this type of moisture pins, the risk exists that during building the test wall a crack in the surrogate mortar sample occurs. If such a crack occurs inbetween the two electrical wires, the electrical resistance between both wires will be larger. Furthermore, with these surrogate moisture pins, a hydraulic interface resistance might occur between the surrogate mortar and the real mortar layer, which might influence the moisture exchange with the surrogate mortar.

Therefore, a second type, referred to as 'in-situ' mortar moisture pins, was embedded in the masonry test walls. For this second type, two insulated nails were positioned in a small distance holder to keep a fixed 3 cm-distance between the pins during masoning (Figure 10-4a). This way, no interface resistance is present and curing conditions of the mortar around the moisture pins are similar to the curing condition in the masonry test wall. Due to the difference in curing conditions with the surrogate moisture pins, the in-situ moisture pins show however a different relationship between electrical resistance and moisture content. Hence, for the in-situ moisture pins, a new calibration is needed.

To be as representative as possible, simultaneously with masoning the masonry test walls, a smaller masonry wall with embedded moisture pins was built in front of the VLIET-test building, and after curing a number of in-situ moisture pins was taken out of the small test wall for calibration later on. For the other positions (in the CaSi and XPS glue mortar), insulated surrogate moisture pins based on the respective materials are applied. Finally, moisture pins were positioned at the warm and cold side of the calcium silicate as shown in Figure 10-4b. For all the moisture pins, the distance between both nails or wires was 3 cm. The electrical resistance measurements were perfomed by use of a Campbell Scientific logger. For the moisture pins a preliminary calibration took place, of which an example for the in-situ mortar moisture pins is given in Figure 10-5.

At half height of the test walls, additionally a heat flux sensor was glued at the warm side of the masonry. The position of the different sensors is shown in Figure 10-6.

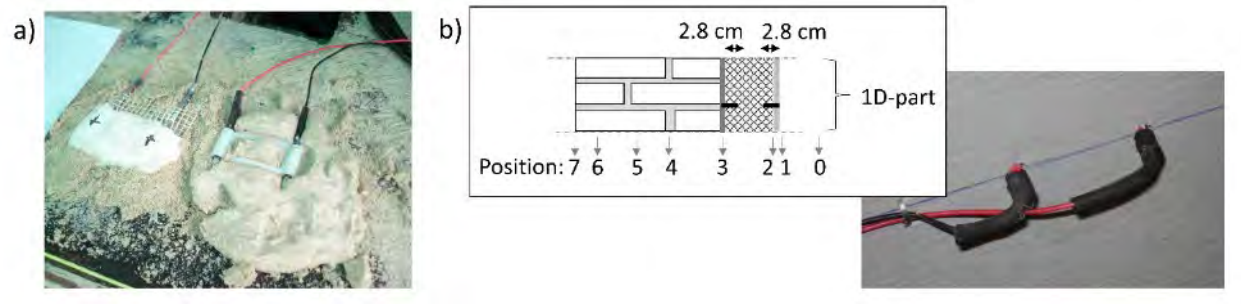

Figure 10-4: (a) Surrogate (left) and in-situ (right) mortar moisture pins, (b) position and execution of a CaSi moisture pin.

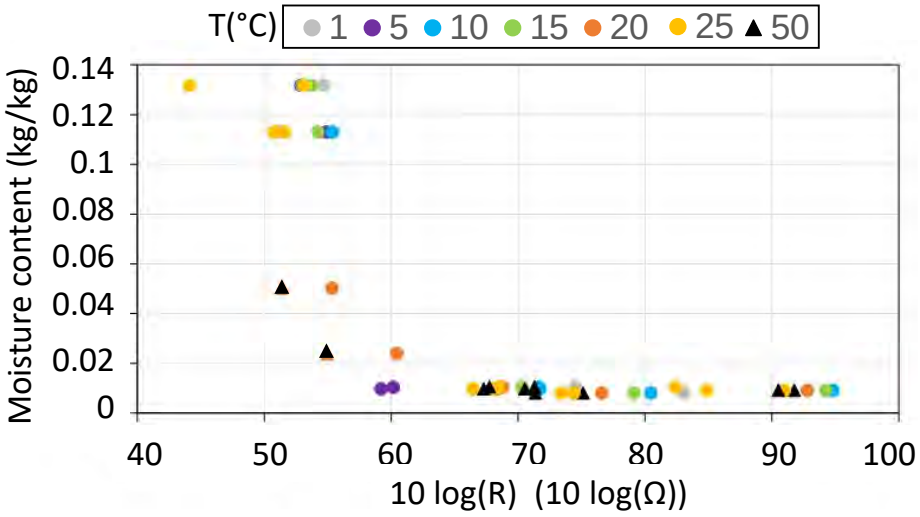

Figure 10-5: Preliminary calibration curve for the in-situ mortar moisture pin.

10.3 Results

Hourly-averaged data are used for the analysis of the hygrothermal performance of the test walls. In what follows, the measurements achieved in the period from June 2018 till the end of January 2020 are shown. Thus, a period in which the walls were all non-hydrophobized and non-insulated is included. In the legend of the graphs, from the start however, these walls are indicated by their final state of hydrophobization and internal insulation system. Focus is put on the moisture conditions in the mortar layer in the 1D-part of the masonry, as measured by the in-situ mortar moisture pins, the moisture conditions in the insulation system and on the moisture conditions of the wooden beam ends.

To analyse the data measured by the moisture pins, it is important to keep in mind the inverse relation between electrical resistance and moisture content. A lower electrical resistance represents a higher moisture content. Furthermore, a preliminary calibration of the in-situ mortar moisture pins (Figure 10-5) showed an electrical resistance above 60 x 10 log(Ω) to correspond to a similar moisture content. The electrical resistance at which this phenomenon occurs can however slightly vary depending on the material the moisture pins are embedded in (Brischke et al., 2008). Hence, at this point, the moisture pins don't allow an absolute comparison of the measurement data in the lower moisture range (above an electrical resistance in the range of 60 x 10 log(Ω)).

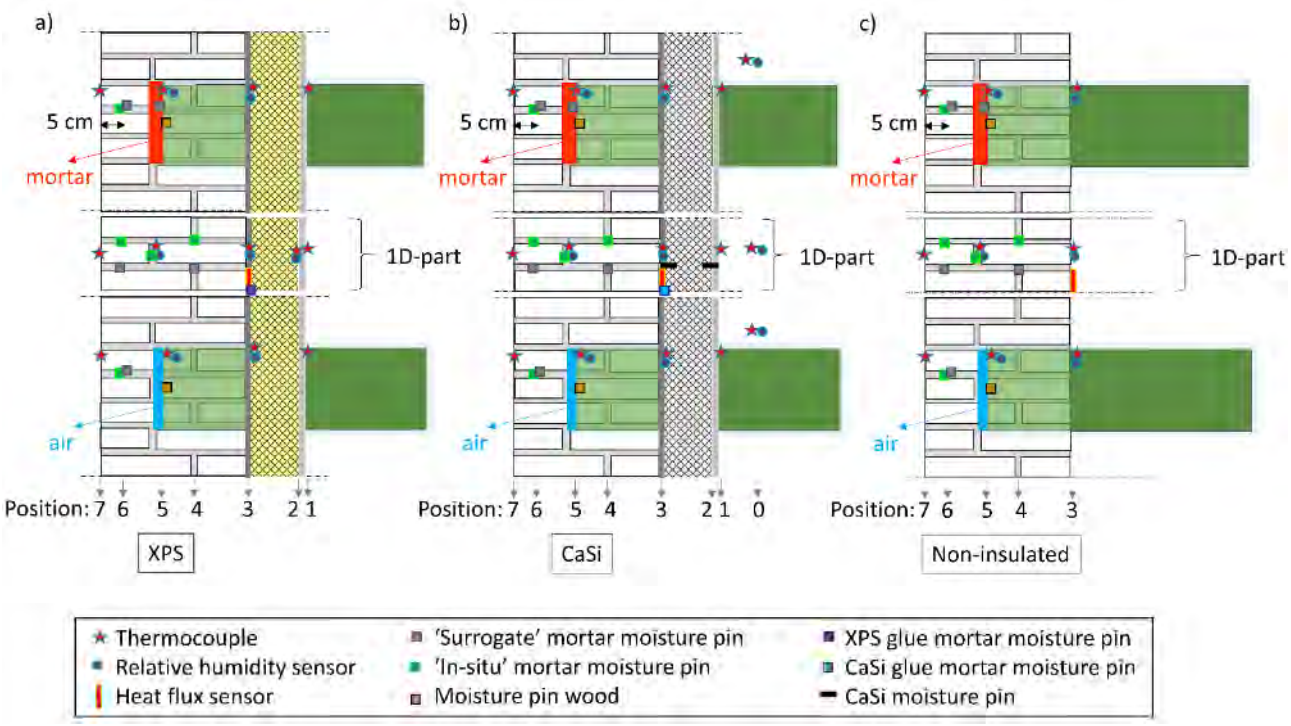

Figure 10-6: Position of the thermocouples, humidity sensors, moisture pins and heat flow sensors for the wall with (a) a XPS-system, (b) a calcium silicate system, (c) no insulation.

10.3.1 Moisture conditions in the 1D-masonry part

Figure 10-7b, c and d show the electrical resistance as measured by the in-situ mortar moisture pins in the middle (1D) part of the test walls. Additionally, the relative humidity at Position 5 is shown (Figure 10-7e). Both the relative humidity and the electrical resistance show a drying behaviour in the period before the water repellent agent was applied. When applying the hydrophobization, for the hydrophobized walls an abrupt drop in electrical resistance is shown at Position 6, which is closest to the outer surface. After this, the electrical resistance starts increasing again slowly, which indicates a drying of this outer masonry region. For Position 5, a decrease in electrical resistance occurs over a longer time period after the hydrophobization (pink rectangle), which can be attributed to an inward redistribution of the water used for the water repellent solution. For the hydrophobized wall with a CaSi-internal insulation system, the measurement data seem to be shifted upward compared to the other walls. No explanation is found for this behaviour and a malfunctioning of the moisture pin is assumed; though the decreasing trend is also visible here. For the three hydrophobized walls, the inward redistribution indicated by the moisture pins is confirmed by the relative humidity sensor at Position 5 (Figure 10-7e). Deeper in the wall (Position 4), no distinct changes are found during or shortly after the application of the hydrophobization (Figure 10-7d).

In December 2018 (yellow rectangle), a reverse behaviour can be observed. In a part of this period the sensors were disconnected to install the internal insulation systems. Though, a comparison of the data before and after this interruption shows, especially for Position 6, a strong decrease in electrical resistance for the three non-hydrophobized walls. This can be attributed to wind-driven rain absorbed by the walls (see Figure 10-7a). The electrical resistance measured in the hydrophobized walls remains substantially the same. A similar behaviour is found in October 2019. Other WDR loads (e.g. in February/March 2019) are less visible, since the moisture level in the wall is already high at that time.

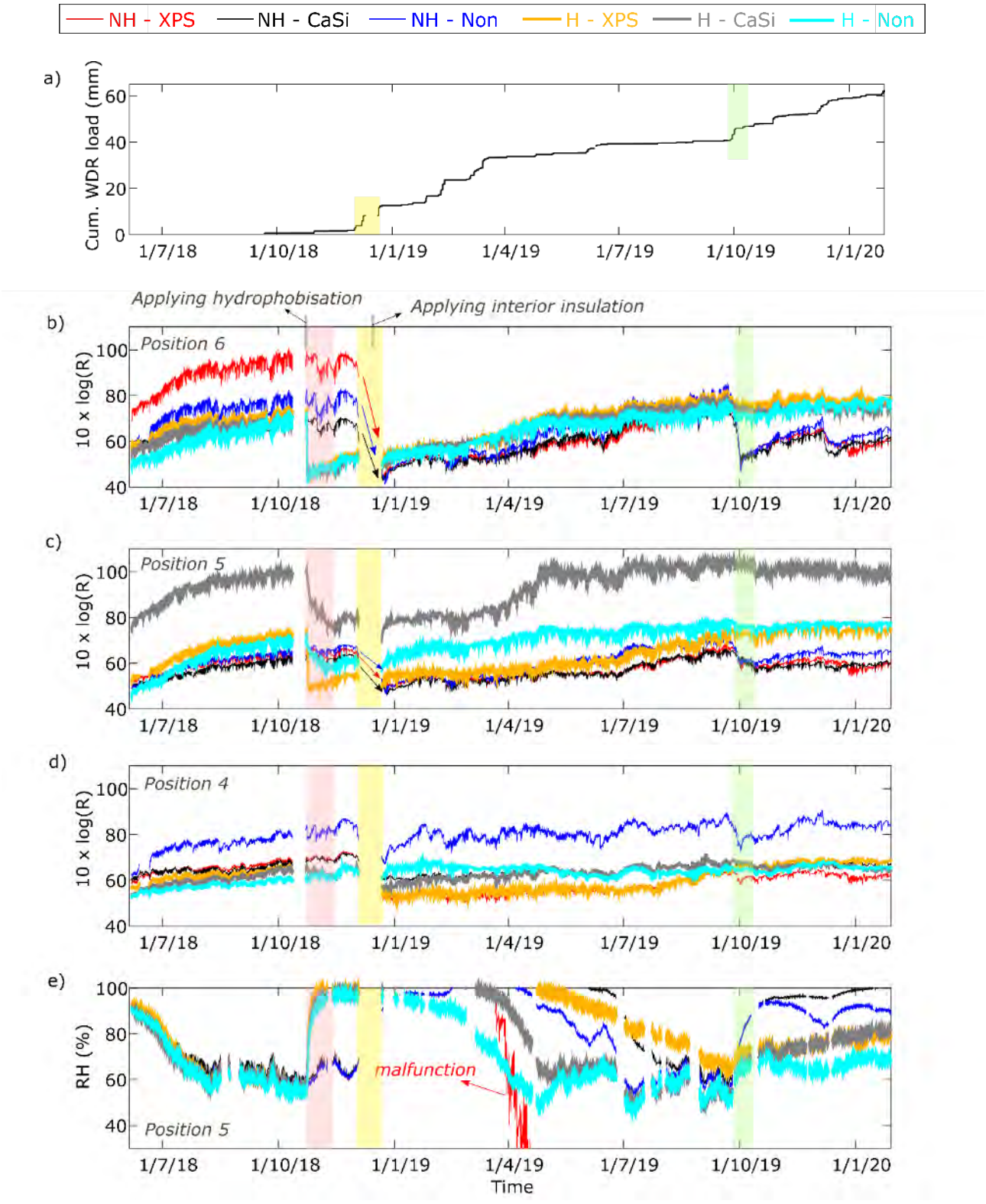

Figure 10-7: (a) Cumulative wind-driven rain load measured by the top WDR gauge, (b,c,d) electrical resistance measured by the in-situ mortar moisture pins in the 1D-part of the walls for (b) Position 6, (c) Position 5 and (d) Position 4, (e) relative humidity measured in the 1D-part at Position 5 (see Figure 10-6 for an indication of the positions).

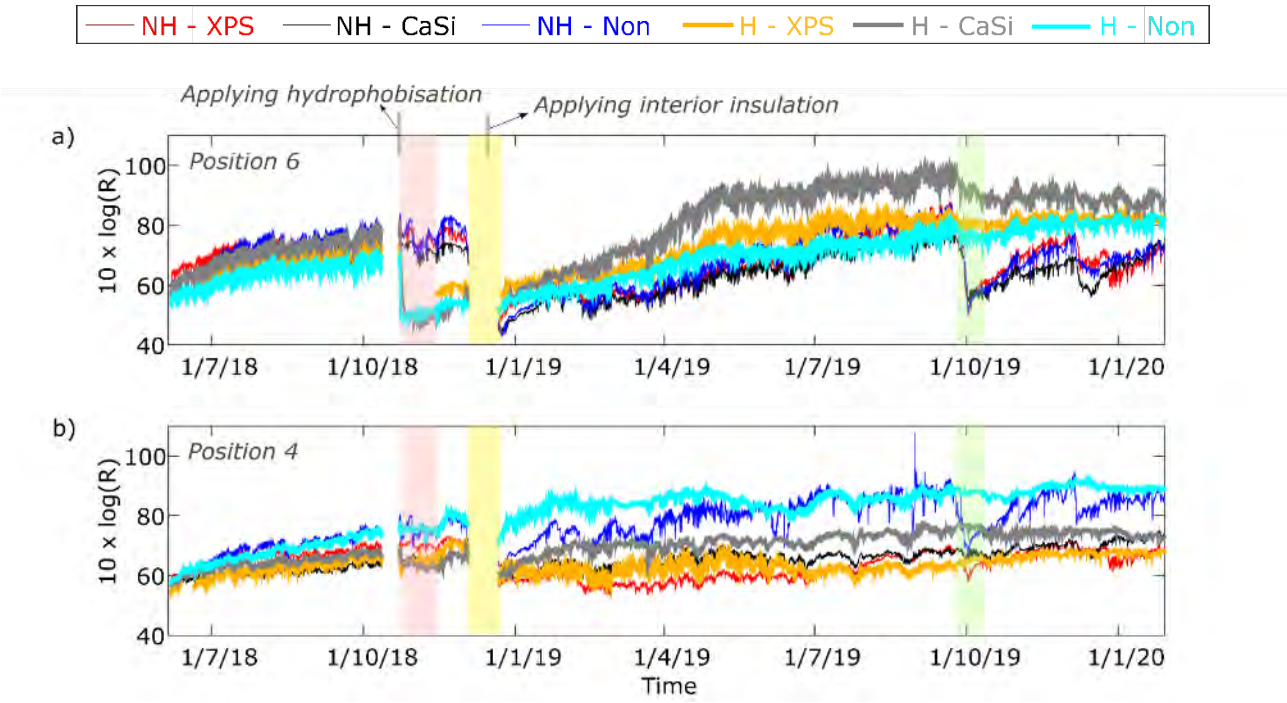

Figure 10-8: Electrical resistance measured by the surrogate mortar moisture pins in the 1D-part of the walls for (a) Position 6 and (b) Position 4 (see Figure 10-6 for an indication of the positions).

The impact of the internal insulation systems is visible in the relative humidity at Position 5 (Figure 10-7e). In spring and summer, a decrease in relative humidity is observed, which occurs first for the hydrophobized non-insulated wall, followed by the hydrophobized wall with the CaSi-system and the non-hydrophobized non-insulated wall. Next, the relative humidity in the hydrophobized wall with XPS starts decreasing, but this occurs slower than found for the non-hydrophobized wall with the CaSi-system. The relative humidity sensor in the non-hydrophobized wall with XPS showed some malfunctioning due to the high moisture load. In October and December 2019, the relative humidity increases again for the non-hydrophobized test walls and reaches a relative humidty above 80%. Again, the increase in relative humidity coincides with a drop in electrical resistance near the exterior surface (Position 6 in Figure 10-7b) and can thus be linked to the WDR load (Figure 10-7a).

As mentioned in Section 10.2.2, two types of mortar moisture pins were embedded in the masonry. As a comparison to the electrical resistance measured by the in-situ moisture pins (Figure 10-7), Figure 10-8 shows the electrical resistance in the 1D-part as measured by the surrogate mortar moisture pins. In general, a similar behaviour can be observed. The increase in moisture level (decrease in electrical resistance) due to an inward liquid distribution during the hydrophobization process and due to wind-driven rain in case of the non-hydrophobized test walls is visible at Position 6. Further in the wall (Position 4), the highest moisture content (lowest electrical resistance) is found for the (non-hydrophobized and hydrophobized) wall with an XPS-system, which was also visible in Figure 10-7d.

10.3.2 Moisture conditions in the glue mortar

As a first indication of the difference in moisture conditions in the glue mortar of the calcium silicate and XPS-system, Figure 10-9a shows the relative humidity in the glue mortar. For both insulation systems, the case with and without hydrophobization is shown. In January 2019, the four cases show

a relative humidity close to 100%. This is due to the initial moisture content, as the insulation material was only recently adhered to the wall at that moment. For the (hydrophobized and non-hydrophobized) walls with calcium silicate, the glue mortar starts to dry out rather fast. Only a negligible difference between hydrophobized and non-hydrophobized wall is visible. For the walls with an XPS-system, on the other hand, the decrease in relative humidity starts much later (i.e. during summer). Though, during the second winter in the measurement campaign, in general, the lowest relative humidity in the glue mortar is achieved for the hydrophobized wall with an XPS-system. For the hydrophobized case with calcium silicate, an outward vapor flow during the heating season might lie at the basis of the higher moisture content than found for the XPS-system.

Based on the glue mortar moisture pins (Figure 10-9b), a similar behaviour can be found. At the start of the measurements, a low electrical resistance is measured due to the initial moisture content. During the second winter period, the lowest moisture content (highest electrical resistance) is measured for the hydrophobized wall with XPS-system. It should however be noticed that for both systems a different glue mortar (and thus a different type of glue mortar moisture pin) is applied. Both types of glue mortars might have a different calibration curve for the relation between electrical resistance and moisture content. This might explain the rather similar electrical resistance measured during Spring 2019 for both systems, while the relative humidity shows a large difference.

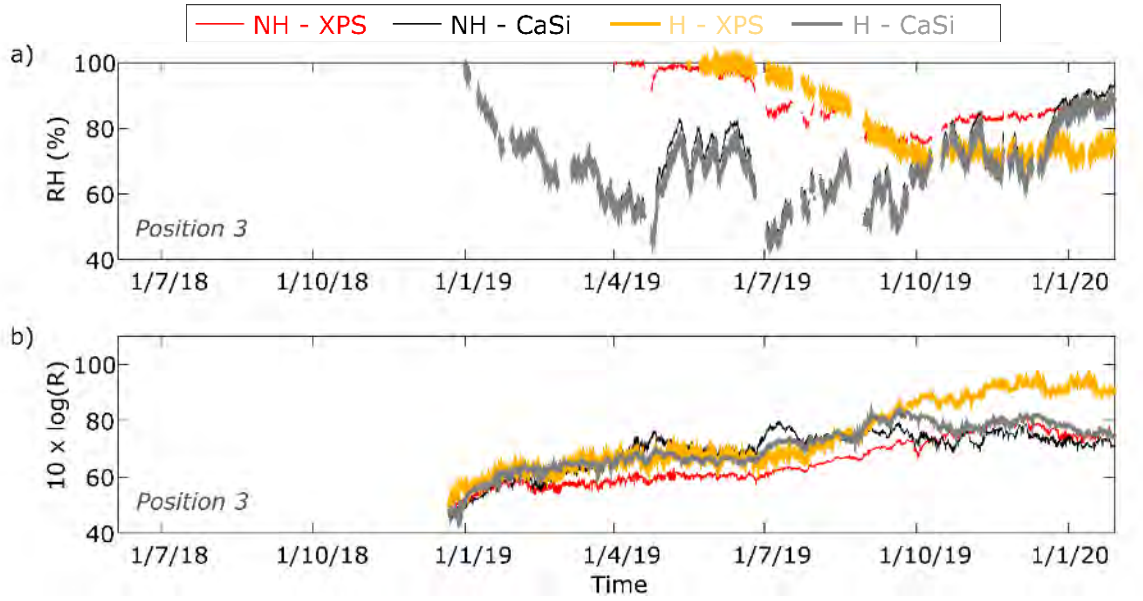

Figure 10-9: (a) Relative humidity and (b) electrical resistance measured in the glue mortar at Position 3 (see also Figure 10-4 for the position).

10.3.3 Moisture conditions at the wooden beam ends

Figure 10-10 shows the relative humidity at Position 5 on the wooden beam ends. For the beam ends in contact with mortar (Figure 10-10a) the relative humidity at the beginning of June 2018 is found to be above 90%. The test walls are at that moment still non-hydrophobized and non-insulated, and hence show a relative humidity that is in close agreement for the different walls. During the next half year, a drying out takes place until a quasi-equilibrium is found close above 60% RH. For the lower beam ends provided with an air gap between beam and masonry (Figure 10-10b), the relative humidity level is found to be between 40 and 65% during this entire period.

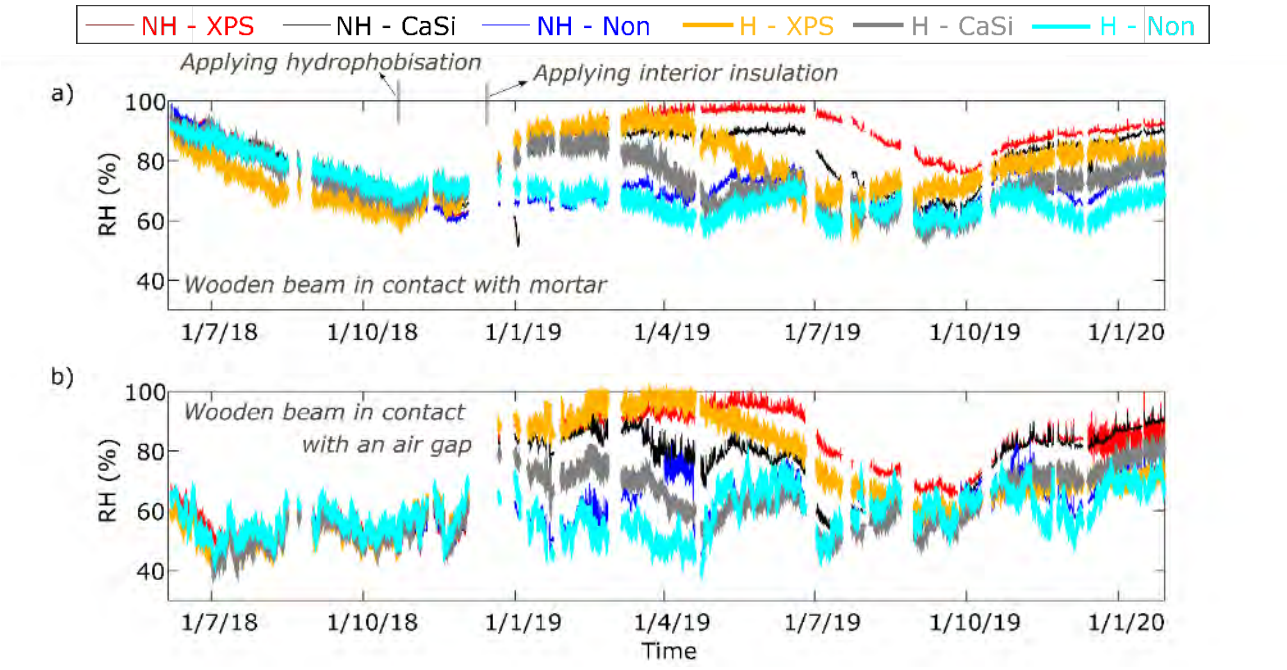

Figure 10-10: Relative humidity at Position 5 (see Figure 10-6) at (a) the upper and (b) the lower wooden beam end.

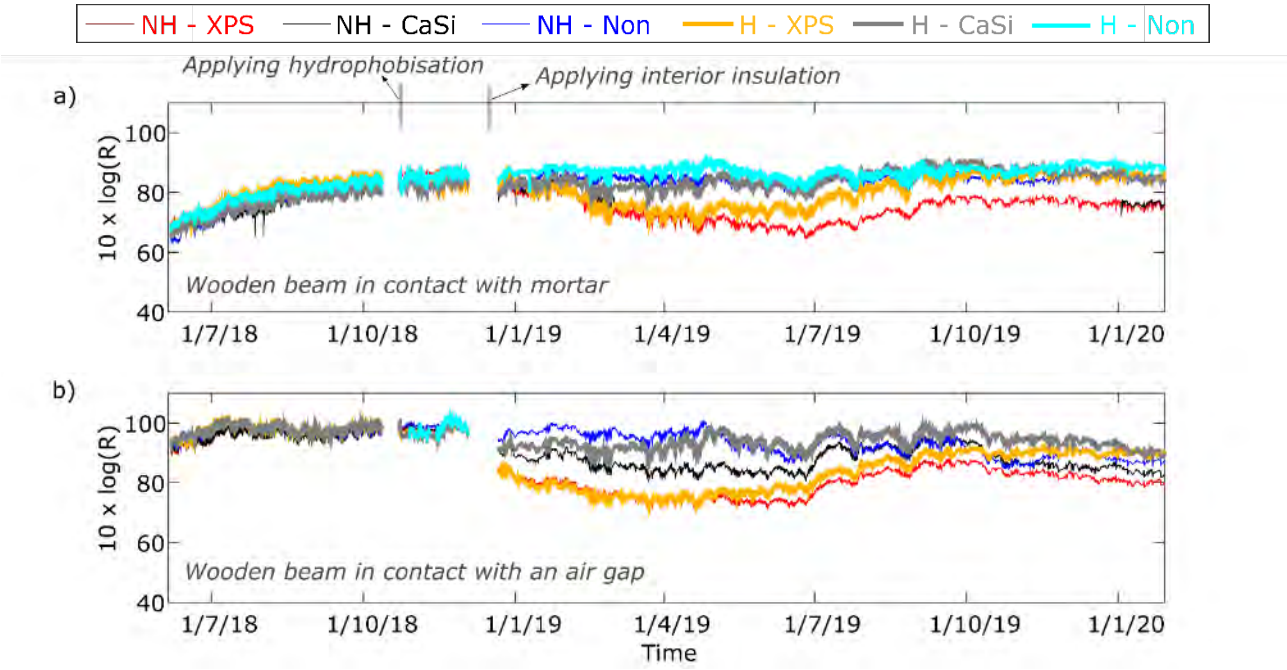

Figure 10-11: Electrical resistance at Position 5 (see Figure 10-6) measured by the wood moisture pins in (a) the upper and (b) the lower wooden beam end.

For the period after January 2019, for both the upper and lower wooden beam end an increase in relative humidity is measured for the walls with internal insulation. This can be partially explained by the lower wall temperature. Apart from this, also a higher moisture content in the wall as indicated by the moisture sensors (Figure 10-7d) can contribute to this, especially for the upper wooden beam

which is in contact with mortar. During spring and summer, the relative humidity starts decreasing again. As found for the relative humidity at Position 5 in the 1D-part (Figure 10-7d), the slowest decrease is found for the non-hydrophobized wall with XPS and the fastest for the hydrophobized system with CaSi. The relative humidity level for the non-insulated walls remains rather stable over the entire period. In the second winter period, the non-hydrophpobised walls with an internal insulation system show a slightly higher relative humidity. As the hydrophobized wall with an XPS-system shows in the second winter period a relative humidity around 60%-80%, the high relative humidity in the first winter period will be attributed to moisture that was absorbed by the wall before and during the application of the hydrophobic agent.

Figure 10-11 shows the electrical resistance measured by the wood moisture pins at the back of the wooden beam end. Also based on these measurements, the largest moisture conditions are found for the non-hydrophobized wall with an XPS-system. For the hydrophobized wall with an XPS-system, in the first winter period a high moisture level is found, while in the second winter period the moisture level in the wood lays in the same order of magnitude as found for the wall with a calcium silicate system. A similar behaviour was found based on the relative humidity sensor.

10.4 Analysis of the impregnation depth

In Section 10.3, the hydophobization process was shown to induce a large increase in moisture content in the mortar at 5 cm from the outer surface of the masonry (Position 6). In order to achieve a view on the extent to which also the hydrophobic agent was transported in the wall, the impregnation depth was further analysed via an additional laboratory test setup. Thereto, a small test wall masoned with the same type of bricks and mortar as applied in the VLIET test setup and hydrophobized in a similar way (Figure 10-12a) was built. This wall was cut in half (Figure 10-12b) and tilt such that the center plane became a horizontal plane on which the impregnation depth of the hydrophic agent could be analysed via the droplet method. Water droplets were dropped on the surface by use of a pipette and the contact angle of the droplet was analysed. For the bricks, three zones were detected (Figure 10-12c). In the zone closest to the outer (hydrophobized) surface a fully hydrophobized effect was observed. Droplets with a contact angle larger than 90° were clearly noticed (Figure 10-12e).

The impregnation depth in the bricks seemed to be larger than the pursued 3 cm, which might be due to the dynamic way of spraying the hydrophobization. This zone passed into a second zone where the droplets collapsed and were next absorbed slowly by the brick layer (Figure 10-12d). Deeper in the wall the bricks seemed not impregnated. After this droplet measurement, a small brick-mortar sample (Figure 10-12f) was sawn out of the middle surface of the smaller test wall. The non-hydrophobized surface was brought in contact with a water level, while the moisture content in the test sample was analysed by the X-ray projection technique (Roels and Carmeliet, 2006). At the end of this experiment, the moisture front had reached the boundary of the first impregnation zone (Figure 10-12g). In the mortar layer, the impregnation depth was found to be much smaller (1 to 2 cm). Hence, the increase in moisture content observed in Section 3 is expected to be attributed to liquid transport only. The active ingredient is not transported with it to the position of the moisture pins in the mortar.

10.5 Conclusions

Preliminary results of a field study on the impact of internal insulation and hydrophobization on the hygrothermal performance of solid masonry walls with embedded wooden beam ends has been presented. In-house made moisture pins yielded valuable information on the moisture transfer in the

masonry during and after spraying the water repellent agent. After all, installing RH sensors in the wet mortar entails a risk on malfunction of the sensors and is not obvious in the high moisture range. A further calibration of the moisture pins is however required to make a conversion to the moisture content and a further analysis of the measurements possible. Below the over-hygroscopic range, standard relative humidity sensors are preferredpreferred above moisture pins.

In the current study, an increased moisture level was induced during the hydrophobization process. A drying period was needed to again reduce the moisture level near the outer surface. When disregarding the period shortly after applying the water repellent agent, hydrophobization showed a positive impact on the wall's hygric performance. Deeper in the wall, near the wooden beams ends, the highest relative humidity was observed for the non-hydrophobized wall with a vapor tight internal insulation system. The non-insulated test walls showed the lowest relative humidity, regardless of the presence of a hydrophobization.

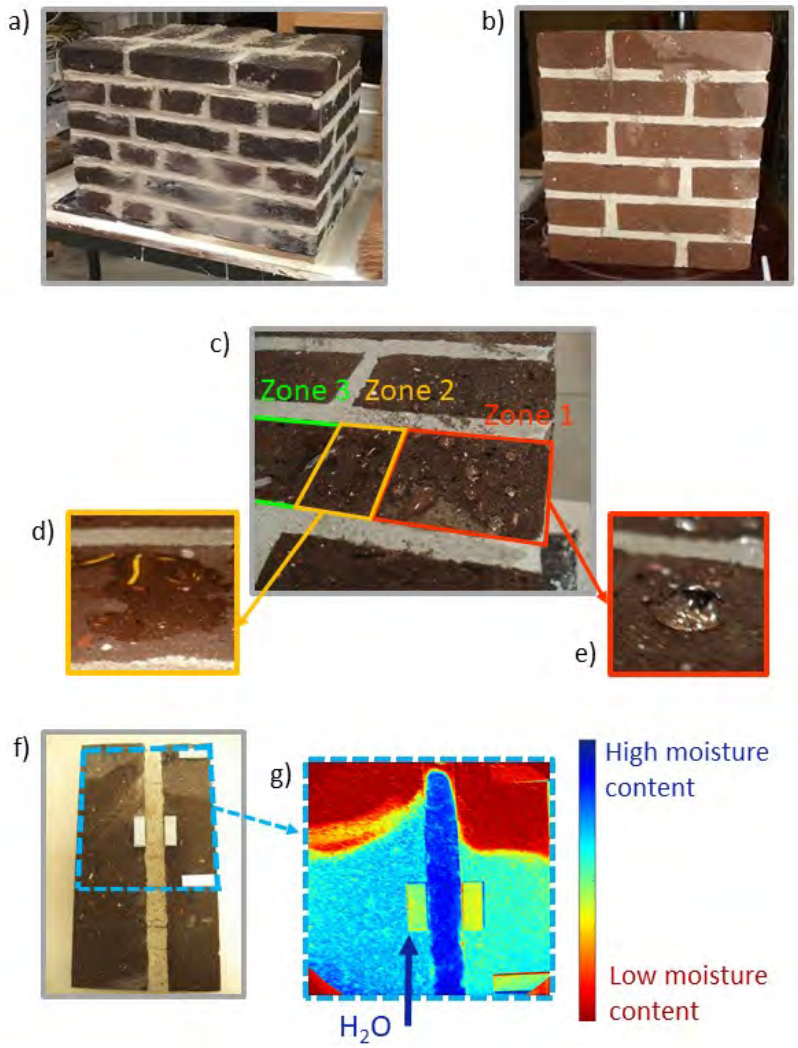

Figure 10-12: Study on the impregnation depth for a small semi-duplicate test wall: (a) the test wall, (b) test wall vertically cut in half, (c,d,e) droplets and collapsed droplets indicating different hydrophobized zones, (f) test sample sawn out the test wall for the X-ray test with metal dummy's as position references, (g) moisture content measured by the X-ray projection method after bringing the non-hydrophobized surface in contact with water.

The moisture level in the hydrophobized masonry wall internally insulated with calcium silicate was found to be lower than measured in the walls with a vapor tight internal insulation system. The moisture level in the non-hydrophobized wall with calcium silicate, however, was often found to be higher than measured in the hydrophobized wall insutaled with a vapor tight XPS-system.

For the vapor tight XPS-system, in the first winter period a high moisture level was found for both the hydrophobized and non-hydrophobized wall, which is due to moisture absorpbed before or during the application of the hydrophobization. In the second winter period, in general, the moisture level in the hydrophobized wall with XPS was lower.

In respect to the moisture level in the glue mortar between the masonry and the internal insulation, the largest drying rate was measured for the walls with calcium silicate insulation. In the second winter period, however, the relative humidity in the calcium silicate glue mortar was found to increase and to become higher than measured in the glue mortar layer between the hydrophobized wall and the vapor tight XPS-system.

Further research will include an analysis over a longer time period, to further exclude the initial effect of the application of the water repellent agent, and this for the total set of sensors and moisture pins embedded in the test walls. Furthermore, a further study and calibration of the moisture pins is ongoing in order to translate the measured electrical resistance into the material's moisture content.

References

Blocken B., Carmeliet J. 2006. On the accuracy of wind-driven rain measurements on buildings. Building and Environment, 41(12):1798-1810.

ISO 13788, 2012. EN, Hygrothermal Performance of Building Components and Building Elements – Internal Surface Temperature to Avoid Critical Surface humidity and Interstitial Condensation – Calculation Methods, European Committee for Standardization, Brussels.

Kopecký P., Staněk K., Bureš M., Richter J., Ryparová P., Tywoniak J. 2019. Experimental investigations of wooden beam ends in masonry with internal insulation: Measured data in real-scale experimental walls exposed to semi-continental climate conditions. Journal of Building Physics 43(3):147-170.

Otten K., Brischke C., Meyer C. 2017. Material moisture content of wood and cement mortars – electrical resistance-based measurements in the high ohmic range. Construction and Building Materials, 153:640-646.

Roels S., Carmeliet J. 2006. Analysis of moisture flow in porous materials using microfocus X-ray radiography. International Journal of Heat and Mass Transfer 49:4762-4772.

Vereecken E., Roels S. 2018. Wooden beam ends in combination with internal insulation: An experimental study on the impact of convective moisture transport. Building and Environment 148:524-534.

Vereecken E., Deckers D., Janssen H., Roels S. 2020. Field study on hydrophobized internally insulated masonry walls. Accepted for publication in "XV International Conference on Durability of Building Materials and Components' proceedings, DBMC 2020, 30 June – 3 July 2020, Barcelona, Spain.